Crosstalk of TDP-43 and Optineurin in Amyotrophic Lateral Sclerosis Models

Mohović, Nikolina

UNIVERSITY OF RIJEKA

DEPARTMENT OF BIOTECHNOLOGY

Nikolina Mohović

CROSSTALK OF TDP-43 AND OPTINEURIN IN AMYOTROPHIC LATERAL SCLEROSIS MODELS

DOCTORAL THESIS

Rijeka, 2023

UNIVERSITY OF RIJEKA

DEPARTMENT OF BIOTECHNOLOGY

Nikolina Mohović

CROSSTALK OF TDP-43 AND OPTINEURIN IN AMYOTROPHIC LATERAL SCLEROSIS MODELS

DOCTORAL THESIS

Mentor: Associate Prof. Ivana Munitić, PhD, Department of Biotechnology, University of Rijeka

Rijeka, 2023

Mentor: Associate Prof. Ivana Munitić, PhD, Department of Biotechnology, University of Rijeka

Doctoral thesis was defended 08th of November 2023 at the University of Rijeka, Department of Biotechnology, in front of Evaluation Committee:

1. associate prof. Jelena Ban, PhD, Department of Biotechnology, University of Rijeka
2. assistant prof. Silva Katušić Hećimović, PhD, Ruđer Bošković Institute
3. assistant prof. Katarina Kapuralin, PhD, Department of Biotechnology, University of Rijeka

Acknowledgments

I am deeply grateful for the opportunity to work in the Laboratory for Molecular Immunology under the supervision of my mentor Ivana Munitić, and for her support, guidance, and expertise throughout my doctoral journey. Her dedication to my academic growth has been invaluable.

Dear Ivana, thank you.

I extend my heartfelt appreciation to my laboratory colleagues, both past and present, who have been an essential part of my journey. Special thanks to Valentina, Matea, Josip, and Andrea. Valentina's attentive ear and willingness to listen to my problems almost every day, Matea's distant but always present support, Josip's collaboration, and Andrea's initial encouragement have all played vital roles during my doctoral journey.

For every coffee we shared and time we enjoyed together, I want to express my deepest gratitude to my wonderful colleagues: Patrizia Jankovic, Martina Muskovic, Beti Zaharija, Bobana Samardžija, and Robert Kolman. I also want to thank my lab neighbours Ivana Bertović and Ana Bura.

Thank you all for being a cherished part of this experience.

My heartfelt thanks also go to my best friend, Iris, for her enduring friendship, unwavering support, and endless walks that we took during this period. I also extend my gratitude to Petra, Silvia, and Vedrana for their friendship and encouragement. Moments and time spent with you provided the balance I needed during this challenging academic journey.

A very special thanks goes to my family, especially to my parents and my brother, whose strong belief in my abilities and endless encouragement have been my constant source of strength in this challenging phase of my life. Your sacrifices and love have been priceless in my academic achievements.

Mama, tata, Dino, hvala!

And last, to my loving husband, Josip, your support, encouragement, and understanding have been the core of my success. Your belief in me has been my motivation, and I am grateful for your presence in every chapter of my life.

Hvala ti i volim te!

This thesis would not have been possible without the support and contributions of all those mentioned above in ways words cannot fully capture.

Thank you all for being a part of my academic and personal journey!

Za nonota i didota

Abstract

Optineurin is a multifunctional polyubiquitin-binding protein implicated in autophagy and inflammatory signalling, processes that have been described as pathogenic mechanisms in neurodegenerative diseases. Notably, more than 40 mutations in the *OPTN* gene, which encodes for optineurin, were linked to amyotrophic lateral sclerosis (ALS) and frontotemporal dementia (FTD), neurodegenerations marked with excessive motor neurons loss, loss of neurons from frontal and temporal lobes, chronic inflammation, and protein aggregation in the central nervous system (CNS). However, the pathogenic role of optineurin mutations is still largely unclear. The autopsies of ALS and FTD patients carrying the optineurin mutations show TAR DNA-binding protein 43 (TDP-43) aggregates, which could elicit its nuclear depletion and loss-of-function. Since optineurin acts as an adaptor protein in autophagy and inflammatory signalling, and chronic inflammation could exacerbate TDP-43 aggregation, here we tested if optineurin ALS-mimicking mutations could lead to impaired TDP-43 proteostasis, excessive inflammation, and/or inefficient immune responses. Moreover, as ageing is a major risk factor for ALS and FTD, and untreated young mice carrying optineurin ALS-linked mutations do not develop the disease, here we investigated whether ageing could trigger neurological, neuropathological, and/or immunological alterations. To this end, we used (1) $Optn^{470T}$ mouse model, that mimics loss-of-function Q398X truncation found in ALS patients both of which express a lower level of truncated optineurin (henceforth termed optineurin insufficiency) and (2) optineurin deficient microglial BV2 cells made using CRISPR/Cas9 technology (BV2 Optn KO). We found elevated basal TDP-43 protein levels in primary mouse $Optn^{470T}$ myeloid cells and cortical neurons, which were post-translationally regulated. Moreover, we demonstrated that optineurin deficiency did not sensitize cells to apoptosis upon autophagy inhibition and that TDP-43 accumulation in $Optn^{470T}$ primary microglia was not caused by an autophagy block. In contrast, we showed that optineurin insufficiency caused an altered TDP-43 turnover, which was unaffected by experimental block in autophagy in both bone marrow-derived macrophages (BMDMs) and primary neurons. To further evaluate the role of optineurin in inflammation and TDP-43 accumulation, we stimulated BV2 cell lines and primary microglia with lipopolysaccharide (LPS) to mimic bacterial infection.

We observed a significant increase in TDP-43 protein levels in WT cells without changes in optineurin levels. However, LPS failed to increase already elevated TDP-43 levels in untreated optineurin-deficient and-insufficient myeloid cells, suggesting that they already reached a plateau at basal conditions. Moreover, we demonstrated no nuclear depletion or aggregation of TDP-43 in Optn^{470T} primary microglia in basal state or with LPS. Characterization of aged Optn^{470T} mice did not show motor or cognitive defects, or differential TDP-43 insolubility in the whole-brain lysates compared to WT mice. In addition, we demonstrated enhanced expression of certain cytokines and chemokines in the CNS during ageing, but with neglectable differences between old WT and Optn^{470T} mice. Moreover, spleen immunophenotyping uncovered signs of ageing of the immune system (inflammageing and immunosenescence) in old Optn^{470T} mice that were comparable to WT mice. These included an increase in memory and regulatory T lymphocytes, a drop in naïve T lymphocytes, and an increase in the number of macrophages and neutrophils. However, we showed that macrophages and conventional dendritic cells (cDC) exhibited increased expression of activation markers in old Optn^{470T} mice, although we could not link it to any phenotype. Altogether, a combination of ageing and optineurin insufficiency did not induce ALS and/or FTD-like immune imbalance and neuropathology in mice. To further evaluate crosstalk between optineurin insufficiency and TDP-43 we established a new two-hit ALS and/or FTD model by crossing Optn^{470T} mice with the transgenic mice carrying a human TDP-43 patient mutation (G348C) but did not observe an ALS-like phenotype either. In conclusion, we showed TDP-43 accumulation in optineurin-insufficient neurons and microglia. In microglia, the accumulation was not caused by an autophagy block, and it was unresponsive to inflammation, while in neurons it was likely caused by a block in autophagy. Furthermore, the Optn^{470T} mouse model during ageing, even when crossed to mutant transgenic TDP-43 did not show motor or cognitive defects, TDP-43 aggregation, or immunological alterations typical for ALS and/or FTD. Thus, further research is necessary to elucidate the mechanistic links between optineurin mutations and TDP-43-mediated pathology.

Key words: optineurin, amyotrophic lateral sclerosis, frontotemporal dementia, TDP-43, chronic inflammation, autophagy, inflammageing

Sažetak

Optineurin je multifunkcionalni ubikvitin-vezujući protein koji ima ulogu u upalnoj signalizaciji i autofagiji, procesima koji su opisani kao patološki mehanizmi u neurodegenerativnim bolestima. Više od 40 mutacija u genu *OPTN*, koji kodira za optineurin, je povezano s amiotrofičnom lateralnom sklerozom (ALS) i frontotemporalnom demencijom (FTD), neurodegenerativnim bolestima koje karakterizira prekomjeran gubitak neurona u motoričkom, temporalnom i frontotemporalnom korteksu, kronična upala i agregacija proteina. Međutim, uloga mutacija optineurina u patogenezi ALS-a još je uvelike nejasna. Autopsije pacijenata s ALS-om i FTD-om koji nose mutacije optineurina pokazale su agregaciju TAR DNA-vezujućeg proteina 43 (TDP-43) u središnjem živčanom sustavu koja je usko povezana s njegovom deplecijom u jezgri i gubitkom funkcije. Budući da optineurin djeluje kao adaptorski protein u autofagiji i upalnoj signalizaciji, a kronična upala može pogoršati agregaciju TDP-43-a, u ovom radu smo testirali dovode li mutacije optineurina u ALS-u do poremećene proteostaze TDP-43-a, pretjerane upale i/ili neučinkovitog imunosnog odgovora. Štoviše, budući da je starenje glavni čimbenik rizika za ALS/FTD spektar neurodegenerativnih bolesti, te uz činjenicu da netretirani mladi miševi s mutacijama optineurina povezanih s ALS-om ne razvijaju bolest, ovdje smo istraživali ukoliko starenje može potaknuti neurološke, neuropatološke i imunsne promjene. U tu svrhu smo koristili (1) mišji $Optn^{470T}$ model, koji oponaša Q398X mutaciju optineurina pronađenu u ALS pacijenatima koju nazivamo proteinskom insuficjencijom zbog manjka mutiranog proteina i (2) mikroglijalnu BV2 staničnu liniju s nedostatkom optineurina dobivenu pomoću CRISPR/Cas9 tehnologije (BV2 Optn KO). Utvrdili smo povišene bazalne razine TDP-43 proteina u primarnim mišjim $Optn^{470T}$ mijeloidnim stanicama i kortikalnim neuronima čije su razine bile posttranslacijski regulirane. Nadalje, pokazali smo da nedostatak funkcionalnog optineurina nije povećao osjetljivost stanica na apoptozu nakon inhibicije autofagije te da blokada autofagije ne izaziva nakupljanje TDP-43 u primarnoj mikrogliji i BV2 staničnoj liniji. Međutim, pokazali smo da nedostatak optineurina uzrokuje nakupljanje TDP-43 putem autofagije u primarnim neuronima i makrofagima. Kako bismo dodatno ispitali ulogu optineurina u upali i nakupljanju TDP-43, stimulirali smo primarnu mikrogliju i BV2 staničnu liniju s lipopolisaharidom (LPS) koji

oponaša bakterijsku infekciju i uočili smo značajno povećanje razine TDP-43 u WT stanicama. Međutim, LPS nije uspio povećati već nakupljeni TDP-43 u netretiranim mijeloidnim stanicama s insuficijencijom optineurina. Štoviše, pokazali smo da TDP-43 ne pokazuje depleciju u jezgri niti agregaciju u Optn^{470T} mikrogliji. Karakterizacija starih Optn^{470T} miševa nije pokazala motoričke ili kognitivne promjene, niti razliku u topljivosti TDP-43 u lizatima cijelog mozga u usporedbi s WT miševima. Osim toga, pokazali smo pojačanu ekspresiju citokina i kemokina u mozgu i leđnoj moždini bez značajnih razlika između dvogodišnjih WT i Optn^{470T} miševa. Štoviše, imunofenotipizacija slezene otkrila je znakove upale povezane sa starenjem u Optn^{470T} koji su bili usporedivi s WT miševima, kao što je povećanje broja memorijskih i regulacijskih T limfocita i pad broja naivnih, te povećan broj makrofaga i neutrofila. Međutim, pokazali smo da makrofagi i konvencionalne dendritičke stanice (cDC) pokazuju povećanu ekspresiju aktivacijskih markera u dvogodišnjim Optn^{470T} miševima. Zaključno, kombinacija nefunkcionalnog optineurina i starenja nije izazvala imunosnu neravnotežu i neuropatologiju sličnu ALS/FTD-u kod miševa. Kako bismo dodatno istražili vezu između nefunkcionalnog optineurina i TDP-43 proteina, uspostavili smo novi model ALS/FTD-a križanjem Optn^{470T} miševa s transgeničnim miševima koji nose ljudsku TDP-43 mutaciju (G348C) pronađenu u pacijentima, ali bez uočenog ALS fenotipa do dvije godine starosti. Zaključno, pokazali smo akumulaciju TDP-43 u neuronima i mikrogliji s nedostatkom funkcinonalnog optineurina. Akumulacija u mikrogliji nije bila uzrokovana blokadom autofagije niti je TDP-43 reagirao na upalu, dok je u neuronima i makrofagima uzrok akumulacije vjerojatno blok u autofagiji. Nadalje, mišji model Optn^{470T}, čak ni nakon križanja s mutiranim transgeničnim TDP-43 mišjim modelom, nije pokazao motoričke ili kognitivne promjene, niti imunosne promjene vezane uz ALS/FTD spektar bolesti. Stoga su daljnja istraživanja potrebna kako bi se razjasnile mehanističke veze između mutacija optineurina i patologije posredovane TDP-43-om.

Ključne riječi: optineurin, amiotrofična lateralna skleroza, frontotemporalna demencija, TDP-43, kronična upala, autofagija, upala povezana sa starenjem

Table of content

1. Introduction

1.1. Amyotrophic lateral sclerosis

Amyotrophic lateral sclerosis (ALS) or Lou Gehrig's disease is a fatal adult-onset neurodegenerative disease that affects upper and lower motor neurons in the central nervous system (CNS), resulting in paralysis and death within one to five years after onset (Hardiman et al., 2017). Upper motor neurons project from the brain motor cortex to the brain stem and spinal cord where they transfer information to lower motor neurons that innervate the muscles. ALS was described by French neurologist Jean-Martin Charcot in 1869, who linked muscle weakness (amyotrophy) with the appearance of axonal degeneration, scarring, and gliosis in the corticospinal and corticobulbar tracts (lateral sclerosis), together with the death of motor neurons in the ventral horns of the spinal cord. The initial symptoms can vary between patients depending on which motor neurons are first affected. Upper motor neuron death causes muscle contractions (spasticity) while lower motor neuron death causes muscle weakness. ALS patients can be divided into two main subgroups, one with spinal-onset and weakness of the limbs, and the other with bulbar-onset characterized by dysarthria (speech alterations) and dysphagia (swallowing alterations) (Brown and Phil, 2017; Hardiman et al., 2017). Nevertheless, during disease progression, both subgroups manifest the same clinical features such as muscle weakness, fasciculations, and atrophy, which in the end leads to paralyses. Finally, paralysis of the respiratory muscles is usually the cause of death in ALS patients (Hardiman et al., 2017).

ALS is a rare disease, with a prevalence of 3-6 per 100 000 individuals and an average onset around 58-60 years (Brown and Phil, 2017; Talbott et al., 2016). However, it is the most common and most rapid motor neuron disease in adults, thus presenting an important medical challenge. First heritability studies have shown that only around 5-10% of ALS patients had a family member affected with ALS, defined as having familial ALS (fALS) (Andersen and Al-Chalabi, 2011; Byrne et al., 2011; Mejzini et al., 2019). Nowadays, genetic studies on twins and European case-control cohorts have found that the heritability of ALS is approximately 40%, from which 40-55% have known genetic mutation, most frequently inherited in an autosomal dominant manner (Al-Chalabi et al., 2010; Ryan et al., 2019; Trabjerg et al., 2020; Zou et al., 2017). The remaining cases are referred to as sporadic (sALS), with no

recorded family history. Notably, in more than 90% of sALS patients, the cause is unknown, meaning that more than half of all ALS cases cannot be linked to the disease cause (Zou et al., 2017). Interestingly, the genes that were found mutated in fALS, are also linked to sALS, demonstrating that sALS also has a strong genetic element. The reasons why uncovering genetic background is so challenging in ALS are diverse – there is a possibility of *de novo* mutations, incomplete penetrance, and/or oligogenic inheritance, previously undetected mutations, late-onset of the disease, and an overlap in the clinical spectrum with other neurodegenerative disorders (Andersen and Al-Chalabi, 2011). Notably, sALS and fALS also share indistinguishable pathological and clinical features, suggesting that they have similar pathogenic mechanism(s) (Hardiman et al., 2017).

ALS is characterized by high genetic heterogeneity, with mutations found in more than 50 different genes thus far (Hardiman et al., 2017). The most frequently affected genes are chromosome 9 open reading frame 72 (*C9orf72*), superoxide dismutase 1 (*SOD1*), transactive response (TAR) DNA binding protein (*TARDBP*), and fused in sarcoma (*FUS*). The mutations in these genes encode proteins or peptides with an increased tendency for aggregation. Notably, although the TAR DNA binding protein of 43 kDa (TDP-43) mutations contribute to less than 5% of fALS, protein aggregates in more than 95% of ALS patients contain WT TDP-43 (Arai et al., 2006; Neumann et al., 2006). In contrast to the aggregate-prone protein variants, less frequent mutations in immune- and autophagy-related genes such as TANK-binding kinase 1 (*TBK1*), sequestosome 1 (*SQSTM1*/*p62*), optineurin (*OPTN*) and cylindromatosis (*CYLD*) were not found in aggregates and, except for CYLD, seem to act by loss-of-function (Dobson-Stone et al., 2020; Fecto et al., 2011; Freischmidt et al., 2017; Maruyama et al., 2010). Interestingly, mutations in those genes also elicit TDP-43 protein aggregation. Genes found mutated in ALS have a wide range of functions in RNA and protein metabolism, trafficking, and roles in non-neuronal cells such as immune cells, but the exact molecular mechanism that triggers ALS is still unclear (Taylor et al., 2016).

No ALS gene has entirely been associated with ALS-only motor alterations (Hardiman et al., 2017). In up to 50% of ALS patients, motor symptoms appear together with cognitive and/or behavioural impairments, and these patients can develop frontotemporal dementia (FTD), characterized by neuronal degradation in

the frontal and temporal cortex (McCauley and Baloh, 2019). Notably, TDP-43 protein aggregates were also found in FTD patients, supporting the idea that ALS and FTD are two different manifestations of a single disease spectrum referred to as ALS/FTD spectrum disorders (Arai et al., 2006; Dobson-Stone et al., 2020; Fecto et al., 2011; Freischmidt et al., 2017; Maruyama et al., 2010; Pottier et al., 2018).

1.1.1. ALS therapy

There is no efficient therapy for ALS, which is at least in part due to high genetic heterogeneity. Current treatment options are only rarely based on disease-modifying therapies and largely target the symptoms. A multidisciplinary approach to care is necessary, involving neurologists, physical therapists, psychologists, and specialized nurses (Mead et al., 2023a). Although more than 50 components with diverse mechanisms of action were researched in the past 30 years, only a few drugs, including the two most common Riluzole and Edaravone have come to market, with Edaravone being approved by the Food and Drug Administration agency (USA) and several other regulatory agencies, but not European Medical Agency (Hardiman et al., 2017). Riluzole belongs to a group of benzothiazoles and has a poorly understood mechanism of action in ALS patients, but it most likely blocks glutamate release and thereby diminishes excitotoxicity (Mead et al., 2023b). Although it was initially reported that it extends life-span for only 2-3 months, recent real-world evidence suggests the patients' survival is prolonged for approximately 6-19 months (Andrews et al., 2020). Edaravone is an antioxidant that is efficient in slowing disease progression only in a limited number of patients (Writing Group and Edaravone (MCI-186) ALS 19 Study Group, 2017). A new drug Relyvrio (AMX0035), which is a combination of two components sodium phenylbutyrate and taurursodiol, has recently been approved in the USA. It slows disease progression by preventing neuronal cell death by blocking ER and mitochondrial stress, without affecting the patients' lifespan (Paganoni et al., 2020). The combination of quinidine sulfate and dextromethorphan (Nuedexta) is used to control uncontrollable/inappropriate laughing and/or crying, and to improve bulbar functions such as speaking and swallowing in ALS patients (Smith et al., 2017). The latest improvement in the treatment of ALS patients with *SOD1* mutations is the first gene-based therapy

named Tofersen. Tofersen is an antisense oligonucleotide designed to decrease mutated SOD1 protein levels (Miller et al., 2022).

Other approaches tested, such as masitinib, an inhibitor of tyrosine kinase receptors that lowers neuroinflammation, and different stem cell therapies failed to show clear-cut efficacy in patients, although the studies are still ongoing. Numerous drug candidates are also in clinical trials (Chiò et al., 2020). To conclude, the search for efficient drugs for ALS patients is still ongoing.

1.1.2. ALS mechanisms

Molecular mechanisms in ALS are still largely elusive, most likely due to wide genetic heterogeneity and the interplay between different environmental and genetic triggers (Hardiman et al., 2017). Several mechanisms were proposed to be disrupted in ALS including RNA metabolism, proteostasis, endosomal, nucleocytoplasmic and vesicular trafficking, excitotoxicity, mitochondrial function and oxidative stress, and neuroinflammation, some of which will be further discussed (Mead et al., 2023a; Van Damme et al., 2017). Moreover, ALS is a non-cell-autonomous disease in which in addition to neurons, various cells such as microglia, astrocytes, oligodendrocytes, and peripheral immune cells contribute to ALS pathogenesis. Notably, regardless of the genes, cells, and mechanism involved, protein aggregation and chronic inflammation occur in all ALS cases.

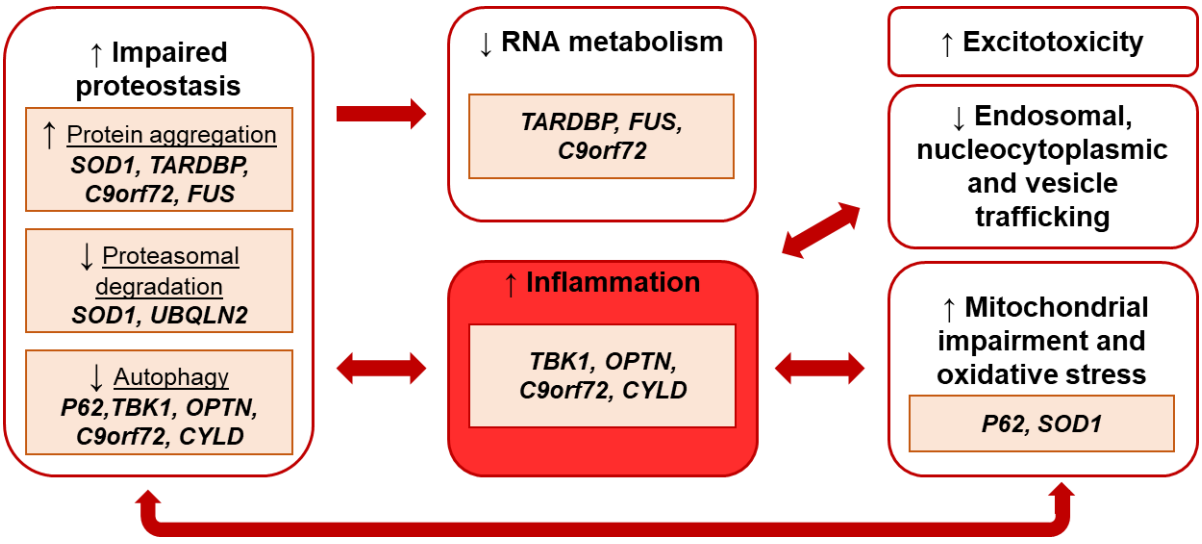

Figure 1. Mechanisms and genes proposed to contribute to ALS pathogenesis. Most genes found mutated in ALS are directly linked to impaired proteostasis by increasing protein aggregation, or diminishing proteasomal and autophagosomal degradation. Moreover, several genes mutated in ALS (*TARDBP* and *FUS*) are RNA/DNA binding proteins that

directly diminish RNA metabolism. Mutations in other genes (*C9orf72, TBK1, OPTN,* and *CYLD*) are directly linked to impaired inflammatory response but also have a role in autophagy. Protein aggregation can directly trigger inflammation and *vice versa,* inflammation can trigger protein aggregation. Inflammation and impaired proteostasis can also be triggered by mitochondrial impairment and increased oxidative stress, as well as excitotoxicity and endosomal, nucleocytoplasmic, and vesicle trafficking. The list of mutated genes that can contribute to disease pathogenesis is even broader, but we focused on the ones linked to proteolysis and inflammation that are the focus of this thesis.

Most ALS-linked mutations disrupt proteostasis by increasing protein aggregation or by altering proteasomal or autophagosomal degradation (Fig. 1.). Since its discovery in 1993, mutations in *SOD1* become the longest and most extensively studied mutations implicated in ALS (Gurney et al., 1994). Since SOD1 is a scavenger for toxic superoxide free radicals, it was first thought that ALS-linked mutations act by loss-of-function, causing mitochondrial dysfunction and oxidative stress, which are toxic to motor neurons (Gurney et al., 1994). However, evidence from transgenic $SOD1^{G93A}$ mice, the first ALS mouse model, demonstrated that mutated SOD1 forms neurotoxic protein aggregates (Bruijn et al., 1998; Urushitani et al., 2002). Consequently, gain-of-function *SOD1* mutations could later on lead to the effect of loss-of-function. Since then, other common ALS-linked mutations in *TARDBP* (encoding for TDP-43), *FUS*, and *C9orf72* were described as gain-of-function mutations with an increased propensity for aggregation (Arai et al., 2006; DeJesus-Hernandez et al., 2011; Kwiatkowski et al., 2009; Neumann et al., 2006; Renton et al., 2011). In addition to *TARDBP* mutations, ubiquitinated and hyperphosphorylated aggregates of WT TDP-43 are present in the majority of ALS cases, except in patients that harbour *SOD1* and *FUS* mutations, and in ~50% of FTD patients, demonstrating that mutations are not necessary for TDP-43 aggregation (Arai et al., 2006; Bruijn et al., 1998; Kwiatkowski et al., 2009; Neumann et al., 2006). Notably, some mutations can disrupt several different functions, such as hexanucleotide repeats in a non-coding region of *C9orf72* that form abnormal RNA species, affect RNA splicing and transcription, cause DNA damage and protein aggregation, but can also disturb autophagy initiation and lysosomal function (Balendra and Isaacs, 2018; Hardiman et al., 2017; Webster et al., 2016). Moreover, both TDP-43 and FUS, as RNA/DNA binding proteins, are implicated in various roles in RNA metabolism, and when aggregated cannot further process their target RNAs,

leading to altered RNA metabolism (Fig. 1.) (Prasad et al., 2019). Numerous other ALS-linked mutations in genes, such as *SQSTM1, OPTN, TBK1, CYLD*, and *ubiqulin-2* (*UBQLN2*), encode for proteins that were reported to disrupt proteostasis and increase TDP-43 protein aggregation at the level of autophagy or proteasomal degradation (Fecto, 2011; Freischmidt et al., 2017; Hjerpe et al., 2016; Maruyama et al., 2010).

Although chronic neuroinflammation is a key contributing factor to ALS, most ALS-linked mutations are not directly related to the immune system. However, protein aggregation and excessive neuronal damage can trigger an inflammatory response in the CNS and promote the infiltration of peripheral immune cells (Brown and Phil, 2017). Moreover, inflammation can also trigger protein aggregation, so the crosstalk between these processes is bidirectional. Other mechanisms disrupted in ALS, including mitochondrial impairment, oxidative stress, and excitotoxicity also trigger inflammation (Fig. 1.). However, several characterized ALS-linked mutations are proposed to directly modulate the immune response, which will further be discussed below (Béland et al., 2020a; Masrori et al., 2022). In conclusion, ALS is likely the result of crosstalk of several altered mechanisms that amplify the damage and lead to motor neuron death.

1.2. Ageing and inflammageing

During ageing individuals increase their susceptibility to intrinsic genetic and epigenetic factors as well as external factors such as environment, nutrition, radiation, temperature, and stress, which leads to changes in the tissues and organs, a decline in function, and increased vulnerability of the organism to death (Jayanthi et al., 2010). Ageing is referred to ‘’unsolved problem in biology’’ (Martin, 1999). Evolutionary theories of ageing propose that ageing is the result of a decline in reproductive fitness in an individual and the force of evolutional selection. Furthermore, systemic theories suggest the ageing is linked to organ system decline, while molecular and cellular theories propose that ageing is the result of a decline at cellular and subcellular levels (Jayanthi et al., 2010). A lot of research is ongoing and knowledge about ageing is expanding rapidly.

Ageing is considered the most prominent risk factor for numerous chronic diseases such as heart disease, cancer, autoimmune disorders, osteoporosis, and

neurodegenerative diseases (Zuo et al., 2019). Chronic, low-grade inflammation termed ‘’inflammageing’’ was linked to age-related diseases in early 2000 by Franceschi *et al.* Inflammageing describes an increase in the levels of pro-inflammatory markers in blood and tissues that in turn lead to inefficient and/or hyperinflammatory immune response and tissue damage (Franceschi et al., 2000). It is proposed that inflammageing is provoked by a continuous antigenic load and stress that leads to alterations in both innate and adaptive immunity and generates a toxic pro-inflammatory environment. In addition to an increased pro-inflammatory environment, the immune system undergoes gradual remodelling termed immunosenescence, which involves diminished responses to pathogens and enhanced susceptibility to infection and cancer, as well as decreased vaccination efficacy (Franceschi et al., 2018).

The immune system remodelling in aged individuals occurs because of functional changes in both innate and adaptive immune systems in which the number of naïve T and B lymphocytes is getting reduced. Notably, the thymus, the primary lymphoid organ responsible for the production of immunocompetent T lymphocytes atrophies and functionally declines during ageing (Ventevogel and Sempowski, 2013). The result of the atrophied thymus is a decreased number of naïve T lymphocytes so antigen-specific memory T lymphocytes become the predominant population (Fig. 2.). However, aged memory T lymphocytes are also functionally impaired – they lose their ability to proliferate, have decreased expression of costimulatory molecules CD27 and CD28, and consequently reduce the ability to help B lymphocytes to produce antigen-specific antibodies (Mittelbrunn and Kroemer, 2021; Murasko et al., 1987). Regulatory T lymphocytes (Tregs) that act as main suppressors of the immune response by maintaining tolerance to self-antigens and downregulating proliferation of effector T lymphocytes in response to foreign antigens are also markedly changed during ageing (Vignali et al., 2008) (Fig. 2.). Tregs accumulation occurs most likely because they try to compete with the overall pro-inflammatory environment and senescence of effector memory T lymphocytes in an attempt to control exaggerated immune reactions (Fessler et al., 2013). Because of this, Tregs are shown to be protective during ageing.

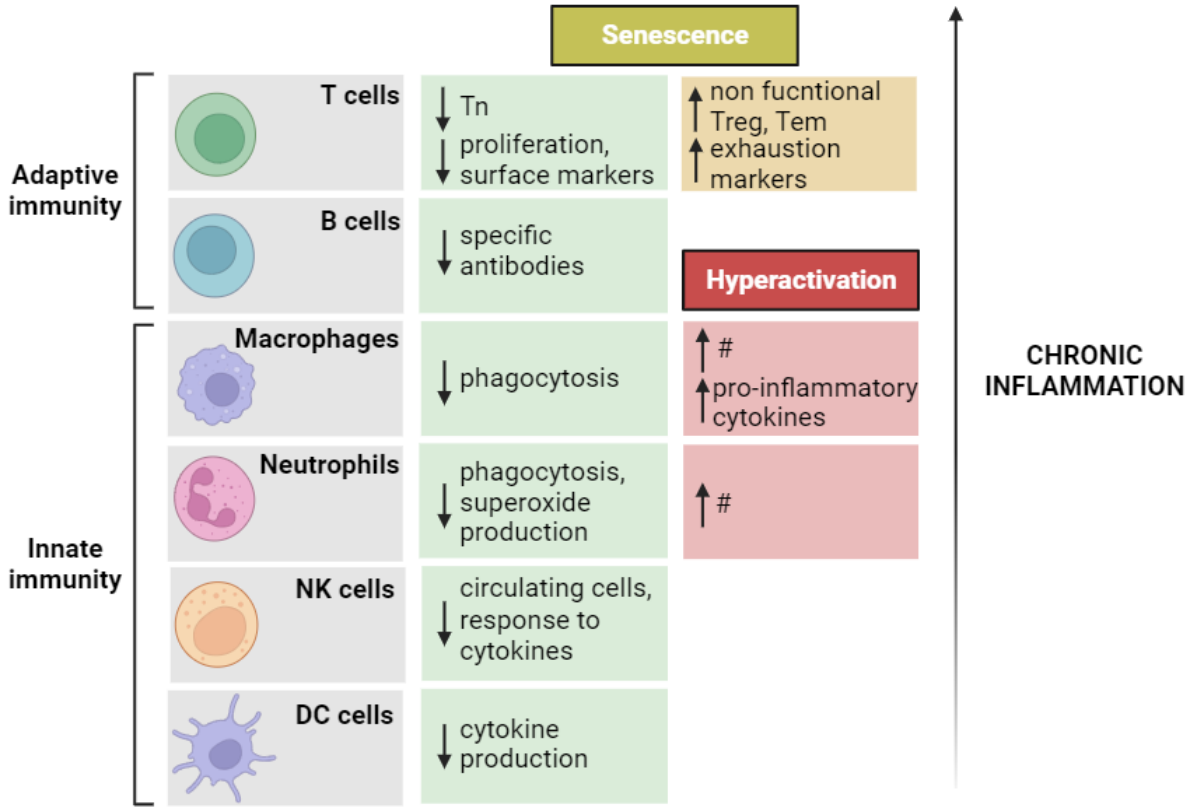

Figure 2. Immune cell alterations in ageing. During ageing adaptive (T and B lymphocytes) and innate immune cells (macrophages, neutrophils, NK and DC cells) undergo changes in number and functions that cause immune system immunosenescence and/or excessive activation, that in the end lead to chronic inflammation. #=number; Tn= naïve; Treg= T regulatory lymphocytes; Tem=effector memory T lymphocytes.

Ageing also directly affects innate immune cells (Fig. 2.). An increased number of hyperactivated macrophages was observed in aged organisms, but with a decline in phagocytic function and increased inflammatory cytokine production (De Maeyer and Chambers, 2021; Peradinovic et al., 2023). Moreover, an increased number of neutrophils, innate immune cells that form the first line of defence against various external and internal insults, were also found in aged individuals. However, they exhibit diminished phagocytosis and superoxide production (Butcher et al., 2000). In contrast to macrophages and neutrophils, the number of mature circulating NK cells drops, and their proliferation ability and response to cytokines decline during ageing (Beli et al., 2014; Gounder et al., 2018). Dendritic cell (DC) numbers were not reported to change, but like other innate immune cells, they display reduced cytokine production (Agrawal and Gupta, 2011). On the molecular level, an increase in pro-inflammatory cytokines and mediators such as C-reactive protein (CRP), interleukin

(IL)-6, and tumor necrosis factor (TNF)-α were found in the blood of ageing individuals (Alvarez-Rodríguez et al., 2012). To sum up, during ageing both adaptive and innate immune functions decline, and because of this, certain cells get more activated and induce a pro-inflammatory environment. Thus, inflammageing is a combination of both decline in function and low-grade chronic activation of the immune system.

1.3. Immunity in ALS

The CNS also undergoes immune alterations linked to ageing and all neurodegenerative diseases are marked with chronic inflammation (Ransohoff, 2016; Zuo et al., 2019). Microglia, as the only immune cell in the brain parenchyma, are the principal modulators of immunity in the CNS, and several studies in the late 20th century demonstrated activated microglia in *post mortem* tissue of ALS patients (McGeer et al., 1988; McGeer and McGeer, 2011). Moreover, the finding that peripheral immune cells can survey and even infiltrate CNS in both health and disease strengthens the idea that crosstalk exists between those systems (Baruch et al., 2014; Ransohoff, 2016). However, outstanding questions remain whether neuroinflammation 1) triggers neurodegeneration, 2) is protective, or 3) acts as a secondary hit in the pathogenesis of neurodegeneration.

1.3.1. Microglia in physiological conditions

Under physiological conditions, microglia, with its ramified processes constantly scan the CNS environment and secrete various neurotrophic factors (Prinz and Priller, 2014). Moreover, the vicinal neurons inhibit activation of microglia by chemokine fractalkine (CX3CL1) and co-stimulatory molecule CD200, while astrocytes secrete anti-inflammatory cytokine transforming growth factor β (TGF-β) (Hellwig et al., 2013; Kettenmann et al., 2013). Microglial activation is triggered in response to neuronal damage (bacterial or viral infections, protein aggregation, or other insults) via several damage receptors such as Toll-like receptors (TLR), complement or scavenger receptors, and cytosolic DNA/RNA sensors. The previous notion that microglia exist in only distinct conditions such as ‘‘resting versus activated’’ and when activated in ‘‘M1 versus M2’’ is now considered outdated. This nomenclature does not address multidimensional states and microglia subsets that

can exist depending on numerous factors such as the local microglial environment, the extent of damage, or the nature of an insult (Paolicelli et al., 2022). For example, upon activation, microglia change to ameboid form, increase body area, proliferate, secrete pro- and anti- inflammatory cytokines and chemokines, and enhance their phagocytic properties (Kettenmann et al., 2013). On the molecular level, activation of TLR receptors and other receptors for pathogen-associated/ damage-associated molecular patterns (PAMP/DAMP) trigger diverse signalling pathways such as nuclear factor kappa-light-chain-enhancer of activated B lymphocytes (NF-κB), interferon regulatory factor 3 (IRF3), and mammalian target of rapamycin (mTOR). Upon sensing different microbial stimuli microglia secret pro-inflammatory cytokines such as TNF-α, IL-1β, and IL-6 and produce reactive oxygen species (ROS) and nitric oxide. On the other hand, alternatively activated microglia secret anti-inflammatory cytokines such as IL-4, IL-10, and IL-13 that suppress inflammation and promote tissue regeneration (Gravel et al., 2016; Kocur et al., 2015; Lobo-Silva et al., 2017; Tang and Le, 2016; X. Zhao et al., 2015). Acute and limited activation of pro-inflammatory microglia is crucial for neuronal protection and CNS homeostasis. However, when microglia exhibit prolonged chronic secretion of neurotoxic factors, it could generate an excitotoxic environment and neuronal death. The exact triggers for such neurotoxic microglia in neurodegeneration are still unclear.

1.3.2. Microglia and astrocytes in ALS pathogenesis

There is a lot of evidence that supports the theory that ALS is a non-cell-autonomous disease and that glial cells contribute to ALS pathogenesis. Most evidence came from transgenic ALS mouse models that carry human mutations in SOD1 (hSOD1) (Gurney et al., 1994). In these mouse models, overexpressed mutated hSOD1 leads to rapidly progressive disease and death within five to six months. Interestingly, neuron-specific expression of hSOD1 in mice was not sufficient for the development of ALS-like symptoms, meaning that both neuronal and non-neuronal cells need to be affected for disease manifestation (Lino et al., 2002; Pramatarova et al., 2001). In line with this, neuron-specific deletion of mutant $hSOD1^{G37R}$ delays the disease onset but does not protect mice from disease manifestation and death (Boillee et al., 2006). The major finding that microglia are crucial in ALS pathogenesis came from the discovery that in transgenic mice

microglia-specific hSOD1^{G37R} deletion significantly slows down the disease progression (Boillee et al., 2006). Moreover, it was seen that during disease microglia shift from early neuroprotective anti-inflammatory to a neurotoxic pro-inflammatory phenotype. Studies from hSOD1^{G93A} showed that at the onset of the disease, microglia express IL-4, IL-10, arginase 1, CD163, and brain- and glial cell-derived neurotrophic factors (BDNF and GDNF). Moreover, during the late phase of the disease, microglia express pro-inflammatory NOX2, TNF, IL-6, and IL-1β, and further exaggerate neuronal death, meaning that microglia had diverse functions in distinct disease phases (Beers et al., 2006; Gravel et al., 2016; Liao et al., 2012; Zhao et al., 2013). Notably, the microglia from the affected spinal cord regions were shown to be less responsive to inflammatory stimuli demonstrating desensitization and/or exhaustion (Nikodemova et al., 2014). The expression of mutant hSOD1 in astrocytes caused astrocytosis but did not trigger motor neuron degradation and disease (Gong et al., 2000). On the other hand, hSOD1^{G37R} deletion in astrocytes did not affect onset but slowed disease progression and postponed microglial activation (Yamanaka et al., 2008). Moreover, studies in astrocytes derived from patient-induced pluripotent stem cells demonstrated that astrocytes from patients carrying mutations in *SOD1* and *C9orf72* trigger the death of motor neurons by soluble toxic factors and oxidative stress (Birger et al., 2019; Re et al., 2014). This indicates that in combination with microglia, astrocytes, although they are not immune cells *per se*, could also orchestrate inflammation and ALS pathology. In summary, glial cells have crucial roles in ALS pathogenesis and can also influence a network of peripheral immune cells, and their infiltration in the CNS.

1.3.3. Peripheral immune responses during ALS pathogenesis

A growing body of evidence suggests that, in addition to glial cells, several innate and adaptive immune cells such as DC, NK cells, macrophages, neutrophils, and T lymphocytes, are implicated in ALS pathogenesis (Fig 3.). Although accumulation of IgG antibodies was found in motor neurons in ALS patient autopsies, currently there is no evidence that B lymphocytes contribute to ALS progression (Engelhardt and Appel, 1990; Naor et al., 2009).

Several lines of evidence from both patients and the hSOD1 mouse models suggest an important role of T lymphocytes in ALS pathogenesis. Infiltration of both

helper ($CD4^+$) and cytotoxic ($CD8^+$) T lymphocytes was found in the ventral horn and corticospinal tracts during autopsies in ALS patients in the late 20th century, but it was not immediately clear if their presence was damaging or beneficial in disease progression (Engelhardt et al., 1993; Troost et al., 1989). Interestingly, the total number of lymphocytes was also found increased in ALS patients' blood compared to healthy individuals (Murdock et al., 2017). Depletion of all T lymphocytes in hSOD1 mice demonstrated faster disease progression, whereas specific $CD8^+$ T lymphocyte depletion reduced inflammation and increased the number of surviving motor neurons (Beers et al., 2008; Chiu et al., 2008; Coque et al., 2019). In addition, *in vitro* data suggested that in co-cultures, SOD1-expressing $CD8^+$ T lymphocytes were selectively killing motor neurons via granzymes, Fas ligand, and secretion of IFN-γ. Moreover, $CD8^+$ T-lymphocyte infiltration was reported in the CNS in the late stage of the disease in both hSOD1 mice and ALS patients (Fig. 3.) (Coque et al., 2019; Holmøy, 2008). Several subsets of $CD4^+$ T lymphocytes such as effector memory Th1 and Th17 were also linked to pro-inflammatory phenotype at the late stage of the disease suggesting they further exaggerate neurotoxicity (Beers et al., 2011b; Henkel et al., 2013; Saresella et al., 2013). On the contrary, the neuroprotective function was reported for the effector memory Th2 subset of $CD4^+$ T lymphocytes and Tregs. The expansion of endogenous Tregs in hSOD1 mice significantly prolonged survival and was associated with preserved motor neurons, suppression of microglia by inducing secretion of IL-4 and IL-10 and inducing its anti-inflammatory phenotype (Mantovani et al., 2009; Sheean et al., 2018). Notably, the decreased number and function of Tregs were found in ALS patients, where their drop correlates with a faster rate of disease progression (Fig. 3.). The same as in hSDO1 mice, in ALS patients autologous expansion or infusion of Tregs in combination with IL-2, a cytokine that drives Treg proliferation, increases Tregs numbers and their suppressive function and therefore slow disease progression during early and later stages (Thonhoff et al., 2022, 2018). In summary, it was seen that individual subsets of T lymphocytes have both neurotoxic and neuroprotective functions during ALS progression (Schwartz and Cahalon, 2022).

Changes in the expression and/or activation of innate immune cells have also been found in the *post mortem* tissues of ALS patients as well as in ALS mouse models (Fig. 3.). Infiltrated NK cells were observed in both the motor cortex and

spinal cords of ALS patients and hSOD1 mice. Moreover, an increased number of NK cells correlates with disease progression in ALS patients, while their depletion delays the onset of paralysis and increases survival in hSOD1 mice (Garofalo et al., 2020; Murdock et al., 2017). When NK cells secret IFN-γ, they polarize macrophages and microglia to pro-inflammatory phenotype, suppress Tregs, and directly kill motor neurons. DC, neutrophils, and macrophages/monocytes have limited access to CNS, and their infiltration in ALS is still under debate (Geissmann et al., 2008; Mrdjen et al., 2018). Notably, the total number of neutrophils and monocytes was found increased, while DCs were decreased and dysfunctional in the blood of ALS patients (Murdock et al., 2017; Rusconi et al., 2017). Furthermore, a high neutrophil-to-lymphocyte ratio correlated with faster ALS progression (Yildiz et al., 2023). Overall, numerous pieces of evidence suggest that adaptive and innate immunity have a role in different stages of ALS, but further research is needed to precisely understand how altered immunity contributes to ALS pathogenesis.

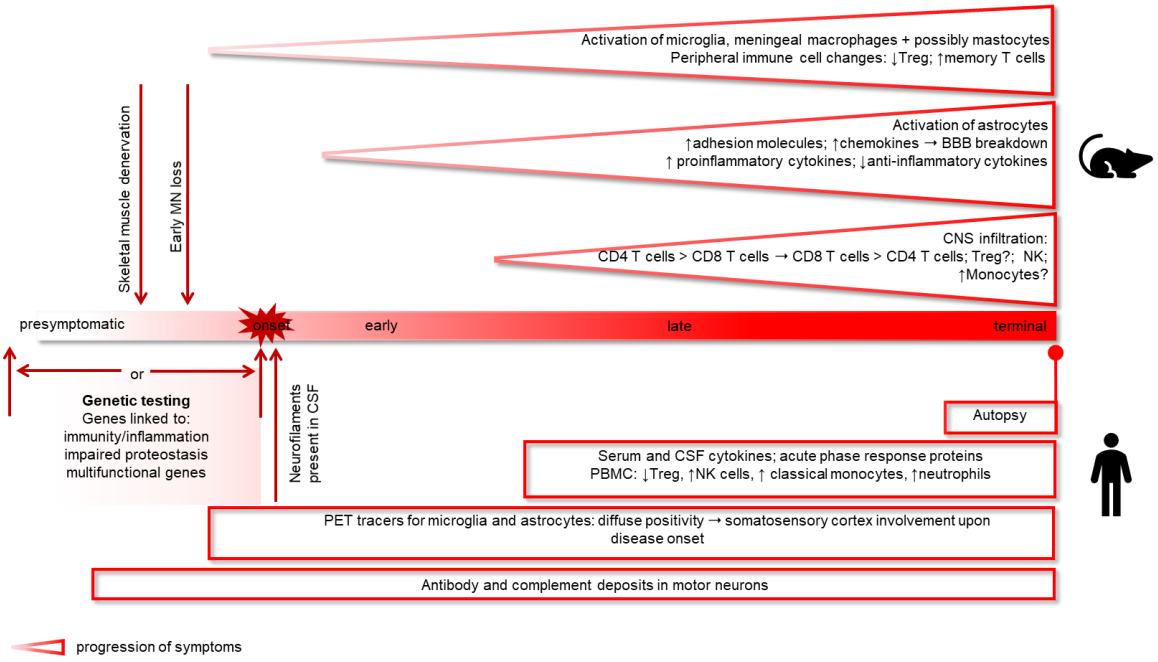

Figure 3. The timeline of immune system alterations found in ALS animal models and patients. The immune responses in animal ALS models (top) and ALS patients (bottom) change throughout the disease. Horizontal arrows mark the conversion of immune biomarkers when applicable, while vertical arrows mark non-immune milestones of disease. Monocyte infiltration is still controversial (*). Abbreviations: blood-brain barrier (BBB), cerebrospinal fluid (CSF), central nervous system (CNS), motor neurons (MN), natural killer (NK), peripheral blood mononuclear cell (PBMC), positron emission tomography (PET), regulatory T cell (Tregs). This figure was taken from our review paper (De Marchi et al., 2021).

1.4. TAR DNA-binding protein 43 (TDP-43)

TDP-43 is 414 amino acids (aa) long DNA- and RNA-binding protein, identified in 1995 as a transcription repressor protein associated with human immunodeficiency virus 1 (HIV-1) (Ou et al., 1995). It is a highly conserved and ubiquitously expressed protein encoded by the *TARDBP* gene, located at chromosome 1, and belongs to the large heterogeneous nuclear ribonucleoprotein (hnRNP) protein family. Normally located in the nucleus, TDP-43 is involved in multiple steps of RNA metabolism including mRNA processing and trafficking, mRNA stability, stress granule formation, and microRNA biogenesis (Prasad et al., 2019). Furthermore, TDP-43 has been shown to regulate mRNAs involved in the development of embryonic neurons and neuronal dendrites where it plays an important role in RNA transport (Sephton et al., 2010). TDP-43 is also a self-regulatory protein that tightly regulates its transcription via a negative feedback loop and promotes the degradation of *TARDBP* mRNA (Ayala et al., 2011). Furthermore, by interfering with lysosomal function TDP-43 has also been shown to control its degradation via lysosomal pathways and autophagy (Leibiger et al., 2018).

Structurally, TDP-43 consists of two highly conserved RNA recognition motifs (RRM1 and RRM2) at the N'-terminus, which enable binding to sequence-specific RNAs (Fig. 4.). Moreover, it contains a nuclear localization signal (NLS), for active transport to the nucleus, and a non-functional nuclear export signal (NES). Recent findings have suggested that TDP-43 can passively diffuse through the nuclear membrane to regulate various aspects of RNA metabolism such as splicing, trafficking, and mRNA stabilisation (Pinarbasi et al., 2018). The C'-terminal region of TDP-43 is a glycine- and glutamine/asparagine-rich highly disordered domain also called prion-like because of its aggregation propensity. It is important for protein-protein interactions, but can also undergo liquid-liquid phase separation and form lipid droplets critical for stress granule formation (Conicella et al., 2016; Prasad et al., 2019). The C'-terminal region of TDP-43 is relevant to the pathological behaviours of TDP-43 and will be further discussed below.

Figure 4. Schematic representation of TDP-43 structural domains. TDP-43 is a 414 aa protein comprised of a nuclear localisation signal (NLS; 82-98 aa) and a non-functional nuclear export signal (NES; 239-250). It contains two highly conserved RNA recognition motifs (RRM1 and RRM2, at 192-262 aa and 239-250 aa, respectively) for binding to RNA. Glycine-rich (274-414 aa) and glutamine/asparagine-rich (Q/N; 345-366 aa) at the C'-terminus is a highly disordered aggregation-prone domain responsible for TDP-43 protein aggregations and also harbours most of *TARDBP* ALS-linked mutations and phosphorylation sites.

1.4.1. TDP-43 in ALS

Since it was first discovered in 2006 as a key component of protein aggregates in the brains of ALS and FTD patients, TDP-43 has become a hot topic in the field of neurodegeneration (Arai et al., 2006; Neumann et al., 2006). Strikingly, more than 95% of ALS and ~50% of FTD cases contain TDP-43 protein aggregates. In a small fraction of ALS patients, TDP-43 mutations have been found in the low-complexity C'-terminal domain (Fig. 4.). The most common *TARDBP* mutations are A382T, and M337V, while the most studied are A315T, Q331K, M337V, D169G, G294A/V, and Q343R. Interestingly, mutations, such as G294V, G348C, A328T, and S393L were found in both the fALS and sALS patients (Prasad et al., 2019). Interestingly, mutations enhance TDP-43 aggregation propensity and increase protein half-life. Moreover, the discovery that the TDP-43 C'-terminal region is similar to prion-like domains of yeast proteins suggests that disease propagation can be mediated in a prion-like manner (Furukawa et al., 2011; Hock and Polymenidou, 2016).

In the disease, TDP-43 is depleted from the nucleus and mislocalized to the cytoplasm where it can form insoluble protein aggregates (Fig. 5.). During disease pathogenesis TDP-43 undergoes various posttranslational modifications such as hyperphosphorylation, ubiquitination, and acetylation, all of which can modify its structure and function (Buratti, 2018; Correia et al., 2015). Moreover, in the disease-affected neurons and glia, TDP-43 undergoes proteolytic cleavage into TDP-35 and TDP-25 C'-terminal toxic fragments, which lack functional N'-terminal NLS and further increase mislocalization, aggregation, and toxicity (Buratti, 2015; Igaz et al., 2009)

(Fig. 5.). The reason why TDP-43 undergoes pathological changes in ALS and FTD pathology is mostly unknown and it is debatable as to whether they are secondary or causative during disease pathogenesis. However, a growing body of evidence exists that supports the important role of impaired proteostasis and neuroinflammation in TDP-43 aggregation in the ALS/FTD disease spectrum.

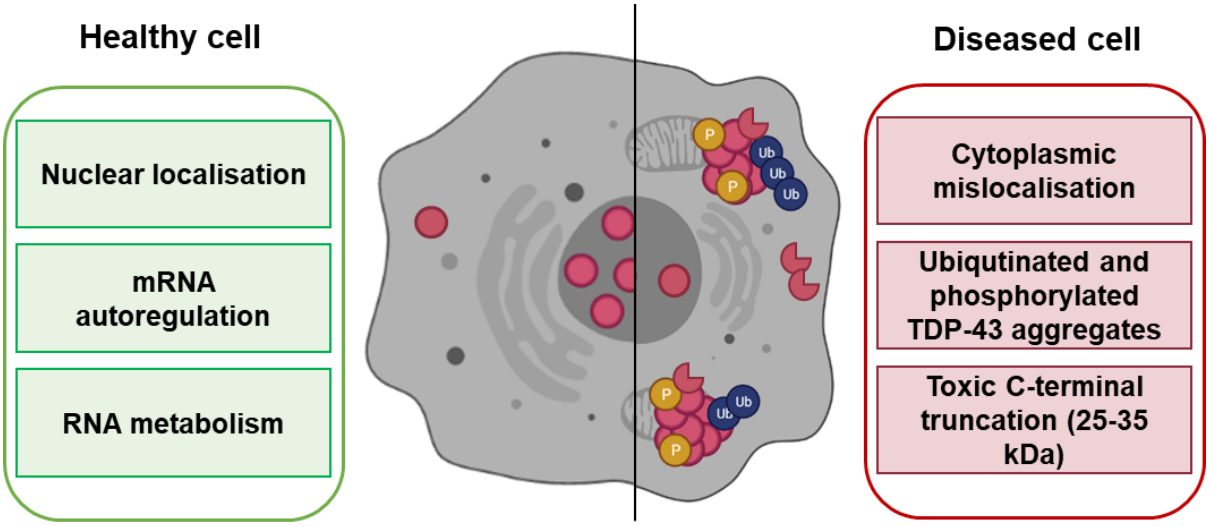

Figure 5. Physiological functions and localization of TDP-43 in healthy cells and diseased cells. In healthy cells, TDP-43 is predominantly located in the nucleus where it regulates its mRNA levels. It is also implicated in various steps of RNA metabolism such as transcription, RNA transport and stability, translation and microRNA, and long non-coding RNA processing. In diseased cells, TDP-43 is depleted from the nucleus, and mislocalized to the cytoplasm where it forms ubiquitinated and hyperphosphorylated aggregates, and can also be fragmented in toxic C'-terminal truncations that lose N'-terminal NLS, and further exaggerate TDP-43 mislocalization and aggregation.

1.4.1.1. Dysregulation of TDP-43 proteostasis in ALS

The TDP-43 turnover is regulated by the ubiquitin-proteasomal system (UPS) and/or autophagy. Several types of polyubiquitin-linked chains direct proteolysis by the addition of ubiquitin on one of the seven lysine residues (K6, K11, K27, K29, K33, K48, and K63) or the first methionine (M1) in the ubiquitin bound to a target protein (Kirisako et al., 2006; Komander and Rape, 2012). If the target protein is tagged with the K48 polyubiquitin chain, the protein preferentially undergoes proteasomal degradation, whereas K63- and M1-tagged proteins are degraded through autophagy (Aman et al., 2021; Leidal et al., 2018). Given that there is a growing body of evidence that suggests that autophagic activity and lysosomal proteolytic function decline with ageing, failure in both autophagy and UPS pathways has been investigated as a potential mechanism of TDP-43 mislocalization and aggregation. Moreover, altered TDP-43 protein turnover has been identified in ALS patients (Dantuma and Bott, 2014; Ramesh and Pandey, 2017).

Early studies have suggested that the full-length soluble TDP-43 and insoluble TDP-43 aggregates are cleared by UPS and/or autophagy (Urushitani et al., 2010; Wang et al., 2010). More recent data has suggested that soluble TDP-43 is primarily degraded by UPS, while aggregated TDP-43 is degraded through autophagy (Scotter et al., 2014). ALS-linked mutation in UBQLN2 causes a decrease in autophagy, leading to an increase in TDP-43 levels, and its aggregation in neurons (Osaka et al., 2016). Furthermore, autophagy adaptor and effector proteins, such as optineurin, p62, and LC3 have been identified in protein aggregates found in ALS and FTD patients' spinal cords. They were also found to colocalize with TDP-43 aggregates in cells expressing aggregate-prone TDP-43, suggesting the involvement of autophagy in the disease (Budini et al., 2017; Götzl et al., 2016; King et al., 2011; Wang et al., 2010). TDP-43 has also been reported to regulate several genes associated with autophagy such as the transcription of autophagy-related gene 7 (Atg7) and localization of transcription factor EB (TFEB), which regulates the expression of autophagy genes in neurons (Prasad et al., 2019). However, some of the TDP-43 mutations were associated with diminished binding to Atg7 and decreased autophagy whereas other mutations such as G288S and A382T showed more rapid turnover compared to WT TDP-43 (Araki et al., 2014; Bose et al., 2011). Despite the complex interplay between these two proteolytic processes, aberrant UPS was detected in

neurons of ALS patients, while there are still conflicting data showing that autophagy can either enhance or decrease disease progression (Barmada et al., 2014; Prasad et al., 2019).

1.4.1.2. Neuroinflammation and TDP-43 in ALS

In addition to diminished protein homeostasis, inflammation is another proposed triggering factor for TDP-43 aggregation. There are several lines of evidence supporting this based on ALS-linked mutations in genes implicated in immunity and inflammatory signalling pathways. One of the most researched inflammatory pathways linked to TDP-43 is the NF-κB signalling pathway, which regulates a large number of inflammatory genes in both neurons and microglia and is a key contributor to inflammageing (Salminen et al., 2008; Swarup et al., 2011b; W. Zhao et al., 2015). TDP-43 has been reported to regulate NF-κB signalling, and *vice versa,* NF-κB affects TDP-43. Overexpression of TDP-43 in breast cancer MCF-7 cells inhibits nuclear translocation p65, the most abundant NF-κB subunit, by competing for the same nuclear transportation mechanism (Zhu et al., 2015). In line with this, TDP-43 silencing in the same cells increased p65 and TNF-α production. In contrast to this, overexpression of WT or mutant TDP-43 enhanced NF-κB activation and pro-inflammatory cytokine production in glial cells and increased neuronal vulnerability (Swarup et al., 2011b). Moreover, Swarup *et al*. demonstrated TDP-43 and p65 colocalization in ALS patients' tissues, and that by binding RRM1 on TDP-43, p65 interferes with TDP-43 protein function, resulting in TDP-43 mislocalization and aggregation (Swarup et al., 2011b, 2012). In the follow-up study, it was demonstrated that the addition of lipopolysaccharide (LPS), an endotoxin from the outer membrane of gram-negative bacteria that activates NF-κB, triggers TDP-43 mislocalization and aggregation in both astrocytes and microglia. Moreover, LPS further increased TDP-43 protein aggregates in the glial cells and cytoplasm of the spinal motor neurons of transgenic TDP-43^{A315T} mice (Correia et al., 2015). In addition to enhancing NF-κB activation, transgenic TDP-43, and toxic TDP-43 fragments upregulated pro-inflammatory microglial response, suggesting that TDP-43 neurotoxicity is mediated via microglia (Swarup et al., 2011b; Zhao et al., 2015).

The most common ALS-linked mutation, the hexanucleotide repeat expansion in *C9orf72,* also elicits TDP-43 pathology and increases the expression of IL-6 and

IL-1β pro-inflammatory cytokines in microglia in ALS and FTD mouse models and patients (Cook et al., 2020; Lall and Baloh, 2017). Similarly, loss-of-function, missense, and in-frame deletions in the gene encoding for TBK1 protein, the main regulator of interferon regulatory factor 3 (IRF3) innate immune signalling pathway, were liked to ALS and FTD (Cirulli et al., 2015; Freischmidt et al., 2017). *TBK1* mutations, also lead to the accumulation of TDP-43 in the temporal lobe of diseased patients (van der Zee et al., 2017). Notably, TBK1 could also influence the pathology by regulating autophagy, whereby it acts by phosphorylating p62 and optineurin and enhancing their binding to ubiquitinated proteins. In line with this, mutations in the genes encoding for autophagy adaptor proteins optineurin and p62 were also linked to ALS and FTD. Therefore, inflammation may be a mediator of TDP-43 proteinopathy, a pathological hallmark of ALS and FTD.

1.5. Optineurin

Optineurin is a 577 aa long multifunctional polyubiquitin-binding protein, encoded by the *OPTN* gene located on the human chromosome 10. It is ubiquitously expressed in the cytoplasm of various cells, with higher levels observed in several tissues including the brain, spinal cord, skeletal muscles, spleen, and heart (Ito et al., 2011). Moreover, it is well conserved between species: human *OPTN* has 80% homology with the murine *Optn* gene (Rezaie et al., 2005). It was initially characterized in 1998 in a two-yeast-hybrid screen, as an adenoviral E3-14.7K interacting protein 2, hence termed FIP-2 (Li et al., 1998). Since then, it has been renamed several times, linked to discoveries of its involvement in multiple cellular processes. Because of its high homology with NF-κB essential modulator (NEMO), it was termed NEMO-related protein (NPR), and TFIIIA-intP because of its function as transcription factor IIIA interacting protein (Moreland et al., 2000; Schwamborn et al., 2000). Finally, when optineurin mutations were linked to primary open-angle glaucoma (POAG), the name optineurin was adopted and standing for optic neuropathy-inducing protein (Rezaie, et al., 2002). Since then optineurin has been described in an unusually wide number of cellular functions including inflammatory signalling, autophagy, vesicle trafficking, maintenance of the Golgi apparatus, and cell death (Markovinovic et al., 2017a; Prtenjaca, 2020). This is due to a wide range of protein-protein interactions that occur via its ubiquitin-binding domain, microtubule-associate protein 1A/1B-light chain 3 (LC3)-interacting region (LIR), TBK1-interacting domains, and others. In 2010 three pathogenic optineurin mutations were found in ALS patients, and since then more than 40 different ALS-linked mutations have been identified (Maruyama et al., 2010; reviewed in Markovinovic et al., 2017a). The pathogenicity of many of them is still unclear. Moreover, optineurin mutations were found in the ALS/FTD spectrum but were also identified in FTD patients only (Ito et al., 2011; Kamada et al., 2014; Pottier et al., 2018). In addition, optineurin polymorphisms were also identified in Crohn's disease and Paget's disease of the bone (Albagha et al., 2010; Smith et al., 2015). Interestingly, optineurin mutations and polymorphisms linked to these diseases were proposed to have different functional outcomes. Specifically, optineurin mutations linked to ALS and FTD act by loss-of-function and haploinsufficiency. On the other hand, dominant-negative effect or gain-of-function mutations were linked to POAG suggesting that regulation of

cellular processes by optineurin is complex, and most likely differs in various cell types, and during the pathogenesis of different diseases. The precise role of optineurin in human disease pathology is thus still largely elusive and differs in distinct experimental settings (Prtenjaca, 2020).

1.5.1. Optineurin domains and protein interactions

Optineurin is a non-enzymatic protein with several structurally different functional domains and it is considered to be an adaptor protein (Fig. 6.). Optineurin has two coiled-coil (CC) domains, N'-terminal CC1 (38-170 aa) and C'-terminal CC2 (239-508 aa), which cover around 70% of protein and mediate its self-oligomerization and oligomerization with other proteins with CC domains (Li et al., 2016, 2016) (Fig. 6.). In the N'-terminus optineurin harbours the LIR domain (176-181 aa), which is important for binding to LC3 on the autophagosomal membranes (P. Wild et al., 2011). On the C'-terminus optineurin has two distinct ubiquitin-binding domains: ubiquitin-binding region of A20 binding inhibitor of NF-κB (ABIN) proteins and NF-kB essential modulator (NEMO) termed UBAN (445-502 aa) and zinc finger (ZF; 547-577 aa), further referred jointly as ubiquitin-binding region (Li et al., 2016; Markovinovic et al., 2017a) (Fig. 6.). The main proposed optineurin-binding partners and their functions are listed in Table 1., and further explained in the subsequent sections.

Table 1. Optineurin binding partners and their functions

Binding partner	Binding site (aa)	Function	References
TBK1	1-127 aa, CC1	autophagy and inflammation	Meena et al., 2016; Morton et al., 2008; Munitic et al., 2013; Pourcelot et al., 2016; Richter et al., 2016; Wild et al., 2011
caspase 8	121-230 aa, CC1	apoptosis	Nakazawa et al., 2016
Rab8	141-209 aa, CC1, LIR	vesicular trafficking	Hattula and Peränen, 2000
p62	193 aa*	autophagy	Liu et al., 2014
TFIIIA	160-469 aa CC2	transcription	Moreland et al., 2000

LC3	178-181 aa, LIR	autophagy	Wild et al., 2011
HACE1	411-456 aa, CC2, UBAN	autophagy	Liu et al., 2014
htt	411-461 aa, CC2	vesicular trafficking	Hattula and Peränen, 2000
CYLD	424-509 aa, CC2, UBAN	inflammation	Nagabhushana et al., 2011
myosin VI	412-520 aa, UBAN	exocytosis	Sahlender et al., 2005; Tumbarello et al., 2012
RIPK1	461-493 aa, UBAN	inflammation/ necroptosis	Ito et al., 2016; Zhu et al., 2007

*Needs to be ubiquitinated; modified from: (Toth and Atkin, 2018).

1.5.1.1. Ubiquitin-binding region

It has been proposed that optineurin arose by gene duplication from NEMO, as they share high homology within their ubiquitin-binding regions (Laplantine et al., 2009; Tumbarello et al., 2015). Through this region optineurin binds with high affinity to K63- and M1-linked linear poly-ubiquitin chains, facilitating:

(1) inflammatory signalling by recruitment of regulatory proteins for signal transduction. It has been proposed that optineurin negatively regulates NF-κB activation by binding to polyubiquitinated receptor-interacting protein 1 (RIPK1), thus outcompeting positive NF-κB regulator NEMO, and by direct binding to deubiquitinase cylindromatosis (CYLD), which deubiquitinates RIPK1 (Ito et al., 2016a; Nagabhushana et al., 2011a). In addition to activation of the IRF3 signalling pathway, optineurin binds to ubiquitinated TBK1 and facilitates its proper activation (Meena et al., 2016b; Pourcelot et al., 2016b).

(2) autophagy and protein degradation, acting on several autophagy steps, as further detailed below; in brief, optineurin controls autophagy by binding to ubiquitinated protein aggregates, intracellular bacteria, damaged mitochondria, and motor protein myosin VI (Korac et al., 2012; Lazarou et al., 2015; Tumbarello et al., 2012; P. Wild et al., 2011).

(3) vesicle trafficking, by linking myosin VI to the Golgi complex and facilitating Golgi formation and exocytosis (Sahlender et al., 2005b).

1.5.1.2. LC3-interacting region

Upon binding the ubiquitinated damaged mitochondria, intracellular bacteria, and protein aggregates (henceforth referred to as cargo) with its ubiquitin-binding region, optineurin bridges it to LC3 on autophagosomal membranes through its LIR domain (Wild et al., 2011). This is a key event in the autophagy elongation step and results in the formation of autophagosomes. Notably, posttranslational modifications are necessary to enhance optineurin binding to both LC3 and the ubiquitinated cargo. To this end, optineurin is phosphorylated in its LIR domain on serine 177 (Ser177) and ubiquitin-binding region on serine 473 (Ser473) by TBK1 (Cirulli et al., 2015; Richter et al., 2016b), that will be further discussed below. Furthermore, by interacting with HECT Domain and Ankyrin Repeat Containing E3 Ubiquitin Protein Ligase 1 (HACE1), optineurin promotes its ubiquitination on Lys193, thus facilitating interaction with p62 and autophagic flux (Liu et al., 2014a).

1.5.1.3. TBK1 interaction

The interaction between optineurin and TBK1, a serine-threonine kinase is induced upon cell activation by PAMPs and DAMPs. It is important in autophagy and the IRF3 signalling pathway. Two proteins initially bind via the CC1 region on optineurin and C'-terminal CC2 on TBK1 (Li et al., 2016; Morton et al., 2008b). This interaction stabilizes TBK1, and allows its K63-linked polyubiquitination and subsequent binding by the ubiquitin-binding region of optineurin (Pourcelot et al., 2016b). Upon binding, TBK1 gets activated by autophosphorylation and phosphorylates IRF3, which enables its nuclear translocation and stimulates interferon-β (IFN-β) production (Meena et al., 2016b; Morton et al., 2008b; Munitic et al., 2013; Pourcelot et al., 2016b). Furthermore, upon stabilization, TBK1 phosphorylates optineurin on Ser177, and Ser473, enhancing optineurin binding to ubiquitinated cargo and LC3 and promoting autophagy-mediated degradation of protein aggregates, damaged mitochondria and cytosolic bacteria *Salmonella enterica* (Korac et al., 2012; Lazarou et al., 2015; Richter et al., 2016b; P. Wild et al., 2011).

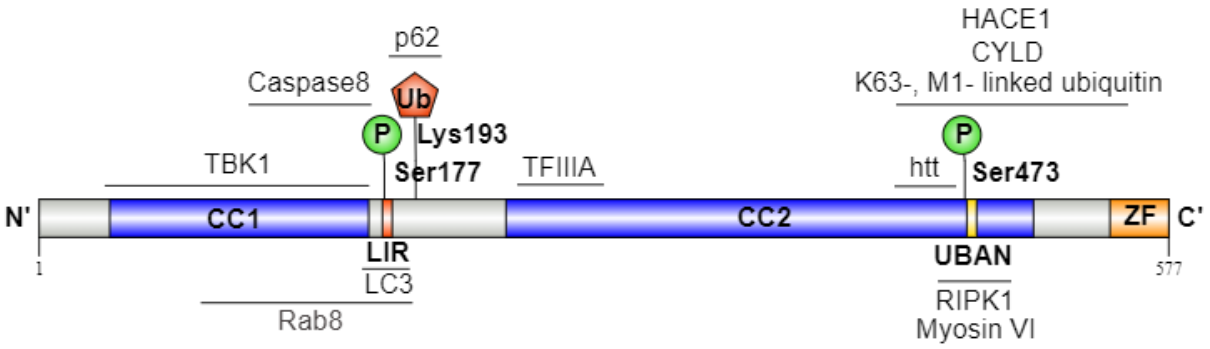

Figure 6. Schematic representation of optineurin domains, posttranslational modifications, and interacting partners. The N'-terminus of optineurin contains the CC1 domain that interacts with TBK1 and LIR that contains Ser177, which is phosphorylated by TBK1 to enhance binding between optineurin and LC3. Optineurin ubiquitination on position Lys193 is mediated by a ubiquitin ligase HACE1 and is required for p62 binding to optineurin. The CC2 domain is crucial for the self-oligomerization of optineurin and for binding to linear ubiquitin. The C'-terminus of optineurin has a ubiquitin-binding domain (UBAN) and a ZF domain (referred to as ubiquitin-binding region) for binding polyubiquitinated signalling proteins and cargo destined for autophagosomal degradation. The ubiquitin-binding region is also important for binding RIPK1, a regulator of the NF-κB pathway, and myosin VI, a motor protein important in vesicle trafficking and autophagy. Phosphorylation on Ser473 enhances optineurin binding to the ubiquitinated cargo. Rab8 and caspase 8 bind to the N'-terminus, TFIIIA to the intermediate region, and deubiquitinase CYLD and htt to the C'-terminus of optineurin.

1.5.2. Optineurin in ALS

Around 40 different optineurin mutations were found in sALS and fALS patients, although it is still unclear which ones are pathogenic. Most mutations with confirmed pathogenicity are situated in the ubiquitin-binding region and CC domains, suggesting that oligomerization and ubiquitin-binding are crucial for disease pathogenesis. Due to its oligomerization capacity, optineurin has the predisposition to aggregate, but mutated forms of optineurin were not found in protein aggregates in autopsy materials of ALS patients (Ito et al., 2011; Maruyama et al., 2010). This suggests that optineurin ALS- and FTD-linked mutations are most likely loss-of-function mutations (Markovinovic et al., 2017b; Prtenjaca, 2020). One of the first optineurin mutations found in fALS was homozygous frameshift deletion of exon 5 (Δex5), supporting the idea that null mutation in both alleles and complete loss of protein is necessary for disease manifestation (Maruyama et al., 2010; Ying et al., 2010). However, the majority of ALS-linked mutations are point mutations, including both missense and nonsense mutations. Homozygous nonsense mutations Q398X and S174X cause a premature stop codon and also suggest that loss of ubiquitin-binding and mutations in both alleles are required for the occurrence of the disease (Gotkine et al., 2021; Kamada et al., 2014; Maruyama et al., 2010). However, several heterozygous mutations like most studied missense mutations E478G and A481V which directly affect the ubiquitin-binding region, and nonsense Q165X mutations suggest that haploinsufficiency is sufficient to cause ALS (Belzil et al., 2011; Maruyama et al., 2010; Tümer et al., 2012). These heterozygous mutations could also exert a dominant-negative effect, where truncated optineurin could interfere with full-length protein and disrupt its normal function, suggesting a potential distinct mechanism of individual mutations. Further studies for a complete understanding of the pathogenicity of optineurin mutations are required.

The autopsies of patients carrying homozygous Q398X and heterozygous E478G optineurin mutations have shown TDP-43 mislocalization and aggregation in the spinal cord and brainstem motor neurons (Ito et al., 2011; Kamada et al., 2014). In addition, optineurin deficient ($Optn^{-/-}$) mice showed TDP-43 cytoplasmic protein aggregates and multivesicular body protein 2B (CHMP2B) positive vacuoles in the motor neurons in the spinal cord (Kurashige et al., 2021). There are only a few studies that have investigated the interaction of TDP-43 and/or SOD1 and optineurin

in ALS, and the majority of results were done on immortalized cell lines rather than in the relevant CNS cells. Upon overexpression of aggregate-prone hSOD1^{G93C} in HeLa cells, phosphorylated optineurin was found in the SOD1 aggregates (Korac et al., 2012). Moreover, in microglia optineurin was reported as an autophagy receptor for protein aggregates of amyloid beta, typical for Alzheimer's disease, and was found enriched in the brain regions affected by Parkinson's disease (Cho et al., 2014; Korac et al., 2012; Wise et al., 2018). Similarly, optineurin was found recruited to TDP-43 in TDP-43 overexpressing cells, but the mechanistic link between these proteins is still largely elusive (Shen et al., 2015; Wang, 2016.). When mutated, optineurin is not found in protein aggregates and since it is directly involved in inflammatory signalling and autophagy (further explained in detail in sections 1.5.3. and 1.5.4.), it is an interesting molecule in the field of neurodegeneration and ALS pathogenesis. It still has to be clarified by which precise mechanism its mutations lead to ALS, or if the breakdown in multiple mechanisms that optineurin regulates is necessary for the appearance of the disease.

1.5.3. Optineurin mouse models

Several optineurin mouse models were designed to study the role of optineurin in neurodegeneration. Unlike the most studied transgenic aggregate-prone hSOD1^{G93A} mouse model in which hSOD1 mutation is expressed at the artificially high level, these models were designed to more closely mimic the conditions found in patients (Table 2.) (Gurney et al., 1994; Markovinovic et al., 2017a). The first reported mouse model was a knock-in D477N point mutation (Optn^{D477N}), similar to the human E478G mutation that is not able to bind ubiquitin (Gleason et al., 2011). Optn^{470T} mouse lacks the distal part of CC2 and the whole ubiquitin-binding region and thus mimics the C'-terminal human Q398X mutation (Munitic et al., 2013) (Table 2.). Both Optn^{D477N} and Optn^{470T} models disrupt ubiquitin-binding and show altered inflammatory signalling in primary cells (further discussed in 1.5.4.4.) but demonstrated no neurodegeneration and/or ALS pathology (tested up to one year of age) (Gleason et al., 2011; Markovinovic et al., 2018; Munitic et al., 2013). Furthermore, to study the relevance of the TBK1-optineurin axis, a mouse model that harbours deletion in the N'-terminal TBK1 binding region (Optn$^{\Delta 157}$) was generated (Meena et al., 2016b). Optn$^{\Delta 157}$ mouse is not related to human mutations but

research on this model established optineurin as a positive regulator of TBK1. Several groups also designed optineurin deficiency mouse models ($Optn^{-/-}$) which mimic homozygous null mutations in patients (Chew et al., 2015; Dermentzaki et al., 2019; Ito et al., 2016a; Kurashige et al., 2021; Moharir and Swarup, 2021; Slowicka et al., 2016). Similar to ubiquitin-binding deficient mouse models, $Optn^{-/-}$ did not exhibit overt ALS pathology. One group reported a slight motor deficit in vertical rearing activity and axonal dysmyelination in the spinal cord in three-month-old $Optn^{-/-}$ mice, with no progression of the dysmyelination for up to two years (Ito et al., 2016b). Furthermore, Ito et al. reported a mild increase in pro-inflammatory cytokines in the spinal cords of unmanipulated mice. In the follow-up study, the dysmyelination phenotype was not confirmed (Dermentzaki et al., 2019). In two other $Optn^{-/-}$ models alterations in motor deficits were not detected (Kurashige et al., 2021; Moharir and Swarup, 2021), although one of them found TDP-43 cytoplasmic aggregates and a diminished number of spinal cord motor neurons. Notably, no ALS pathology was observed up until one year in neuron-specific $Optn^{-/-}$ mice, suggesting that optineurin deficiency is not enough to cause ALS-like phenotype in young and middle-aged mice. Several immune phenotypes were reported unrelated to the CNS: Moharir and Swarup *et al.* demonstrated that the $Optn^{-/-}$ mice exhibit patchy hair loss possibly by T cell-mediated damage of hair follicles, whereas Slowicka *et al.* showed that optineurin deficiency makes mice more susceptible to infection with *Salmonella enterica* (Moharir and Swarup, 2021; Slowicka et al., 2016). A summary of optineurin mouse models and their functional readouts in primary cells and *in vivo* are shown in Table 2.

Table 2. Optineurin mouse models and functional readouts

Mouse model	Domain/mutation	Related human mutation	Functional readouts in primary cells or *in vivo*
Optn^{D477N}	A point mutation in ubiquitin-binding region ➔ lacks the ubiquitin-binding activity	**E478G**	- impaired TBK1 activation, IRF3 phosphorylation and IFN-β production - reduced phosphorylation of mutated optineurin by TBK1 - no differences in NF-κB activation (Gleason et al., 2011)
Optn^{470T}	Truncation of the ubiquitin-binding region and the distal part of CC2 ➔ lacks the ubiquitin-binding activity; lower expression level	**Q398X**	- impaired TBK1 activation, IRF3 phosphorylation and IFN-β production - disbalance in gene expression of pro- and anti-inflammatory factors - no differences in NF-κB activation (Markovinovic et al., 2018; Munitic et al., 2013; Pourcelot et al., 2016b)
OptnΔ^{157}	N-terminal deletion ➔ lacks TBK1-binding activity	***/***	- impaired TBK1 activation, IRF3 phosphorylation and IFN-β production - reduced phosphorylation of OptnΔ^{157} by TBK1 (Meena et al., 2016b)
Optn$^{-/-}$	Total protein deletion ➔ complete loss-of-function	**Null mutations**	- impaired TBK1 activation, IRF3 phosphorylation and IFN-β production - no differences in NF-κB activation (Slowicka et al., 2016) - mildly increased pro-inflammatory cytokines *in vivo* (in unmanipulated mice) (Ito et al., 2016a) - mice more susceptible to *Salmonella* infection (Slowicka et al., 2016) - motor deficit in vertical rearing activity and axonal dysmyelination (Ito et al., 2016b) - patchy hair loss (Moharir and Swarup, 2021)
			- TDP-43 cytoplasmic inclusions and CHMP2B vacuoles in spinal cord motor neurons (Kurashige et al., 2021)

* This table was modified from our review paper (Prtenjaca, 2020). *In vivo* functional redouts are marked in orange.

1.5.4. Optineurin: proposed cellular functions

1.5.4.1. Autophagy mechanism

Autophagy (from the Greek words auto, meaning ‘self’, and phagein ‘to eat’) is a highly conserved cellular process by which ubiquitinated molecules and subcellular elements are getting degraded via lysosome-mediated removal (Aman et al., 2021). In times of starvation, decreased levels of glucose, amino acids, or adenosine triphosphate (ATP) initiate non-selective autophagy via 5' adenosine monophosphate-activated protein kinase (AMPK) and mTOR, allowing the cells to survive. The autophagy process can also be selective, and this represents a mechanism for disposing of ubiquitinated cargo such as aggregated proteins, damaged organelles, and intracellular pathogens (Stolz et al., 2014). Both non-selective and selective autophagy pathways depend on a set of autophagy-related genes (Atg) and can be divided into four major phases: nucleation, elongation, maturation, and degradation (Fig. 7). Moreover, both pathways lead to the activation of unc-51 like autophagy activating kinase 1 (ULK1) by phosphorylation, which subsequently forms a complex with focal adhesion kinase family interacting protein of 200 kD (FIP200), Atg13, and Atg101. This complex activates the phosphatidylinositol 3-kinase (VPS34) complex that generates phosphatidylinositol 3-phosphate (PI3P) required for the nucleation by forming a double membrane for cargo enclosure called phagophore (Aman et al., 2021; Kirkin, 2020; Stolz et al., 2014). After nucleation, the phagophore elongation process requires the recruitment of the Atg12-Atg5-Atg16L1 complex via WD repeat domain phosphoinositide-interacting protein 2 (Wipi2). The Atg12-Atg5-Atg16L1 complex facilitates the conjugation of phosphatidyl ethanolamine (PE) to LC3 (LC3-I shifts to LC3-II), allowing its incorporation into autophagosomal membranes. Simultaneously, autophagic adaptor proteins trap ubiquitinated cargo via their ubiquitin-binding domains and deliver them to the LC3-II on autophagosome by their LIR domains (Aman et al., 2021; Stolz et al., 2014). Autophagosome maturation requires the incorporation of additional endosomal membranes, which allows their fusion with lysosomes and the degradation of cargo by lysosomal hydrolases (Fig. 7).

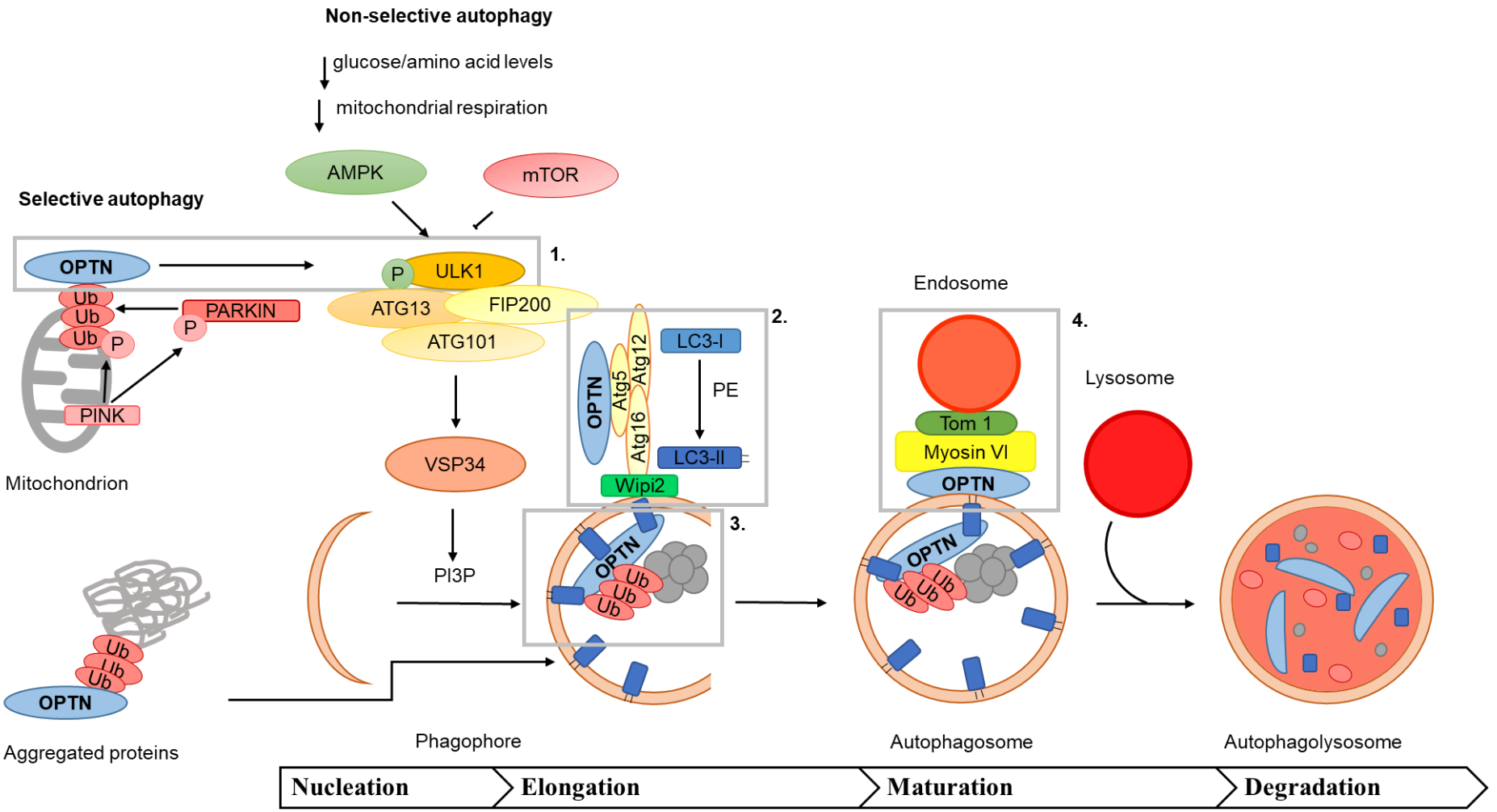
Non-selective autophagy
glucose/amino acid levels
mitochondrial respiration
AMPK
mTOR
Selective autophagy
OPTN
Ub
Ub
Ub
P
PARKIN
P
PINK
Mitochondrion
1.
P
ULK1
ATG13
FIP200
ATG101
VSP34
PI3P
2.
OPTN
Atg5
Atg12
Atg16
LC3-I
PE
LC3-II
Wipi2
3.
OPTN
Ub
Ub
Ub
Endosome
4.
Tom 1
Myosin VI
OPTN
Lysosome
Ub
Ub
Ub
OPTN
Aggregated proteins
Phagophore
Autophagosome
Autophagolysosome
Nucleation
Elongation
Maturation
Degradation

Figure 7. Key steps of autophagy mechanism and proposed roles of optineurin during autophagy. The four major phases of autophagy are nucleation, elongation, maturation, and degradation. In times of starvation, cells undergo non-selective autophagy via AMPK and mTOR. The process of autophagy can also be selective for disposing of damaged organelles (such as mitochondria), aggregated proteins, and intracellular pathogens. Both these autophagy pathways lead to the activation of ULK1 by phosphorylation, forming several complexes and a double membrane called a phagophore. After nucleation, the phagophore elongation requires LC3-II incorporation into autophagosomal membranes, and bridging ubiquitinated cargo by autophagic adaptor proteins. Autophagosome maturation requires binding to endosomes and fusion with lysosomes where degradation of cargo occurs. Optineurin has been proposed to act in four distinct steps of autophagy: (1 and 3) in the selective binding of damaged mitochondria, protein aggregates, and cytosolic bacteria and delivery of cargo to autophagosomes by bridging polyubiquitinated cargo to LC3-II, (2) in the recruitment of the Atg12-Atg5-Atg16L1 complex to the autophagosomal membrane which allows the formation of LC3-II and (4) in bridging Tom1 on endosome with protein myosin VI allowing proper lysosome and autophagosome fusion.

1.5.4.2. Optineurin in autophagy

Optineurin has been proposed to act in four distinct autophagy steps: as a receptor protein in selective autophagy, the protein that recruits ULK1 and Atg12-Atg5-Atg16L1, and for the fusion of lysosome and autophagosome (Fig. 7). Firstly, optineurin was initially described as an autophagy receptor in the nucleation step for selective clearance of cytosolic bacteria *S. Typhimurium* in HeLa cells (Wild et al., 2011). This has been corroborated in multiple studies for different types of cargo. It was also proposed as a receptor for aggregated proteins and damaged mitochondria. In the latter upon PTEN-induced kinase 1 (PINK1)-mediated phosphorylation and activation of ubiquitin ligase Parkin, optineurin binds to ubiquitinated mitochondria (Heo et al., 2015; Korac et al., 2012; Lazarou et al., 2015; Moore and Holzbaur, 2016; Shen et al., 2015; Wong and Holzbaur, 2014.). Notably, ALS-linked optineurin mutations Q398X and E478G or complete depletion of optineurin are unable to recruit damaged mitochondria to phagophore membrane (Lazarou et al., 2015; Moore and Holzbaur, 2016; Wong and Holzbaur, 2014.). Interestingly, pharmacological blockade, silencing, or ALS-linked E696K TBK1 mutation resulted in an inability of optineurin to bind to autophagosomal membranes, suggesting that coordinated crosstalk of TBK1 and optineurin is crucial in optineurin-mediated autophagy (Moore and Holzbaur, 2016; Richter et al., 2016b). Secondly, in addition to its role as an autophagy receptor in the nucleation step, optineurin also recruits ULK1 and initiates phagophore formation in HeLa cells (Lazarou et al., 2015; Moore

and Holzbaur, 2016). Thirdly, optineurin was proposed to interact with Atg5 and recruits it to Atg12-Atg5-Atg16L1 and potentiate LC3-II production in the elongation autophagy step. In optineurin deficient and cells harbouring E478G mutation, the number of Atg12-Atg5-Atg16L1-positive puncta and recruitment of the Atg12-Atg5-Atg16L1 complex to Wipi2 is reduced. In addition, fibroblasts from $Optn^{-/-}$ mice showed diminished LC3-II formation and a lower number of autophagosomes during both basal and starvation-induced autophagy (Bansal et al., 2018). Finally, optineurin is also implicated in autophagosome maturation by binding actin-based motor protein myosin VI in complex with Tom1 on endosomes and allows the fusion of the vesicles (Tumbarello et al., 2015). Overexpressed optineurin E478G mutant was unable to bind to myosin VI, consequently inhibiting protein trafficking and inducing ER stress and Golgi fragmentation in the NSC-34 motor neuron-like cell line (Sundaramoorthy et al., 2015).

Of note, the vast majority of autophagy results were obtained from *in vitro* overexpression models, which can lead to experimental artifacts and could be of limited relevance (Prtenjaca, 2020). Unfortunately, there are only a few reports analysing optineurin in autophagy in primary cells. A recent investigation in primary neurons showed that optineurin colocalises with damaged mitochondria and α-synuclein aggregates in dopaminergic neurons but it is still not clear how optineurin mutations affect autophagy and if this is relevant to disease pathogenesis (Evans and Holzbaur, 2020; Wise et al., 2018)

1.5.4.3. The overview of inflammatory signalling

Innate immunity receptors such as cytoplasmic DNA/RNA sensors and TLRs detect various PAMPs and DAMPs and simultaneously activate NF-κB and TBK1 signalling pathways, which lead to the secretion of pro-inflammatory cytokines and type I IFN, respectively (Akira et al., 2006). Both pathways are highly regulated by a series of ubiquitination and phosphorylation events that create feedback loops to either amplify or block signalling, thus orchestrating appropriate immune responses for diverse stressors (Chen, 2012; Tu et al., 2013). Upon ligand binding, TLRs undergo conformational changes, which results in the recruitment of several adaptor proteins and ubiquitin ligases like tumor necrosis factor receptor-associated factors (TRAFs) and cellular inhibitors of apoptosis proteins (cIAPs), which generate K63-

linked polyubiquitin chains. Moreover, the recruited linear ubiquitin chain assembly complex (LUBAC) generates M1 linear polyubiquitin chains (Markovinovic et al., 2017b; Tokunaga, 2013). Upon polyubiquitination of receptor-interacting serine/threonine-protein kinase 1 (RIPK1) and activation of transforming growth factor-β-activated kinase 1 (TAK1), IKK complex, comprised of ubiquitin-binding adaptor protein NEMO and two kinases - inhibitor of kappa B kinase (IKK)α and IKKβ, is docked to ubiquitinated RIPK1, and phosphorylated and activated by TAK1 (Chen, 2012). IKKα and IKKβ phosphorylate inhibitor of κB (IκB), which keeps the transcription factor NF-κB from entering the nucleus. Phosphorylated IκB then gets K48-polyubiquitinated, which directs it to degradation. NF-κB gets translocated to the nucleus, where it binds to promotors for various proinflammatory factors, including cytokines TNF-α, IL-1β, and IL-6, and prosurvival genes. To prevent hyperactivation, NF-κB signalling acts in the autoregulatory feedback loop, where NF-κB also binds to the promotor for IκB, promotes its expression, and NF-κB inhibition. NF-κB can also be neutralized by deubiquitinase CYLD, which degrades polyubiquitin chains and stops the downstream signalling cascade (Wertz et al., 2004). Polyubiquitination of TBK1 kinase, homologous to IKKα and IKKβ, is also mediated by TRAFs and cIAPs, upon which TBK1 recruits optineurin, providing its own proper activation and phosphorylation of IRF3. Upon phosphorylation, IRF3 dimerizes and translocates to the nucleus where it triggers type I IFN production (Akira et al., 2006; Fitzgerald et al., 2003).

1.5.4.4. Optineurin in inflammatory signalling

Optineurin has been proposed to act as an adaptor in both NF-κB and TBK1 inflammatory signalling pathways (Markovinovic et al., 2017b). Due to its high homology with NEMO and its ability to inhibit the NF-kB pathway by binding to K63-polyubiquitinated RIPK1, optineurin was proposed to be a competitive inhibitor of NEMO (Schwamborn et al., 2000). In line with this, *in vitro* studies in HEK293 cells showed that overexpression of WT optineurin inhibits, while optineurin silencing led to an enhanced TNF-mediated NF-κB activation (Nakazawa, 2016.; Zhu et al., 2007). Conversely, overexpression of WT but not ubiquitin-deficient E478G and Q398X optineurin inhibited NF-κB upon TNF-α stimulation in neuronal cell line NSC-34, opening a possibility that NF-κB hyperactivation caused by optineurin mutations

could trigger neurodegeneration (Akizuki et al., 2013; Maruyama et al., 2010). Notably, optineurin was also proposed to recruit the deubiquitinase CYLD to polyubiquitinated RIPK1 thus facilitating deubiquitination and inhibition of the NF-κB signalling pathway (Nagabhushana et al., 2011b). However, in contrast to results from different cell lines, research in various primary cells from several models of optineurin deficiency and insufficiency ($Optn^{-/-}$, $Optn^{D477N}$, $Optn^{470T,}$ and $Optn^{\Delta 157}$) demonstrated that optineurin is dispensable for NF-κB activation and TNF-α secretion (Gleason et al., 2011; Markovinovic et al., 2018; Meena et al., 2016b; Munitic et al., 2013; Pourcelot et al., 2016b; Slowicka et al., 2016). Since optineurin expression is under the NF-κB promotor, it was also tested if optineurin regulates late phases of inflammation but the results were negative as well (Markovinovic et al., 2018; Munitic et al., 2013). Therefore, because of the discrepancies in cell lines and primary cells, most likely due to overexpression or silencing artefacts, which are common for ubiquitin-binding proteins, the role of optineurin in the NF-κB signalling pathway is still debatable.

As a protein that binds poly-ubiquitinated TBK1, optineurin was proposed to impact IRF3 signalling and type I IFN production and elimination of viruses and bacteria (Fitzgerald et al., 2003; Pourcelot et al., 2016b). It was first reported that optineurin acts as a negative regulator of the IRF3 pathway induced by the Sendai virus and RNA in HEK293 cells (Mankouri et al., 2010). Again, in contrast to the data from the cell lines, various studies in primary cells from optineurin deficiency and insufficiency models have shown that optineurin and/or its ubiquitin-binding region are necessary for adequate TBK1 activation and IFN-β production, suggesting that it is a positive regulator for TBK1 (Gleason et al., 2011; Markovinovic et al., 2018; Meena et al., 2016b; Munitic et al., 2013; Pourcelot et al., 2016b; Slowicka et al., 2016). In line with this, truncated optineurin in primary microglia led to a diminished expression of several pro- and anti-inflammatory factors downstream of IFN-β including IL-10, IRF7, CXCL1, and CXCL10 (Markovinovic et al., 2018). Overall, the results in primary cells reveal the relevance of optineurin in the activation of the TBK1–type I IFN axis. This is particularly important since mutations in TBK1 have also been reported in ALS patients, and opens a possibility that insufficient immune responses could participate in ALS and FTD onset and pathogenesis (Cirulli et al., 2015; Freischmidt et al., 2017; Pottier et al., 2015).

2. Thesis Aims and Hypothesis

Since optineurin was proposed to be an adaptor protein in autophagy and inflammatory signalling, and both of these mechanisms are thought to contribute to neurodegeneration, here we aimed to test if optineurin insufficiency and deficiency would impair proteostasis, trigger inflammation, and/or lead to inefficient immune responses. Several groups established optineurin mouse models carrying different optineurin mutations that mimic those found in ALS patients, but they did not replicate the patients' disease phenotype(s). As ageing is one of the major risk factors for ALS, here we also tested whether alterations during ageing could contribute to the neuro- or immunopathology in the mice carrying the ALS-mimicking mutation Optn^{470T}.

To pinpoint the molecular mechanism(s) by which optineurin mutations could stimulate TDP-43 accumulation, and test if ageing provides a sufficient second hit that triggers an ALS- or FTD-like phenotype, we used Optn^{470T} mice, primary cells from Optn^{470T} mice and BV2 Optn KO microglial cell lines as research models. The goals and hypotheses were the following:

(1) Testing if optineurin deficiency and insufficiency cause TDP-43 protein accumulation, which is present in the CNS of patients carrying the ALS-linked *OPTN* mutations. For this purpose, we established BV2 Optn KO microglial cell lines, and isolated primary myeloid cells (microglia and macrophages) and cortical neurons from the Optn^{470T} mouse model in which we tested *TARDBP* transcription and TDP-43 protein levels. We hypothesised that loss of functional optineurin would cause an accumulation of TDP-43.

(2) Since optineurin is a ubiquitin-binding adaptor protein with proposed roles in autophagy and inflammatory signalling, we tested if Optn^{470T} mutation could cause TDP-43 accumulation by affecting protein homeostasis and/or inflammation. We tested TDP-43 levels and cellular localization upon different stimuli that block protein degradation and/or cause inflammation in the *in vitro* experiments on primary myeloid cells and cortical neurons from the Optn^{470T} mouse model and BV2 Optn KO microglia. We hypothesised that optineurin insufficiency would cause a block in autophagy and increased inflammatory responses that trigger TDP-43 accumulation.

(3) As most of the research was thus far done on young Optn^{470T} mice, and ALS is an adult-onset disease, here we analysed if a combination of two hits, optineurin mutation, and ageing, would accelerate immunosenescence and/or inflammageing to uncover ALS and/or FTD-like neuropathology. We hypothesised that ageing will precipitate ALS/FTD pathology in Optn^{470T} mice. Therefore, we analysed motor and cognitive neurological symptoms, TDP-43 aggregation, and innate and adaptive immune systems in WT and Optn^{470T} mice up to two years of age.

(4) Since we anticipated the possibility that Optn^{470T} mice will not by itself exhibit an ALS-like phenotype, as was the case for many loss-of-function ALS-like mouse models, including the recently reported TBK1 models (Brenner et al., 2019), we established a new two-hit ALS mouse model. To this end, we crossed optineurin-insufficient Optn^{470T} mice with mice that carry a human mutation in TDP-43 (TDP-43^{G348C}), the ALS/FTD model that develops cytoplasmic inclusions of TDP-43 protein and neuroinflammation around ten months of age (Swarup et al., 2011a). We hypothesised that optineurin insufficiency will aggravate ALS/FTD pathology and lead to faster disease onset.

3. Materials and Methods

3.1. Materials

3.1.1. Chemicals, reagents, buffers, and experimental kits

Table 3. List of chemicals and reagents

Chemical	Catalog number	Manufacturer
Acrylamide (Rotiphorese gel 40)	3030.1	Carl Roth
Agarose Universal peqGOLD	35-1020	Peqlab a VMR company
Ammonium peroxodisulfat (APS)	9592.2	Carl Roth
Aqua-Poly/Mount	18606-20	Polyscience, Inc.
β-mercaptoethanol	M3148	Sigma Aldrich
Bovine serum albumin (BSA)	3854.3	Carl Roth
Bromophenol blue	T116.1	Carl Roth
CH_3COOH (Acetic acid)	64-19-7	Alkaloid
Dithiothreitol (DTT)	R0862	Thermo Scientific
DNAse I	10104159001	Roche
Ethylenediamine tetraacetic acid (EDTA)	205-358-3	AppliChem
EDTA-free Protease Inhibit	11873580001	Roche
Ethanol 96%	133124	Kefo
Ethylene glycol	107-21-1	T.T.T. doo
Glycerol	P121003	Gram Mol
Glycine	3908.3	Carl Roth
HCl	30721	Sigma Aldrich
Horse serum	P30-0702	Pan Biotech
Isopropanol	20842.323	VMR
KCl	7447-40-7	T.T.T. doo
Ketamidor	QN01AX03	Richter pharma
KH_2PO_4	3904.2	Carl Roth
Liberase TM	5401020001	Roche
Methanol	20897.295	VMR
NaCl	31434	Honeywell Fluka
Na_2HPO_4	P143790	Gram Mol
Nuclease-free H_2O	AM9937	Ambion
Paraformaldehyde (PFA)	0335.3	Carl Roth

Phosphatase inhibitor (PhosSTOP EASYpack)	04906837001	Roche
Proteinase K	70663-4	Sigma Aldrich
Rompun (Xylazine)	KP09X0N	Bayer
Sarkosyl (N-Lauroylsarcosine Sodium Salt)	L5125-50G	Sigma Aldrich
Sodium azide	K305.1	Carl Roth
Sodium deoxycholate	D6750	Sigma Aldrich
Sodium dodecyl sulfate (SDS)	0183.2	Carl Roth
Saccharose D(+)	4621.1	Carl Roth
N, N, N', N'-Tetramethylenthylenediamine (TEMED)	2367.3	Carl Roth
Thiourea	T8656	Sigma Aldrich
Tris	4855.3	Carl Roth
Triton X-100	9002-93-1	Fisher Scientific
TrueBlack	23007	Biotium
Tween-20	9055-64-5	J.T. Baker
Urea	U5128	Sigma Aldrich
4',6-diamidino-2-phenylidole (DAPI)	D9542	Sigma Aldrich
3-((3-cholamidopropyl) dimethylammonium)-1-propane sulfonate (CHAPS)	C3023	Sigma Aldrich

3.1.1.1. Buffers and reagents for DNA isolation and genotypization

Table 4. Buffer composition for DNA isolation and genotypization

Buffer name	Composition
DNA lysing buffer	10 mM Tris-HCl pH 8.0 10 mM EDTA pH 8.0 150 mM NaCl 0.2% SDS (w/v) 0.4 mg/mL proteinase K (added freshly before use)
50x TAE (stock solution)	2 M Tris-HCl pH 8.0 50 mM EDTA pH 8.0 1 M CH_3COOH
1x TAE (diluted in 1:50 in dH_20)	40 mM Tris-HCl pH 8.0 1 mM EDTA pH 8.0 20 mM CH_3COOH

Other reagents for DNA isolation and genotyping were: 2% agarose gel ((w/v) in 1x TAE buffer), GelStar gel dye (50535, Lonza), DNA ladder 100 bp (N3231S, New England BioLabs), EmeraldAmpGT PCR Master Mix (RR310A, Takara).

3.1.1.2. Buffers and reagents for protein isolation, SDS-polyacrylamide gel electrophoresis (PAGE), and western blot (WB)

Table 5. Buffer composition for protein isolation, biochemical fractionation, SDS-PAGE, and western blot

Buffer name	Composition
10x PBS (stock solution)	1.37 M NaCl 27 mM KCl 100 mM Na_2HPO_4 18 mM KH_2PO_4
1x PBS (diluted in 1:10 in dH_20)	137 mM NaCl 2.7 mM KCl 10 mM Na_2HPO_4 1.8 mM KH_2PO_4
RIPA lysis buffer pH 8.0	50 mM Tris 150 mM NaCl 0.5% sodium deoxycholate (w/v) 1% Triton X-100 (v/v) phosphatase inhibitor (added freshly before use) protease inhibitor (added freshly before use)
4x Laemmli buffer	50 mM Tris-HCl, pH 6.8 10% glycerol (v/v) 2% SDS (w/v) 10 mg bromophenol blue 2% β-mercaptoethanol (v/v) (added freshly before use)
6x SDS loading buffer	375 mM Tris-HCl 12% SDS 60% glycerol 10 mg bromophenol blue 600 mM DTT
Low salt (LS) buffer	10 mM Tris-HCl pH 7.5 5 mM EDTA pH 8.0 10% saccharose (w/v)

	1 mM DTT (added freshly before use) protease inhibitor (added freshly before use)
Triton-X-100 buffer	10 mM Tris-HCl pH 7.5 5 mM EDTA pH 8.0 10% saccharose (w/v) 1% Triton-X-100 (v/v) 0.5 M NaCl 1 mM DTT (added freshly before use) protease inhibitor (added freshly before use)
Sarkosyl buffer	10 mM Tris-HCl pH 7.5 5 mM EDTA pH 8.0 10% saccharose (w/v) 1% sarkosyl (w/v) 0.5 M NaCl 1 mM DTT (added freshly before use) protease inhibitor (added freshly before use)
Urea buffer	7 M Urea 2 M Thiourea 30 mM Tris-HCl pH 8.5 4% CHAPS (w/v)
10x SDS running buffer (stock solution)	30 mM Tris 150 mM glycine 1% SDS (w/v)
1x SDS running buffer (diluted in 1:10 in dH_20)	30 mM Tris 150 mM glycine 1% SDS (w/v)
1x Transfer buffer	25 mM Tris 192 mM glycine 20% methanol (v/v)
10 x TBS pH 7.4 (stock solution)	500 mM Tris 1.5 M NaCl 20 mM KCl
0.1% TBS-Tween pH 7.4 (diluted in 1:10 in dH_20)	50 mM Tris 150 mM NaCl 2 mM KCl 0.1% Tween-20 (v/v)
Blocking buffer	3% BSA in 1x TBS-Tween (w/v)
Primary antibody probing solution	3% BSA in TBS-Tween (w/v) 0.5% sodium azide (v/v)

Secondary antibody probing solution	3% BSA in 1x TBS-Tween (w/v)

Table 6. Gels for SDS-PAGE

Gels	Composition
Stacking gel	250 mM Tris-HCl pH 6.8 6% acrylamide (v/v) 0.1% SDS (w/v) 0.1% APS (w/v) 0.01% TEMED (v/v)
Resolving gel (12%)	375 mM Tris-HCl pH 8.8 12% acrylamide (v/v) 0.1% SDS (w/v) 0.1% APS (w/v) 0.01% TEMED (v/v)
Resolving gel (15%)	375 mM Tris-HCl pH 8.8 15% acrylamide (v/v) 0.1% SDS (w/v) 0.1% APS (w/v) 0.01% TEMED (v/v)

Other reagents for protein isolation, SDS-PAGE, and western blot were: ROTI®Mark TRICOLOR (8271.1, Carl Roth), Nitrocellulose membrane pore size: 0.45 µm (10600001, Cytiva), Immobilon®-P polyvinylidene fluoride (PVDF) membrane pore size: 0.45 µm (IPVH00005, Merck Millipore), Trans-Blot Turbo RTA Transfer kit (1704270), Lumi-Light western blotting substrate (12015200001, Roche).

3.1.1.3. Reagents and kits for RNA extraction, cDNA synthesis, and RT-qPCR

Table 7. List of kits for RNA extraction and gene expression analyses

Experimental kit	Catalog number	Manufacturer
RNeasyMini Kit	74106	Qiagen
HighCapacity cDNA ReverseTranscription Kit	4368814	Applied Biosystems
LightCycler® 480 SYBR Green I Master	04887352001	Roche

3.1.1.4. Buffers and reagents for immunocytochemistry

Table 8. Buffer composition for cell immunofluorescence

Buffer	Composition
Fixation buffer pH 7.4	4% PFA (w/v) 137 mM NaCl 2.7 mM KCl 10 mM Na_2HPO_4 1.8 mM KH_2PO_4
Permeabilization buffer	0.1% Triton X-100 in 1x PBS (v/v)
Blocking buffer	0.5% BSA in 1x PBS (w/v)

3.1.1.5. Reagents for immunofluorescence on tissue

Table 9. Buffer composition for tissue immunofluorescence

Buffer	Composition
Fixation buffer pH 7.4	4% PFA (w/v) 137 mM NaCl 2.7 mM KCl 10 mM Na_2HPO_4 1.8 mM KH_2PO_4
Tissue storage solution	30% sucrose in 1x PBS (w/v)
Antifreeze solution pH 7.4	30% ethylene glycol (v/v) 30% glycerol (v/v) 24.4 mM NaH_2PO_4 buffer
Permeabilization/blocking buffer	10% horse serum (v/v) 0.25% Triton X-100 (v/v) in 1x PBS
Primary antibody probing solution	1% horse serum (v/v) 0.25% Triton X-100 (v/v) in 1x PBS
Washing buffer	0.25% Triton X-100 (v/v) in 1x PBS
TrueBlack staining solution	20% TrueBlack in 70% ethanol (v/v)

Other reagents for tissue immunofluorescence were: Tissue-Tek optimal cutting temperature (O.C.T.) Compound (4583, Sakura), PAP pen (Z377821-1EA, Sigma Aldrich), Vectashield (H-1200, Vector Laboratories).

3.1.1.6. Reagents for cytokine array

Table 10. List of kits for cytokine analyses

Experimental kit	Catalog number	Manufacturer
Pierce BCA Protein Assay Kit	23227	Thermo Scientific
RayBio® C-Series Mouse Inflammation Antibody Array C1	126AAM-INF-1-8	Raybiotech

3.1.1.7. Reagents and kits for flow cytometry

Table 11. Composition of buffers for flow cytometry

Buffer	Composition
FACS flow buffer	2% FBS (v/v) 0.05% sodium azide (w/v) in 1x PBS
Fc block buffer	10 µg/mL anti-mouse CD16/CD32 diluted in FACS flow buffer
Stock isotonic Percoll (SIP)	9:1=Percoll: 10x HBSS
70% SIP (per brain)	3.1 mL SIP and 0.9 mL 1x HBSS
37% SIP (per brain)	1.65 mL SIP and 2.35 mL 1x HBSS
30% SIP (per brain)	1.3 mL SIP and 2.7 mL 1x HBSS

Other reagents for flow cytometry were: Ammonium-Chloride-Potassium (ACK) lysing buffer (A10492-01, Gibco), UltraComp eBeads™ Compensation Beads (01-2222-42, Invitrogen), Foxp3/Transcription Factor Staining Buffer Set (00-5523-00, eBioscience), Percoll (GE17-0891-02, GE Healthcare).

3.1.2. Antibodies

3.1.2.1. Antibodies for Western blot and immunofluorescence analyses

3.1.2.1.1. Primary antibodies

Table 12. List of primary antibodies for Western blot and immunofluorescence analyses

Antigen	Host	Catalog number	Manufacturer	Dilution
β-tubulin	mouse	T8328	Sigma Aldrich	WB 1:10000 IF 1:1000
Caspase 3	rabbit	9662	Cell Signaling	WB 1:1000
Cleaved caspase 3	rabbit	9661	Cell Signaling	WB 1:1000
LC3	rabbit	PM036	MBL	WB 1:1000
Optineurin	rabbit	100000	Cayman Chemical	WB 1:1000
TDP-43 (C')	rabbit	12892-1-AP	Proteintech	WB 1:1000
TDP-43 (N')	rabbit	10782-2-AP	Proteintech	WB 1:1000 IF 1:500

3.1.2.1.2. Secondary antibodies

Table 13. List of secondary antibodies for Western blot and immunofluorescence analyses

Antibody	Conjugate	Catalog number	Manufacturer	Dilution
anti-mouse	Alexa Fluor 488	A11029	Invitrogen	IF 1:1000
anti-rabbit	Alexa Fluor 546	A11035	Invitrogen	IF1:1000
anti-mouse	HRP	115-035-174	Jackson ImmunoResearch	WB 1:2500
anti-rabbit	HRP	111-035-144	Jackson ImmunoResearch	WB 1:2500

3.1.2.2. Antibodies for flow cytometry

Table 14. List of antibodies for flow cytometry

Antibody	Conjugate	Catalog number	Manufacturer	Dilution for cells	Dilution for beads
B220	Alexa Fluor 700	103231	BioLegend	1:1000	1:1000
CD4	APC-H7	560181	BD Pharmingen	1:1000	1:500
CD8a	BV605	100744	BioLegend	1:1000	1:1500
CD11b	APC	553312	BD Pharmingen	1:400	1:400
CD11c	PE	12-0114-82	eBioscience	1:200	1:100
CD25	APC	101910	BioLegend	1:100	1:1500
CD25	PE-Cy7	25-0251-82	eBioscience	1:1000	1:1000
CD38	PE	102707	BioLegend	1:10000	1:2000
CD44	PE/Dazzle	103055	BioLegend	1:1500	1:500
CD45	FITC	11-0451-82	eBioscience	1:2000	1:2000
CD62L	PerCP-Cy5.5	104431	BioLegend	1:1000	1:100
CD69	APC	104514	BioLegend	1:800	1:800
CD86	PE-Cy7	25-0862-80	eBioscience	1:200	1:1000
CD90.2	BV786	105331	BioLegend	1:2000	1:2000
FOXP3	PE	126404	BioLegend	1:200	1:1000
F4/80	PerCP-Cy5.5	45-4801-82	eBioscience	1:200	1:50
KLRG1	FITC	11-5893-82	eBioscience	1:1500	1:1000
Ly6C	APC-eFluor780	47-5932-82	eBioscience	1:100	1:100
Ly6G	FITC	127606	BioLegend	1:1000	1:400
MHC-II	PE/Dazzle	107648	BioLegend	1:8000	1:200
NK1.1	BV605	108739	BioLegend	1:100	1:1000
CD16/CD32 (clone 2.4G2)	/	553142	BD Pharmingen	1:1000	/

3.1.3. DNA oligonucleotides

DNA synthetic oligonucleotides (primers) for mouse genotyping and specific gene expression used in the polymerase chain reaction (PCR) and real-time polymerase chain reaction (RT-qPCR), respectively were purchased from Metabion. Primers were received as a stock solution of 100 µM, and working stocks were diluted to a concentration of 10 µM in dH20.

Table 15. List of primers

Gene	Primer	Sequences (5' → 3')	Final concentration
Optineurin^{WT}	Forward	GCTACCATGCTCAGCCAGAGTTTC	0.2 µM
	Reverse	GGCTTCAGGGATGCATGAATC	0.2 µM
Optineurin^{470T}	Forward	GCAACACAGACCTGAACAGACG	0.2 µM
	Reverse	ACTCCACCCATAAGTCATCAAAGC	0.2 µM
TDP^{G348C}	Forward	TTATTACCCGATGGGCA	1 µM
	Reverse	CTCTTTGTGGAGAGGAC	0.5 µM
TARDBP	Forward	CGAGTCCAGAAAACATCTGACC	0.4 µM
	Reverse	ACACCSTCGCCCATCTATCAT	0.4 µM
Gapdh	Forward	GTGCTGAGTATGTCGTGGA	0.4 µM
	Reverse	GTGGTTCACACCCATCACAA	0.4 µM
G3bp1	Forward	GCAGAAGGAAATCCACAGGA	0.4 µM
	Reverse	TCATTCAGAGTTGCGTGAGC	0.4 µM
Poldip3	Forward	ATGGGCAACCTATGAAGTGC	0.4 µM
	Reverse	TTTTTCACTGAGGGGCTGTC	0.4 µM

3.1.4. Reagents and treatments used in cell culture

Table 16. List of reagents and treatments used in cell culture

Reagents	Catalog number	Manufacturer
AlbuMAXTM I	11020-013	Gibco
Antibiotic/Antimycotic Solution (100x)	AAS-B	Capricorn Scientific GmbH
Bafilomycin A1 (Baf A1)	B1793	Sigma Aldrich
Borax (di-Sodium tetraborate decahydrate)	27727.231	VMR
Boric acid	5935.1	Carl Roth
B27 50X supplement	17504-044	Gibco
Deoxyribonuclease I (DNase I) for microglia	DN25	Sigma Aldrich
Deoxyribonuclease I (DNase I) for neurons	D5025	Sigma Aldrich
Dimethyl sulfoxide (DMSO)	445103	CARLO ERBA reagents
Dulbecco's Modified Eagle Medium (DMEM)	P04-04510	Pan Biotech
1x Hank's Balanced Salt Solution (HBSS), with Ca^{2+}, Mg^{2+} (+/+)	HBSS-1A	Capricorn Scientific GmbH
1x Hank's Balanced Salt Solution (HBSS), w/o Ca^{2+}, Mg^{2+} (-/-)	HBSS-2A	Capricorn Scientific GmbH
Fetal bovine serum (FBS)	P30-3306	Pan Biotech
HEPES	HEP-B	Capricorn Scientific GmbH
L-glutamine	GLN-B	Capricorn Scientific GmbH
Glutamine (stabile) for neurons	STA-B	Capricorn Scientific GmbH
Lipopolysaccharide from E. coli O111:B4 (LPS)	L4391	Sigma Aldrich
MG132	133407-82-6	Calbiochem
Neurobasal medium	21103-049	Gibco
1x Dulbecco's PBS, w/o Ca^{2+}, Mg^{2+}	PBS-1A	Capricorn Scientific GmbH
Poly-D-lysine	P6403	Sigma Aldrich
Poly-L-lysine	P1274	Sigma Aldrich
Puromycin	0240.2	Carl Roth
RPMI 1640	RPMI-A	Capricorn Scientific GmbH
Trehalose	T9531	Sigma Aldrich

Trypan blue	17-924E	Lonza
Trypsin inhibitor	T9003	Sigma Aldrich
2.5% (10x) Trypsin solution	15090-46	Invitrogen
Trypsin-EDTA (0.5%) in DPBS (10x)	TRY-1B10	Capricorn Scientific GmbH

3.1.4.1. Reagents for isolation and cultivation of primary microglia

Poly-L-lysine was dissolved in a concentration of 10 mg/mL in sterilized dH_20, and DNAse I was dissolved in sterile 0.9% NaCl (w/v) at a final concentration of 5 mg/mL. Both solutions were filtered sterile and frozen in 1 mL aliquots until use.

Primary microglia isolated from P0-3 old pups were cultured in Dulbecco's Modified Eagle Medium supplemented with 10% FBS (v/v), 2 mM L-glutamine, and antibiotic/antimycotic solution (10 000 U/mL Penicillin, 10 mg/mL Streptomycin, 25 µg/mL Amphotericin B), referred to as complete DMEM.

3.1.4.2. Reagents for cortical neuron isolation, cultivation, and treatment

Poly-D-lysine solution was prepared in 0.1 M borate buffer (0.1 M boric acid, 0.025 M borax pH 8.5) at a concentration of 4 mg/mL, and the final concentration of 0.02 mg/ml, and DNase I in HBSS with Ca^{2+} Mg^{2+} at a concentration of 10 mg/mL, and the final concentration of 10 µg/mL, filtered sterile and frozen in aliquots until use. The triturating solution was prepared in Ca^{2+}, Mg^{2+}- free HBSS with 1% AlbuMAXTM I, 0.05% trypsin inhibitor (v/v) from soybean, and 10 µg/mL DNase I.

Primary cortical neurons isolated from E15.5 old embryos were cultured in Neurobasal medium supplemented with 2% B27 50X supplement (v/v), stable glutamine, and antibiotic/antimycotic solution (10 000 U/mL Penicillin, 10 mg/mL Streptomycin, 25 µg/mL Amphotericin B).

3.2. Cell lines generation, maintenance, and treatment

WT BV2 cells were a kind gift from Dr. Jasna Kriz. Optineurin knockout (KO) microglial BV2 cell line was generated by the CRISPR/Cas9 technology as previously described (Prtenjaca et al., 2022). In brief, WT BV2 cell lines were transfected with optineurin-directed gRNA-guided Cas9 endonuclease that was targeting the third exon with translational initiation codon, and puromycin N-acetyl-transferase, and selected based on puromycin resistance. BV2 Optn KO cells were maintained in a complete DMEM (see below) medium with 2 μg/mL puromycin, until seeding for the experiment. The L929 cell line was a kind gift from Dr. Jonathan D. Ashwell and was cultured in complete DMEM (see below), and their supernatant was used as a source of macrophage colony-stimulating factor (M-CSF) in bone marrow-derived macrophages (BMDM) differentiation.

WT BV2, KO BV2, and L929 cell lines were cultured in DMEM supplemented with 10% FBS (v/v), 2 mM L-glutamine, and antibiotic/antimycotic solution (10 000 U/mL Penicillin, 10 mg/mL Streptomycin, 25 μg/mL Amphotericin B), referred to as complete DMEM.

TDP-43 mechanism of degradation was analysed by blocking the ubiquitin-proteasomal system with 1μM MG132 for 4 h and 8 h, and autophagy with 50 nM Baf A1 for 4 h or with their combination. To determine TDP-43 levels and localization upon inflammatory stimuli BV2 WT and KO cells were treated with 0.3 μg/mL or 2 μg/mL LPS for 24 h.

3.3. Mice

Mice were maintained at 24°C under a 12 h/12 h light/dark cycle and had ad libitum access to food and water. C57BL/6 mice, hereafter referred to as wild-type (WT) mice were purchased from Jackson and have been expanded in the animal facility at the Medical School of the University of Rijeka. Generation of the optineurin truncated $Optn^{470T}$ mice has been previously described; these mice are considered optineurin insufficient because of two reasons: the presence of loss-of-function C'-terminal truncation and ~7-fold lower protein level (Munitic et al., 2013). In brief, whole-body homozygous optineurin truncation was achieved by crossing the mice carrying flanked exon 12 with loxP-neoR-loxP cassette with β-actin-cre mice that express Cre recombinase under the control of endogenous mouse β-actin promoter. In that way, the last 114 amino acids were removed from the C'-terminus, including the ubiquitin-binding region. $Optn^{470T}$ mice used in this study were backcrossed to C57BL/6 genetic background 11 times. For a generation of primary BMDMs, the three-month-old WT and $Optn^{470T}$ males were used. In all other experiments young adult (three-month-old), middle-aged (one-year-old), and old (two-year-old) male and female mice were used, as noted. To establish a new two-hit ALS model, $Optn^{470T}$ mice were crossed with the mice carrying the human transgenic TDP-43 (TDP-43^{G348C}) (see section 4.3.). Aged-matched WT, $Optn^{470T}$, and TDP-43^{G348C} were used as control mice at the indicated time points used in experiments. All experimental procedures were performed according to the European Communities Council Directive of 24 November 1986 (86/609/EEC) and approved by the Ministry of Agriculture of the Republic of Croatia, Ethics Committees of the Department of Biotechnology, and Medical School of the University of Rijeka.

3.4. Methods

3.4.1. Mice euthanasia, for perfusion and tissue isolation

Mice were euthanized by cervical dislocation or deep anaesthesia following blood perfusion, depending on the tissues isolated and the purpose of the experiments. For multi-colour flow cytometry analyses, mice were euthanized by cervical dislocation, placed on the back, the skin and peritoneum were opened, and the spleen was removed. After isolation, spleens were immediately processed for immune cell isolation and characterization. To collect brain and spinal cord for biochemical fractionation, cytokine array, flow cytometry, and immunofluorescence analyses mice were subjected to blood perfusion with ice-cold 1x PBS to avoid contamination with blood cells. First, mice were deeply anesthetized with intraperitoneal injection with a combination of ketamine and xylazine in the final concentrations of 0.1 mg/g and 0.02 mg/g, respectively. When mice reached a surgical plane of anaesthesia, they were placed on the back, and a lateral incision beneath the rib cage through the skin and abdominal wall was made to reach the sternum and diaphragm. To expose the heart, parallel cuts on both sides of the rib cage and diaphragm were performed, followed by lifting of the sternum. A small incision to the right atrium of the heart using iris scissors was made to allow blood and 1x PBS to run out from circulation. Immediately after, a 25G butterfly needle connected to a 50 mL syringe filled with ice-cold 1x PBS was placed in the apex of the left ventricle and ice-cold 1x PBS was slowly injected into the circulation. Mice were perfused with a total of 60 mL of ice-cold 1x PBS. Indication of successful perfusion was a loss of blood and pale colour of the liver. After perfusion, mice were placed on the abdomen and decapitated. To reach the cranium, the skin between the ears was removed. Parallel cuts on both sides of the cranium from interparietal to parietal bone, and one through sagittal suture were carefully done to expose, but not damage the brain. The cranium was lifted from the cut through the sagittal suture to parallel cuts on the side, and the brain was carefully removed with the rounded spatula. To extract the spinal cord, the skin from the back was removed, and small parallel cuts were done on both sides of the cervical part of the vertebrae. To uncover the whole spinal cord up to the sacral part, the cervical part of the vertebrae was held with tweezers, and vertebrae were cut on both sides with iris scissors. Nerves exiting the spinal cord were carefully separated from the spinal cord, making the spinal cord

accessible for extraction from vertebrae. For the isolation of immune cells from the brain, brain tissue was immediately proceeded for enzymatic digestion (See section 3.4.5.2.). To perform biochemical fractionation and cytokine array analyses, after extraction of the brain and spinal cords, tissues were snap-frozen in liquid nitrogen, and stored at −80°C until use.

3.4.2. Isolation, cultivation, and treatments of bone marrow-derived macrophages (BMDMs)

To generate bone marrow-derived macrophages (BMDMs), bone marrow from the femurs and tibias of three-month-old WT and $Optn^{470T}$ male mice was used. Mice were sacrificed by cervical dislocation, placed on the back, and the skin was removed from the abdomen to the hindlimbs. Hindlimbs were cut in the hip, and adherent muscles and connective tissue were removed from the bones with the scalpel. After cutting the upper and lower bone epiphyses, bone marrow was flushed using a 25G needle in RPMI 1640 medium supplemented with 10% FBS (v/v), 2 mM L-glutamine, antibiotic/antimycotic solution (10 000 U/mL penicillin, 10 mg/mL streptomycin, 25 µg/mL amphotericin B), and 10 mM HEPES, referred to as complete RMPI 1640, filtered through a 70 µm cell strainer, and centrifuged for 5 minutes (min) at 1500 rpm. At this point, bone marrow was cryopreserved at -80°C in a freezing medium (10% DMSO (v/v) and 90% FBS(v/v)), or left in the culture. To differentiate BMDMs, the pellet was resuspended in a complete RPMI 1640 medium in the presence of 30% L929 cell line supernatant as a source of macrophage colony-stimulating factor (M-CSF) in a standard humidified incubator at 37°C with 5% CO_2 for 5 days. After differentiation, BMDMs were detached with 10 mM EDTA 1x PBS for 15 min and seeded onto a 24-well plate at a density of 2 x 10^5 cells/mL. Number and cell viability were determined on the Neubauer haemocytometer using Trypan blue, a dye that penetrates only the dead cells. To determine TDP-43 levels upon inflammatory stimuli and autophagy inhibition 24 h upon seeding, BMDMs were left untreated or stimulated with 0.3 µg/mL or 2 µg/mL LPS for 24 h, and autophagy was blocked with 50 nM Baf A1 for the last 4 h of the experiment.

3.4.3. Isolation, cultivation, and treatments of primary microglia

Primary microglia were isolated from the brains of WT and Optn^{470T} neonatal pups (0–3 days postnatally). To obtain neonatal pups, scheduled timed pregnancies of WT and Optn^{470T} mice were set up (the gestation period lasted for typically 19-21 days). Neonatal pups were decapitated, the skin between ears was removed, and the brains were extracted after the removal of the cranium. To avoid contamination with peripheral myeloid cells and meningeal fibroblasts, the meninges were carefully separated from the brains in 1x HBSS (-/-) under a dissecting microscope, together with removing the olfactory bulbs and cerebella. The remaining brain tissue was transferred to fresh 1x HBSS (-/-), chopped into small pieces, and trypsinized in 0.125% trypsin in a standard humidified incubator at 37°C with 5% CO_2 for 15 min. To stop trypsinization, brain tissue was transferred to a 15 mL Eppendorf tube containing 6 mL complete DMEM. When the tissue settled down, the supernatant was aspirated and 6 mL of fresh complete DMEM was added with 625 µg/mL of DNase I. Brain tissue was triturated by pipetting up and down up to 20 times, filtered through the 70 µm cell strainers, and centrifuged at 500 rpm for 5 min. Cell pellets from three brains were resuspended in 10 mL of complete DMEM and plated onto a 0.1 mg/mL poly-L-lysine coated T75 flask. The medium was changed the following day and subsequently, every 2nd day, until cell cultures reached complete confluence, usually after 7-10 days. To detach microglia from the astrocyte layer, 1M HEPES was added to maintain physiological pH, parafilm was put on the flask cap, and the T75 flask was shaken for 16 h at 120 rpm at 37°C. The following day, T75 flasks were additionally shaken for 4 h at 300 rpm, and the supernatant containing microglia was collected and centrifuged for 5 min at 1000 rpm. Number and cell viability were determined using Trypan blue, and microglia were seeded onto a PLL-coated 24-well plate at a density of 2 x 10^5 cells/mL for protein and RNA isolation, and 10^5 cells/mL on 13 mm coverslips for immunofluorescent analyses. 48 h after seeding, microglia were used for functional analyses. TDP-43 degradation mechanism was analysed by blocking the ubiquitin-proteasomal system with 1 µM MG132 and autophagy with 50 nM Baf A1 for 4 h, or with their combination. To determine TDP-43 levels and localization upon inflammatory stimuli microglia were treated with 0.3 µg/mL or 2 µg/mL LPS for 24 h.

3.4.4. Isolation, cultivation, and treatments of primary neurons

Primary cortical neurons were obtained from WT and Optn^{470T} mice embryos. To obtain mouse embryos, scheduled time pregnancy of WT and Optn^{470T} mice were set up, and pregnant females were taken on E15.5 days of the gestation period when extensive neurogenesis occurs. Females were euthanized by cervical dislocation and cut through skin and peritoneum to expose internal organs and the uterus. The two horns of the uterus with amniotic sacs were removed by cutting connective tissue and transferred to the sterile Petri dish. Embryos were dissected from amniotic sacs, decapitated, and brains were extracted from the cranium in 1x HBSS (-/-). Under the dissecting microscope, meninges were removed from the brain and cortices were transferred to fresh 1x HBSS (-/-). The cortices were washed once with 1x HBSS (-/-), and treated with 0.125% trypsin in a standard humidified incubator at 37°C with 5% CO_2 for 20 min followed by the addition of 10 µg/mL of DNase I solution and mixing by inversion. When the tissue settled down, the supernatant was aspired. The remaining tissue was dissociated in 1 mL trituration solution followed by the addition of Neurobasal medium (1 mL per embryo) and passed through a 70 µm cell strainer. The cell suspension was centrifuged at 1000 rpm for 5 min, and the number and cell viability were determined using Trypan blue on a Neubauer haemocytometer. Cells were seeded on the poly-D-lysine coated 12-well plate at a density of 1.8 x 10^5 cells/mL for protein and RNA isolation. Five days after seeding, neurons were used for functional analyses. To determine TDP-43 levels and the mechanism of TDP-43 degradation neurons were treated with 1 µM MG132 and 50 nM Baf A1 for 4 h and 8 h, or with their combination. Induction of autophagy was done using 100 mM trehalose for 24 h.

3.4.5. Functional and biochemical assays

3.4.5.1. Immunoblotting and protein analyses

3.4.5.1.1. Cell lysis and protein isolation

For isolation of proteins for western blotting, cells were washed three times with ice-cold 1x PBS and lysed in 110 µL RIPA lysis buffer containing protease and phosphatase inhibitors. Lysates were transferred to a 1.5 mL Eppendorf tube and kept on ice for 30 min. After 30 min of incubation, lysates were centrifuged at 14 000 rpm for 10 min at 4°C, and 90 µL of supernatant was carefully transferred to a new 1.5 mL Eppendorf tube. Supernatants were mixed with 4X Laemmli buffer and frozen at -20°C, or left at 4°C (for LC3 protein) until sodium dodecyl sulphate-polyacrylamide gel electrophoresis (SDS-PAGE) analysis.

3.4.5.1.2. Biochemical fractionation

For distinguishing soluble and insoluble proteins from brains upon extraction and storage at −80°C, biochemical fractionation was performed. One hemisphere of the brain was taken, weighed, and homogenized in 5 mL/g of low-salt (LS) buffer on ice. Brain lysates were centrifuged at 14 000 rpm for 30 min at 4°C and the supernatants were saved as LS fraction. The remaining pellet was washed once more in LS fraction and centrifuged at 14 000 rpm for 30 min at 4°C. The supernatant was discarded and the pellet was resuspended in 5 mL/g of Triton-X (TX) buffer and ultracentrifuged at 180 000 g for 30 min at 4°C. Supernatants were saved as TX fractions. To wash the remaining pellet, the pellet was resuspended again in TX buffer and ultracentrifuged at 180 000 g for 30 min at 4°C. After ultracentrifugation, the supernatant was discarded and the pellet was homogenized in 1 mL/g sarkosyl (SARK) buffer and shaken at 800 rpm for 1 h at RT. Next, the lysate was ultracentrifuged at 180 000 g for 30 min at RT, and the supernatant was saved as a sarkosyl fraction. The remaining pellet was resuspended in 0.5 ml/g urea buffer and centrifuged at 14 000 rpm for 30 min at 4°C. Supernatants were saved as urea fractions. Samples were mixed with 6x SDS loading buffer and frozen at -20°C until SDS-PAGE analysis.

3.4.5.1.3. SDS-polyacrylamide gel electrophoresis (PAGE) and western blot analyses

Isolated proteins were separated using SDS-PAGE in Mini-PROTEAN Tetra Vertical Electrophoresis Cell (Bio-Rad). Samples were heated for 10 min at 95 ◦C (except urea fraction from biochemical fractionation) before loading on the 12% or 15% polyacrylamide gels (the latter were used only for CC3 and LC3), For identification of protein size, a protein ladder marker (Roti-Mark TRICOLOR) was loaded onto the gel. The gels were first run at 100 V in 1x SDS running buffer until samples did not compress to separating gel, and then the currency was increased to 130 V until the loading dye from 1x Laemmli buffer did not reach the end of the gel. All gels were then transferred to nitrocellulose membranes, except for those that were later blotted for CC3 and LC3 which were transferred to PVDF membranes. Transfer sandwich consisting of a sponge, blotting paper, gel, and membrane was locked into a gel holder cassette and placed into a Mini Trans-Blot Electrophoretic Transfer Cell (Bio-Rad) in 1x transfer buffer and run at 100 V for 60-80 min depending on the protein size. For proteins isolated by biochemical fractionation, semi-dry transfer was done using Trans-Blot® Turbo™ Transfer RTA kit and System (Bio-Rad). Proteins were transferred to the membrane at 1.3 A for 10 min. After transferring proteins from the gel to the membrane, membranes were blocked with blocking buffer to reduce unspecific antibody binding for 1 h at RT and incubated with primary antibodies in antibody probing solution O/N at 4°C. The next day, membranes were washed three times for 10 min with 0.1% TBS-Tween and probed with secondary anti-rabbit or anti-mouse antibodies conjugated with HRP in antibody probing solution for 1 h at RT. Membranes were then washed three times for 10 min with 0.1% TBS-Tween and visualized with Chemiluminescence Blotting Substrate using ChemiDocTM imaging system (Bio-Rad).

3.4.5.1.4. Western blot densitometric analyses and protein quantification

Densitometric analyses were done using Fiji ImageJ software (National Institutes of Health). Obtained protein levels were normalized to loading control (β-tubulin). Protein quantification from biochemical fractionation is shown as a fold-change difference from a WT sample.

3.4.5.2. Methods for protein gene expression analyses

3.4.5.2.1. RNA isolation

The first step of gene expression and RNA sequencing analyses was the isolation of total RNA using the Total RNA RNeasy Mini Kit according to the manufacturer's instructions. Briefly, cells were washed with 1x PBS and lysed with 350 µL RLT buffer, following the addition of the same volume of 70% ethanol prepared in nuclease-free water to precipitate RNA. Samples were then transferred to the RNeasy Mini spin column placed in a 2 mL collection tube and centrifuged for 1 min at 8000 x g to selectively bind RNA to the membrane. Flow-through was discarded, and 700 µL of RW1 buffer was added to the spin column and centrifuged for 1 min at 8000 x g to remove possible DNA contamination. The washing step was repeated two times with RPE to remove traces of salts, from buffers used earlier in the protocol, and RNA was eluted from the column with 30 µL nuclease-free water in the new collection tube. RNA concertation and purity were measured using UV/VIS spectrophotometer BioDrop Duo at 260 nm wavelength, and 280/260, and 280/230 ratio was determined for protein concentration and phenol contamination, respectively. If both 280/260 and 280/230 ratios were ~ 2, RNA was pure enough to continue with the reverse transcription or be sent for RNA sequencing.

3.4.5.2.2. Reverse transcription and complementary DNA (cDNA) synthesis

After isolation, total RNA was transcribed to complementary DNA (cDNA) with the High-Capacity cDNA Reverse Transcription Kit following the manufacturer's instructions. 2x Master mix for reverse transcription was prepared with the reagents provided in the kit, containing: RT buffer, 100 mM dNTPs, random primers, 50 U/µL reverse transcriptase, 20 U/µL RNase inhibitor, and nuclease-free water. Isolated RNA was mixed with 2x Master Mix in the final volume of 20 µL, and put in the thermocycler for cDNA synthesis using the protocol listed in Table 17. Upon the end of transcription, synthesised cDNA was diluted 1:10 in dH2O and stored at -20°C.

Table 17. Protocol for cDNA synthesis

Step	Temperature	Time
Primer annealing	25°C	10 minutes
Reverse transcription	37°C	120 minutes
Enzyme inactivation	85°C	5 minutes
Cooling	4°C	∞

3.4.5.2.3. Quantitative Real-Time polymerase chain reaction (RT-qPCR)

Gene expression was analysed by RT-qPCR using SYBR green I Master Mix, following the manufacturer's instructions. Primers for the selected genes (listed in Table. 15) were added to Master Mix and finally mixed with 1:5 diluted cDNA in dH_2O in a ratio of 4:1 in the final volume of 20 µL. Duplicates were made for each gene. RT-qPCR was performed on LightCycler® 96 System (Roche) using the protocol listed in Table 18.

Table 18. Protocol for RT-qPCR

Step	Temperature	Time	Number of cycles
Preincubation	95°C	600 sec	1x
3 Step Amplification	95°C	10 sec	45x
	55°C	10 sec	
	72°C	30 sec	
Melting	95°C	10 sec	1x
	65°C	60 sec	
	97°C	1 sec	
Cooling	37°C	30 sec	1x

3.4.5.2.4. Gene expression analyses

Gene expression analyses were done with the LightCycler 480 Software. The presence of more than one peak in the melting curves was checked for each gene (to rule out non-specific amplification) and in the case of multiple peaks for certain gene, this gene was excluded from the analyses. The mean value of cycle threshold (Ct) per each gene was calculated from duplicates and was subtracted from the mean Ct value of the housekeeping gene, glyceraldehyde 3-phosphate dehydrogenase

(GAPDH), and expressed as a difference in threshold cycles (ΔCt). Each ΔCt from different samples was subtracted from ΔCt of untreated WT control and expressed as ΔΔCt value. Relative fold gene expression ($2^{-\Delta\Delta Ct}$) of *TARDBP*, *Poldip3,* and *G3bp1* genes was shown as a difference compared to untreated WT control.

3.4.5.3. Microscopy

3.4.5.3.1. Immunofluorescence

For the immunofluorescence analyses primary microglia were plated onto PLL-coated chamber slides (#177402; LabTek). Cells were washed once in 1x PBS and fixed in 4% PFA for 15 min. After fixations, cells were washed three times in 1x PBS and subsequently permeabilized with permeabilization buffer (0.1% Triton X-100 in 1x PBS) for 15 min. After permeabilization, cells were blocked with blocking buffer (0.5% BSA in 1x PBS) for 1 h at RT and incubated with primary antibodies diluted in blocking buffer in a humid chamber O/N at 4°C. The cells were washed three times in 1x PBS and incubated with secondary antibodies diluted in a blocking buffer for 1 h at RT in the dark. Finally, after washing three times with 1x PBS, nuclei were stained with 0.5 ng/mL DAPI in 1x PBS for 5 min in the dark, washed ones, and cells were mounted on glass slides with the Aqua-Poly/Mount mounting medium. Cells were imaged using a 60X objective on an Olympus IX83 microscope (Tokyo, Japan).

3.4.5.3.2. Image analyses

The nuclear/cytoplasmic TDP-43 ratio and percentage of TDP-43 in the cytoplasm in primary microglia were measured using Fiji (Image J) software. The cytoplasmic area was marked based on β-tubulin and the nuclear by DAPI staining. Briefly, TDP-43 integrated density (sum of the area and mean fluorescence intensity (MFI)) was measured in the whole cell and only in the nucleus. To get integrated density from the cytoplasm, nuclear-integrated density was subtracted from the whole cell integrated density. To get cytoplasmic TDP-43 MFI, calculated cytoplasmic integrated density was divided by the area of the cytoplasm. The nuclear/cytoplasmic TDP-43 ratio was obtained by dividing cytoplasmic and nuclear TDP-43 MFI values.

3.4.5.4. Cytokine array

To assess the inflammatory profile in the brains and spinal cords of three-month and two-year-old WT and Optn^{470T} male mice, simultaneous detection of 40 different cytokines and chemokines was analysed with a RayBio® C-Series Mouse Inflammation Antibody Array C1 kit according to the manufacturer's instructions. All reagents were provided in the kit. One hemisphere of the brain and the whole spinal cord were lysed in 0.5 mL of the lysing buffer, and protein concentrations were determined using Pierce BCA Protein Assay Kit, according to the manufacturers' instructions. In brief, 10 µL of diluted brain or spinal cord lysates (1:50 in lysing buffer) were pipetted to 96 well plates with a flat bottom and incubated for 30 min at 37°C with 25 µL A+B mixed solution from the kit. As a protein standard, 1 mg/mL to 0.0625 mg/mL concentration of BSA provided in the kit was used diluted in lysing buffer from Array kit and also incubated with A+B solution for 30 min at 37°C. Upon the end of incubation, absorbance at 562 nm was measured on a spectrophotometer, and protein concentrations were determined based on a standard curve calculated from known BSA concentrations and absorbance measured. At this step, two distinct sets of three-month and two-year-old WT and Optn^{470T} mice were pooled together and diluted in 1x blocking buffer to obtain the final concentration of 300 µg/mL. In the meantime, array membranes were blocked with 1x blocking buffer for 1 h at RT. Each set of diluted brain lysates was incubated on the separate array membrane O/N at +4°C. The following day, membranes were washed three times with wash buffer I and two times with wash buffer II for 5 min and incubated with a cocktail of biotinylated detection antibodies diluted in 1x blocking buffer O/N at +4°C. On the final day, membranes were washed again (as previously described), incubated with streptavidin labelled antibody diluted in 1x blocking buffer (1:1000) for 1 h at RT, washed, and incubated with a Detection Buffer C+D mixture (1:2) for 2 min. Array membranes were developed using the ChemiDocTM MP Imaging System (Bio-Rad).

3.4.5.4.1. Cytokine array analyses

After developing array membranes, densitometric analyses were done using Fiji (ImageJ) software (National Institutes of Health) by measuring the mean grey values of duplicates for each cytokine. The average of the duplicates for each cytokine was normalized to the average of positive controls on each membrane and

shown in the tables as means from two sets ± SD for three-months-old and three sets ± SEM for two-year-old male mice.

3.4.6. Multi-colour flow cytometry

3.4.6.1. Isolation of the immune cells from the spleen

Upon spleen removal, cells were released from the tissue by gentle grinding, filtered through the 70 µm cell strainers, and rinsed with FACS flow buffer. After centrifugation at 1500 rpm for 3 min, spleen cell suspensions were incubated with 1 mL of ACK lysing buffer for 5 min at RT to lyse red blood cells, rinsed again with 10 mL FACS flow buffer to dilute ACK lysing buffer, and centrifuged again. Cell pellets were resuspended in 5 mL of FACS flow buffer and filtered through the 70 µm cell strainers to get rid of the debris. Numbers and cell viability were determined using Trypan blue on a Neubauer haemocytometer and 10^6 cells were transferred to a 96-well round bottom plate for staining (described below).

3.4.6.2. Isolation of the immune cells from the brain

After perfusion, the brain was dissected and placed in 2 mL of ice-cold 1x PBS in a 15 mL Falcon tube and kept on ice. Brains were cut into smaller pieces and digested with 13 U/mL Liberase TM and 350 kU/mL DNAse I for 45 min at 37°C and mixed by vortexing every 10 min. After incubation, tissue was triturated, filtered through the 70 µm cell strainers, and centrifuged at 1500 rpm for 8 min. Supernatants were resuspended in 4 mL 37% Stock isotonic Percoll (SIP) and carefully pipetted on 4 mL 70% SIP previously added in a 15 mL Falcon tube. On the top 4 mL of 30%, SIP was carefully added, and brain homogenates in the Percoll gradient were separated by centrifugation for 40 min at 500 g and 18°C without brake to avoid mixing of the interphases. Immune cells were collected from the 37%/70% Percoll interphase, washed once with 1x HBSS, and counted using Trypan blue on a Neubauer haemocytometer, and 10^6 cells were transferred to the 96-well round bottom plate. Immune cells from the brain were analysed unstained or stained as described in section 3.4.5.3. Unstained samples were also seeded on coverslips, fixed, stained with 300 nM DAPI, and analysed on Olympus IX83 fluorescent microscope for autofluorescence (Tokyo, Japan).

3.4.6.3. Immune cell staining for multi-colour flow cytometry

96-well round bottom plate with isolated cells was centrifuged at 1500 rpm for 3 min and then incubated with 50 μL of Fc blocking antibody (anti-CD16/CD32, clone 2.4G2) for 5 min at RT to avoid any nonspecific binding of antibodies to Fc receptor on the immune cell surface. Cells were then stained with 50 µL of the 2x mixture of primary antibodies in FACS flow buffer for 30 min at +4°C in the dark. For each antibody, concentration was previously determined with antibody titration as listed in Table 14. Simultaneously, UltraComp eBeads™ compensation beads were stained with each antibody from the mix separately (single colour staining) with concentrations listed in Table 14., to perform compensation on flow cytometry. For the staining of nuclear FOXP3 Foxp3/Transcription Factor Staining Buffer Set was used according to the manufacturer's instructions. Briefly, after staining cell surface markers as described above, cells were incubated for 30 min at RT with 1x fixation/permeabilization concentrate diluted in fixation/permeabilization diluent, washed, and then permeabilized with 1x permeabilization buffer diluted in distilled water for 15 min at +4°C. After permeabilization, cells were incubated with Fc blocking antibody prior to staining with 50 µL of diluted FOXP3 primary antibody in FACS flow buffer for 30 min at +4°C. After staining, cells were washed three times by resuspending in FACS flow buffer and centrifugation, and incubated with 300 nM DAPI for 5 min in the dark, except for cells that were fixed and stained for FOXP3, respectively. Cells were washed once more, resuspended in 400 µL FACS flow buffer, passed through a 70 µm cell strainer, and kept in FACS tubes on ice until analysis. UltraComp eBeads™ Compensation Beads were centrifuged, washed once, resuspended in 200 µL FACS flow buffer, and kept in FACS tubes on ice until analysis.

3.4.6.4. Multi-colour flow cytometry

Analysis of surface marker and FOXP3 intracellular staining was done using BD FACSAria III flow cytometer and BD FACSDiva software (BD Biosciences). Compensation was performed to prevent fluorescent spillover and overlap of different fluorophores since each fluorophore emits a distinct wavelength range that can be detected with more than one detector. Unstained cells and single-colour stained-UltraComp eBeads™ Compensation Beads were then recorded and BD FACSDiva

software calculated compensation. Approximately 3-5*10^5 cells were collected per sample.

3.4.6.5. Multi-colour flow cytometry analyses

Gating and cell frequency analysis was done using FlowJo software as shown in Figure 8. for adaptive immunity and in Figure 9. for innate immunity. Cell debris was excluded based on forward (FSC) and side scatter (SSC) area parameters. Dead cells and doublets were eliminated based on positivity for DAPI and FSC area/height gating, respectively. After the elimination of cell debris, dead cells, and doublets, live cells were gated on T and B lymphocytes based on the positivity for specific markers for T lymphocyte Thy1.2 (CD90.2) and B lymphocyte B220 (CD45R). Cells negative for Thy1.2 and B220 were gated as innate immune non-T/non-B cells. The T cell population was further divided into $CD4^+$ and $CD8^+$ T lymphocytes based on positivity for $CD4^+$ and $CD8^+$, respectively. $CD4^+$ and $CD8^+$ were further analysed as naïve ($CD44^{lo}CD62L^+$), central memory (T_{CM}; $CD44^{hi}CD62L^+$), effector memory (T_{EM}; $CD44^{hi}CD62L^-$) and activated T lymphocyte subsets ($CD44^{hi}CD38^+$, $CD44^{hi}CD69^+$, and CD44hiKLRG1$^+$). Regulatory T lymphocytes (Treg) were gated as functional ($CD4^+CD25^+FOXP3^+$), and non-functional ($CD4^+CD25^+FOXP3^-$) $CD4^+$ T lymphocytes, as reported in (Nishioka et al., 2006). Non-T non-B (T^-/B^-) cells were separated based on positivity for several surface markers as follows: conventional dendritic cells (cDC; $CD11c^+$MHC-II$^+$), neutrophils ($Ly6C^+Ly6G^+$), macrophages/monocytes ($Ly6C^+Ly6G^-CD11b^+F4.80^+$), and natural NK cells ($NK1.1^+$). Activation of macrophages and cDC were analysed by MFI of CD86, CD11c, and MHC Class II. Absolute cell numbers of indicated populations were calculated from the number of live cells determined using Trypan blue on a Neubauer haemocytometer multiplied by the frequency of that population obtained in FlowJo software.

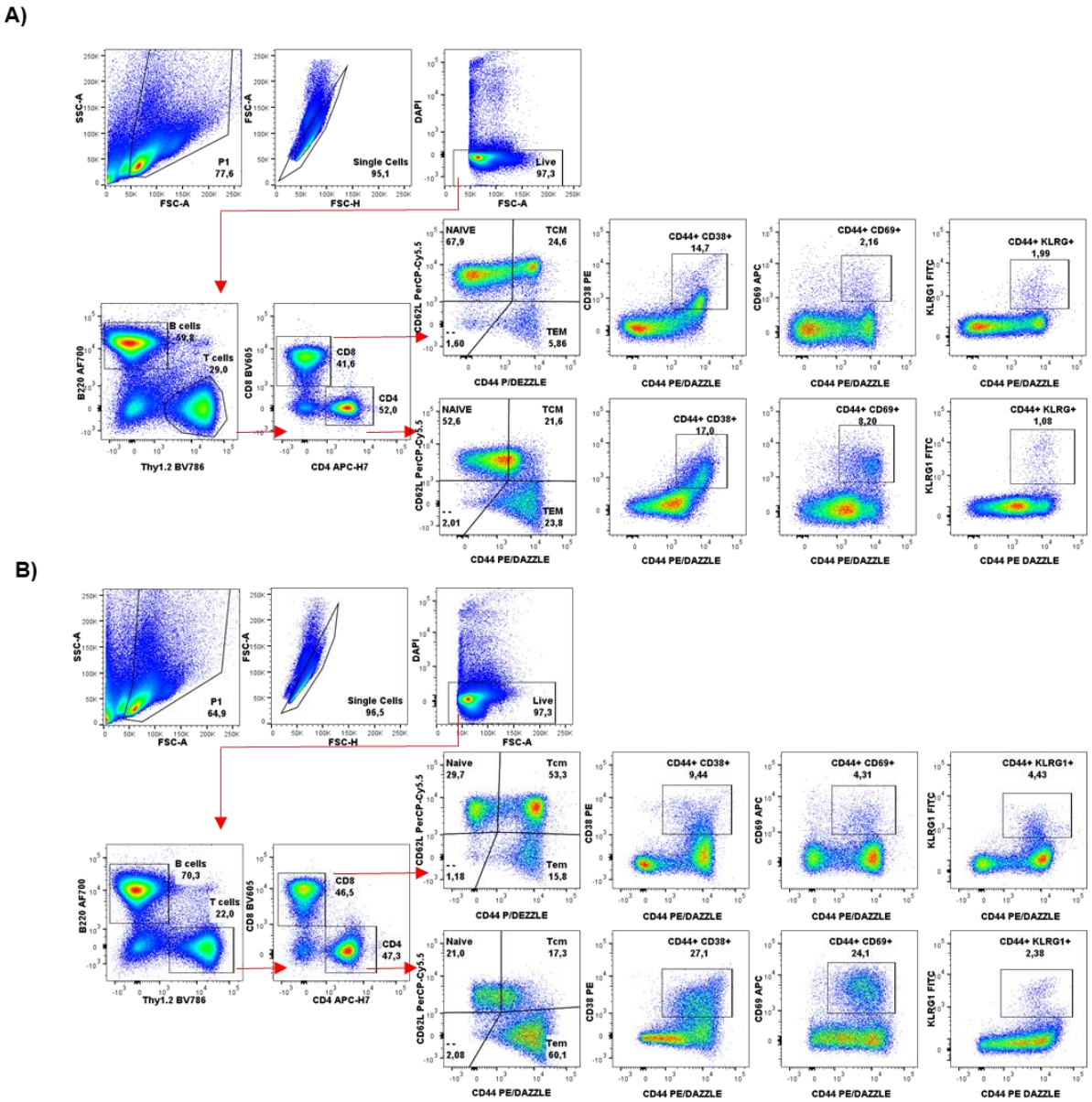

Figure 8. Representative gating strategy for peripheral immune cell characterization in young adult and old mouse spleens. Splenocytes were isolated from spleens of WT and Optn^{470T} male mice and gated as shown in (A) three-month-old and (B) two-year-old male mice. In brief, upon discarding doublets and dead cells, live cells were gated for T and B lymphocytes. T lymphocytes were gated on helper (CD4$^+$) and cytotoxic (CD8$^+$) subsets and further separated onto naive (CD44^{lo}CD62L$^+$), memory (central: CD44^{hi}CD62L$^+$, effector: CD44^{hi}CD62L$^-$), and activated subsets (CD44$^+$ CD38$^+$, CD44$^+$ CD69$^+$, and CD44$^+$ KLRG1$^+$).

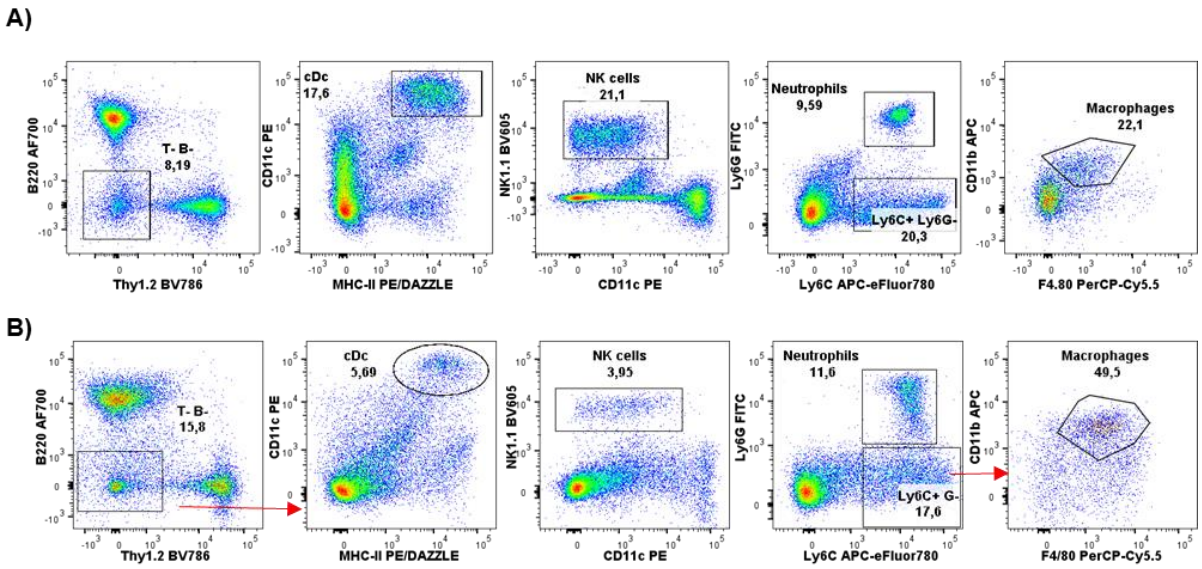

Figure 9. Representative gating strategy for myeloid and NK cells in young adult and old mouse spleens. Splenocytes were isolated from spleens of WT and Optn^{470T} male mice and gated as shown in (A) three-month-old and (B) two-year-old male mice. In brief, upon discarding doublets and dead cells, live cells were gated for cells negative for T and B cell markers (T^-B^-), and further separated on neutrophils ($Ly6C^+Ly6G^+$), macrophages/monocytes ($Ly6C^+Ly6G^-CD11b^+F4.80^+$), conventional dendritic cells (cDC; $CD11c^+MHC\text{-}II^+$) and NK cells ($NK1.1^+$).

3.4.7. Mice genotypization

3.4.7.1. DNA isolation and quantification

Mice genotypization was done using DNA isolated from individual mouse tails. Briefly, mouse tails were shaken at 900 rpm at 55°C O/N in 400 µL DNA lysing buffer in the presence of 0.4 mg/mL proteinase K. The next day, tail lysates were centrifuged at 12 000 rpm for 1 min at 4°C to get rid of residual hair. After the centrifugation, supernatants containing DNA were transferred to a new 1.5 mL Eppendorf tube, and an equal volume of isopropanol (400 µL) was added to the supernatants. The 1.5 mL Eppendorf tubes were strongly vortexed and centrifuged at 12 000 rpm for 10 min at 4°C. Supernatants were discarded and the DNA pellets were resuspended in 1 mL 70% ethanol and centrifuged again at 12 000 rpm for 10 min at 4°C. Supernatants were discarded again, and the DNA pellet was left to dry for 10 min at RT. DNA pellets were then resuspended in 100-200 µL dH20 (depending on the size of the pellet), and shaken at 900 rpm at 55°C for 1 h until DNA was fully dissolved. DNA purity and concertation were measured using UV/VIS spectrophotometer BioDrop Duo (BioDrop) at 260 nm wavelength, and the samples were stored at 4°C until further analyses.

3.4.7.2. Polymerase chain reaction (PCR)

The $Optn^{WT/WT}$ x $TDP\text{-}43^{G348C}$ and $Optn^{470T/470T}$ x $TDP\text{-}43^{G348C}$ transgenic mice were identified by PCR amplification of the human transgenic *TARDBP*, and WT and truncated optineurin gene using the primer pairs at the concentrations indicated in Table 15. The three separate PCR reactions for WT optineurin, truncated optineurin, and transgenic $TDP\text{-}43^{G348C}$ were performed. PCR reactions contained 1x EmeraldAmpGT PCR Master Mix buffer with dNTPs and DNA polymerase, forward and reverse primers, ~200 ng DNA isolated from mice tails, and DNase-free water to a final volume of 20 µL. The DNA was amplified in a thermocycler as shown in Table 19. in different programs for optineurin WT and truncated form, and transgenic *TARDBP* gene, because of different primer annealing temperatures.

Table 19. PCR program steps

Step	Temperature	Time	Number of cycles
Initial denaturation	95°C	30 sec	1x
Denaturation	95°C	30 sec	35x
Primer annealing	55°C (WT and $Optn^{470T}$) 59°C ($TDP\text{-}43^{G348C}$)	30 sec	
Elongation	72°C	60 sec	
Final elongation	72°C	600 sec	1x
Cooling	4°C	∞	/

3.4.7.3. Agarose gel electrophoresis

For DNA electrophoresis, agarose was dissolved in 1x TAE buffer to a final concentration of 2%. For DNA visualization, Gel Star dye (dilution 1:10000) was added to the agarose gel before polymerization, and DNA ladder 100 bp was the molecular weight standard. The agarose gel was run in 1x TAE buffer at 110 V till the dye reached the end of the gel. The DNA was visualized on Bio-Rad ChemiDocTM MP Imaging System (Bio-Rad). Optineurin WT band was visualized at 363 bp, truncated optineurin at 288 bp, and transgenic *TARDBP* at 365 bp, respectively.

3.4.8. Motor and behavioral tests on mice

3.4.8.1. RotaRod

To test motor coordination in mice, the RotaRod test was performed and measured as the latency time before falling off a rotating rod using the RotaRod apparatus (#47600, Ugo Basile S.R.L). The experiment is performed over two days. On the first (training) day, mice were familiarized with the RotaRod apparatus. Each mouse was given two trials at a fixed speed of 5 rpm for 4 min and the third trial at a fixed speed of 8 rpm for 3 min. Trials were 1 h apart from each other. On the second day, mice were tested three times at an accelerated mode from 5 rpm to 50 rpm for 300 s, with a 1 h pause in between each trial. Results are shown as an average time of three trials per mouse at indicated time points.

3.4.8.2. Passive avoidance

To test learning and fear-motivated memory, a passive avoidance test was performed and measured as the time needed for a mouse to enter the dark compartment (latency). Mice, as nocturnal animals, are primarily active during the night and physiologically choose dark areas (Steinlechner, 2012). In this experiment, however, mice tend to avoid entering the dark because they should associate discomfort due to electrical shock with darkness. In more detail, the experiment is performed over three days. On the first day, mice were left to explore the passive avoidance apparatus that consists of light and dark sections connected by an open door for 5 min. On the second day, mice were placed in the bright section, and the door was opened after 30 s. Upon entering the dark section, a mouse received a mild foot shock of 0.3 mA. The mouse was left to calm down and then returned to its cage. On the final day of the experiment, the mouse was placed in the bright section and the latency before entering the dark section was measured. Mice who remembered the previous exposure to shock tended to avoid entering the dark compartment during the 300 s of the test. Results are shown as one trial per mouse at the indicated time points.

3.4.9. Statistics

Statistical analysis was done using GraphPad Prism Software 8.0.1. Since all data met the criteria for normal distribution, statistical analyses were performed by Student's t-test and ordinary one-way and two-way ANOVA. A *p*-value of < 0.05 was considered statistically significant.

4. Results

4.1. Crosstalk of optineurin and TDP-43 in protein homeostasis and inflammation

4.1.1. Optineurin insufficiency led to increased TDP-43 protein levels in mouse myeloid cells

Due to the finding that patients carrying the *OPTN* mutations and optineurin deficient ($Optn^{-/-}$) mice have shown TDP-43 aggregation and TDP-43 nuclear depletion, we aimed to test the effects of homozygous C'-terminal truncation of optineurin on TDP-43 protein levels and *TARDBP* gene expression in optineurin insufficient ($Optn^{470T}$) mice. Previous findings from our group showed that optineurin deficiency (generated by CRISPR/Cas9 technology) in the BV2 microglial cell line led to an accumulation of TDP-43 (results from Matea's Rob Master thesis: https://urn.nsk.hr/urn:nbn:hr:193:162533) (Prtenjaca et al., 2022). To corroborate these findings in primary myeloid cells, neonatal microglia and bone marrow-derived macrophages (BMDMs) were isolated and differentiated from WT and $Optn^{470T}$ mice. Approximately two-fold higher TDP-43 protein levels were observed in $Optn^{470T}$ microglia (Fig. 10 A-B), and BMDMs (Fig. 10 D-E) compared to WT cells. Since TDP-43 binds and autoregulates its own mRNA expression (Polymenidou et al., 2011), RT-qPCR was performed to test if TDP-43 protein accumulation in $Optn^{470T}$ myeloid cells is due to the change in *TARDBP* gene expression. Interestingly, *TARDBP* mRNA expression was similar in primary WT and $Optn^{470T}$ microglia (Fig. 10 C) and BMDMs (Fig. 10 F), indicating that the elevated TDP-43 protein levels in $Optn^{470T}$ microglia and macrophages were due to post-translational modifications. Given that TDP-43 can be subjected to phosphorylation, ubiquitination, acetylation, and other post-translational modifications it remains to be seen which are altered in $Optn^{470T}$ primary myeloid cells (Prasad et al., 2019). In conclusion, optineurin insufficiency led to an increased level of TDP-43 protein in primary myeloid cells, and this effect was post-translationally regulated.

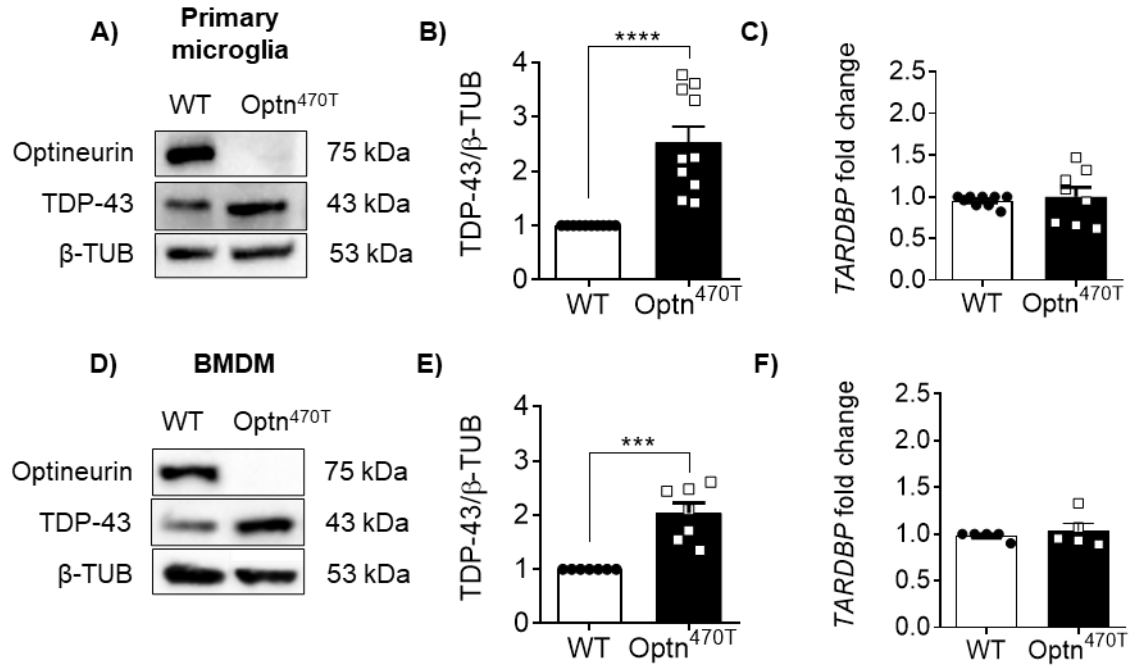

Figure 10. The basal level of TDP-43 is elevated in Optn^{470T} mouse primary microglia and BMDMs without changes in *TARDBP* mRNA levels. (A) Western blotting for TDP-43 and optineurin in WT and Optn^{470T} primary microglia. (B) Bar charts show the densitometric analysis of TDP-43 protein levels normalized to β-tubulin (β-TUB) in primary microglia. (C) mRNA for *TARDBP* in WT and Optn^{470T} microglia was assessed by RT-qPCR. (D) Western blotting for TDP-43 and optineurin in WT and Optn^{470T} BMDMs. (E) Bar charts show the densitometric analysis of TDP-43 protein levels normalized to β-tubulin (β-TUB) in BMDMs. (F) mRNA for *TARDBP* in WT and Optn^{470T} BMDMs was assessed by RT-qPCR. An average ± SEM from 5 (F), 7 (B), 9 (C), and 10 (E) independent experiments are shown; replicates are depicted as individual data points. Statistical analysis was performed by Student's t-test: *** $p<0.001$, **** $p<0.0001$.

4.1.2. Ubiquitin-proteasomal system inhibition causes apoptosis in WT and KO BV2 microglia cells

To assess the routes of TDP-43 degradation in the myeloid cells, two main mechanisms of protein degradation were investigated: UPS and autophagy. We first determined if inhibition of UPS and/or autophagy causes apoptosis that can affect TDP-43 protein levels. Since optineurin has several proposed roles in autophagy, we hypothesised that optineurin-deficient cells would be more sensitive to autophagy inhibition. We analysed BV2 Optn KO microglial cell lines and confirmed that optineurin was successfully knocked out with an efficiency of ~90% (Fig. 11 A and B). Caspases are crucial mediators of apoptosis, and among them, caspase-3, and its autoproteolytic cleavage fragment cleaved caspase 3 (CC3), catalyses the cleavage of many cellular proteins. Caspase 3 and CC3 can thus be monitored by Western blotting to assess the early steps of apoptosis initiation (Porter and Jänicke, 1999). We treated BV2 WT and Optn KO cells with UPS inhibitor MG132 for 4 h and 8 h, with or without the addition of an autophagy inhibitor Baf A1 for the last 4 h of the experiment, and tested caspase 3 and CC3 levels. Caspase 3 did not show a significant change upon UPS and/or Baf A1 treatment in WT or Optn KO cells (Fig. 11 A and C). Upon 4 h of UPS inhibition CC3 was present at low levels, not significantly different from untreated cells in both WT and Optn KO cells. On the contrary, 8 h of UPS inhibition led to significantly increased CC3 in WT cells, indicating activation of apoptosis (Fig. 11 A and D). However, there was no obvious difference in CC3 levels between WT and Optn KO cells. Interestingly, additional blockade of autophagy did not further exaggerate apoptosis activation upon UPS inhibition, as CC3 was not increased in the presence of Baf A1 (Fig. 11 A and D). Overall, 8 h of UPS inhibition activated apoptosis in both BV2 WT and Optn KO cells and affected TDP-43 protein levels (see section below). In addition, we did not observe increased sensitivity in optineurin-deficient cells upon autophagy blockade.

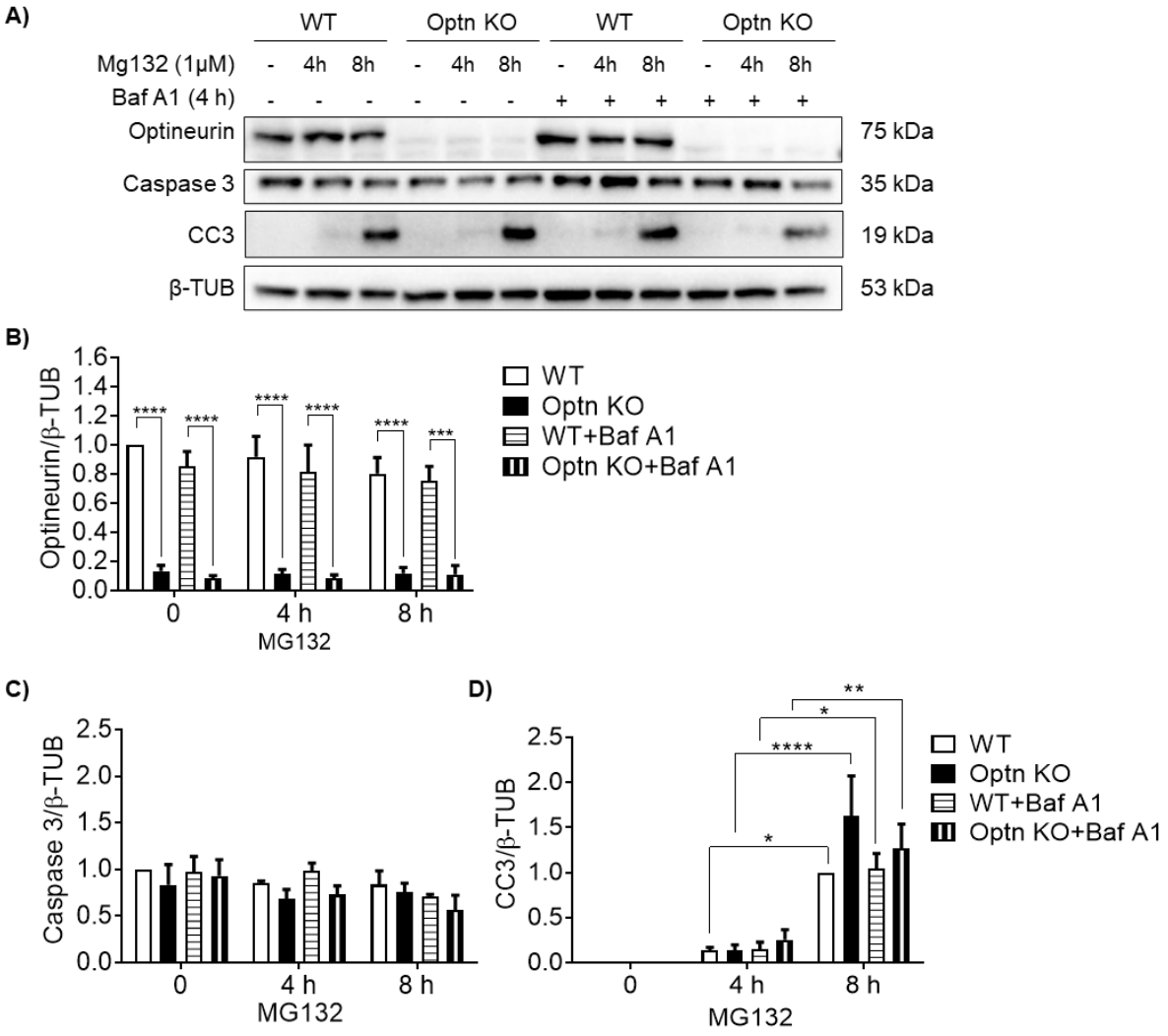

Figure 11. UPS inhibition activates apoptosis similarly in BV2 WT and Optn KO cells. (A) Western blotting was done for caspase 3, cleaved caspase 3 (CC3), and optineurin in BV2 WT and Optn KO microglial cell lines treated with UPS inhibitor MG132 (1 μM) for 4 h and 8 h, and/or autophagy inhibitor Baf A1 (50 nM) for 4 h. Bar charts show the densitometric analysis for (B) optineurin, (C) caspase 3 and (D) CC3 protein levels normalized to β-tubulin in microglial cell lines. An average ± SEM from 4 independent experiments is shown. Statistical analysis was performed by two-way ANOVA; * p<0.05, ** p<0.01, *** p<0.001, **** p<0.0001.

4.1.3. Block in autophagy did not trigger TDP-43 accumulation in BV2 Optn KO microglia cell line

To analyse if optineurin-deficient microglial cells have increased TDP-43 due to impaired turnover by UPS or autophagy, we blocked UPS with MG132 inhibitor for 4 h, with or without the addition of autophagy inhibitor Baf A1 in BV2 WT and Optn KO cells, and assessed the TDP-43 protein levels by Western blotting. No major optineurin degradation happened upon 4 h by UPS inhibition in BV2 WT cells, whereas the degradation by autophagy showed a non-significant trend (Fig. 12 A-B). Of note, we could not analyse the level of truncated optineurin due to the inability of commercial antibodies to detect this fragment since most antibodies target the C'-terminus. Inhibition of UPS or autophagy for 4 h showed a small but significant accumulation of TDP-43 in WT cells, demonstrating that around ~20% of TDP-43 was separately degraded through both UPS and autophagy (Fig. 12 A and C). Optn KO cells again showed significantly more TDP-43 in the basal state. Moreover, a trend in the accumulation of TDP-43 was also observed in Optn KO cells upon autophagy inhibition meaning that an accumulation of TDP-43 was not due to the block in autophagy in optineurin-deficient cells (Fig. 12 A and C). Interestingly, simultaneous inhibition of both UPS and autophagy did not further increase TDP-43 protein levels in WT cells. Surprisingly, it decreased the levels of TDP-43 in both BV2 WT and Optn KO cells suggesting that the blockade of both degradation mechanisms could exert some toxic effects. In Optn KO cells, the simultaneous inhibition of both degradation mechanisms decreased TDP-43 levels, suggesting the potential higher toxicity in optineurin-deficient cells, but we could not directly confirm this as we did not see increased apoptosis in Optn KO microglial cells. To conclude, block in either autophagy or UPS is not a cause for the observed accumulation of TDP-43 protein in optineurin-deficient microglial cells.

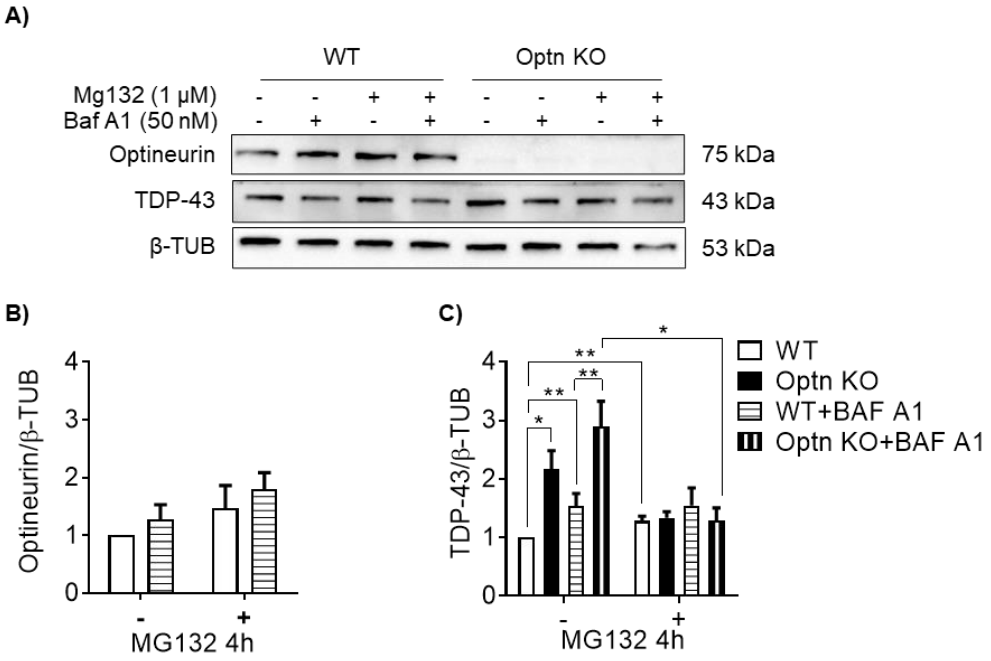

Figure 12. TDP-43 protein accumulation in BV2 Optn KO cells is not caused by a block in autophagy or UPS. (A) Western blotting for TDP-43 and optineurin in BV2 WT and Optn KO microglial cell lines treated with UPS inhibitor MG132 (1 μM) and autophagy inhibitor Baf A1 (50 nM) for 4 h. Bar charts show the densitometric analysis of (B) optineurin and (C) TDP-43 protein levels normalized to β-tubulin (β-TUB) in BV2 microglial cells. An average ± SEM from 9 (without MG132) and 4 (with MG132) independent experiments is shown. Statistical analysis was performed by two-way ANOVA: * $p<0.05$, ** $p<0.01$.

4.1.4. Block in autophagy did not trigger TDP-43 accumulation in Optn^{470T} mouse primary microglia

Observed results in BV2 Optn KO microglia could be due to some unknown genetic mutation(s) linked to immortalized cell lines, so we next performed an analysis of TDP-43 degradation in WT and Optn^{470T} primary microglia. No optineurin degradation in WT primary microglia happened upon 4 h of UPS and/or autophagy inhibition (Fig. 13 A-B). Moreover, TDP-43 turnover by each degradation mechanism showed a small, but non-significant trend in WT cells (Fig. 13 A and C). This means that TDP-43 protein degradation was slower in primary microglia cells than in BV2 microglial cell lines. Although higher levels of TDP-43 were present in the basal state in Optn^{470T} compared to WT microglia, we detected the same trend in TDP-43 turnover by UPS. Notably, the inhibition of autophagy did not change the TDP-43 protein levels in Optn^{470T} microglia (Fig. 13 A and C). Simultaneous inhibition of UPS and autophagy led to a small but non-significant accumulation of TDP-43 in WT microglia. Moreover, similar to findings in BV2 Optn KO cells, we observed an unexpected drop in TDP-43 in Optn^{470T} primary microglia in these conditions. Notably, we did not detect CC3 in neither WT nor Optn^{470T} microglia upon simultaneous UPS and autophagy inhibition. Because there was no apoptosis initiation, we cannot explain the drop of TDP-43 in Optn^{470T} microglia at this moment nor we can conclude that the accumulation of TDP-43 in these cells is related to a block in autophagy.

Since we did not observe that optineurin affects TDP-43 degradation through autophagy, we further characterized if optineurin insufficiency causes autophagy block in general. We analysed autophagy flux by monitoring LC3-I to LC3-II conversion by Western blot (Fig. 13 A and D). Inhibition of UPS did not affect LC3-I to LC3-II conversion or LC3-II protein level in both WT or Optn^{470T} primary microglia. Moreover, autophagy inhibition in WT microglia led to the accumulation of LC3-II demonstrating an active autophagy flux. Interestingly, inhibition of basal autophagy in Optn^{470T} microglia showed the same accumulation of LC3-II, demonstrating that a loss of functional optineurin did not cause a block in autophagy flux. Moreover, simultaneous inhibition of UPS and autophagy did not exaggerate the levels of LC3-II in both WT and Optn^{470T} microglia cells, meaning that UPS inhibition did not further increase autophagy. To sum up, the elevated levels of TDP-43 in optineurin-

insufficient primary microglia, same as in optineurin-deficient BV2 cell lines, could not be explained by a block in neither autophagy nor UPS.

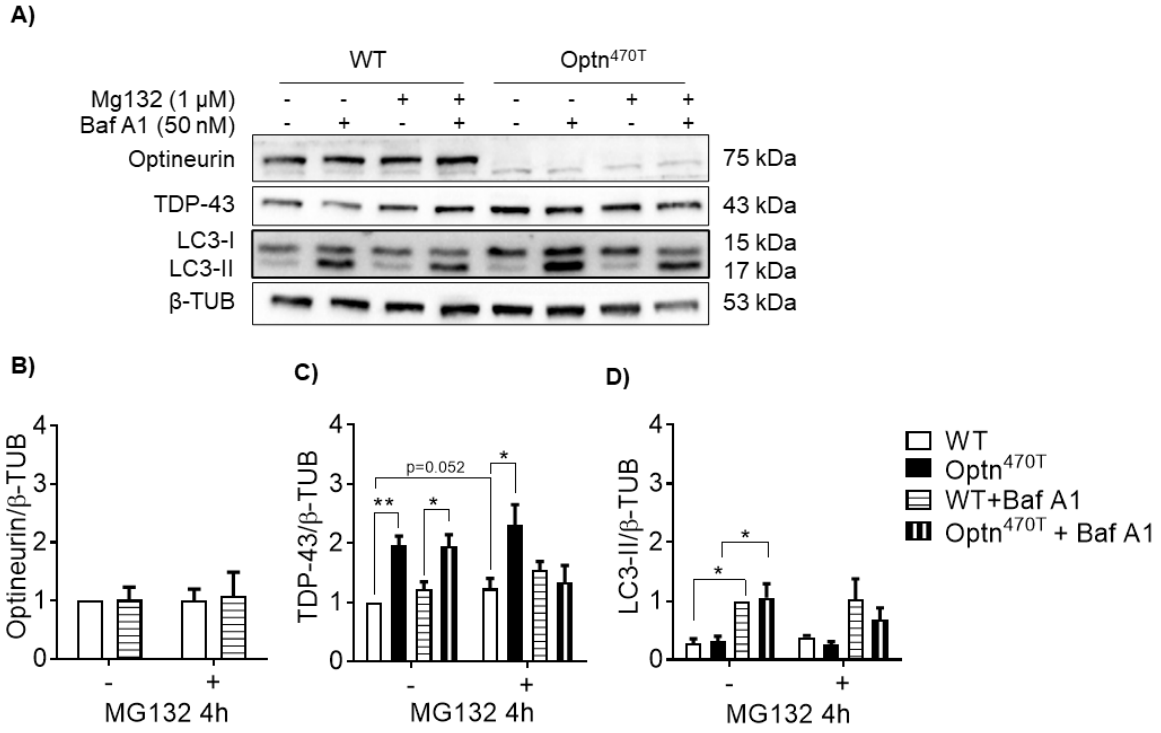

Figure 13. TDP-43 protein accumulation in Optn^{470T} mouse primary microglia was not caused by a block in autophagy or UPS. (A) Western blotting for TDP-43, optineurin, and LC3-I and LC3-II in WT and Optn^{470T} primary microglia treated with MG132 (1 μM) and Baf A1 (50 nM) for 4 h. Bar charts show the densitometric analysis of (B) optineurin, (C) TDP-43, (D) LC3-I, and LC3-II protein levels normalized to β-tubulin (β-TUB) in primary microglia cells. An average ± SEM from 9 (without MG132) and 3-4 (with MG132) independent experiments are shown. Statistical analysis was performed by two-way ANOVA: * $p<0.05$, ** $p<0.01$, *** $p<0.001$.

4.1.5. TDP-43 turnover in WT BMDMs requires autophagy but autophagy inhibition did not trigger TDP-43 accumulation in Optn^{470T} mouse BMDMs

Given the unexpected lack of autophagy block in optineurin-deficient or -insufficient microglia, which contrasted recent literature (Kurashige et al., 2021), we also analysed an autophagy flux in primary BMDMs. To this end, we treated WT and Optn^{470T} mouse BMDMs with an autophagy inhibitor Baf A1 for 4 h and assessed the TDP-43, LC3-I, and LC3-II protein levels by Western blotting (Fig. 14 A). We observed elevated TDP-43 protein levels upon autophagy inhibition in WT BMDMs, demonstrating that TDP-43 turnover requires autophagy (Fig. 14 A-B). Upon autophagy inhibition, TDP-43 stayed at an already elevated state as in the basal conditions in Optn^{470T} BMDMs suggesting a block in TDP-43 degradation via autophagy. Interestingly, we observed similar LC3-II levels upon autophagy inhibition in Optn^{470T} BMDM, thus showing that the basal autophagy flux was comparable to WT BMDMs (Fig. 14 A and C). In conclusion, by blocking the final step of autophagy (fusion of autophagosome and lysosome) by Baf A1 we observed the accumulation of TDP-43 in WT BMDMs, demonstrating that TDP-43 turnover requires autophagy. However, TDP-43 accumulation in Optn^{470T} BMDMs could not be explained by general block in LC3-mediated autophagy as we observed a similar LC3-I to LC3-II conversion as in WT BMDMs.

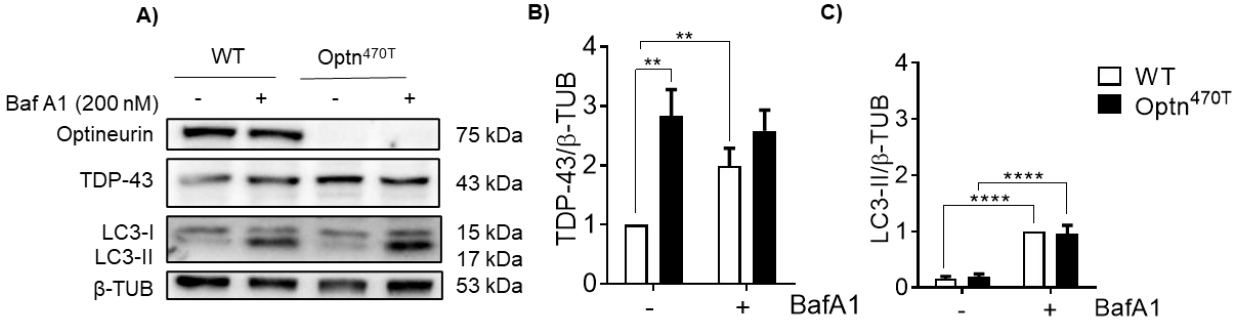

Figure 14. TDP-43 protein accumulation in Optn^{470T} mouse BMDMs was not caused by a block in autophagy. (A) Western blotting for optineurin, TDP-43, and LC3-I and LC3-II in WT and Optn^{470T} BMDMs upon treatment with Baf A1 (200 nM) for 4 h. Bar charts show the densitometric analysis of (B) TDP-43, and (C) LC3-II protein levels normalized to β-tubulin (β-TUB). An average ± SEM from 6 (B) and 7 (C) independent experiments is shown. Statistical analysis was performed by Student's t-test: ** p<0.01, **** p<0.0001.

4.1.6. Optineurin insufficiency caused diminished degradation of TDP-43 protein in mouse primary cortical neurons

In contrast to myeloid cells, previous findings from our group did not show TDP-43 accumulation in optineurin-deficient neuronal Neuro2A and NSC-34 cell lines (results from Matea's Rob Master thesis: https://urn.nsk.hr/urn:nbn:hr:193:162533) (Prtenjaca et al., 2022). To confirm this, we isolated primary cortical neurons from E15.5 days-old WT and Optn^{470T} mouse embryos. This is the period of strongest neurogenesis which occurs in the absence of gliogenesis *i.e.* generation of glial cells (happening as sequential and largely non-overlapping processes) to ensure only neuronal cell presence (Miller and Gauthier, 2007). After five days of cultivation, we analysed UPS and autophagy in WT and Optn^{470T} mouse primary cortical neurons by blocking UPS with MG132 inhibitor for 4 h and 8 h, with or without the addition of autophagy inhibitor Baf A1, and assessed the TDP-43 protein levels. The levels of optineurin demonstrated negligible changes upon blocking of UPS and/or autophagy (Fig. 15 A). TDP-43 was degraded through both autophagy and UPS in WT primary neurons, seen as an accumulation of TDP-43 upon UPS or autophagy inhibition already after 4 h (Fig 15 A-B). Notably, more TDP-43 was degraded through UPS than autophagy. Simultaneous inhibition of UPS and autophagy did not further increase TDP-43 in WT primary neurons. Notably, these findings confirm our results from microglia that TDP-43 is getting degraded independently through both UPS and autophagy and that inhibition of UPS is not increasing autophagy. Surprisingly, in comparison to our finding in the neuronal N2A and NSC-34 cell lines, Optn^{470T} primary neurons had significantly elevated TDP-43 protein levels in the basal state. Similar to microglia, TDP-43 accumulation in Optn^{470T} primary neurons was also post-transcriptionally regulated, as we did not observe the difference in *TARDBP* expression (Fig. 15 E). Furthermore, in Optn^{470T} primary neurons, TDP-43 was not accumulating upon inhibition of UPS or autophagy suggesting that optineurin-insufficiency caused the block in TDP-43 degradation. Simultaneous inhibition of UPS and autophagy caused a drop in TDP-43 in Optn^{470T} primary neurons, similar to results obtained in primary microglia. Again, as we did not detect apoptosis initiation (presence of CC3) in Optn^{470T} cortical neurons, we cannot explain the potential toxicity of TDP-43 drop at this moment.

As autophagy is particularly important in neurons, and we observed a block in TDP-43 turnover via autophagy in optineurin-insufficient neurons to further test this, we treated WT and Optn^{470T} primary cortical neurons with trehalose, an mTOR-independent inducer of autophagy that most likely acts by inducing lysosomal enlargement and membrane permeabilization (Benito-Cuesta et al., 2021; Rusmini et al., 2018; Sarkar et al., 2007). In WT primary neurons there was a significant accumulation of TDP-43 upon trehalose, demonstrating that in contrast to our hypothesis, TDP-43 was not getting more degraded through trehalose-induced autophagy (Fig. 15 C-D). Compared to WT neurons, trehalose did not cause an accumulation of an already elevated TDP-43 in Optn^{470T} primary neurons. Interestingly, we again observed a decrease in TDP-43 upon simultaneous treatment with trehalose and Baf A1 in Optn^{470T} primary neurons. In conclusion, optineurin-insufficiency leads to the accumulation of TDP-43 in the basal state in primary cortical neurons, similar to our results in primary myeloid cells from Optn^{470T} mice. Moreover, TDP-43 in WT primary neurons is degraded by both autophagy and UPS. However, we demonstrated that Optn^{470T} primary cortical neurons had a block in TDP-43 turnover via autophagy that should be further tested.

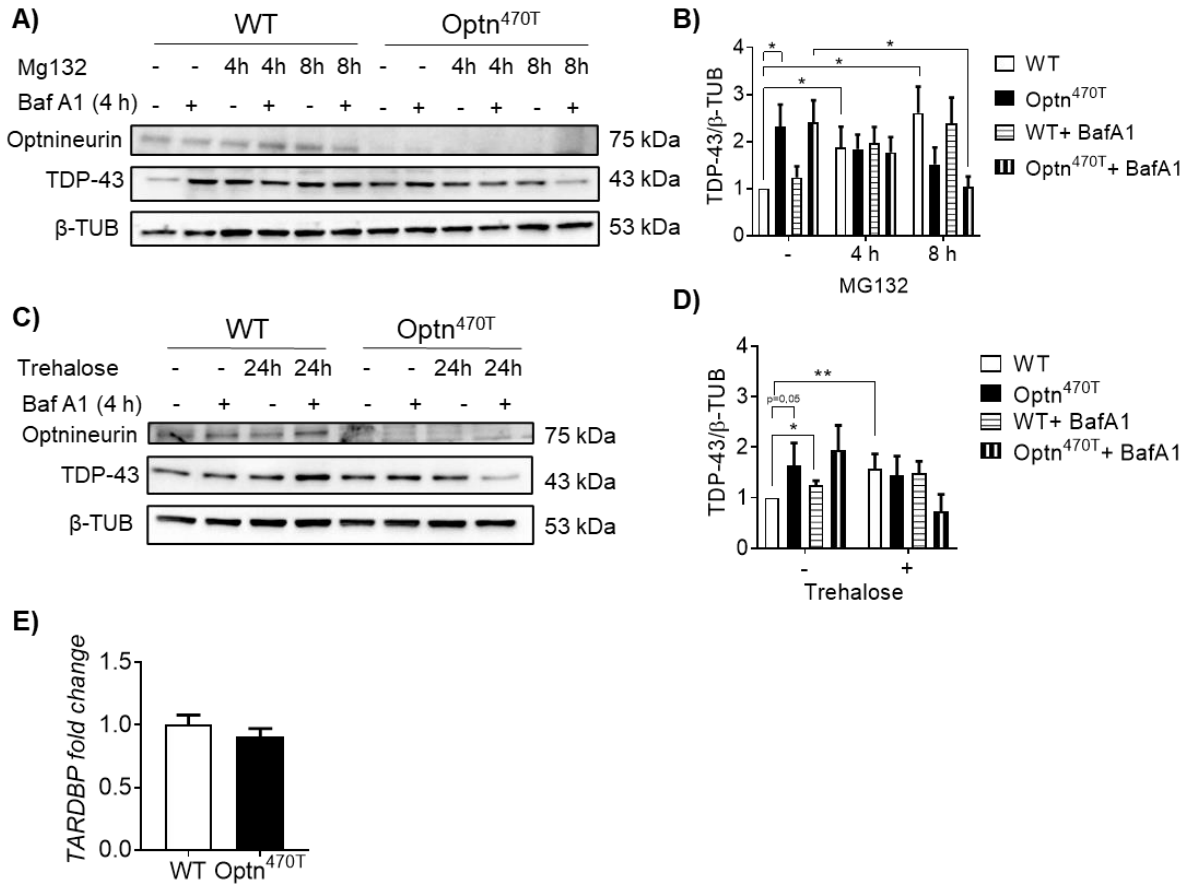

Figure 15. TDP-43 protein accumulation in Optn^{470T} mouse primary neurons is caused by a block in TDP-43 degradation by autophagy. (A) Western blotting for TDP-43 and optineurin in WT and Optn^{470T} primary neurons treated with MG132 (1 μM) for 4 and 8 h and Baf A1 (50 nM) for the last 4 h of the experiment. (B) Bar charts show the densitometric analysis of TDP-43 protein levels normalized to β-tubulin (β-TUB) in primary neurons. (C) Western blotting for TDP-43 and optineurin in WT and Optn^{470T} primary neurons treated with Trehalose (100 mM) for 24 h and Baf A1 (50 nM) for the last 4 h of the experiment. (D) Bar charts show the densitometric analysis of TDP-43 protein levels normalized to β-tubulin (β-TUB) in primary neurons. E) mRNA for *TARDBP* in WT and Optn^{470T} primary neurons was assessed by RT-PCR. An average ± SEM 3-4 independent experiments are shown. Statistical analysis was performed by Student's t-test: * $p<0.05$, ** $p<0.01$.

4.1.7. LPS treatment increased TDP-43 in WT cells but failed to increase an already elevated TDP-43 in optineurin-deficient and insufficient microglia

As we did not detect diminished TDP-43 protein turnover in optineurin-deficient and -insufficient microglia, we next tested if increased TDP-43 levels in these cells were due to their activation. Activation of microglia is crucial for the removal of bacterial and viral infections and the clearing of cellular debris. It was previously reported that LPS triggers TDP-43 aggregation and mislocalization in microglia (Correia et al., 2015), so we further tested how the lack of functional optineurin affects TDP-43 protein levels upon inflammatory stimuli. To test this, both BV2 WT and Optn KO microglial cells and WT and Optn^{470T} primary microglia were treated with two doses of LPS for 24 h, and TDP-43 protein levels were determined by Western blotting. Optineurin levels did not change upon LPS treatment in WT cells (Fig. 16 B and E). In line with the previous finding by Correia *et al*., we detect elevated TDP-43 protein levels upon LPS in a dose-dependent manner in BV2 WT cells (Fig. 16 A and C), and WT primary microglia (Fig. 16 D and F). On the contrary, in the BV2 Optn KO cells (Fig. 16 A and C) and Optn^{470T} primary microglia (Fig. 16 D and F) LPS did not cause any further increase in the already elevated TDP-43 protein levels. In conclusion, TDP-43 protein levels reached a plateau in the basal state in optineurin-deficient and -insufficient microglial cells that could not further increase upon LPS treatment in comparison to WT cells. As TDP-43 functions in a very narrow concentration window, we speculate that optineurin-deficiency or - insufficiency leads to a TDP-43 plateau, possibly due to a low level of chronic activation but this hypothesis should be further tested.

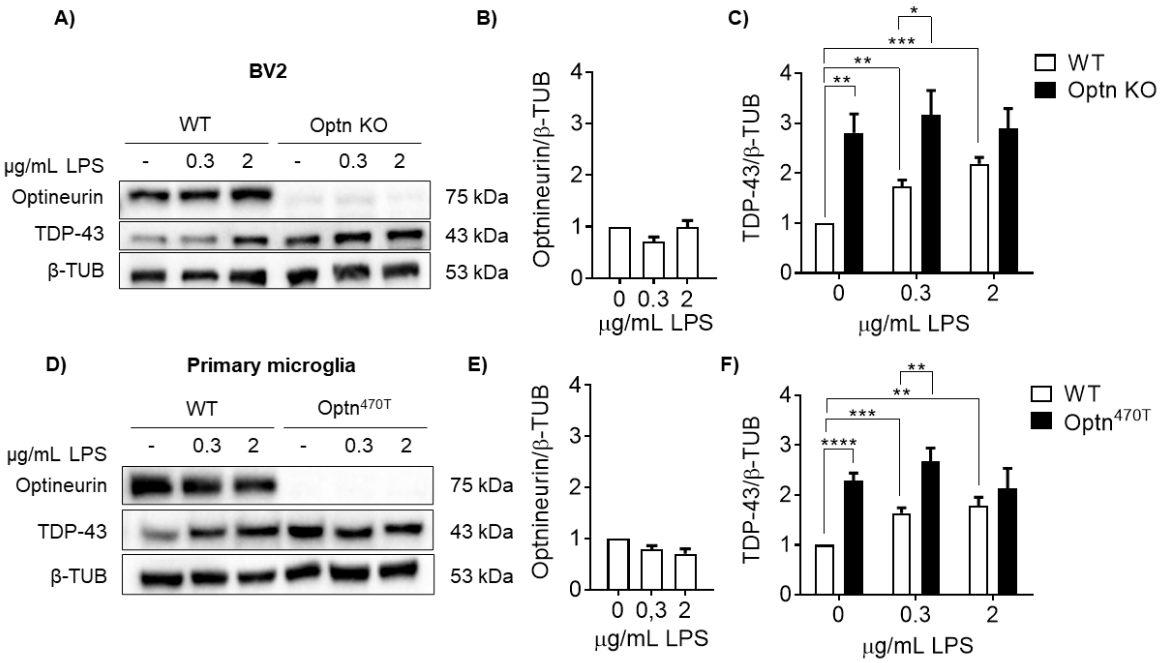

Figure 16. LPS treatment did not cause the further increase of TDP-43 levels in BV2 Optn KO and Optn^{470T} mouse primary microglia. (A) Western blotting for TDP-43 and optineurin in BV2 WT and Optn KO cell lines upon two different doses of LPS (0.3 µg/mL and 2 µg/mL) for 24 h. Bar charts show the densitometric analysis of (B) optineurin and (C) TDP-43 protein levels normalized to β-tubulin (β-TUB) in the BV2 WT and Optn KO cell line. (D) Western blotting for TDP-43 and optineurin in WT and Optn^{470T} primary microglia upon two different doses (0.3 µg/mL and 2 µg/mL) of LPS for 24 h. Bar charts show the densitometric analysis of (E) optineurin and (F) TDP-43 protein levels normalized to β-tubulin (β-TUB) in WT and Optn^{470T} primary microglia. An average ± SEM from 5 independent experiments is shown. Statistical analysis was performed by Student's t-test: * p<0.05, ** p<0.01, *** p<0.001, **** p<0.0001.

4.1.8. Increased TDP-43 did not elicit TDP-43 protein aggregation in optineurin insufficient mouse primary microglia

TDP-43 protein is the main component of protein aggregates found in the neuronal and glial cell cytoplasm of ALS and FTD patients (Arai et al., 2006; Neumann et al., 2006). Previous findings reported that inflammatory stimuli, such as LPS, deplete both WT and aggregation-prone mutated TDP-43 from the nucleus and form cytoplasmic aggregates in microglia (Correia et al., 2015). To test if TDP-43 accumulation in Optn^{470T} microglia and LPS-treated WT microglia causes TDP-43 nuclear depletion and aggregation, we treated primary microglia with LPS for 24 h and performed immunocytochemistry for TDP-43 and β-tubulin. In the basal state in WT microglia, TDP-43 showed normal distribution with predominantly nuclear localization while around 20% of TDP-43 was present in the cytoplasm. (Neumann et al., 2006) (Fig. 17 A-B). Therefore, TDP-43 in basal state in Optn^{470T} microglia did not result in increased TDP-43 cytoplasmic aggregation or nuclear depletion. Interestingly, TDP-43 in Optn^{470T} microglia demonstrated normal distribution with no aggregates and a small increase in nuclear TDP-43 compared to WT cells (Fig. 17 A and C). Upon 24 h of LPS, both WT and Optn^{470T} primary microglia changed their shape from ramified to an ameboid form, which was visualised by the change in β-tubulin, demonstrating an efficient microglial activation (Fig. 17 A). Surprisingly and in contrast to Correia et al., there was no TDP-43 nuclear depletion or aggregation upon 24 h of LPS treatment in WT microglia. However, we demonstrated a significant decrease in cytoplasmic (Fig. 17 B), and an increase in TDP-43 nuclear/cytoplasmic ratio (Fig. 17 C). This suggested that increased TDP-43 in WT microglia, which were observed upon LPS by Western blotting, were localised in the nucleus. Furthermore, TDP-43 in the Optn^{470T} microglia upon LPS demonstrated a non-significant drop in the percentage of cytoplasmic TDP-43 and a smaller increase in nuclear/cytoplasmic ratio compared to WT microglia. This could mean that elevated TDP-43 in Optn^{470T} microglia, which upon LPS showed the same protein levels as in basal condition, is also less responsive to cellular redistribution than TDP-43 in WT cells. Interestingly, a similar phenotype was observed in the lumbar spinal cord in rats, where microglia were less responsive to inflammatory stimuli, most likely demonstrating exhaustion and/or desensitization (Nikodemova et al., 2014). In conclusion, elevated TDP-43 protein levels in basal state in Optn^{470T} and LPS-treated WT microglia did not trigger

nuclear depletion, nor cytoplasmic aggregation of TDP-43. In inflammatory conditions, TDP-43 showed increased nuclear localization that was slightly more prominent in WT microglia.

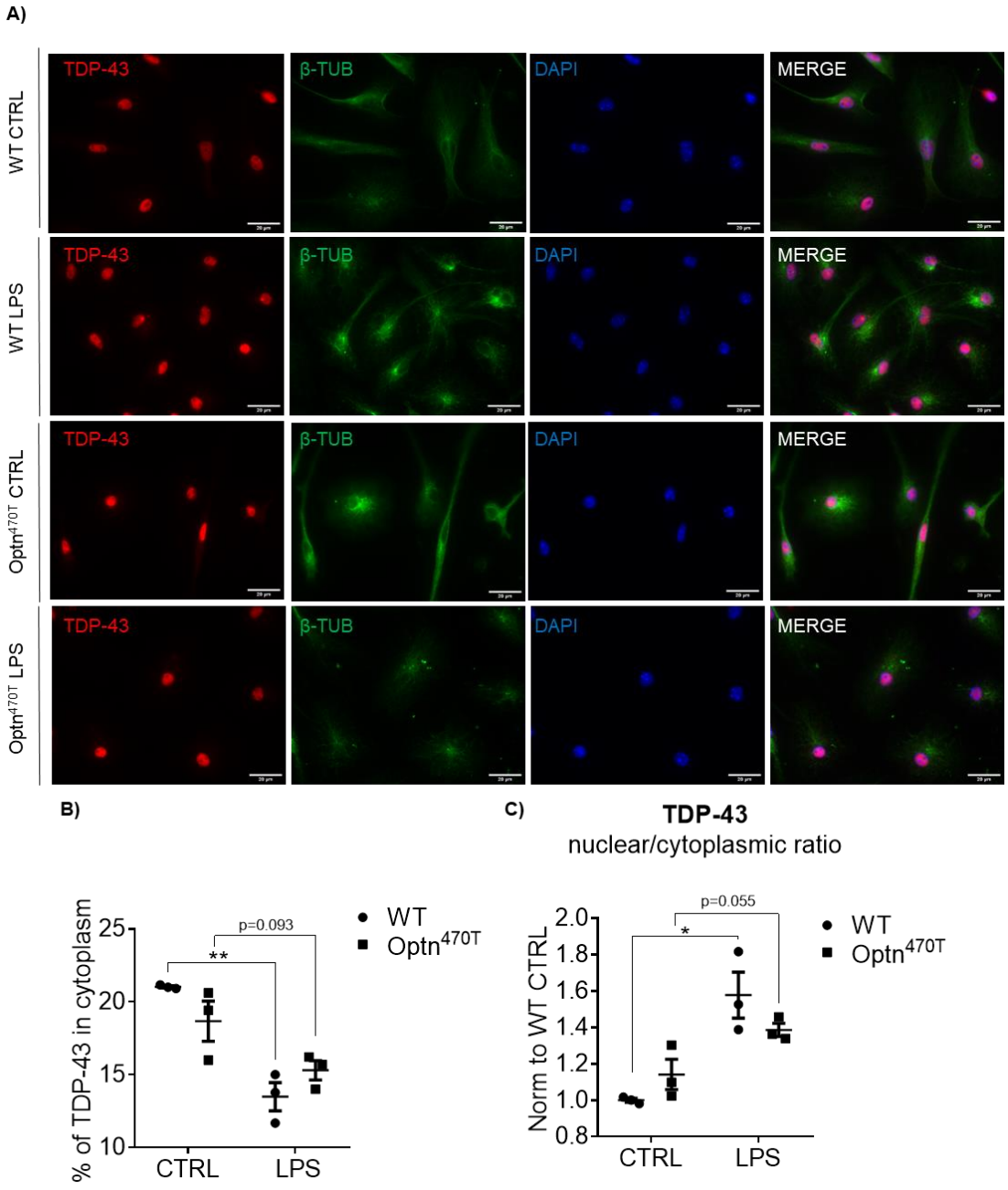

Figure 17. TDP-43 is predominantly nuclear in untreated or LPS-treated WT and Optn^{470T} mouse primary microglia. (A) Representative images of immunofluorescence staining for TDP-43 (red), β-tubulin (β-TUB; green), and DAPI (blue) in WT and Optn^{470T} microglia in the basal state and stimulated with 2 µg/mL of LPS for 24 h. (B) The graph shows % of TDP-43 in the cytoplasm in the basal state and upon LPS treatment. (C) The nuclear to cytoplasmic ratio of TDP-43 MFI is shown in WT and Optn^{470T} microglia. An average ± SEM from 3 independent experiments is shown. Statistical analysis was performed by Student's t-test: * $p<0.05$, ** $p<0.01$.

4.1.9. Upon LPS treatment TDP-43 accumulated in WT mouse BMDMs was not further enhanced by autophagy inhibition, while in Optn^{470T} mouse BMDMs TDP-43 did not show additional accumulation upon any stimuli

We have previously detected elevated TDP-43 protein levels in Optn^{470T} mouse primary microglia and BMDMs that did not change upon LPS treatment. Moreover, we observed a block in TDP-43 turnover in Optn^{470T} BMDM, so we wanted to further examine if TDP-43 protein levels during inflammation are regulated by autophagy. WT and Optn^{470T} BMDMs were treated with two doses of LPS for 24 h, with the addition of autophagy inhibitor Baf A1 for the last 4 h, and optineurin and TDP-43 protein levels were analysed by Western blotting. In contrast to WT microglial cells, optineurin decreased upon LPS treatment in WT BMDMs, but autophagy inhibition did not change its levels suggesting that was not degraded through autophagy in BMDMs (Fig. 18 A-B). Same as in WT BV2 and primary microglia, TDP-43 protein levels were elevated in a dose-dependent manner upon LPS in WT BMDMs. As observed before, TDP-43 was degraded through autophagy in basal state in WT BMDMs, but surprisingly not upon LPS treatment (Fig. 18 A and C). In contrast to WT BMDMs, we observed elevated TDP-43 protein levels in the basal state in Optn^{470T} BMDMs that were autophagy-independent. Moreover, upon simultaneous stimulation with LPS and autophagy inhibition TDP-43 is decreased in Optn^{470T} BMDMs, but for now, we could not explain this drop in TDP-43.

To further investigate autophagy upon LPS treatment in optineurin-insufficient BMDMs, we analysed autophagy markers p62, LC3-I, and LC3-II (Fig. 18 A, D-E). We observed minor accumulation in p62 in the basal state in Optn^{470T} compared to WT BMDMs. However, we showed a small basal p62 turnover via autophagy only in WT cells. The p62 levels were significantly increased upon LPS treatment in both WT and Optn^{470T} BMDMs, but its turnover was independent of autophagy (Fig. 18 A and D). The latter suggests that p62 did not act as an autophagy adaptor upon LPS treatment in BMDMs, but was rather increased due to the activation of inflammatory signalling pathways. Moreover, LPS did not significantly change an autophagy flux as we observed similar LC3-II levels in the basal state and upon LPS treatment in both WT and Optn^{470T} BMDM (Fig. 18 A and E). To sum up, TDP-43 accumulated in WT BMDMs upon LPS, and this accumulation was not further enhanced by autophagy inhibition. Optineurin-insufficient BMDMs, similar to results observed in microglia, did

not show additional TDP-43 protein accumulation upon LPS. Finally, we showed that general autophagy flux, measured by LC3-I to LC3-II conversion was comparable in WT and Optn^{470T} BMDMs and was unaffected by LPS stimulation.

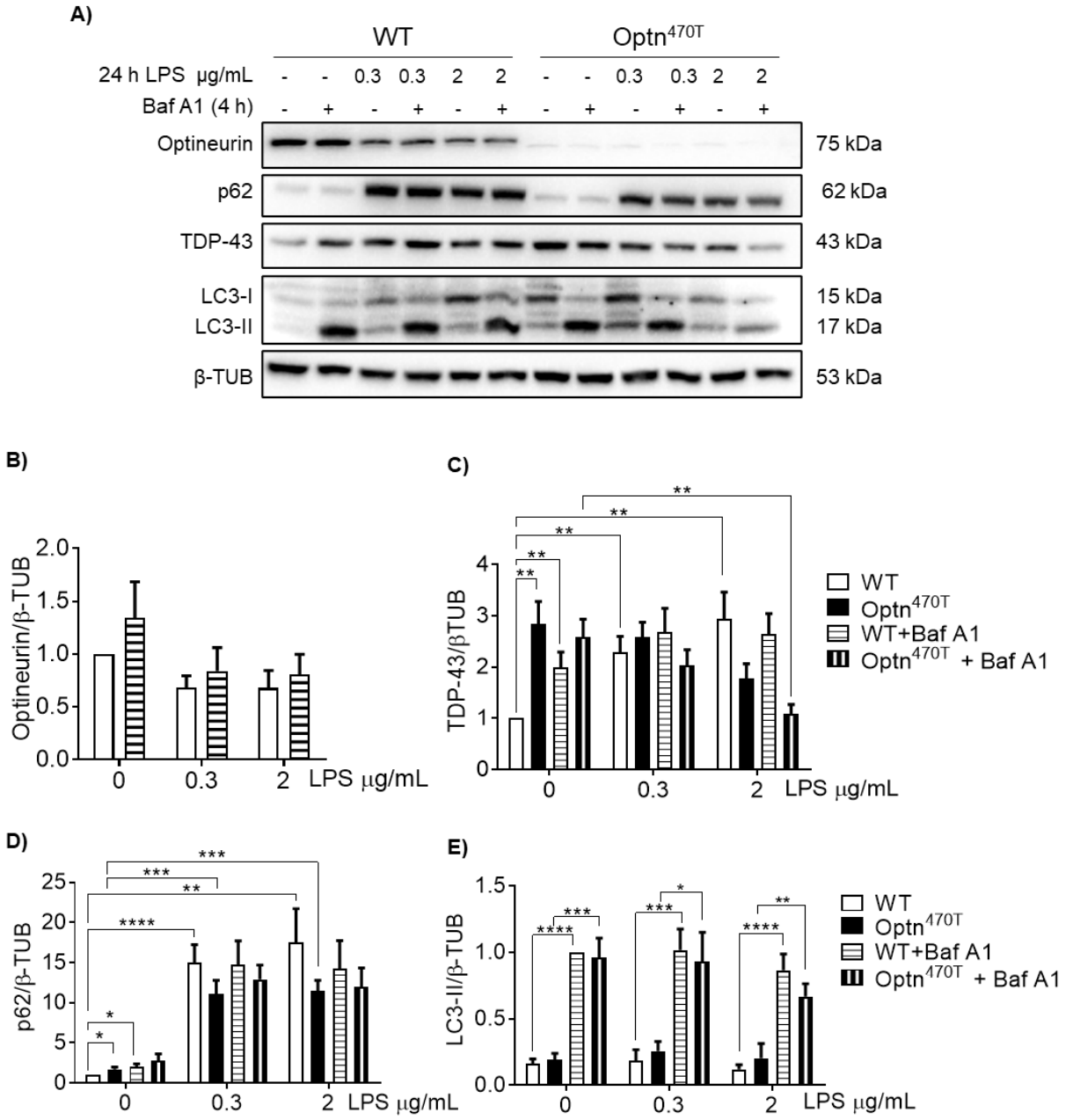

Figure 18. Autophagy flux is comparable in WT and Optn^{470T} mouse BMDMs and is not required for the turnover of accumulated TDP-43 in LPS-treated WT and Optn^{470T} BMDMs. (A) Western blotting for optineurin, p62, TDP-43, and LC3-II in WT and Optn^{470T} BMDMs upon two different doses (0.3 µg/mL and 2 µg/mL) of LPS for 24 h and autophagy inhibitor Baf A1 (50 nM) for 4 h. Bar charts show the densitometric analysis of (B) optineurin, (C) TDP-43, (D) p62 and E) LC3-II protein levels normalized to β-tubulin in WT and Optn^{470T} BMDMs. An average ± SEM from 6 independent experiments is shown. Statistical analysis was performed by Student's t-test: * p<0.05, ** p<0.01, *** p<0.001, **** p<0.0001.

4.1.10. LPS treatment changed the transcription of genes downstream of TDP-43 in WT and Optn^{470T} mouse BMDMs and primary microglia

TDP-43 regulates the transcription of various genes as well as its own transcription by binding on 3' UTR regions of mRNA (Buratti and Baralle, 2008). Since we observed elevated TDP-43 in basal state in Optn^{470T} and LPS-treated WT myeloid cells we analysed whether this affects its transcriptional activity. To test this, we performed RT-qPCR in WT and Optn^{470T} BMDMs and primary microglia upon 24 h of LPS treatment. In WT BMDMs *TARDBP* expression was reduced only upon 2 µg/mL of LPS, while in Optn^{470T} cells a significant decrease occurred with both doses (Fig. 19 A). There were minor changes in *TARDBP* expression in WT upon 0.3 µg/mL of LPS, while Optn^{470T} primary microglia showed neglectable changes (Fig. 19 D). These results suggested that the LPS-mediated TDP-43 increase in WT BMDMs and microglia and the increase in basal TDP-43 in Optn^{470T} were not transcriptionally regulated. To test if loss of functional optineurin was directly linked to impaired TDP-43 function, we analysed TDP-43 mRNA targets Polymerase delta-interacting protein 3 (*Poldip3*), which has multiple roles in RNA and DNA-related cellular processes and Ras-GAP SH3 domain-binding protein 1 (*G3bp1*), a protein crucial for stress granule formation. Upon LPS stimulation *Poldip3* was significantly increased in WT BMDMs, while there was no change in expression in Optn^{470T} BMDMs (Fig. 19 B). The same expression pattern was observed in primary microglia (Fig. 19 E), suggesting that elevated TDP-43 protein levels in Optn^{470T} myeloid cells inhibit *Poldip3* expression upon LPS. *G3bp1* expression was decreased upon LPS in both WT and Optn^{470T} BMDMs and primary microglia (Fig. 19 C and F). Although TDP-43 has been reported as a regulator of *G3bp1* in human cells (Sidibé et al., 2020), it is possible that in mouse cells *G3bp1* is regulated differently. In conclusion, *G3bp1* was decreased in both WT and Optn^{470T} cells upon LPS-, whereas only in WT and not in optineurin-insufficient cells did LPS increase *Poldip3* expression.

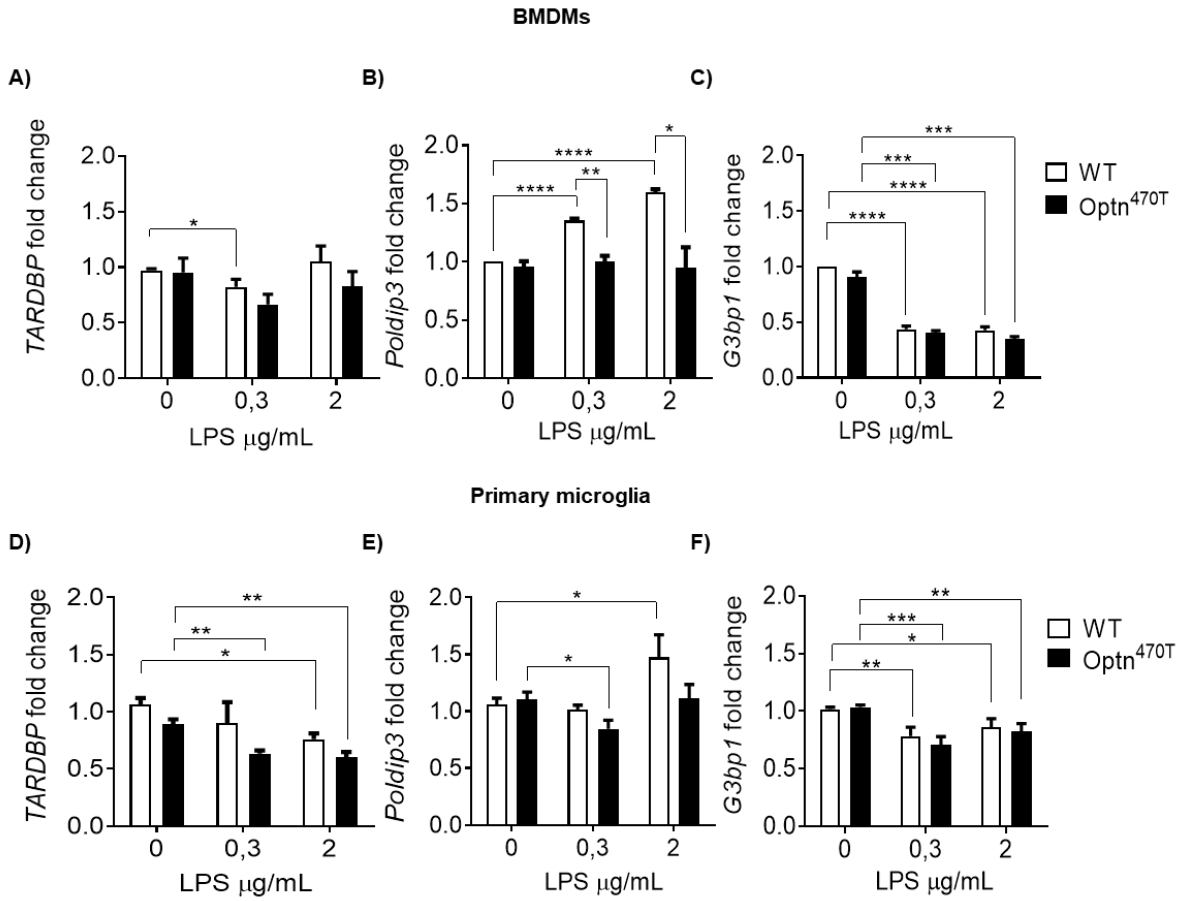

Figure 19. *TARDBP* and its downstream genes show different expression patterns upon inflammation in WT and Optn^{470T} mouse BMDMs and primary microglia. WT and Optn^{470T} BMDMs and primary microglia were treated with 0.3 µg/mL and 2 µg/mL of LPS for 24 h. Gene expression in WT and Optn^{470T} BMDMs were assessed by RT-PCR 24 h upon LPS treatment for (A) *TARDBP*, (B) *Poldip3*, and (C) *G3bp1.* An average ± SEM from 3-4 independent experiments is shown. Gene expression in WT and Optn^{470T} primary microglia was assessed by RT-qPCR 24 h upon LPS treatment for (D) *TARDBP*, (E) *Poldip3*, and (F) *G3bp1*. An average ± SEM from 4-8 independent experiments is shown. Statistical analysis was performed by Student's t-test: * p<0.05, ** p<0.01, *** p<0.001, **** p<0.0001.

4.2. Neuroimmune characterization of aged Optn^{470T} mouse model

4.2.1. Peripheral immune cell characterization

4.2.1.1. Optineurin insufficiency did not affect ageing-induced changes in B and T lymphocytes

Ageing is a major risk factor for neurodegeneration, including ALS/FTD spectrum disorder, and is accompanied by alterations in both adaptive and innate immune responses (Franceschi et al., 2000; Mattson and Arumugam, 2018). Since ALS is a systemic disease, peripheral immune cells, despite having limited access to the CNS, also play a key role in ALS pathogenesis (Béland et al., 2020b). As optineurin is proposed to regulate several inflammatory pathways, we tested if optineurin insufficiency affects ageing-induced changes in the peripheral immune system. We compared splenocytes of young adults (three-month-old), middle-aged (one-year-old), and old (two-year-old) WT and Optn^{470T} male (Fig. 20), and middle-aged and old WT and Optn^{470T} female mice (Fig. 21) by flow cytometry (gated as shown in Fig. 8). Absolute splenocyte numbers were comparable between the genotypes at all tested time points in males (Fig. 20 A) and females (Fig. 21 A), with a higher mouse-to-mouse variability seen in old mice. The percentage of B lymphocytes was significantly increased between young adults, middle-aged and old Optn^{470T} compared to WT males in which it didn't reached statistical significance (Fig. 20 B). The absolute numbers of B lymphocytes remained unchanged over time and between genotypes (Fig. 20 C). Compared to males, old females showed a drop in B lymphocytes percentage, which was statistically significant only in Optn^{470T} females (Fig. 21 B). Moreover, the absolute number of B lymphocytes was decreased in both WT and Optn^{470T} females (Fig. 21 C). The T lymphocyte percentage was comparable between the genotypes, with a small, but significant decrease in absolute numbers from middle-aged to old WT males (Fig. 20 D-E). Moreover, we observed an increased percentage in CD8$^+$, and a decrease in CD4$^+$ T lymphocytes from young adults to old males in both genotypes, while they were comparable in middle-aged and old WT and Optn^{470T} males (Fig. 20 F). In addition, we observed a decline in the CD4$^+$/CD8$^+$ ratio, which has previously been associated with ageing, but we did not detect differences between the genotypes (Fig. 20 H). Notably, the absolute number of CD8$^+$ and CD4$^+$ significantly declined in old compared to young adults and middle-aged WT males, while this was not observed in Optn^{470T} mice (Fig. 20 G). Compared

to males, the frequency and number of T lymphocytes, $CD4^+$ and $CD8^+$, and $CD4^+/CD8^+$ ratio remain constant during ageing in middle-aged and old females (Fig. 21 D-H). In summary, we showed a mild increase in B lymphocytes in optineurin-insufficient males and a decreased percentage in females. However, both WT and $Optn^{470T}$ mice showed T lymphocyte alterations previously described during ageing, with minor changes between the genotypes.

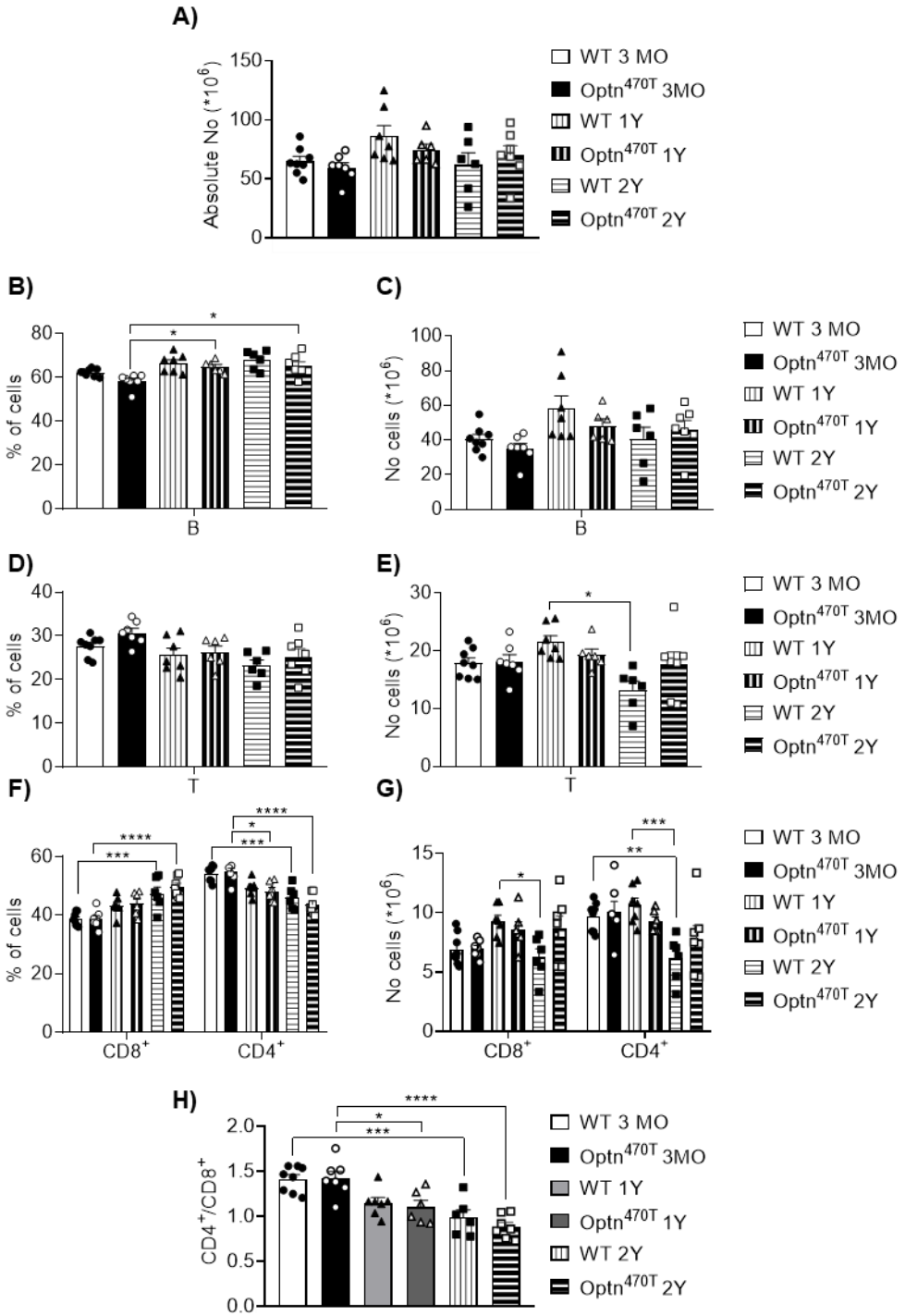

Figure 20. B and T lymphocyte subsets in aged Optn^{470T} mice were comparable to those in WT male mice. B and T lymphocytes were analysed based on the gating strategy shown in Figure 8. (A) Absolute splenocyte numbers from three-month (young adults), one-(middle-aged), and two-year-old (old) male WT and Optn^{470T} mice are shown. Population frequency (%) and absolute number (No) of (B-C) B lymphocytes, (D-E) T lymphocytes, and CD8$^+$ and CD4$^+$ T lymphocyte subsets (F-G) are shown. (H) CD4$^+$/CD8$^+$ ratio is shown. The data from 6-8 males are shown as means ± SEM and analysed ordinary one-way ANOVA (A-E) and two-way ANOVA (F-G): * p<0.05, ***p<0.001, ****p<0.0001.

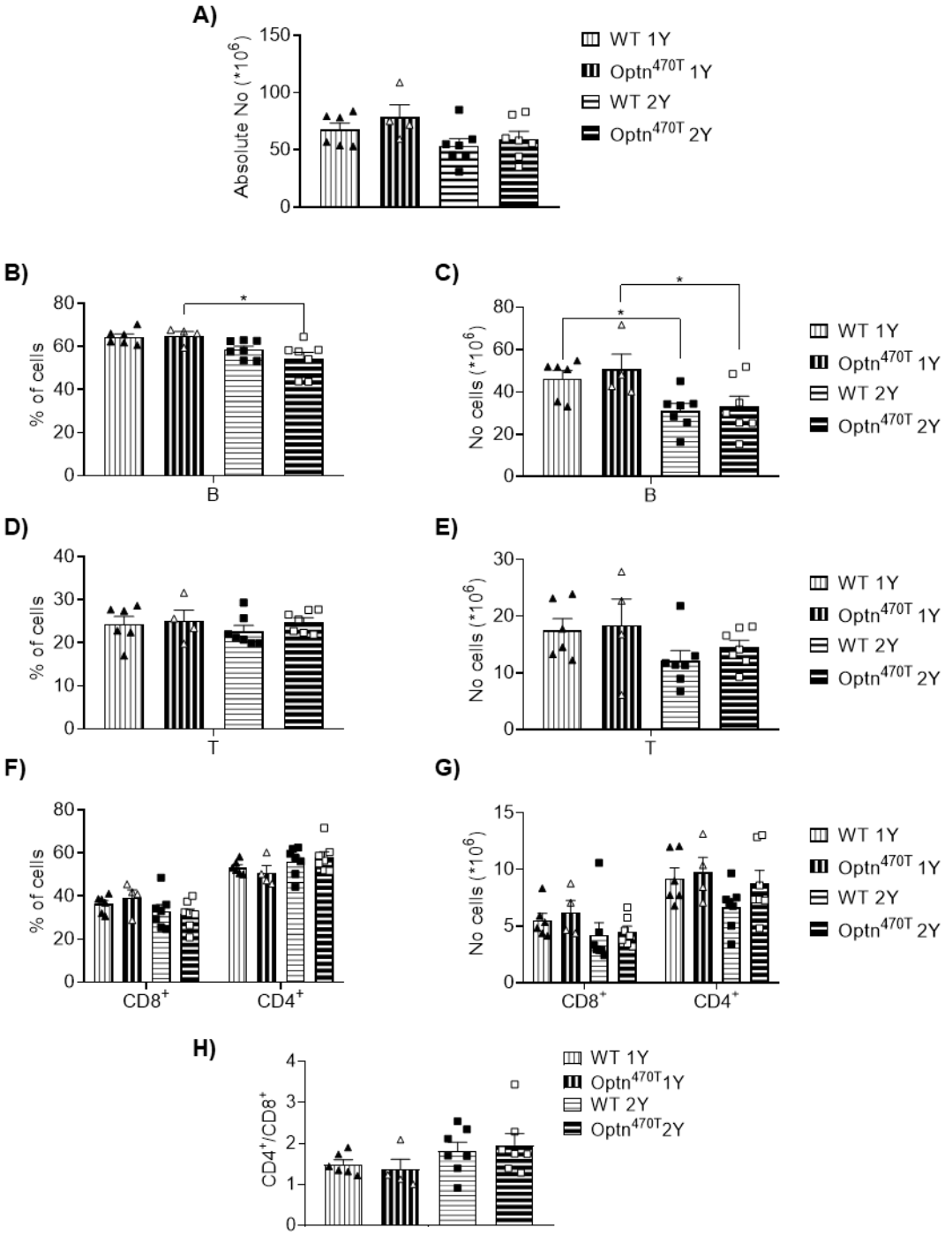

Figure 21. B lymphocyte frequency and number decline during ageing in WT and Optn^{470T} female mice. B and T lymphocytes were analysed based on the gating strategy shown in Figure 8. (A) Absolute splenocyte numbers from one- (middle-aged) and two-year-old (old) female WT and Optn^{470T} mice are shown. Population frequency (%) and absolute number (No) of (B-C) B lymphocytes, (D-E) T lymphocytes, and CD8^{+} and CD4^{+} T lymphocyte subsets (F-G) are shown. The data from 4-8 females are shown as means ± SEM and analysed by ordinary one-way ANOVA (A-E) and two-way ANOVA (F-G): * $p<0.05$.

4.2.1.2. Ageing-induced cytotoxic T lymphocyte activation and changes toward the memory phenotype in both WT and Optn^{470T} mice

To further evaluate CD8$^+$ T lymphocytes during ageing in WT and Optn^{470T} male and female mice, we analysed naïve and memory subsets, and several markers that are linked to activation. Compared to young adults, both WT and Optn^{470T} middle-aged and old males had a significant reduction in the percentage of naïve CD8$^+$ (Fig. 22 A). On the contrary, a significant increase in the percentage of central and effector memory CD8$^+$ were observed during ageing in both genotypes (Fig. 22 A). Moreover, compared to middle-aged males, a significant reduction in the frequency of naive CD8$^+$ and an increase in the percentage of central memory CD8$^+$ were observed in old mice. Interestingly, a decrease in the absolute number of naïve, and an increase in central memory CD8$^+$ were observed only in old WT males during ageing, likely due to the high mouse-to-mouse variability in absolute numbers in CD8$^+$ T lymphocytes in Optn^{470T} mice (Fig. 22 B). Similar to males, females also demonstrated a reduction in naïve lymphocytes between middle-aged and old mice in both genotypes. Compared to males, a higher percentage was observed in effector, but not central memory CD8$^+$, without changes in absolute numbers or differences between the genotypes in middle-aged and old females (Fig. 22 A-B). We also analysed several activated CD8$^+$ subsets. An increased percentage and number in the CD44$^+$CD38$^+$ subset was observed in both WT and Optn^{470T} mice in old compared to young adults and middle-aged males, but significantly more CD44$^+$CD69$^+$ was observed only in Optn^{470T} mice (Fig. 22 C-D). Interestingly, the percentage and number of CD44$^+$KLRG1$^+$ subset, marking the exhausted cell phenotype, were not changed during ageing in neither WT nor Optn^{470T} males. Old WT and Optn^{470T} females demonstrated the same increase in the percentage of CD44$^+$CD38$^+$ subset compared to middle-aged mice, but significant increases in number were observed only in old WT females (Fig. 22 C-D). Moreover, in comparison to males, a significant increase in CD44$^+$CD69$^+$ was observed only in WT females. The results from our group also demonstrated that these minor differences in percentage and the absolute number of CD8$^+$ subsets found between WT and Optn^{470T} mice during ageing did not affect functional outcomes since cytokine secretion was similar ((Mohovic et al., 2023), results obtained by J. Peradinovic). To conclude, we showed that both old male and female WT and Optn^{470T} mice showed

changes in CD8$^+$ T lymphocytes typical for ageing (drop in naïve, more memory, and increased activation), but otherwise with negligible differences between the genotypes.

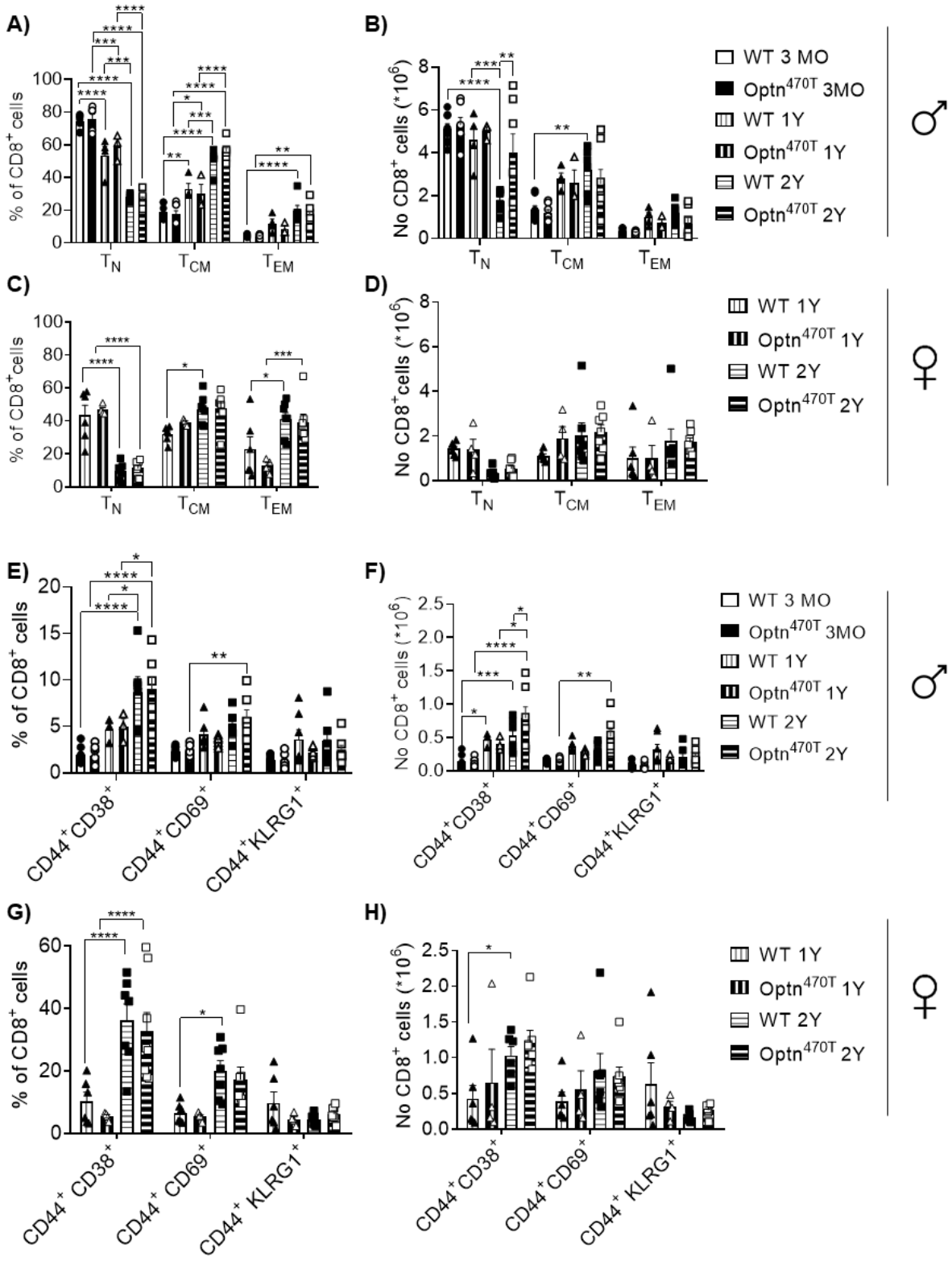

Figure 22. Ageing induced CD8$^+$ T cell activation and a shift from naive to memory phenotype in WT and Optn^{470T} mice. Ageing induced CD8$^+$ T cell activation and shifts from naive to memory phenotype in WT and Optn^{470T} mice. Memory and activation status of cytotoxic CD8$^+$ T lymphocytes from three-month (young adults), one- (middle-aged) and two-year-old (old) WT, and Optn^{470T} male mice and one- (middle-aged) and two-year-old (old) females were analysed. Population frequency (%) and absolute number (No) of naïve (T_N), central memory (T_{CM}), and effector memory (T_{EM}) in (A-B) males and (C-D) females are shown. Population frequency (%) and absolute number (No) of activated CD44$^+$CD38$^+$, CD44$^+$CD69$^+$, and CD44$^+$KLRG1$^+$ populations in (E-F) males and (G-H) females are shown. The data from 6-7 males, and 4-8 females are shown as means ± SEM and analysed by two-way ANOVA: * p<0.05, ** p<0.01, ***p<0.001, ****p<0.0001.

4.2.1.3. Ageing-induced helper T lymphocyte activation and changes toward the memory phenotype in both WT and Optn^{470T} mice

Next, we evaluated naïve and memory CD4$^+$ T lymphocytes, and activation during ageing in WT and Optn^{470T} male and female mice. Same as in CD8$^+$, a strong drop in percentage and absolute numbers in naïve CD4$^+$ were observed between young adult and old WT and Optn^{470T} males (Fig. 23 A-B). Moreover, we observed a decrease in central memory CD4$^+$ frequency and absolute numbers in old WT compared to Optn^{470T} males. Notably, the percentage and number of effector memory lymphocytes significantly increased between young adult, middle-aged and old WT, and Optn^{470T} males (Fig. 23 A-B). The same CD4$^+$ phenotype was observed between middle-aged and old females with negligible differences between the genotypes (Fig. 23 C-D). We also observed an increase in the percentage and absolute numbers of activated CD44$^+$CD38$^+$CD4$^+$ subset in young adults compared to old mice in both genotypes, with a significant increase in old Optn^{470T} males (Fig. 23 E-F). Moreover, CD4$^+$ showed an increased percentage of CD44$^+$CD69$^+$ subset in old males, with a higher number observed in Optn^{470T} mice. We did not detect activation of the CD44$^+$ KLRG1$^+$ subset in males in both genotypes. In addition, middle-aged and old WT and Optn^{470T} females demonstrated the same increase in the percentage of CD44$^+$ CD38$^+$ and CD44$^+$ CD69$^+$ subsets, but significantly higher absolute numbers were observed only in old Optn^{470T} females (Fig. 23 G-H). To sum up, CD4$^+$ from old WT and Optn^{470T} mice shifted toward effector memory phenotype. Furthermore, CD4$^+$ from old mice demonstrated stronger activation of CD44$^+$CD38$^+$ and CD44$^+$CD69$^+$ subsets, which was exaggerated in Optn^{470T} compared to WT

males. Similar to findings in $CD8^+$ subsets, minor differences in $CD4^+$ subsets did not result in functional outcomes since secreted cytokines showed negligible differences between genotypes ((Mohovic et al., 2023), results obtained by J. Peradinovic). In summary, $CD4^+$ T lymphocytes from both old WT and $Optn^{470T}$ mice showed alterations typical for ageing (decrease of naïve and increase of memory cells; increased activation), but otherwise with negligible differences between the genotypes.

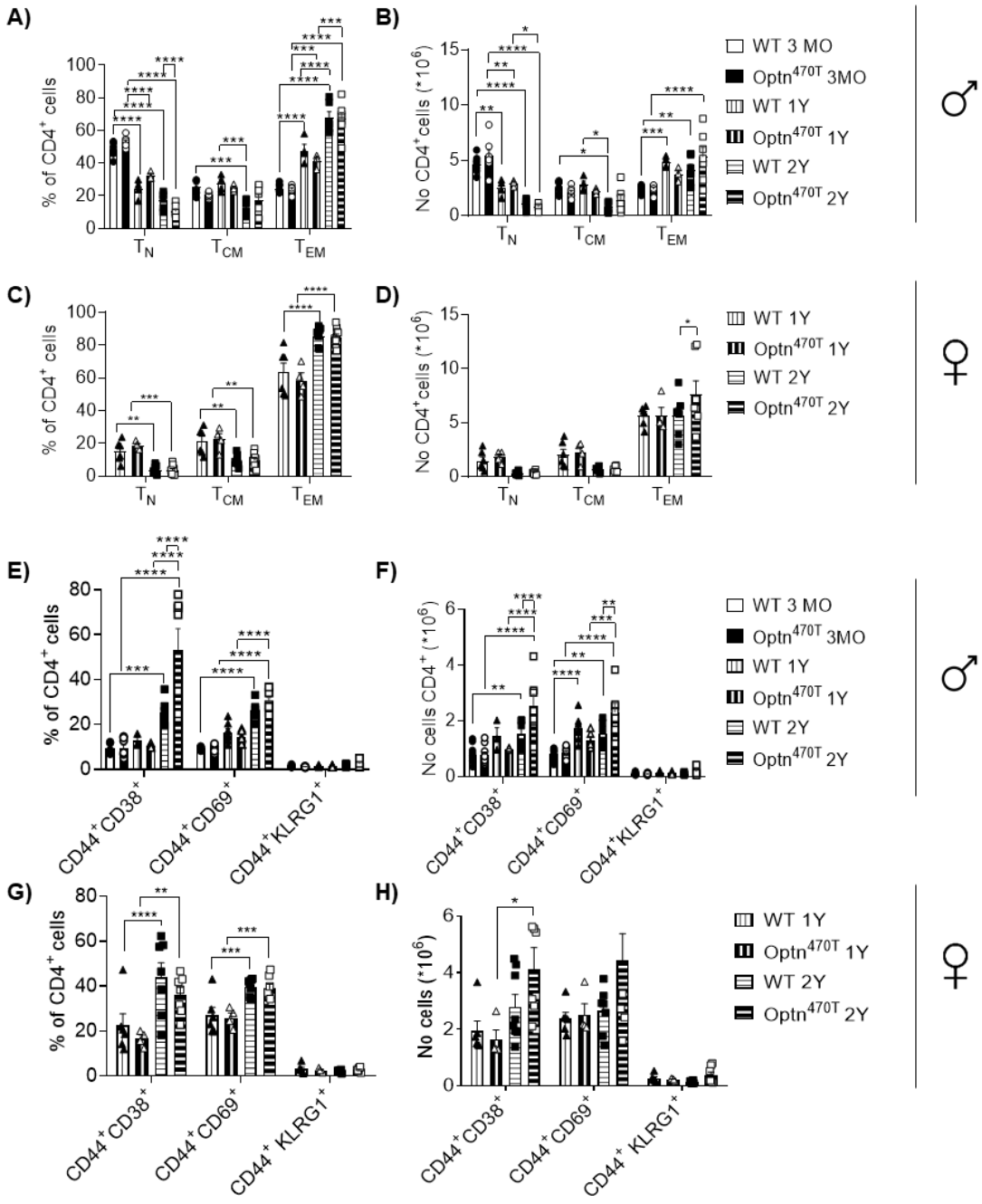

Figure 23. Ageing induced $CD4^+$ T cell activation and a shift from naive to effector memory phenotype in WT and $Optn^{470T}$ mice. Memory and activation status of helper

$CD4^+$ T lymphocytes from three-month (young adults), one- (middle-aged) and two-year-old (old) WT and $Optn^{470T}$ male mice and one- (middle-aged) and two-year-old (old) females were analysed. Population frequency (%) and absolute number (No) of naïve (T_N), central memory (T_{CM}), and effector memory (T_{EM}) in (A-B) males and (C-D) females are shown. Population frequency (%) and absolute number (No) of activated $CD44^+CD38^+$, $CD44^+CD69^+$, and $CD44^+KLRG1^+$ populations in (E-F) males and (G-H) females are shown. The data from 6-7 males, and 4-8 females are shown as means ± SEM and analysed by two-way ANOVA: * p<0.05, ** p<0.01, ***p<0.001, ****p<0.0001.

4.2.1.4. Non-functional Tregs increase during ageing in WT and $Optn^{470T}$ mice

Decreased Tregs were observed in ALS patients' blood and hSOD1 mice model at the later stage of the disease and correlated with more rapid disease progression (Beers et al., 2011a; Mantovani et al., 2009). In contrast, during ageing the number of Tregs is increasing (Fessler et al., 2013). To determine if optineurin insufficiency affects Treg cell number and function during ageing, we performed intracellular staining for the FOXP3 transcription factor, a Treg-specific marker. As shown in the gating strategy (Fig. 24 A-B) Tregs were subdivided into functional ($CD4^+FOXP3^+CD25^+$) and non-functional ($CD4^+$ $FOXP3^+$ $CD25^-$) lymphocytes, as previously reported in aged mice (Nishioka et al., 2006). Compared to young adults, both old WT and $Optn^{470T}$ males showed an increased percentage of non-functional, while the percentage of functional Tregs was significantly increased only in WT males (Fig. 24 C). However, the percentage and absolute number of non-functional Tregs were also higher between middle-aged and young adult WT males (Fig. 24 D). In addition, between middle-aged and old males the percentage and number of both functional and non-functional Tregs were not changed. Old females showed an increased percentage of non-functional Tregs, while functional Tregs were increased only in WT females. Moreover, the absolute number of Tregs was not changed during ageing (Fig. 24 E-F). To test the expression of FOXP3 in functional Tregs, we analysed FOXP3 MFI. FOXP3 MFI was comparable between WT and $Optn^{470T}$ males and did not substantially change during ageing (Fig. 24 G). Surprisingly, FOXP3 MFI significantly declined in old $Optn^{470T}$ compared to WT females, meaning there was less FOXP3 in functional Tregs (Fig. 24 H). To sum up, ageing induced an accumulation of non-functional Tregs in both WT and $Optn^{470T}$ mice, and functional only in WT mice during ageing. Notably, functional Tregs in old $Optn^{470T}$ exhibited

slightly lower FOXP3 MFI compared to WT females. To conclude, we did not observe a decrease in Tregs in optineurin insufficient mice that was found in ALS patients and hSOD1 mice, but rather an increase in Tregs linked to ageing.

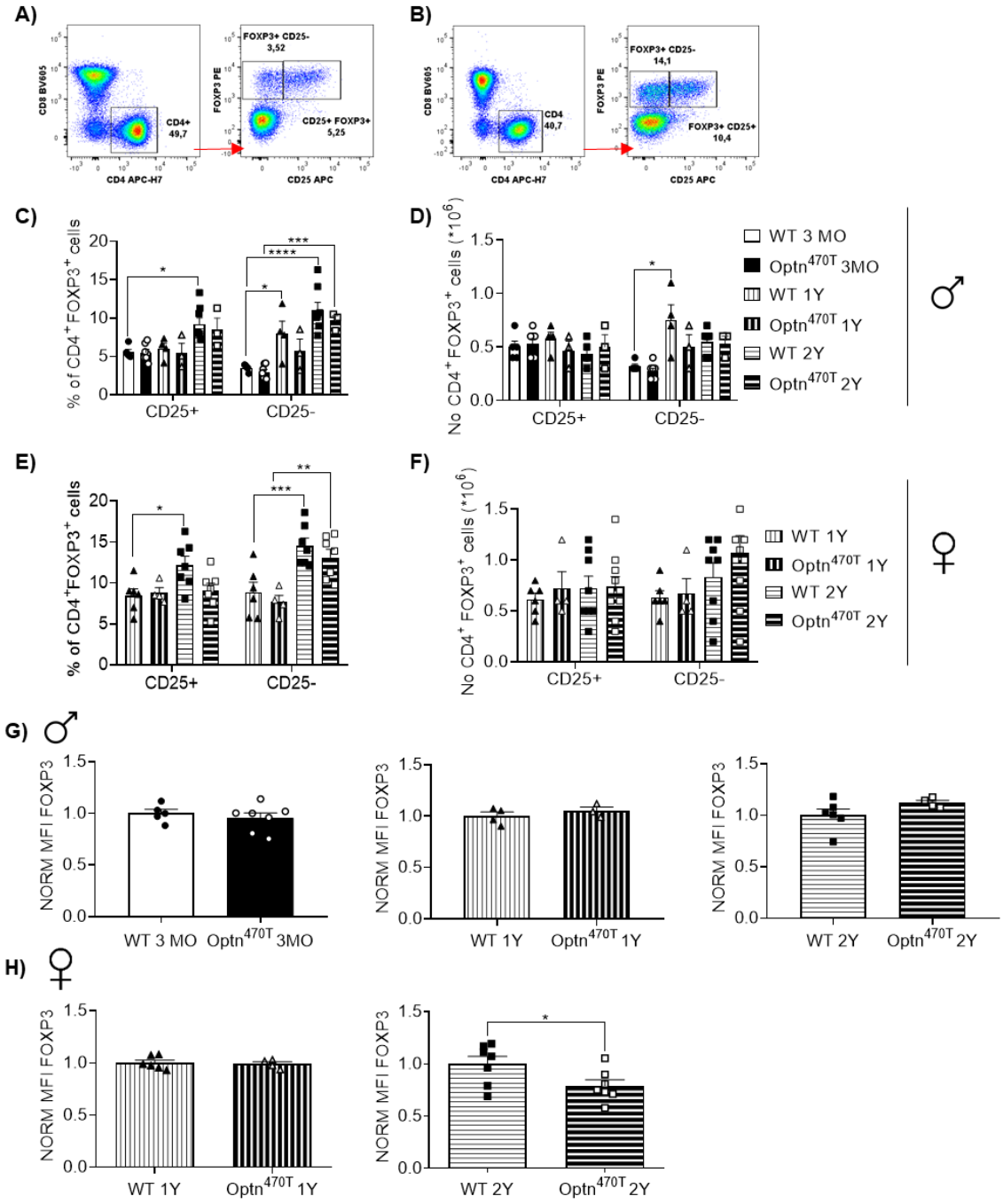

Figure 24. The number of non-functional lymphocytes increased during ageing in both WT and Optn^{470T} mice and while ageing decreased FOXP3 levels in Optn^{470T} two-years-old female mice. The gating strategy for representative Treg lymphocyte subsets in (A) three-month (young adults) and (B) two-years-old (old) mouse spleens. Functional Tregs were gated as CD4^{+}FOXP3^{+}CD25^{+} and non-functional as CD4^{+}FOXP3^{+} CD25^{-} lymphocytes. Treg subsets are shown as frequency (%) and absolute numbers (No) in (C-D) one- (middle-aged) and two-year-old (old) males and (E-F) one- (middle-aged) and two-year-old (old)

females. (G) The graph shows the MFI of FOXP3 in Optn^{470T} normalized to WT males in functional Tregs. (H) The graph shows the MFI of FOXP3 in Optn^{470T} normalized to WT females in functional Tregs. The data from 6-7 males, and 4-8 females are shown as means ± SEM and analysed by two-way ANOVA (C-F) and Student's t-test (G-H): * $p<0.05$, ** $p<0.01$, ***$p<0.001$.

4.2.1.5. Optineurin insufficiency did not affect the percentages and numbers of innate immune cells in aged mice

To further evaluate inflammageing in Optn^{470T} mice, we analysed innate immune cells in the spleens of three-month (young adults), one- (middle-aged), and two-year-old (old) WT and Optn^{470T} males (Fig. 25), and one- (middle-aged) and two-year-old (old) WT and Optn^{470T} females (Fig. 26) by flow cytometry as shown in Figure 9. The percentage of total non-T/non-B cells decreased between young adults and middle-aged males, but in old mice, it again reached the level found in young adults, without changes in absolute numbers (Fig. 25 A-B). A similar increase in total non-T/non-B cells was observed in females, but it reached statistical significance only in old Optn^{470T} mice (Fig. 26 A-B). The percentage of cDCs was significantly dropping only in Optn^{470T} males during ageing. However, a similar trend, although statistically not significant, was present in WT mice (Fig. 25 C). Interestingly, the absolute number of cDCs was not changed during ageing (Fig. 25 D). Moreover, as previously described, the percentage of macrophages and neutrophils was significantly increased in WT males during ageing with negligible differences in absolute numbers. However, a similar trend was also observed in Optn^{470T} mice (Fig. 25 E-H). In old compared to middle-aged females there were no changes in the percentage and total numbers of cDCs and neutrophils (Fig. 26 C-D and G-H). In addition, the higher percentage of total non-T/non-B cells was mostly caused by an increase in the total number of macrophages, which showed significance only in Optn^{470T} females (Fig. 26 G-H). It was previously seen that NK cells increase during ALS progression while ageing leads to a decline in the number and cytotoxic functions of these cells (Brauning et al., 2022; Murdock et al., 2017). Notably, here we demonstrated a strong drop of NK cells in middle-aged and old compared to young adult WT and Optn^{470T} males (Fig. 25 I-J). Furthermore, a similar drop in NK cells was observed in females (Fig. 26 I-J), demonstrating that NK cells showed an ageing phenotype, rather than the one linked to ALS. In summary, ageing led to an increase in

neutrophils and macrophages and a decrease in cDC and NK cells in old mice. However, we did not detect differences between optineurin insufficient and WT mice.

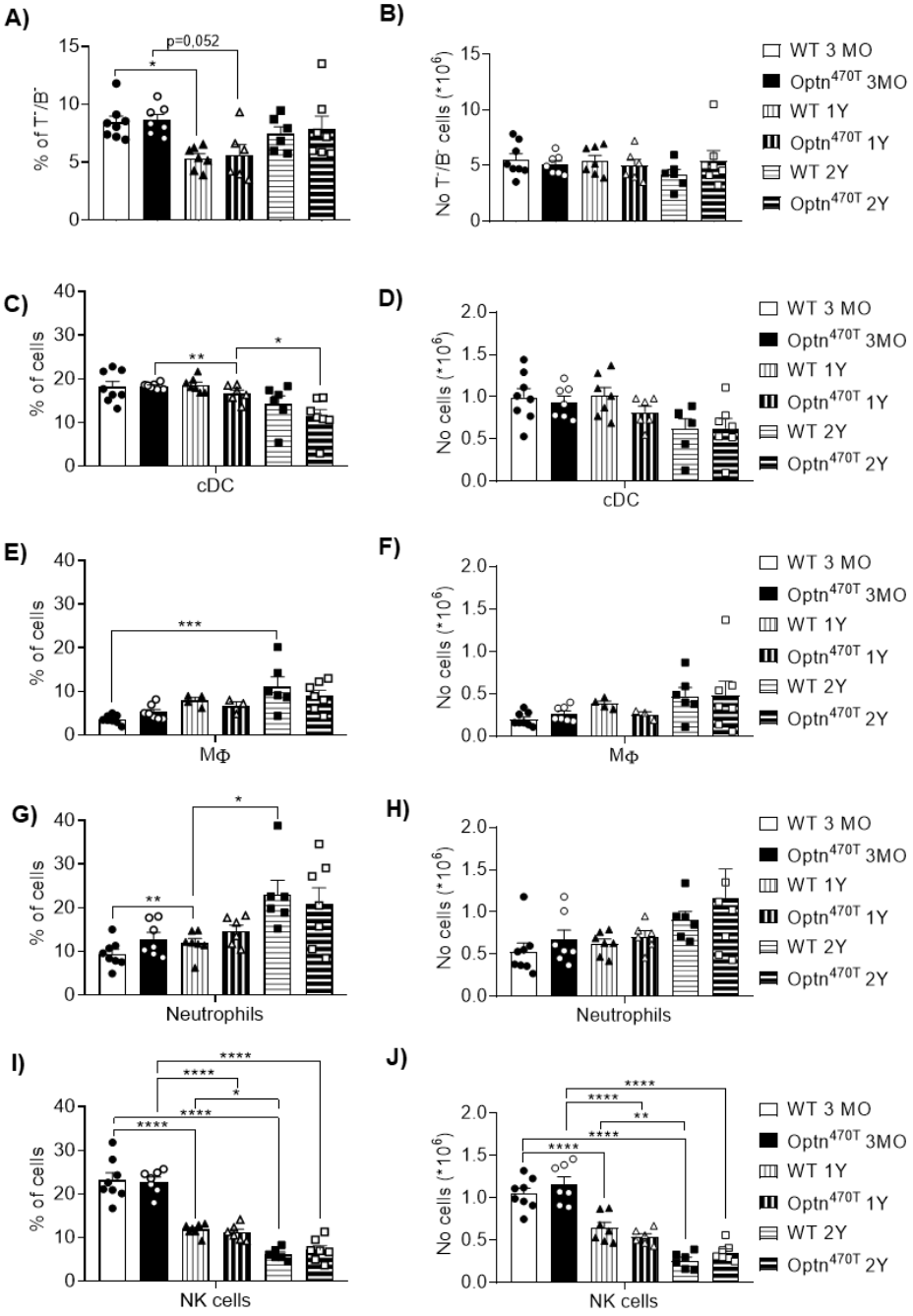

Figure 25. Ageing-induced changes in innate immune cells are unaffected by optineurin insufficiency in male mice. Myeloid and NK cells were analysed based on the gating strategy in Figure 9 in three-month (young adults), one- (middle-aged) and-two-year-old (old) WT and Optn^{470T} males. Population frequency (%) and absolute number (No) of (A-B) non-T/non-B cells (T^- B^-), (C-D) conventional dendritic cells (cDC), (E-F) macrophages (MΦ), (G-H) neutrophils and (I-J) NK cells were shown. The data from 6-7 males are shown as means ± SEM and analysed by ordinary one-way ANOVA: * p<0.05, ** p<0.01, ***p<0.001, ****p<0.0001.

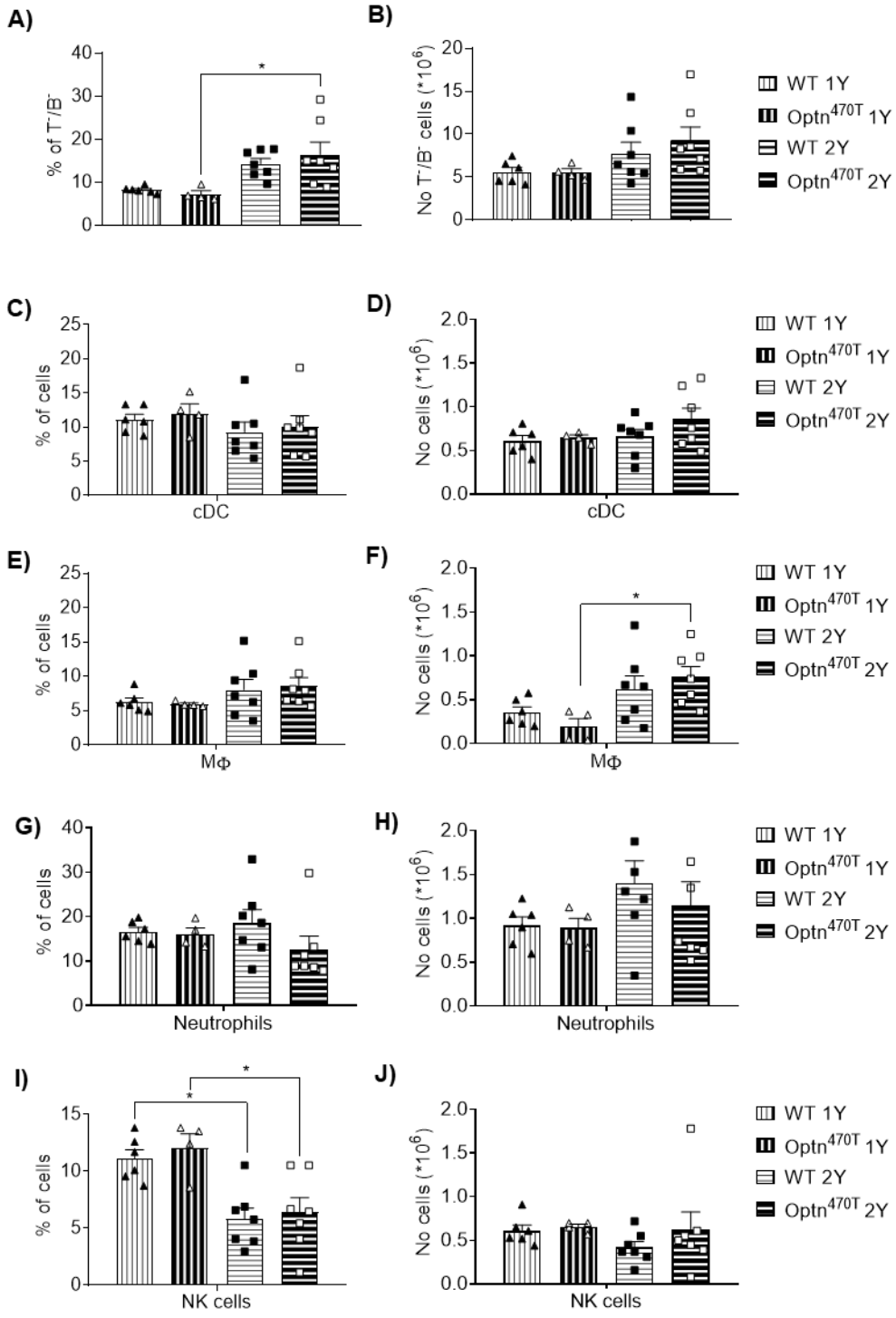

Figure 26. Ageing-induced changes in innate immune cells are unaffected by optineurin insufficiency in female mice. Myeloid and NK cells were analysed based on the gating strategy in Figure 9 in one- (middle-aged) and-two-year-old (old) WT and Optn^{470T} females. Population frequency (%) and absolute number (No) of (A-B) non-T/non-B cells (T-B-), (C-D) conventional dendritic cells (cDC), (E-F) macrophages (MΦ), (G-H) neutrophils and (I-J) NK cells were shown. The data from 4-8 females are shown as means ± SEM and analysed by ordinary one-way ANOVA: * $p<0.05$.

4.2.1.6. Optineurin insufficiency caused increased activation of cDC and macrophages in two-year-old male mice

To check the activation of innate immune cells we analysed the expression of activation markers CD86 and MHC-II in cDC, and CD86, MHC-II, and CD11c in macrophages by measuring their MFI during ageing in WT and Optn^{470T} mice. We did not observe alterations in cDC activation in young adults and middle-aged Optn^{470T} compared to WT males. However, we observed increased cDC activation in old Optn^{470T} males, which was detected as higher expression of both CD86 and MHC-II activation markers (Fig. 27 A, from left to right: young adult, middle-aged and old males). Macrophages from middle-aged Optn^{470T} males demonstrated higher activation by expressing more CD11c and MHC-II than WT males, and the expression was rising from young adult to old males (Fig. 27 B, from left to right: young adult, middle-aged, and old males). However, in contrast to males, old Optn^{470T} females did not demonstrate alterations either in cDC (Fig. 27 C, from left to middle-aged and old females) or macrophage (Fig. 27 D, from middle-aged and old females) activation. To conclude, optineurin insufficiency caused a significant decrease in the cDC percentage that was followed by increased activation of these cells and macrophages in Optn^{470T} males, but not in female mice.

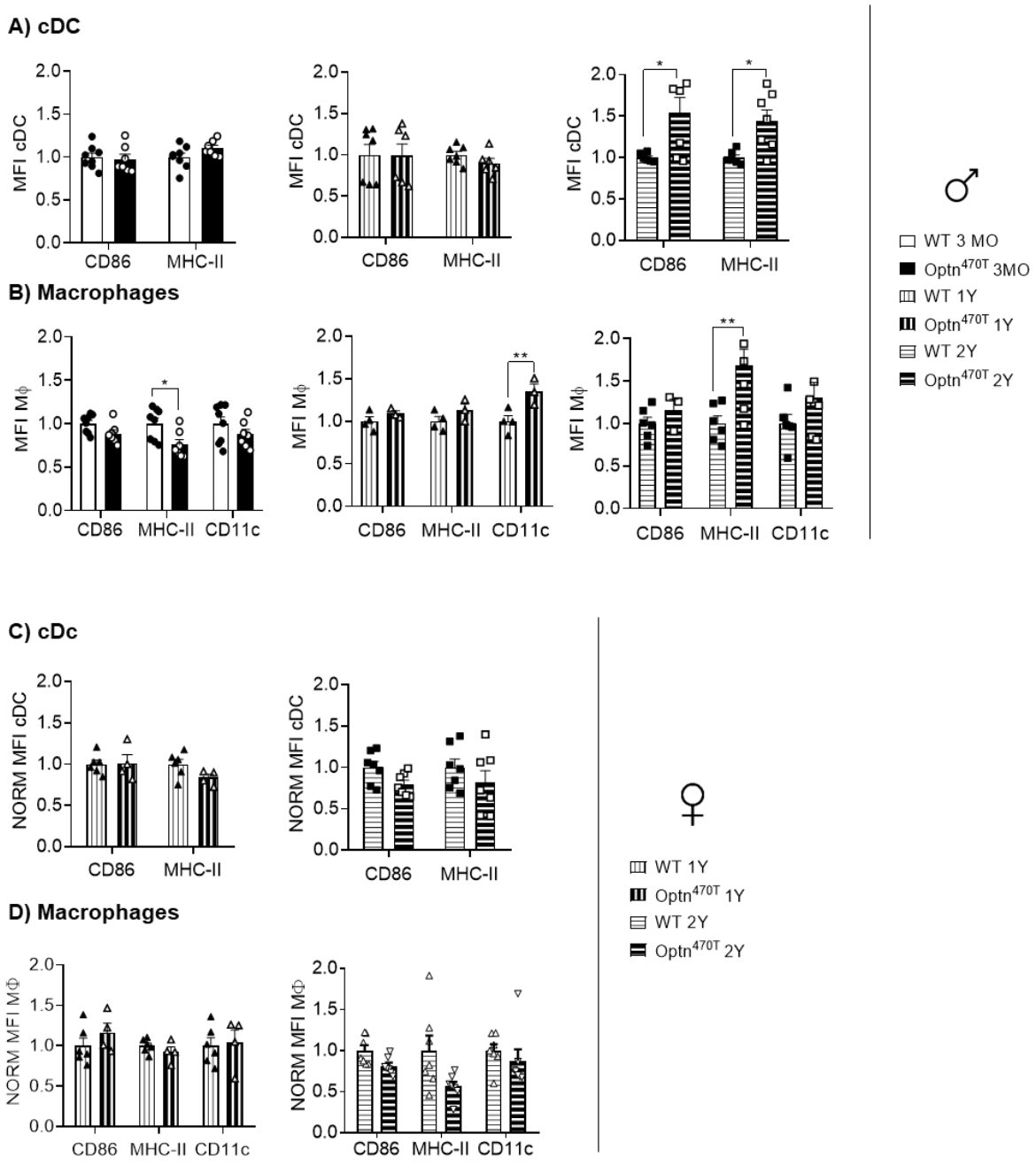

Figure 27. Optineurin insufficiency increased activation of cDC in two-year-old male mice. The mean fluorescence intensity (MFI) for CD86 and MHC-II activation markers in cDC and CD86, MHC-II, and CD11c in macrophages were analysed in three-months-old (young adult) male, and one- (middle-aged) and two-years-old (old) WT and Optn^{470T} males and females. MFI is shown normalized to WT at indicated time points for (A) cDC and (B) macrophages in males and (C) cDC and (D) macrophages in females. The data from 6-7 males, and 4-8 females are shown as means ± SEM and analysed by two-way ANOVA: * $p<0.05$, ** $p<0.01$.

4.2.2. Analysis of immune cells and their function in the central nervous system of Optn^{470T} and WT mice

4.2.2.1. Immune cells isolated from aged mouse brains showed high autofluorescence

In an attempt to investigate microglia and other immune cells in the brains of aged optineurin-insufficient mice, we performed a Percoll-based enrichment of immune cells and analysed isolated cells by flow cytometry. Unfortunately, we encountered a technical problem because of a strong autofluorescence of cells isolated from the old mice, which was prominent in several channels. To investigate this, we performed Percoll-enrichment from young and middle-aged mice and analysed it as shown in Figure 28 A. Dead cells were excluded based on positivity for DAPI (*i.e.* live cells were gated as DAPI negative). Cells from young mice were stained with CD45-FITC (green channel) and CD11b-APC (red channel), or left unstained. Analyses of MFI from both channels showed that the unstained cells from young mice showed substantially lower signals in both red and green channels compared to stained cells (blue peaks) (Fig. 28 B). However, the unstained cells isolated from middle-aged mice (red peaks) showed two peaks, one negative for the red and green channels, and one that demonstrated even stronger MFI than stained cells from young mouse. These results suggested that one fraction of cells from the aged mice brain demonstrated very high autofluorescence. We hypothesised that autofluorescence is coming from lipofuscin, pigment granules composed of lipid-containing residues of lysosomal digestion. The autofluorescence was also confirmed by fluorescence microscopy, which most likely represents the accumulation of lipofuscin in middle-aged but not young mice (Fig. 28 C). Our findings go in line with the autofluorescence of the cells isolated from the aged brains analysed on flow cytometry and fluorescence microscopy previously described by O'Neill *et al.* (O'Neil et al., 2018). In summary, we encountered a technical problem during an analysis of immune cells from the brain because of a large accumulation of autofluorescent material, precluding further immunophenotyping of cells from aged CNS by flow cytometry.

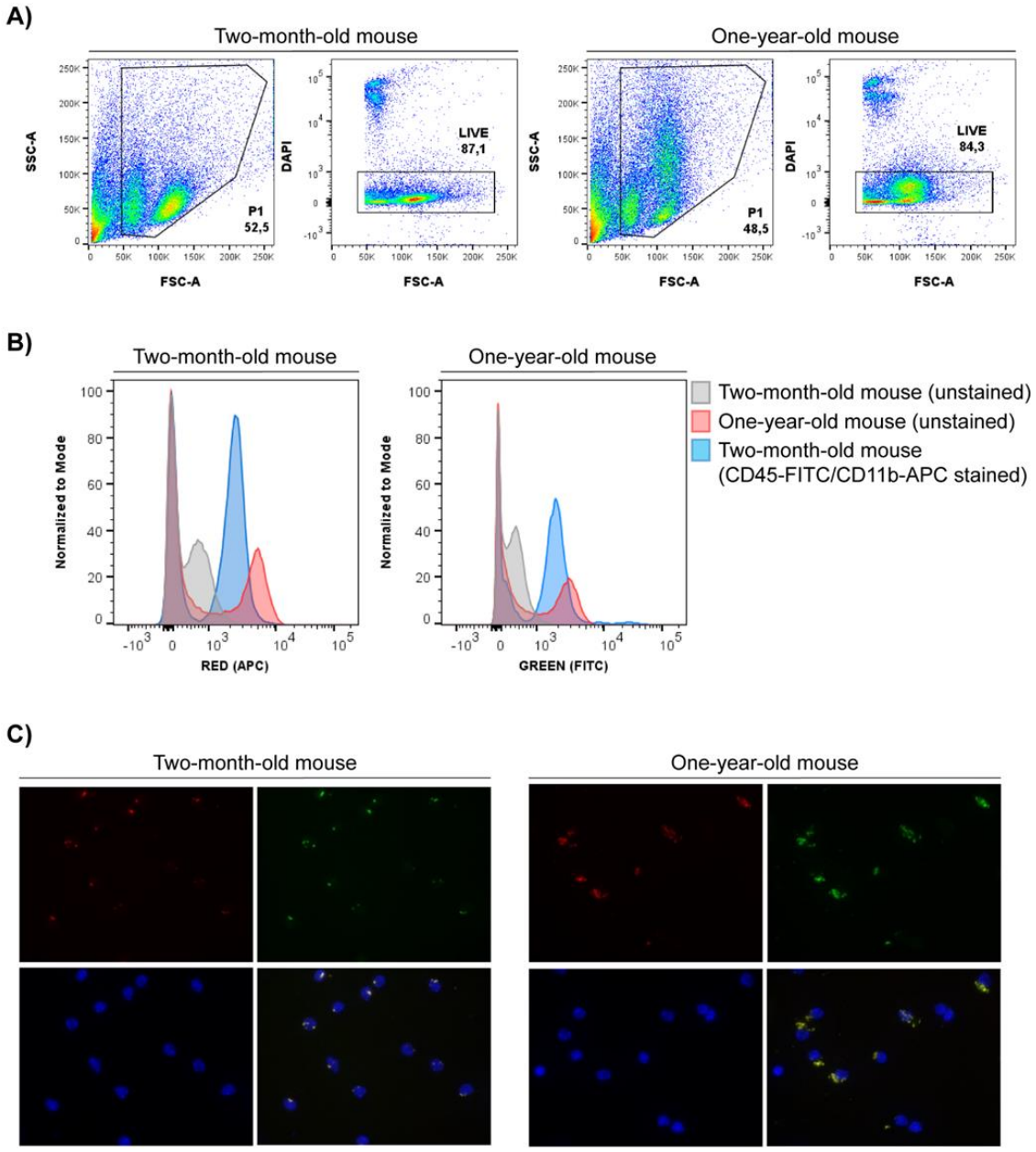

Figure 28. Immune cells isolated from the aged brains showed high autofluorescence. (A) Gating strategy for the immune cells isolated from the brains of young (two-month) and middle-aged (one-year-old mice) left unstained or stained for the indicated markers analysed by BD FACSAriaTM III cytometer. (B) Overlaid histograms show MFI from unstained and stained two-month-old, and unstained one-year-old immune cells in red (left) and green (right) channels. (C) Unstained immune cells isolated from two-month-old (left) and one-year-old (right) brains were seeded on coverslips, fixed, stained with DAPI (blue), and analysed using red and green channels to evaluate autofluorescence on an Olympus IX83 fluorescent microscope.

4.2.2.2. Cytokine and chemokine expression is higher in the aged compared to young brains of Optn^{470T} and WT mice

In order to overcome the problem with high autofluorescence observed in the immune cells from aged CNS, and still analyse potential functional immune alterations during ageing, we performed protein array analyses. Specifically, we analysed the levels of 40 different pro- and anti-inflammatory cytokines, chemokines, and growth factors in the brain lysates of three-month (young adults) and two-year-old (old) WT and Optn^{470T} male mice. In the young adult WT and Optn^{470T} brain lysates, the strongest expression was seen in anti-inflammatory cytokine IL-4, and chemoattractants and/or growth factors for neutrophils and macrophages LIX, M-CSF, and TCA-3 (Fig. 29 A, left side, quantified in B). Moreover, intermediate expression of pro-inflammatory cytokines IL-1α and IL-12 p70 was observed in the brains of young adults, and fractalkine (CX3CL1), a chemokine by which neurons suppress microglial activation, respectively. Notably, old mice demonstrated a robust increase in expression of almost all proteins analysed by protein array, confirming our results from peripheral immune cell flow cytometry analyses, that older mice exhibited age-related changes in the immune system (Fig. 29 A, right side, quantified in C). Interestingly, the strongest signal was observed in the same proteins as in young adult mice: IL-4, IL-1α, IL-12p70, LIX, M-CSF, and TCA-3, but they were significantly more expressed in old mice (Fig. 29 D). Notably, only a minor difference between the genotypes was observed in a higher level of I-TAC (CXCL11), a chemoattractant for activated T lymphocytes in old Optn^{470T} brains (Fig. 29 C). Interestingly, the levels of major pro-inflammatory cytokines TNF-α and its receptors TNF-RI and TNF-RII, IFN-γ, IL-1β, and CD30 although present in low levels in old mice, were significantly higher compared to young adults. These results confirm our findings from the periphery that optineurin-insufficient brains show typical signs of inflammageing. Surprisingly, the levels of IL-1β and IL-6, a key mediator of the pro-inflammatory response were expressed in low levels at all tested time points. Overall, we observed robust expression of pro- and anti-inflammatory cytokines, chemokines, and growth factors in the brain lysates of old mice, with no changes in major pro- and anti-inflammatory factors in Optn^{470T} and WT brains, with a minor difference detected only in I-TAC.

A)

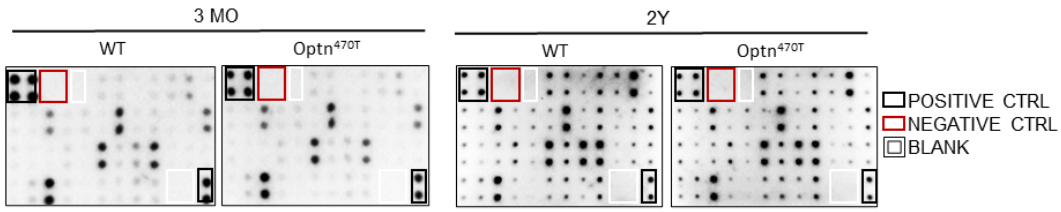

B) Young

						CXCL13	CD30	CCL11	CCL24	FasL	Fractalkine	G-CSF
					WT	0,14 +/- 0,01	0,13 +/- 0,01	0,04 +/- 0,01	0,011 +/- 0,02	0,15 +/- 0,03	0,27 +/- 0,03	0,07 +/- 0,00
					Optn470T	0,24 +/- 0,01	0,18 +/- 0,00	0,05 +/- 0,01	0,11 +/- 0,00	0,14 +/- 0,02	0,29 +/- 0,06	0,02 +/- 0,01
	GM-CSF	IFN-γ	IL-1α	IL-1β	IL-2	IL-3	IL-4	IL-6	IL-9	IL-10	IL-12	IL-12p70
WT	0,08 +/- 0,02	0,05 +/- 0,00	0,40 +/- 0,01	0,07 +/- 0,00	0,11 +/- 0,01	0,07 +/- 0,00	0,80 +/- 0,07	0,10 +/- 0,00	0,15 +/- 0,00	0,07 +/- 0,00	0,08 +/- 0,00	0,49 +/- 0,02
Optn470T	0,17 +/- 0,07	0,13 +/- 0,00	0,56 +/- 0,04	0,16 +/- 0,02	0,19 +/- 0,03	0,13 +/- 0,01	0,94 +/- 0,15	0,10 +/- 0,01	0,11 +/- 0,01	0,01 +/- 0,01	0,03 +/- 0,02	0,54 +/- 0,09
	IL-13	IL-17A	I-TAC	CXCL1	Leptin	LIX	XCL1	CCL2	M-CSF	CXCL9	CCL3	MIP-1γ
WT	0,05 +/- 0,03	/	0,02 +/- 0,01	0,12 +/- 0,02	0,04 +/- 0,01	0,81 +/- 0,09	0,20 +/- 0,04	0,34 +/- 0,03	0,74 +/- 0,05	/	/	/
Optn470T	0,10 +/- 0,05	/	0,07 +/- 0,01	0,20 +/- 0,02	0,08 +/- 0,00	0,98 +/- 0,16	0,20 +/- 0,07	0,24 +/- 0,05	0,60 +/- 0,05	/	/	/
	CCL5	CXCL12	TCA-3	CCL25	TIMP-1	TIMP-2	TNF-α	TNF RI	TNF RII			
WT	/	0,16 +/- 0,01	0,98 +/- 0,07	0,10 +/- 0,03	/	0,11 +/- 0,03	0,10 +/- 0,02	0,18 +/- 0,01	0,17 +/- 0,02			
Optn470T	/	0,21 +/- 0,02	1,31 +/- 0,17	0,12 +/- 0,04	/	0,07 +/- 0,03	0,06 +/- 0,05	0,13 +/- 0,04	0,08 +/- 0,05			

C) Old

						CXCL13	CD30	CCL11	CCL24	FasL	Fractalkine	G-CSF
					WT	1,2+/- 0,14	1,08+/- 0,16	0,6+/- 0,08	1,33+/- 0,20	0,93+/- 0,16	3,02+/- 0,28	0,28+/- 0,04
					Optn470T	1,18+/- 0,17	0,55+/- 0,19	0,41+/- 0,17	0,92+/- 0,12	0,66+/- 0,16	2,54+/- 0,20	0,28+/- 0,04
	GM-CSF	IFN-γ	IL-1α	IL-1β	IL-2	IL-3	IL-4	IL-6	IL-9	IL-10	IL-12	IL-12p70
WT	0,49+/- 0,02	0,51+/- 0,09	1,36+/- 0,15	0,08+/- 0,05	0,29+/- 0,05	0,3+/- 0,06	2,96 +/- 0,33	0,34+/- 0,04	1,12+/- 0,13	0,29+/- 0,04	0,49+/- 0,05	0,96+/- 0,1
Optn470T	0,46+/- 0,07	0,44+/- 0,08	1,44+/- 0,15	0,18+/- 0,01	0,44 +/- 0,03	0,37+/- 0,05	2,72+/- 0,37	0,35+/- 0,08	0,91+/- 0,13	0,17+/- 0,07	0,51+/- 0,11	0,96+/- 0,09
	IL-13	IL-17A	I-TAC	CXCL1	Leptin	LIX	XCL1	CCL2	M-CSF	CXCL9	CCL3	MIP-1γ
WT	0,32+/- 0,005	0,29+/- 0,05	0,08+/- 0,04	0,56+/- 0,06	0,14+/- 0,01	2,54+/- 0,32	0,87+/- 0,05	2,6+/- 0,24	2,81+/- 0,23	0,07+/- 0,04	0,33+/- 0,08	0,26+/- 0,12
Optn470T	0,45+/- 0,05	0,39+/- 0,07	**0,34+/- 0,05***	0,74+/- 0,04	0,26+/- 0,04	2,58+/- 0,11	0,96+/- 0,09	2,44+/- 0,29	2,54+/- 0,38	0,17+/- 0,08	0,51+/- 0,05	0,37+/- 0,04
	CCL5	CXCL12	TCA-3	CCL25	TIMP-1	TIMP-2	TNF-α	TNF RI	TNF RII			
WT	0,3+/- 0,02	0,66+/- 0,13	2,13+/- 0,43	/	/	0,48+/- 0,09	0,59+/- 0,07	1,02+/- 0,12	0,44+/- 0,18			
Optn470T	0,47+/- 0,16	0,9+/- 0,1	2,62+/- 0,19	/	/	0,65+/- 0,05	0,82+/- 0,09	1,23+/- 0,09	0,62+/- 0,14			

D)

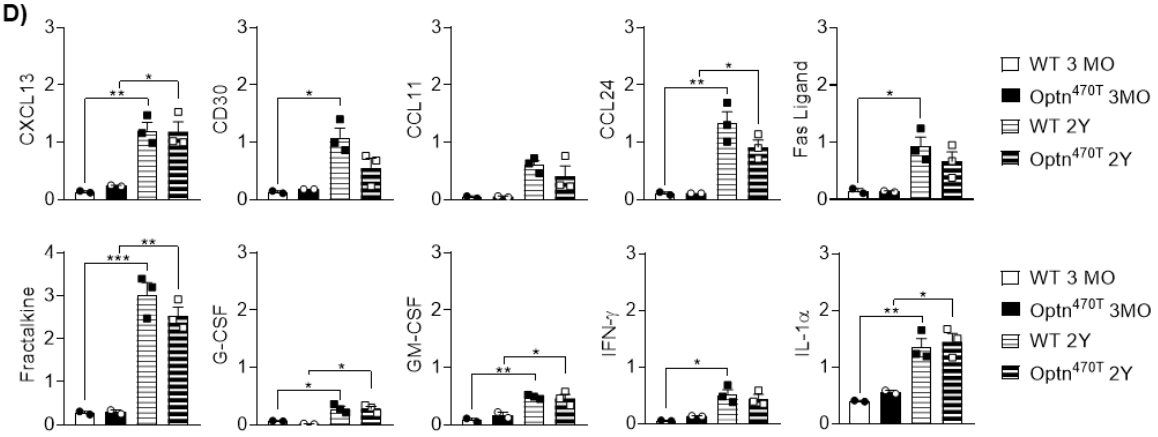

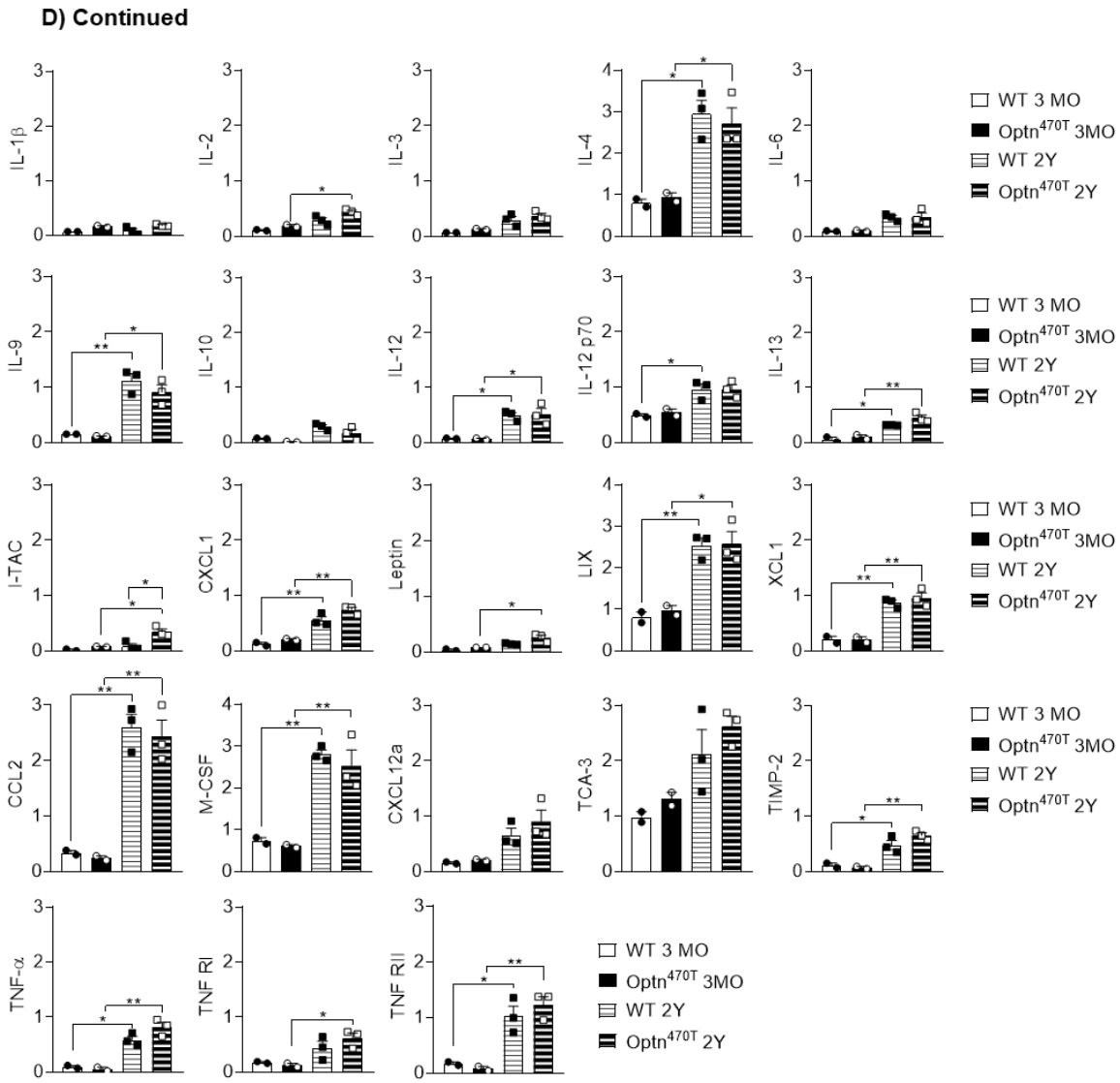

Figure 29. The brains of aged Optn^{470T} and WT mice showed higher cytokine and chemokine expression compared to the brains of young mice without overt differences between the genotypes. (A) Representative RayBio® C-Series Mouse Inflammation Antibody Array C1 membranes incubated with brain lysates from three-month (left) and two-year-old (right) male WT and Optn^{470T} mice are shown. (B) Mean values for individual proteins obtained by densitometric analyses ± SD are shown for three-month-old mice. Two independent experiments were performed from the following groups of mice: 1) 3 WT and 3 Optn^{470T}; 2) 5 WT, 4 Optn^{470T}. C) Mean values for individual proteins obtained by densitometric analyses ± SEM are shown for two-year-old mice. Three independent experiments were performed from the following groups of mice: 1) 4 WT and 5 Optn^{470T}; 2)1 WT, 5 Optn^{470T}; 3) 4 WT, 3 Optn^{470T}. D) Graphs show the comparison of individual cytokines from the brains of three-month and two-year-old WT and Optn^{470T} mice. The data were analysed by Student's t-test: * $p<0.05$, ** $p<0.01$, *** $p<0.001$.

4.2.2.3. Cytokine and chemokine expression is higher in aged spinal cords of Optn^{470T} and WT mice

The mouse models with ALS-like pathology mainly exhibit it in the spinal cord (Philips and Rothstein, 2015). Because of this, we evaluated inflammatory status in the spinal cord by performing the same protein array analyses as on brains in three-month (young adult) and two-year-old (old) male mice. Similar to the brain lysates, the strongest expression was observed in IL-4, LIX, M-CSF, and TCA-3 in both WT and Optn^{470T} spinal cord lysates (Fig. 30 A, left side, quantified in B). Notably, the levels of pro-inflammatory cytokines IL-1α, IL-12 p70, and fractalkine were lower than in brains. In comparison to spinal cord lysates from young adults, lysates from old mice demonstrated a robust increase in expression of almost all analysed proteins together with various major pro-inflammatory cytokines TNF-α, TNF-RI, TNF-RII, IL-1β, IFN-γ and CD30 (Fig. 30 A, right side, quantified in C). Moreover, the strongest expression in old mice was again observed for IL-4, LIX, CCL2, M-CSF, and TCA-3, and it was significantly increased in old compared to young adult mice (Fig. 30 D). Interestingly, in comparison to brain lysates, fractalkine, and pro-inflammatory cytokines IL-1α and IL-12p70 were not increased in aged WT and Optn^{470T} males, while pro-inflammatory IL-1β and TNF-α, and its receptors TNF-RI and TNF-RII showed higher expression than in brain lysates. Notably, aged spinal cord lysates from Optn^{470T} mice had a higher expression of XCL1, a chemokine that recruits T lymphocytes and NK cells (Fig. 30 C). To conclude, similar to the brains, the spinal cords from old mice demonstrated increased expression of pro- and anti-inflammatory cytokines, chemokines, and growth factors. Moreover, optineurin insufficiency in old mice led to a significant increase only in XCL-1, but otherwise with negligible differences between the genotypes.

A)

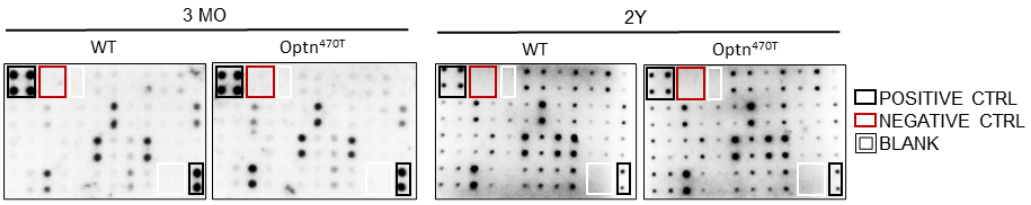

B) Young

						CXCL13	CD30	CCL11	CCL24	Fas L	Fractalkin	G-CSF
					WT	0,16 +/- 0,04	0,13 +/- 0,03	0,04 +/- 0,01	0,16 +/- 0,07	0,14 +/- 0,03	0,25 +/- 0,08	0,10 +/- 0,05
					Optn470T	0,16 +/- 0,01	0,20 +/- 0,09	0,06 +/- 0,04	0,13 +/- 0,00	0,15 +/- 0,01	0,21 +/- 0,07	0,06 +/- 0,05
	GM-CSF	IFN-γ	IL-1α	IL-1β	IL-2	IL-3	IL-4	IL-6	IL-9	IL-10	IL-12	IL-12 p70
WT	0,09 +/- 0,07	0,04 +/- 0,04	0,24 +/- 0,1	0,03 +/- 0,02	0,08 +/- 0,02	0,06 +/- 0,05	0,76 +/- 0,25	0,09 +/- 0,04	0,13 +/- 0,03	/	/	0,55 +/- 0,18
Optn470T	0,17 +/- 0,08	0,07 +/- 0,01	0,42 +/- 0,1	0,10 +/- 0,08	0,11 +/- 0,09	0,10 +/- 0,10	0,88 +/- 0,31	0,08 +/- 0,08	0,12 +/- 0,09	/	/	0,52 +/- 0,26
	IL-13	IL-17 A	I-TAC	CXCL1	Leptin	LIX	XCL1	CCL2	M-CSF	CXCL9	CCL3	MIP-1 γ
WT	0,03 +/- 0,02	/	/	0,07 +/- 0,04	/	0,82 +/- 0,22	0,17 +/- 0,07	0,23 +/- 0,07	0,65 +/- 0,04	/	/	/
Optn470T	0,06 +/- 0,04	/	/	0,19 +/- 0,13	/	0,89 +/- 0,34	0,18+/- 0,011	0,31 +/- 0,15	0,67 +/- 0,17	/	/	/
	CCL5	CXCL12 a	TCA-3	CCL25	TIMP-1	TIMP-2	TNF-α	TNF RI	TNF RII			
WT	/	0,09 +/- 0,00	0,69 +/- 0,29	0,06 +/- 0,04	/	0,12 +/- 0,05	0,08 +/- 0,03	0,29 +/- 0,01	0,12 +/- 0,03			
Optn470T	/	0,12 +/- 0,01	0,99 +/- 0,23	0,13 +/- 0,09	/	0,11 +/- 0,08	0,06 +/- 0,05	0,24 +/- 0,02	0,13 +/- 0,04			

C) Old

						CXCL13	CD30	CCL11	CCL24	FasL	Fractalkine	G-CSF
					WT	1,5+/-0,26	1,37+/-0,22	/	1,38+/-0,29	0,92+/-0,27	1,86+/-0,66	0,34+/-0,18
					Optn470T	1,81+/-0,32	1,18+/-0,11	/	1,37+/-0,15	0,69+/-0,12	1,59+/-0,19	0,33+/-0,07
	GM-CSF	IFN-γ	IL-1α	IL-1β	IL-2	IL-3	IL-4	IL-6	IL-9	IL-10	IL-12	IL-12p70
WT	0,58+/-0,06	0,63+/-0,07	1,5+/-0,15	0,86+/-0,14	0,2+/-0,10	0,21+/-0,12	3,74+/-0,56	/	0,84+/-0,15	/	0,63+/-0,11	1,07+/-0,23
Optn470T	0,6+/-0,01	0,86+/-0,1	2,00+/-0,49	1,19+/-0,30	0,43+/-0,25	0,43+/-0,20	3,93+/-0,53	/	1,02+/-0,15	/	0,69+/-0,07	0,96+/-0,1
	IL-13	IL-17A	I-TAC	CXCL1	Leptin	LIX	XCL1	CCL2	M-CSF	CXCL9	CCL3	MIP-1γ
WT	0,6+/-0,06	0,5+/-0,09	1,05+/-0,16	0,89+/-0,07	/	3,6+/-0,53	0,98+/-0,05	3,22+/-0,38	3,6+/-0,49	/	0,64+/-0,06	0,54+/-0,11
Optn470T	0,69+/-0,01	0,68+/-0,17	1,32+/-0,28	1,18+/-0,29	/	3,96+/-0,42	**1,32+/-0,1***	3,33+/-0,28	3,45+/-0,40	/	0,71+/-0,01	0,32+/-0,03
	CCL5	CXCL12	TCA-3	CCL25	TIMP-1	TIMP-2	TNF-α	TNF RI	TNF RII			
WT	0,91+/-0,02	1,43+/-0,25	4,1+/-0,61	/	/	0,99+/-0,24	1,27+/-0,21	1,18+/-0,19	2,14+/-0,36			
Optn470T	1+/-0,04	1,66+/-0,24	4,35+/-0,54	/	/	0,83+/-0,07	1,02+/-0,1	0,69+/-0,1	1,39+/-0,21			

D)

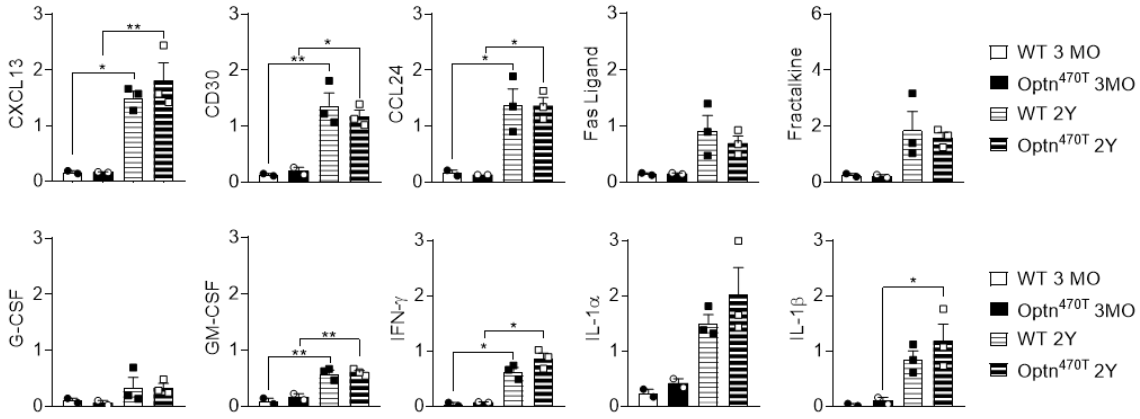

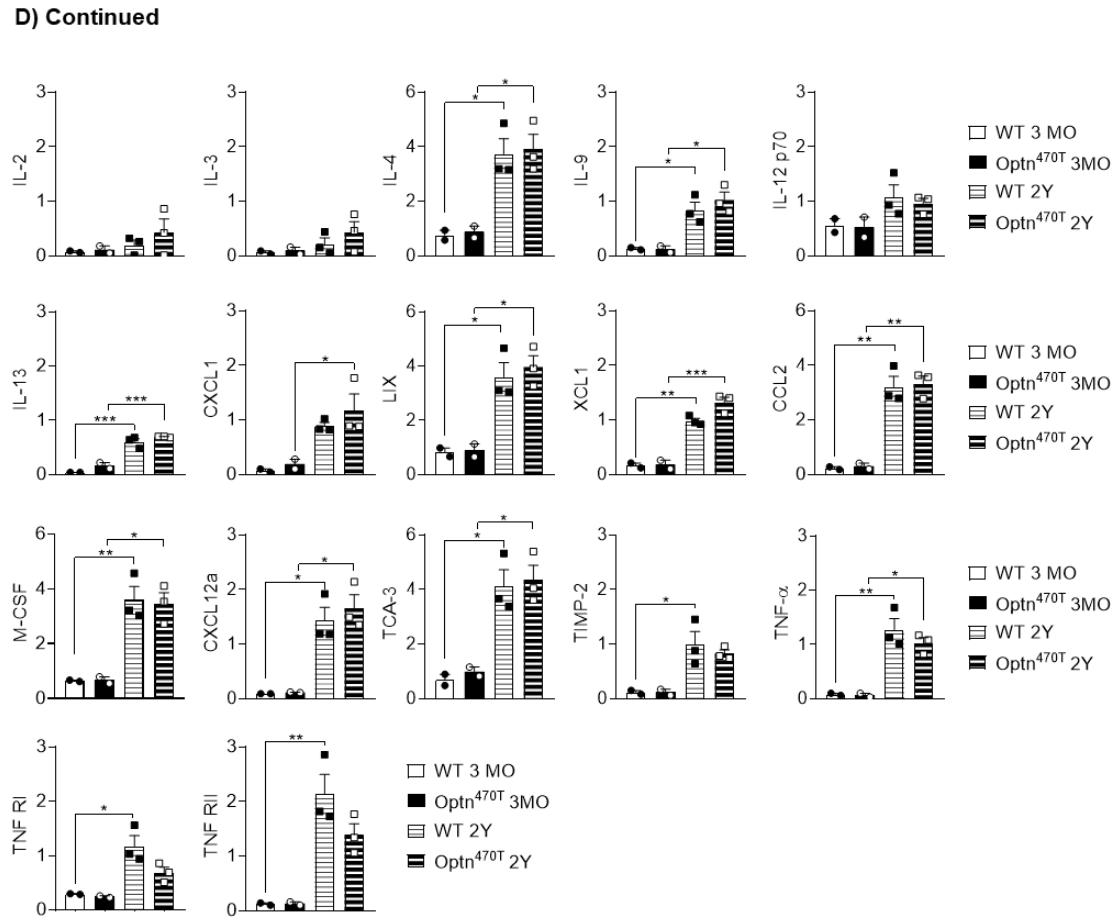

Figure 30. Aged Optn^{470T} and WT mice showed higher cytokine expression in the spinal cord compared to young mice. (A) Representative RayBio® C-Series Mouse Inflammation Antibody Array C1 membranes incubated with spinal cord lysates from three-month (left) and two-year-old (right) male WT and Optn^{470T} mice are shown. (B) Mean values for individual proteins obtained by densitometric analyses ± SD are shown for three-month-old mice. Two independent experiments were performed from the following groups of mice: 1) 3 WT and 3 Optn^{470T}; 2) 3 WT, 3 Optn^{470T}. C) Mean values for individual proteins obtained by densitometric analyses ± SEM are shown for two-year-old mice. Three independent experiments were performed from the following groups of mice: 1) 4 WT and 5 Optn^{470T}; 2)1 WT, 5 Optn^{470T}; 3) 4 WT, 3 Optn^{470T}. D) Graphs show the comparison of individual cytokines from the spinal cords of three-month and two-year-old WT and Optn^{470T} mice. The data were analysed by Student's t-test: * $p<0.05$, ** $p<0.01$, *** $p<0.001$.

4.2.3. Ageing did not induce accumulation of TDP-43 in the brains of optineurin-insufficient mice

Hyperphosphorylated and ubiquitinated TDP-43 aggregates are present in more than 95% of ALS and 50% of FTD patients, including those carrying *OPTN* mutations, and are shown to be detergent-insoluble (Arai et al., 2006). Therefore, we tested TDP-43 protein levels and solubility in WT and Optn^{470T} two-year-old male brain homogenates by biochemical fractionation. TDP-43 was found in detergent-soluble LS and TX fractions in both WT and Optn^{470T} mice, without differences between the genotypes (Fig. 31 A and B). It is important to mention, that higher bands on the membrane blotted for TDP-43 present in SARK and urea fraction were most likely a phosphorylated form of TDP-43 (phospho-TDP-43; marked by *). To further strengthen this result, we used an antibody against phospho-TDP-43 (pSer409), which is typically used for assessing pathological hyperphosphorylated TDP-43 aggregates. We observed that phosphorylated forms of TDP-43 were enriched in detergent-insoluble SARK and urea fraction in both WT and Optn^{470T} aged mice (Fig. 31 A and C). In conclusion, no signs of differential TDP-43 insolubility were found between the genotypes when tested on the whole-brain lysates. Moreover, phospho-TDP-43 was observed in insoluble fractions but without differences between the genotypes.

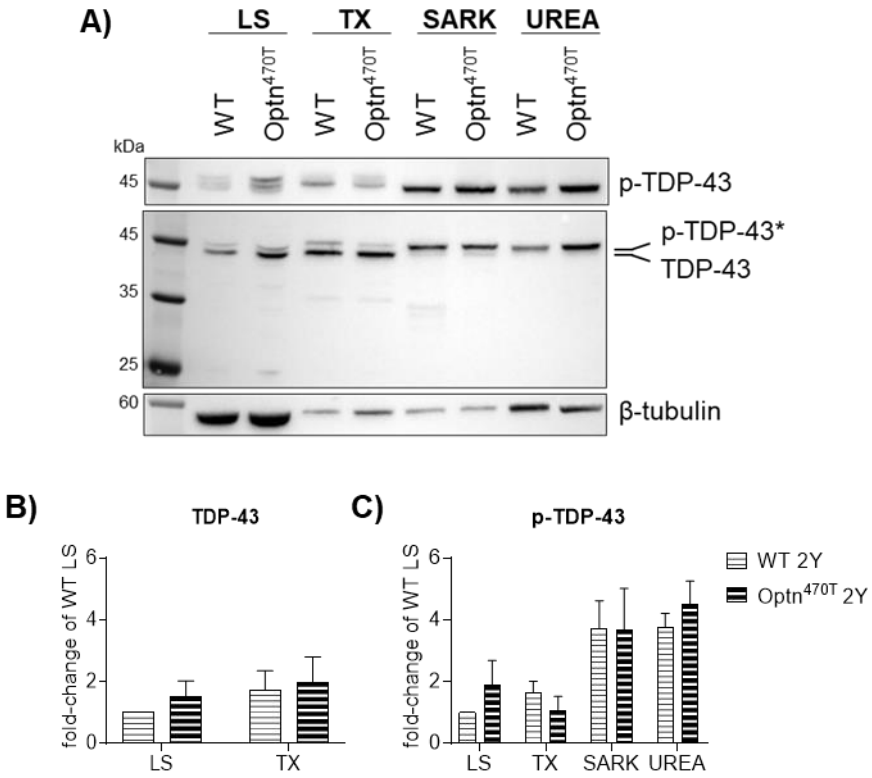

Figure 31. Ageing did not induce TDP-43 protein aggregation in Optn^{470T} compared to WT mouse brains. (A) The brains of individual two-year-old WT and Optn^{470T} male mice were homogenized, biochemically fractionated, and immunoblotted for TDP-43, p-TDP-43, and β-tubulin; β-tubulin is relevant as a loading control only for low-salt (LS) fraction. Densitometric analysis of (B) TDP-43 and (C) phospho-TDP-43 is shown as a fold-change of WT in the LS fraction; TX = Triton X fraction; SARK = sarkosyl fraction; data represent means ± SEM from three mice per genotype and were analysed by Student's t-test.

4.2.4. Optineurin-insufficient mice did not exhibit motor and cognitive deficits

To test if optineurin-insufficient mice, that mimic C'-terminal optineurin truncations found in ALS patients demonstrate an ALS- or FTD-like phenotype we assessed weight, motor functions, and cognition over the course of two years. Between six months and one year, WT males significantly gained weight (~13%), and then lost approximately the same amount by two years (Fig. 32 A). Optn^{470T} males gained less weight by one year (~9%) but overall weighted the same as WT at six months and two years. For this reason, compared to WT males, Optn^{470T} males did not show a significant weight gain from six months to one year, and loss by two years. In contrast to males, both WT and Optn^{470T} female mice increased weight during ageing (Fig. 32 B). As ALS is predominantly a motor neuron disease, and patients exhibit motor coordination deficits, we evaluated motor phenotype in WT and Optn^{470T} mice by performing the rotarod test. The average latency to fall from the rotarod in two years compared to one-year-old WT males dropped from 112 to 99 seconds (11%), which was not statistically significant (Fig. 32 C). Moreover, a similar drop from 113 to 88 seconds (23%) was demonstrated in Optn^{470T} males, showing no significant drop in latency to fall compared to WT males. Furthermore, WT and Optn^{470T} females showed no difference in average latency to fall from 18 months to two years (Fig. 32 D), confirming our results that optineurin-insufficient mice do not exhibit an ALS phenotype. As ALS and FTD share common genetic backgrounds, we also tested if Optn^{470T} mice show deficits in learning and fear-motivated memory by measuring entry latency in a passive avoidance test. We observed high mouse-to-mouse variability in one-year-old males and females in both genotypes. However, we did not demonstrate a difference in cognition or FTD phenotype in optineurin-insufficient compared to WT mice (Fig. 32 E-F). Notably, we did not detect a different survival rate between WT and Optn^{470T} mice (data not shown). To summarize, Optn^{470T} males showed slightly lower average weight gain at one year compared to WT mice, but overall, no ALS or FTD phenotype.

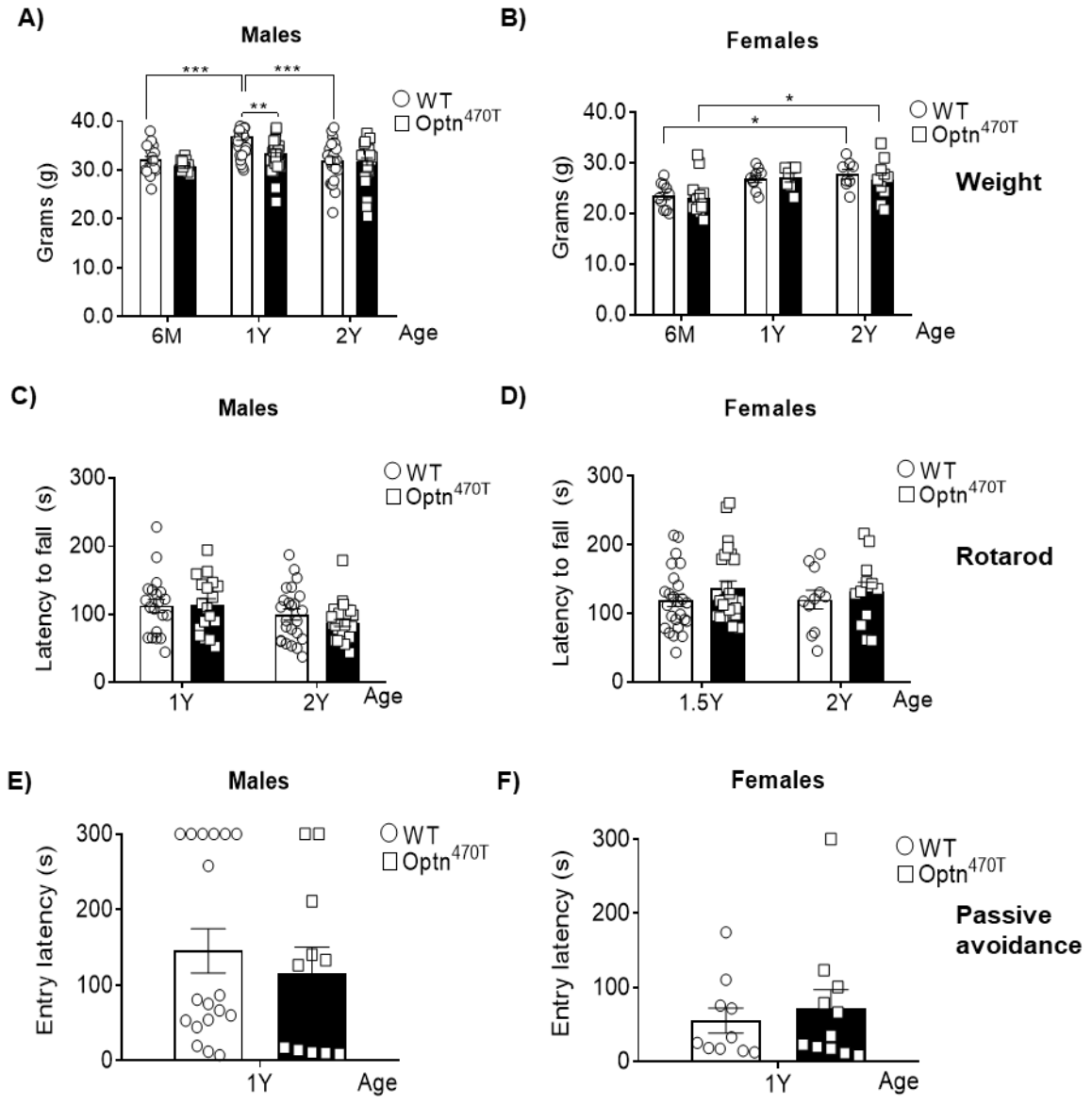

Figure 32. Optineurin insufficiency did not affect motor coordination and cognition in Optn^{470T} mice. Bar diagrams show body weight (in grams) for individual (A) males at the age of six months (20 WT, 17 Optn^{470T}), one year (35 WT, 39 Optn^{470T}), and two years (26 WT, 29 Optn^{470T}), and (B) females at the age of six months (11 WT, 16 Optn^{470T}), one year (9 WT, 7 Optn^{470T}) and two years (8 WT, 10 Optn^{470T}). Motor coordination on the rotarod measured as the average latency to fall (in seconds) is shown for (C) males at the age of one year (20 WT, 18 Optn^{470T}) and two years (24 WT, 28 Optn^{470T}), and (D) females at the age of one and a half years (25 WT, 26 Optn^{470T}), and two years (11 WT, 12 Optn^{470T}). Evaluation of fear-motivated memory is shown as entry latency (in seconds) in the passive avoidance test for (E) males (18 WT, 11 Optn^{470T}) and (F) females (10 WT, 11 Optn^{470T}). Data are presented as means ± SEM from the indicated number of mice and analysed by two-way ANOVA (A-D) and Student's t-test (E-F): * $p < 0.05$, ** $p < 0.01$, *** $p < 0.001$.

4.3. Establishing a novel two-hit ALS mouse model that carries optineurin truncation and transgenic human TDP-43^{G348C} mutation

As we showed that ageing was not sufficient to initiate ALS- or FTD-like phenotype in optineurin-insufficient mice, we aimed to establish a new two-hit ALS and/or FTD model. We crossed optineurin-insufficient (Optn^{470T}) mice with mice carrying transgenic human TDP-43 mutation (TDP-43^{G348C}), the model that develops cytoplasmic TDP-43 protein aggregates and neuroinflammation (Swarup et al., 2011a). To obtain mice for the experiments, we had to generate three generations of mice, which we screened by PCR for WT and truncated optineurin, and human transgenic TDP-43^{G348C} and analysed by agarose gel electrophoreses (WT band ~365 bp, Optn^{470T} ~288 bp, and TDP-43^{G348C} ~363 bp, respectively). In the first generation, homozygous Optn$^{470T/470T}$ males were crossed with Optn$^{WT/WT}$ TDP-43^{G348C} females, which were previously backcrossed to C57BL/6 (WT) genetic background by Dr. Jasna Križ. We obtained offspring heterozygous for optineurin with or without transgenic TDP-43^{G348C} (Optn$^{WT/470T}$, Optn$^{WT/470T}$ TDP-43^{G348C}) as shown in Figure 33A. In the second generation, non-transgenic heterozygous (Optn$^{WT/470T}$) males were crossed with transgenic heterozygous females (Optn$^{WT/470T}$ TDP-43^{G348C}) and the littermates were both non-transgenic and transgenic homozygotes for WT (Optn$^{WT/WT}$, Optn$^{WT/WT}$ TDP-43^{G348C}) and truncated optineurin (Optn$^{470T/470T}$, Optn$^{470T/470T}$ TDP-43^{G348C}), or the heterozygous mice (Optn$^{WT/470T}$, Optn$^{WT/470T}$ TDP-43^{G348C}); an example of screening is shown in Figure 33 B. To finally establish the cohorts necessary for our experiments, in the third generation non-transgenic Optn$^{470T/470T}$ were crossed with transgenic Optn$^{470T/470T}$ TDP-43^{G348C} mice, and the resulting littermates were homozygous for optineurin either with or without a heterozygous transgenic TDP-43^{G348C} mutation; they are therefore referred to as Optn^{470T} and Optn^{470T} TDP-43^{G348C}, respectively (Fig. 33 C). A similar breeding scheme was performed to obtain age-matched control mice, homozygous Optn$^{WT/WT}$ and Optn$^{WT/WT}$ TDP-43^{G348C}, further referred to as WT and WT TDP-43^{G348C}, respectively. Notably, we observed a normal Mendelian pattern of inheritance and no difference in survival rate between genotypes. To sum up, after three generations of mice, we established a potential new ALS and/or FTD mouse model that had truncated optineurin and carried a human transgenic mutation in TDP-43.

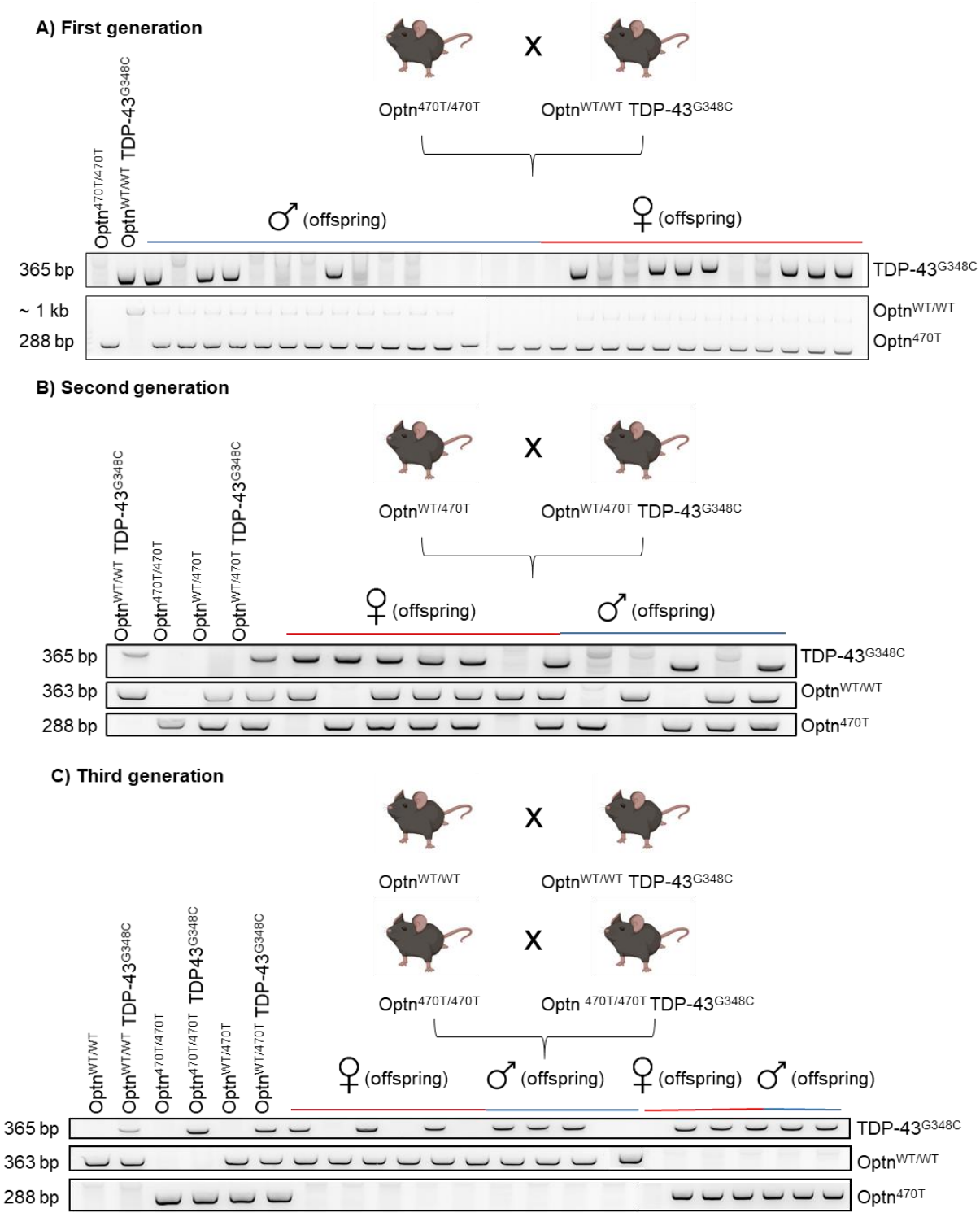

Figure 33. Generation of a novel mouse model with optineurin insufficiency and transgenic human TDP-43 mutation. To generate a novel mouse model several generations of mice were generated and the mouse genotype was checked by PCR for WT and truncated optineurin, and trangenic TDP-43, and analysed on an agarose gel. The control mice for PCR reactions were shown on the left side of the gel. (A) In first-generation homozygous Optn^{470T} mice were crossed with trangenic TDP-43^{G348C} to obtain offspring that

is heterozygous for optineurin with or without the TDP-43^{G348C} transgene. (B) In the second generation, heterozygous Optn^{470T} mice were crossed with heterozygous Optn^{470T} with trangenic TDP-43^{G348C} to obtain homozygous Optn^{470T} trangenic, as well as Optn^{WT} transgenic mice. (C) For a stable line of homozygous Optn^{470T} and Optn^{WT} transgenic mice were crossed with Optn^{470T} and Optn^{WT} without transgene.

4.3.1. The novel two-hit ALS and/or FTD mouse model did not exhibit ALS-like motor deficits

To test if novel two-hit ALS and/or FTD model mice show ALS phenotype, we assessed motor functions by performing rotarod tests from 6 to 20-month-old mice. Because of the (still) limited number of transgenic mice we obtained from breedings, we pooled males and females from the same genotype (WT, TDP-43^{G348C}, Optn^{470T,} and Optn^{470T} TDP-43^{G348C}) and analysed them in the following age groups: from 6-10, 11-15 and 16-20 months of age. The average latency to fall from the rotarod in WT non-transgenic mice (white bars) at 6-10 months was around 185 seconds and it significantly dropped to 108 seconds (~41%) at 11-15 months, without changes at a later test point (Fig 34 A). As we expected, Optn^{470T} non-transgenic mice (black bars) demonstrated similar average latency to fall compared to WT mice (Fig 34 A). Surprisingly, and opposite to the results shown by Swarup *et al*. (Swarup et al., 2011a) we did not detect a difference in latency to fall in TDP-43^{G348C} compared to WT non-transgenic mice at any time point tested, finding a similar significant drop between 6-10 and 11-15 months old mice (Fig 34 A). Furthermore, our novel two-hit ALS Optn^{470T} TDP-43^{G348C} model showed similar latency to fall from rotarod as Optn^{470T} mice, with a significant drop from 6-10 to 15-20 months old mice (Fig 34 A). Moreover, we did not detect the difference in latency to fall between TDP-43^{G348C} and Optn^{470T} TDP-43^{G348C} at any time point tested. To conclude, we did not detect a failure in motor functions between non-transgenic and transgenic WT and Optn^{470T} mice demonstrating no evident ALS phenotype.

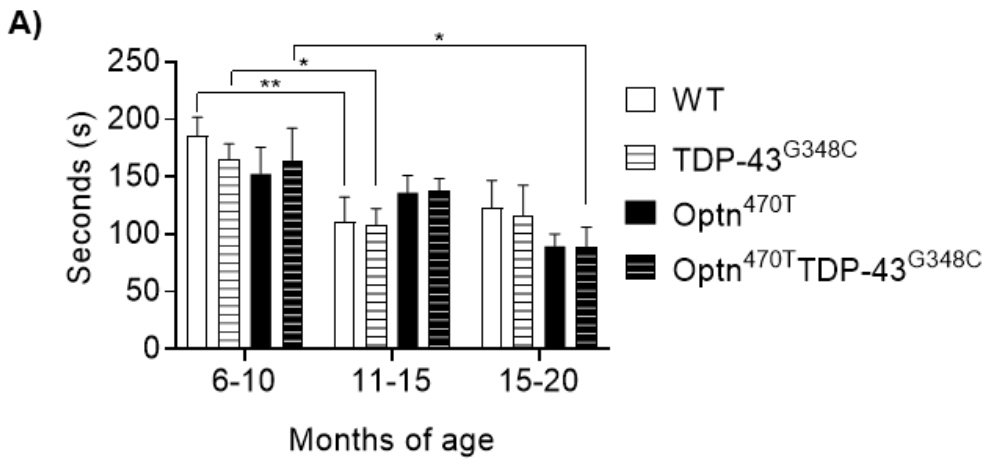

Figure 34. The novel two-hit ALS mouse model did not exhibit deficits in motor coordination. (A) Bar charts show motor coordination on the rotarod measured as the average latency to fall (in seconds) for indicated months of age in WT, WT TDP-43^{G348C}, Optn^{470T}, and Optn^{470T}TDP-43^{G348C} mice. Data are presented as means ± SEM from the indicated number of mice (WT; 19,16 and 11, WT TDP-43^{G348C}; 27, 20 and 6, Optn^{470T}; 9, 25 and 16, Optn^{470T} TDP-43^{G348C}; 10, 37 and 12) and analysed by two-way ANOVA.

5. Discussion

5.1. The role of optineurin deficiency and insufficiency in TDP-43 accumulation

Mutations in optineurin have been linked to ALS and FTD, a neurodegenerative diseases marked by chronic inflammation and protein aggregation (Maruyama et al., 2010). In the majority of sALS and fALS cases, including cases that harbour optineurin mutations, protein aggregates in motor neurons and glial cells contain nuclear RNA/DNA-binding protein TDP-43 (Arai et al., 2006; Ito et al., 2011; Kurashige et al., 2021; Neumann et al., 2006). The exact reason for TDP-43 nuclear depletion and cytoplasmic aggregation in disease is still largely elusive, therefore we aimed to test how the loss of functional optineurin could cause TDP-43 pathology. The initial results from our group demonstrated that complete optineurin genetic depletion (using a conventional CRISPR/Cas9 approach) in cell lines led to the accumulation of TDP-43 in BV2 microglial cell lines, but not in neuronal Neuro2A and NSC-34 cell lines (results from Matea's Rob Master thesis: https://urn.nsk.hr/urn:nbn:hr:193:162533) (Prtenjaca et al., 2022). Upon finding this TDP-43 phenotype in BV2 Optn KO cells, we further tested TDP-43 levels in unmanipulated primary myeloid cells (BMDMs and microglia) from ubiquitin insufficient $Optn^{470T}$ mouse model that mimics C'-terminal Q398X truncation found in ALS patients. Primary $Optn^{470T}$ myeloid cells displayed increased TDP-43 protein levels, thus confirming our results obtained on optineurin-deficient microglia cells. This demonstrated that optineurin deficiency and ubiquitin-binding insufficient optineurin have the same phenotype, suggesting that ubiquitin binding is crucial for increased TDP-43 protein levels. Notably, despite having increased TDP-43 levels, $Optn^{470T}$ primary microglia did not exhibit protein aggregates, and TDP-43 was still predominantly nuclear, which we confirmed by immunofluorescent microscopy. Somewhat similar results were found in HeLa cells, where optineurin siRNA depletion and ALS-associated pathogenic mutations induced an accumulation of ubiquitinated TDP-43 fragments (Kakihana et al., 2021). Moreover, in contrast to our preliminary data in neuronal cell lines, and similar to the finding in Neuro2A cell lines harbouring UBQLN2 ALS-linked mutation, here we demonstrated increased TDP-43 in $Optn^{470T}$ primary neurons (Osaka et al., 2016; Prtenjaca et al., 2022). This is potentially a very interesting observation since it was previously reported in the hSOD1 mouse model

that both neurons and non-neuronal glial cells need to be affected for ALS pathology (Boillee et al., 2006; Lino et al., 2002; Pramatarova et al., 2001). Importantly, as TDP-43 actively binds to its own mRNA and autoregulates its cellular concentration, we found no overt *TARDBP* expression in both microglia and neurons, meaning that increased TDP-43 protein levels are post-translationally regulated in optineurin-deficient and -insufficient primary cells.

5.1.1. Optineurin is dispensable for TDP-43 protein degradation by ubiquitin-proteasomal system and autophagy

Several genetic mutations associated with ALS and FTD, such as p62, VCP, and UBQLN2, were shown to disrupt UPS and autophagy pathways, both of which are involved in the degradation of TDP-43 (Deng et al., 2011; Fecto, 2011; Watts et al., 2004). However, the role of protein degradation in the maintenance of TDP-43 proteostasis is still unclear. Although there is conflicting evidence on whether TDP-43 is predominantly degraded by the UPS or autophagy, recent findings suggested that degradation of the soluble TDP-43 is mediated by the UPS, whereas TDP-43 protein aggregates require autophagy (Scotter et al., 2014; Urushitani et al., 2010; Wang et al., 2010; Zhang et al., 2010). Here we reported that microglial TDP-43 in the basal state is predominantly degraded through UPS, while neuronal TDP-43 turnover requires both UPS and autophagy. Overexpression of ALS-linked optineurin mutations Q398X and E478G or optineurin deletion fails to clear damaged mitochondria and overexpressed mutant TDP-43, as well as bind to myosin VI, thus affecting autophagy flux (Korac et al., 2012; Lazarou et al., 2015; Moore and Holzbaur, 2016; Shen et al., 2015; Sundaramoorthy et al., 2015; Wong and Holzbaur, 2014.). Interestingly, while patients carrying the homozygous Q398X mutation tested positive for TDP-43-positive autophagic vacuoles, ALS patients carrying a heterozygous mutation E478G did not (Ito et al., 2011; Kurashige et al., 2021; Shen et al., 2015). Due to these discrepancies in the role of optineurin in TDP-43 degradation via autophagy, we assessed whether the increased TDP-43 levels in BV2 Optn KO cells and $Optn^{470T}$ primary microglia are due to the impaired protein degradation caused by non-functional optineurin. Perhaps surprisingly, by monitoring the LC3-I to LC3-II conversion, we observed an active autophagy flux in the basal conditions in both WT and optineurin-insufficient microglia, suggesting that optineurin

or its ubiquitin-binding function is dispensable for this process. Notably, our results also demonstrated that optineurin was not acting as an autophagy adaptor protein in this process, as we showed that optineurin itself was not degraded by autophagy. This shows that it's most likely not participating in the process of basal TDP-43 turnover in microglia. Interestingly, in contrast to the results obtained in microglia, we demonstrated that in another type of myeloid cells -macrophages - TDP-43 was degraded by autophagy in WT cells under basal conditions. Nevertheless, in both WT and Optn^{470T} BMDMs, basal autophagy flux (measured by LC3-II turnover) was equally active. These results have suggested that the accumulation of TDP-43 in primary myeloid Optn^{470T} and BV2 Optn KO cells cannot be explained by macroautophagy, an autophagy degradation process that is LC3-mediated within cytosolic double-membrane autophagosomes. Recent findings showed that TDP-43 is also a substrate in chaperone-mediated autophagy (CMA) and that CMA can contribute to the turnover of physiological and pathological forms of TDP-43, suggesting that alterations in other types of autophagy could be the reason for increased TDP-43 protein in optineurin insufficient/deficient myeloid cells (Ormeño et al., 2020; Parzych and Klionsky, 2014). Similar results observed on TDP-43 degradation in BMDMs upon inhibition of autophagy were observed in Optn^{470T} primary neurons. We found this interesting since previous findings from our group showed a mild block in different steps within basal autophagy flux in Optn^{470T} primary neurons and N2A Optn KO neuronal cell lines (results from Tereza's Ljutić and my Master thesis: https://urn.nsk.hr/urn:nbn:hr:193:919801, https://urn.nsk.hr/urn:nbn:hr:193:2653 75). Thus, our results reinforce the conclusion that the role of optineurin in autophagy could differ in various cell types and experimental systems and should be further investigated since there are other proteins within the LC3 family such as GABA Type A Receptor-Associated Protein (GABARAP).

Inhibition of both the UPS and autophagy increased the insoluble TDP-43 protein levels and enhanced its aggregation in human neuronal cell lines (Scotter et al., 2014). However, in contrast to these findings, we demonstrated that the joint blockade of UPS and autophagy did not further increase TDP-43 protein levels in WT or optineurin deficient/insufficient cells, suggesting that these mechanisms work independently of each other under our experimental conditions. One notable

limitation of our study is our inability to precisely determine the half-life of TDP-43. We performed a cycloheximide chase assay, where by blocking protein translation we could measure protein degradation at different time points by Western blot. However, our experimental cells were dying before TDP-43 started to degrade. Microglia showed higher sensibility by entering apoptosis upon 8 h of UPS blockade, with higher incubation times being toxic, whereas TDP-43 is a stabile protein with a half-life around 12-15 h (Austin et al., 2014; Ling et al., 2010; Watanabe et al., 2013). Interestingly, we did not observe a difference in apoptosis between BV2 WT and Optn KO microglia cells. Surprisingly, in BV2 Optn KO cells, as well as Optn^{470T} primary microglia and neurons, the dual inhibition of both UPS and autophagy decreased TDP-43 levels. Although this may have suggested the potential higher toxicity by these blocks in cells lacking functional optineurin, we did not detect increased apoptosis or toxic TDP-25/TDP-35 fragments during 4 h of experiments. We propose several hypotheses that should be tested to clarify our findings. Firstly, the decreased TDP-43 protein levels in optineurin deficient/insufficient cells could be due to increased levels of insoluble TDP-43 and should be tested in buffers of different solubilities, but we do not favour this since we did not observe the loss of TDP-43 when performing immunofluorescent analyses. Secondly, since TDP-43 protein aggregates are hyperphosphorylated and marked with K48- and K63-poly ubiquitin chains, there is a possibility that commercially available antibodies could not detect altered TDP-43. However, we used the same commercial polyclonal TDP-43 and p-TDP-43 antibodies as other groups that reported TDP-43 protein aggregates, so most likely we do not encounter problems with antibodies. Moreover, we could not determine the localisation of WT and truncated optineurin and if it is co-localisation with TDP-43 as commercial optineurin antibody is not working for immunofluorescence analyses, and our attempt to produce a specific N'-terminal antibody for truncated optineurin was unsuccessful. Finally, other degradation mechanisms such as ER stress-activated unfolded protein response (UPR), CMA, or microautophagy could mitigate TDP-43 degradation in cells harbouring non-functional optineurin. Therefore, although we still do not understand the exact mechanism of the TDP-43 increase in optineurin-deficient and -insufficient cells, we did not see significantly diminished protein degradation by UPS and/or autophagy compared to WT cells.

5.1.2. TDP-43 in optineurin-insufficient mouse myeloid cells is unresponsive to inflammatory stimuli

It was proposed that TDP-43 protein aggregation could directly trigger inflammation, and *vice versa*, that inflammation could trigger protein aggregation (Bright et al., 2021). Given that ALS is marked with excessive chronic neuroinflammation and that cytoplasmic TDP-43 has been reported in the circulating monocytes of ALS patients (De Marco et al., 2017), several publications have looked for eventual direct links between TDP-43 and inflammation. In line with results obtained by Correia *et al*., we found increased TDP-43 protein levels upon LPS inflammatory stimuli in WT BV2 cell lines and primary microglia (Correia et al., 2015). Surprisingly, in contrast to their finding that LPS caused TDP-43 nuclear depletion and aggregation, in our experimental settings we could not trigger a proteinopathy similar to what has been observed in ALS or FTD. Interestingly, upon LPS treatment, WT microglia showed a decrease in cytoplasmic and an increase in the nuclear to cytoplasmic TDP-43 ratio, which is opposite to what has been previously reported (Correia et al., 2015). Nevertheless, several reports also suggested that TDP-43 has been difficult to aggregate, even in the presence of patient mutations (Araki et al., 2014; Buratti, 2018). Importantly, in BV2 Optn KO and Optn^{470T} primary microglia, LPS could not further increase TDP-43 levels. We observed that TDP-43 in these cells persisted at the same elevated state as in basal conditions, suggesting that TDP-43 reached the plateau in cells with non-functional optineurin and could not further increase upon inflammatory stimuli. Similar findings were observed in macrophages, where in WT cells LPS increased TDP-43 protein levels, whereas in Optn^{470T} BMDMs TDP-43 stayed at the same elevated state as in basal conditions. We hypothesize that this plateau is reached because TDP-43 functions in a very narrow concentration window and even moderate overexpression can be toxic to cells. Moreover, we did not detect nuclear depletion nor cytoplasmic TDP-43 protein aggregates upon LPS in WT and optineurin-insufficient primary microglia. In contrast to WT cells, we showed a rather small increase in nuclear to cytoplasmic ratio, suggesting that TDP-43 is less responsive to cellular redistribution. A similar phenotype was observed in affected lumbar spinal cord regions in rats, where microglia were less responsive to inflammatory stimuli than healthy microglia, perhaps demonstrating exhaustion and/or desensitization (Nikodemova et al., 2014).

It was previously reported that optineurin mutation could lead to hyperactivation of the NF-κB or IRF3 signalling pathway, but this result should be interpreted with caution because opposing results were obtained within different research groups and experimental settings (Akizuki et al., 2013; Fukushi et al., 2023; Maruyama et al., 2010). Our results could also mean that optineurin deficiency/insufficiency could exaggerate chronic inflammation, but these hypotheses should further be evaluated as we did not detect shape change from ramified to an ameboid form, nor apoptosis activation in basal state. Our recently performed RNA-Seq results could provide additional clues into how optineurin could modulate gene expression upon inflammation.

In addition to inflammation, studies have shown that autophagy is also involved in the defence against bacterial and viral infection and that autophagy dysfunction could lead to excessive inflammation and damage during infection (Choi et al., 2018; Deretic, 2021; Mao and Klionsky, 2017). Here we reported that upon LPS treatment, an autophagy receptor p62 is elevated in both WT and Optn^{470T} BMDMs, confirming the data that NF-κB facilitates autophagy induction by inducing the expression of receptor proteins (Zhong et al., 2016). Surprisingly, we did not detect elevated optineurin levels in WT BMDMs upon LPS treatment, suggesting that optineurin is not a receptor protein in LPS-mediated autophagy. We further tested if the accumulation of TDP-43 upon LPS in WT cells and optineurin insufficient cells is autophagy-dependent, as optineurin was proposed to be an autophagy receptor for protein aggregates (Korac et al., 2012; Shen et al., 2015). We showed that contrary to the basal state, elevated TDP-43 was not degraded through autophagy in WT cells upon inflammation. However, similar to our findings obtained in protein degradation experiments, we detected an inexplicable drop in TDP-43 in Optn^{470T} cells upon both inflammatory stimuli and autophagy inhibition. The possible reason behind this is already emphasised detection of aggregates in our experimental settings since a recent publication reported that some antibodies do not stain the aggregates in human cells (Fernandes et al., 2020). To address this issue, we compared N'- and C'-terminal TDP-43 antibodies by Western blotting and observed the same pattern of TDP-43 staining (data not shown), suggesting that we did not experience staining problems. Taken together, for now, we cannot explain the drop in TDP-43 in some

experimental conditions but we further wanted to test exocytosis, because it is proposed that TDP-43 could be cleared by exocytosis (Hung et al., 2023).

Recent findings suggested that mutations in TDP-43 or its overexpression could lead to perturbed autoregulation, altered RNA splicing, and mRNA stability in motor neuron-like cells and primary cultures of cortical neurons (Neelagandan et al., 2019; White et al., 2018). Here we analysed whether LPS-induced accumulation or increased levels of TDP-43 in basal state in Optn^{470T} myeloid cells could alter gene expression. We reported that *TARDBP* expression upon LPS in both WT and Optn^{470T} myeloid cells is slightly reduced, suggesting that inflammation decreases *TARDBP* gene expression independently of optineurin mutation, and demonstrating that TDP-43 autoregulation is not lost. This finding confirmed our data that accumulated TDP-43 in the optineurin- insufficient and -deficient model is post-translationally regulated. Although TDP-43 regulates thousands of RNA targets, it is largely unknown which ones, if any, directly contribute to disease pathogenesis. Recent findings showed that nuclear depletion of TDP-43 decreased the splicing of *Poldip3*, a gene encoding for RRM-containing protein that participates in the regulation of translation, and also reduces the stability *of G3bp1* gene transcripts, which encode for a protein important in stress granule formation (Shiga et al., 2012; Sidibé et al., 2020). Here we reported that expression levels of *Poldip3* and *G3bp1* in the basal state were comparable between Optn^{470T} and WT myeloid cells arguing that increased TDP-43 protein levels in optineurin insufficient cells do not alter the expression of these genes. Moreover, we showed that LPS stimulation decreased *G3bp1*, and increased *Poldip3* expression in WT myeloid cells. However, LPS did not increase *Poldip3* expression but did stimulate a similar drop in *G3bp1* in optineurin-insufficient cells. Therefore, as mentioned before, we expect that the results from RNA-Seq analyses could pinpoint the altered gene sets and clarify how optineurin and/or accumulated TDP-43 in optineurin-deficient myeloid cells modulate gene expression upon inflammation.

Collectively, our data suggest that optineurin deficiency and insufficiency post-translationally upregulate microglial TDP-43 protein levels. This TDP-43 accumulation does not occur via diminished proteolysis, does not trigger protein aggregation, and cannot be further increased by inflammation.

5.2. The role of ALS-linked optineurin mutation during ageing in Optn^{470T} mice

Diseases such as ALS, FTD, Alzheimer's, and Parkinson's disease are among the most pressuring problems of developed societies within an ageing population, and ageing is considered to be a major risk factor for these neurodegenerative diseases. Thus, the second aim of this thesis was to study whether ageing would provide a sufficient second hit to elicit an ALS-like phenotype and neuropathology in Optn^{470T} mice. During ageing, the immune system undergoes changes that are linked to immune cell senescence and excessive activation in both CNS and periphery (Franceschi et al., 2000). Here we reported that Percoll-enriched immune cells isolated from the CNS of old mice exhibited a strong autofluorescence already in middle-aged mice, most likely due to the accumulation of lipofuscin, an age-related lipid-containing pigment that accumulates in various brain regions in post-mitotic and senescent cells (Moreno-García et al., 2018). Notably, our group reported no difference in lipofuscin accumulation between old WT and Optn^{470T} mice by immunofluorescence, meaning that optineurin-insufficiency does not aggravate lipofuscin accumulation ((Mohovic et al., 2023), results from J. Peradinovic). Although we aimed to evaluate infiltration of both CD4$^+$ and CD8$^+$ T lymphocytes that are previously reported in ALS patients and hSOD1 mice (Coque et al., 2019; Engelhardt et al., 1993; Holmøy, 2008; Troost et al., 1989), because of autofluorescence we could not perform immunophenotyping of immune cells from the CNS. However, because numerous alterations in the periphery were also reported in ALS and FTD patients and animal models (Beers and Appel, 2019; Béland et al., 2020; De Marchi et al., 2021), we performed detailed analyses of splenocytes by flow cytometry. Notably, despite the proposed optineurin roles in inflammatory signalling, detailed immunophenotyping has not been performed in detail in any of the optineurin mouse models. We reported an increase in B lymphocytes in old Optn^{470T} male mice that was absent in WT, but we could not link this to any phenotype as there is currently no experimental evidence that B lymphocytes affect the course of ALS (Béland et al., 2020c; De Marchi et al., 2021; Naor et al., 2009). Interestingly, both WT and Optn^{470T} female mice showed a decrease in B lymphocytes, demonstrating discrepancies between the sexes during ageing. In addition, we showed several notable age-related changes in T lymphocytes, such as an increase in CD8$^+$ T lymphocytes, a

decrease in $CD4^+$ T lymphocytes, and thus a drop in $CD4^+/CD8^+$ T lymphocyte ratio in both WT and $Optn^{470T}$ mice. In addition, a recent study on middle-aged $Optn^{-/-}$ mice reported a slight drop in $CD4^+/CD8^+$ T lymphocyte ratio in blood compared to WT mice (Moharir and Swarup, 2021). Furthermore, we also found a prominent drop in naïve and an increase in both effector and central memory $CD8^+$ and $CD4^+$ lymphocytes between young adults and old mice. However, we did not observe any substantial differences between the WT and $Optn^{470T}$ mice. Furthermore, optineurin insufficiency did not cause an exaggerated activation of T lymphocytes during ageing or an increased exhaustion/senescence phenotype. Interestingly, most of the age-related alterations in T lymphocytes were already observed in middle-aged mice and were not severely aggravated between middle-aged and old mice. One of the major findings from the adaptive immune system in the hSOD1 mice model and ALS patients is that disease progression is accelerated by a decrease in Tregs and that by autologous Treg infusion or by other treatments that boost Treg numbers, the ALS progression is slowed down (Henkel et al., 2013; Thonhoff et al., 2022, 2018). Here we reported an increase in non-functional Tregs in both WT and $Optn^{470T}$ mice during ageing, which was previously reported in the aged mice (Nishioka et al., 2006). Interestingly, an increase in functional Tregs was absent from $Optn^{470T}$ in comparison to WT mice, but higher expression of FOXP3 was observed in old $Optn^{470T}$ female mice, but for now, we could not link this to any functional readouts. We also observed changes in innate immune cells linked to ageing: an increase in the number of macrophages and neutrophils, as well as a decrease in NK cells in both WT and $Optn^{470T}$ mice. However, in contrast to recently reported lower expression of activation markers in young conditional CD11c-specific $Optn^{-/-}$ model, here we found higher levels of MHC-II in cDC of old $Optn^{470T}$ males (Wang et al., 2021). However, Wang *et al.* also observed an increase in Tregs in their model, suggesting that some changes could be age-related. Interestingly, detailed immunophenotyping performed in $C9orf72^{-/-}$ mouse model showed a higher CD86 expression in cDCs which is similar to an increased CD86 expression observed in our analyses in old $Optn^{470T}$ mice (McCauley et al., 2020). Because of this discrepancy between mouse models and studies, which could also be age-related, and because the general role of cDCs in ALS is unclear, further investigations are necessary to understand the importance of optineurin in cDCs and immune cells in general. Taken together, we found no

peripheral immune alterations linked to ALS pathogenesis nor advanced immunosenescence and/or inflammageing in the optineurin insufficient mouse model.

Similar to recently reported cytokine expression in the brain during ageing, here we demonstrated that both brains and spinal cords from old mice have a robust increase in expression of almost all proteins analysed by protein array (Porcher et al., 2021). Recent findings also suggested that spinal cords of $Optn^{-/-}$ mice exhibited an increased expression of multiple proinflammatory cytokines such as TNF-α, IFN-γ, IL-1α, IL-1β, IL-2, and IL-12, whereas a brain expressed higher levels of microglial activation and IL-1β only upon lentivirus-mediated overexpression of $OPTN^{E478G}$ (Ito et al., 2016a; Liu et al., 2018). However, here we demonstrated the neglectable difference between WT and $Optn^{470T}$ mice, confirming our results from peripheral immune analyses. The strongest expression in both young adults and old WT and $Optn^{470T}$ mice was observed for anti-inflammatory cytokine IL-4, and chemoattractants and/or growth factors for neutrophils and macrophages LIX, M-CSF, and TCA-3. Furthermore, fractalkine, chemokine by which neurons suppress microglial activation, and pro-inflammatory cytokines IL-1α and IL-12 p70 were observed both in brains and in the spinal cord. Surprisingly, we did not detect strong expression of major pro-inflammatory cytokine TNF-α, IFN-γ, IL-α, IL-β, IL-2, and IL-12 previously reported as a major functional readout in optineurin deficient mice (Ito et al., 2016b). Our results showed that ageing is by itself insufficient to uncover the difference in the expression of inflammatory factors in the CNS between WT and $Optn^{470T}$ mice. The recent finding also suggested that, during ageing, an increase in cytokine production is more prominent in the hippocampus compared to other brain regions, thus suggesting that cytokine expression depends on the brain region (Porcher et al., 2021). This finding opens a question of whether we should separately test the motor cortex and lumbar spinal cord to detect more subtle changes in cytokine expression and possible phenotype.

It was previously reported that young unmanipulated $Optn^{470T}$ and $Optn^{D477N}$ mice, with a lack of or non-functional ubiquitin-binding region, do not have ALS/FTD-like phenotype (Gleason et al., 2011; Markovinovic et al., 2018; Munitic et al., 2013). To finally determine if ageing could be a second hit to trigger disease, we performed motor and cognitive tests and evaluated the solubility of TDP-43. Despite mild lower average weight in middle-aged $Optn^{470T}$ compared to WT males, we failed to uncover

motor or cognitive alterations linked to ALS and/or FTD in both male and female Optn^{470T} mice. Similar results were obtained by several independent groups on Optn$^{-/-}$ mice, suggesting that loss of the whole or just ubiquitin-binding region of optineurin is unable to induce an ALS/FTD-like phenotype (Dermentzaki et al., 2019; Kurashige et al., 2021; Moharir and Swarup, 2021; Slowicka et al., 2016). However, Ito *et al.* demonstrated a mild decrease in vertical rearing activity and spinal cord dysmyelination demonstrating that optineurin deficiency causes hind-limb weakness that was not confirmed in the follow-up study (Dermentzaki et al., 2019; Ito et al., 2016a). Furthermore, Kurashige *et al*. recently reported TDP-43 and p62 positive inclusions in spinal cord motor neurons and axonal degeneration of the sciatic nerves but no difference in survival time, body weight, or motor function up to two years (Kurashige et al., 2021). Here we demonstrated that optineurin insufficiency in the brain did not provoke a difference in TDP-43 or pathological p-TDP43 solubility compared to WT mice. In line with this, Slowicka *et al.* also demonstrated no TDP-43 protein aggregates in old Optn$^{-/-}$ mice (Slowicka et al., 2016). The latter report also demonstrated that mice are more susceptible to *Salmonella enterica* infection thus opening the possibility that additional environmental stimuli are necessary to induce disease phenotype. Finally, Moharir *et al.* demonstrated that 11-22 months Optn$^{-/-}$ mice have no loss of body weight or neurological phenotype (measuring paw grip and limb muscle strength), but exhibit a patchy loss of hair. Researchers speculated that mice have patchy hair loss most likely because of damage of hair follicles due to the activation of T cells (Moharir and Swarup, 2021). Taken together, the findings in Optn^{470T} mice go in line with previously published results in which optineurin during ageing is dispensable to induce an ALS/FTD-like neuropathology. We argue that optineurin mouse models, that mimic mutation found in patients are still of major relevance for research, but that additional environmental (e.g.: inducing acute and/or chronic inflammation) and genetic challenges should be introduced to provoke the phenotype.

5.3. The novel two-hit ALS mouse model does not exhibit an ALS/FTD-like phenotype

No mouse model fully recapitulates ALS/FTD pathogenesis and disease phenotype. Notably, for over a decade, the transgenic hSOD1 mouse model, that develops a rapid disease was the only available mouse model. However, it represents only 2% of ALS cases, and although it exhibits excessive neuroinflammation and motor neuronal loss, they do not recapitulate TDP-43 pathology that is present in > 95% of ALS patients (Fisher et al., 2023; Gurney et al., 1994). Since then, numerous mouse models harbouring ALS-linked patients' mutations have been designed, most often overexpressing transgenic mutations or mimicking endogenous mutations linked to ALS (De Giorgio et al., 2019). There are various optineurin mouse models, that faithfully represent mutations found in ALS patients, but as emphasized before, do not exhibit ALS phenotype during their life-span (Dermentzaki et al., 2019; Kurashige et al., 2021; Mohovic et al., 2023; Munitic et al., 2013; Slowicka et al., 2016). Here we demonstrated that optineurin is dispensable to induce an ALS/FTD-like neuropathology in old $Optn^{470T}$ mice suggesting that ageing is not a sufficient ''second hit'' that induces disease. Notably, recent findings showed that heterozygous loss of major optineurin-binding partner TBK1 is by itself insufficient to cause motor neuron degeneration and/or dysregulation of autophagy in mice during ageing (Brenner et al., 2019). However, when crossed to the $hSOD1^{G93A}$ mouse model, hemizygous *Tbk1* deletion demonstrated a double-edged role of TBK1 during disease progression; in the early stage it deteriorated clinical onset and muscular denervation whereas in the late stage, it was beneficial and extended survival. For this reason, we established a potential new two-hit ALS/FTD mouse model by crossing $Optn^{470T}$ mice with mice that carry a human transgenic mutation in TDP-43 ($TDP\text{-}43^{G348C}$), an ALS/FTD model that has been reported to develop cytoplasmic inclusions of TDP-43 protein and neuroinflammation around 10 months (Swarup et al., 2011a). We found a normal Mendelian pattern of inheritance and no difference in survival rate between WT $TDP\text{-}43^{G348C}$ and $Optn^{470T}$ $TDP\text{-}43^{G348C}$ mice. In addition, it is important to pinpoint that these mice have the same genetic background. Notably, it was previously seen that background has a significant role in the manifestation of phenotype, as when $Optn^{470T}$ was crossed to 129 X C57BL/6 background was embryonic lethal with

incomplete penetrance (Munitic et al., 2013). Establishing a novel mouse model is a long time-consuming process, so we had limited time to investigate the phenotype in WT TDP-43^{G348C} and Optn^{470T} TDP-43^{G348C} mice. However, our preliminary data showed no ALS/FTD-like pathological hallmarks in WT TDP-43^{G348C} mice, in contrast to Swarup *et al*. These authors demonstrated impaired learning and memory capabilities during ageing in WT TDP-43^{G348C}, as well as motor dysfunction and TDP-43 protein aggregates (Swarup et al., 2011a). Here we showed no motor phenotype in WT TDP-43^{G348C} mice. These mice were rederived in our mouse facility in Rijeka upon importing from Canada, so we speculate that some other environmental factors such as different microbiome or other stressors could lead to lack of ALS-like phenotype. Moreover, preliminary data from our group also demonstrated no TDP-43 protein aggregation in spinal cord and motor cortex showed by immunofluorescence on the tissue (result from Marija's Marošević Master thesis: https://urn.nsk.hr/urn:nbn:hr:193:791592) nor behavioural alterations tested with novel object recognition test in WT transgenic mice (result from J. Peradinovic). Moreover, here we demonstrated that optineurin insufficiency in our novel Optn^{470T} TDP-43^{G348C} mouse model did not induce motor alterations nor ALS-like phenotype. Similar to results in old non-transgenic mice, both WT TDP-43^{G348C} and Optn^{470T} TDP-43^{G348C} demonstrated motor decline linked to ageing. For now, we could not explain discrepancies observed in WT TDP-43^{G348C} mouse model between different research groups, but it is most likely due to different environmental factors, that are proposed to be triggering factors in ALS/FTD pathogenesis (Brown and Phil, 2017; Hardiman et al., 2017). In conclusion, the novel two-hit ALS mouse model does not exhibit ALS/FTD-like phenotype, but further analyses are necessary to verify these results.

6. Conclusions

(1) Optineurin insufficiency caused an accumulation in TDP-43 protein levels in primary myeloid cells and cortical neurons that were post-translationally regulated.

(2) Lack of optineurin in BV2 microglial cell lines did not exaggerate cell sensitivity to apoptosis upon inhibition of autophagy and/or UPS.

(3) Block in either autophagy or UPS did not trigger TDP-43 aggregation in the BV2 Optn KO microglial cell line and Optn^{470T} primary microglia.

(4) TDP-43 turnover in WT BMDMs required basal autophagy but optineurin insufficiency caused diminished TDP-43 turnover via autophagy in primary neurons BMDMs.

(5) Optineurin insufficiency caused diminished TDP-43 turnover via autophagy in primary neurons.

(6) LPS increased TDP-43 in WT but failed to increase already elevated TDP-43 in optineurin-deficient and -insufficient myeloid cells; increased TDP-43 was not degraded via autophagy, it was not depleted from the nucleus, and did not form TDP-43 protein aggregates.

(7) LPS changed the transcription of the P*oldip3* gene downstream of TDP-43 in optineurin-insufficient cells.

(8) Optineurin insufficiency did not affect ageing-induced changes in T lymphocyte numbers, activation, and naïve/memory cell ratio compared to WT mice.

(9) Optineurin insufficiency caused decreased expression of FOXP3 Treg-specific marker in female mice, but not a drop in Treg numbers previously found in ALS patients and hSOD1 mice; Tregs showed phenotype linked to ageing.

(10) Ageing-induced changes in innate immune cells were unaffected by optineurin. However, optineurin-insufficient cDC and macrophages demonstrated increased activation in old male mice.

(11) Immune cells isolated from the CNS of aged mice showed high autofluorescence.

(12) Cytokine and chemokine expression was stronger in CNS of aged WT and Optn^{470T} compared to young mice with neglectable differences between genotypes.

(13) Optineurin-insufficient mice did not exhibit ALS- or FTD-motor and cognitive deficits or TDP-43 pathology linked to ALS.

(14) A novel two-hit ALS mouse model that carries optineurin truncation and transgenic human TDP-43^{G348C} mutation had a normal Mendelian pattern of inheritance and no difference in survival rate and no motor deficits linked to ALS.

7. Literature

Agrawal, A., Gupta, S., 2011. Impact of Aging on Dendritic Cell Functions in humans. Ageing Res Rev 10, 336–345. https://doi.org/10.1016/j.arr.2010.06.004

Akira, S., Uematsu, S., Takeuchi, O., 2006. Pathogen Recognition and Innate Immunity. Cell 124, 783–801. https://doi.org/10.1016/j.cell.2006.02.015

Akizuki, M., Yamashita, H., Uemura, K., Maruyama, H., Kawakami, H., Ito, H., Takahashi, R., 2013. Optineurin suppression causes neuronal cell death via NF-κB pathway. J Neurochem 126, 699–704. https://doi.org/10.1111/jnc.12326

Albagha, O.M.E., Visconti, M.R., Alonso, N., Langston, A.L., Cundy, T., Dargie, R., Dunlop, M.G., Fraser, W.D., Hooper, M.J., Isaia, G., Nicholson, G.C., del Pino Montes, J., Gonzalez-Sarmiento, R., di Stefano, M., Tenesa, A., Walsh, J.P., Ralston, S.H., 2010. Genome-wide association study identifies variants at CSF1, OPTN, and TNFRSF11A as genetic risk factors for Paget's disease of bone. Nat Genet 42, 520–524. https://doi.org/10.1038/ng.562

Al-Chalabi, A., Fang, F., Hanby, M.F., Leigh, P.N., Shaw, C.E., Ye, W., Rijsdijk, F., 2010. An estimate of amyotrophic lateral sclerosis heritability using twin data. J Neurol Neurosurg Psychiatry 81, 1324–1326. https://doi.org/10.1136/jnnp.2010.207464

Alvarez-Rodríguez, L., López-Hoyos, M., Muñoz-Cacho, P., Martínez-Taboada, V.M., 2012. Aging is associated with circulating cytokine dysregulation. Cell Immunol 273, 124–132. https://doi.org/10.1016/j.cellimm.2012.01.001

Aman, Y., Schmauck-Medina, T., Hansen, M., Morimoto, R.I., Simon, A.K., Bjedov, I., Palikaras, K., Simonsen, A., Johansen, T., Tavernarakis, N., Rubinsztein, D.C., Partridge, L., Kroemer, G., Labbadia, J., Fang, E.F., 2021. Autophagy in healthy aging and disease. Nat Aging 1, 634–650. https://doi.org/10.1038/s43587-021-00098-4

Andersen, P.M., Al-Chalabi, A., 2011. Clinical genetics of amyotrophic lateral sclerosis: what do we really know? Nat Rev Neurol 7, 603–615. https://doi.org/10.1038/nrneurol.2011.150

Andrews, J.A., Jackson, C.E., Heiman-Patterson, T.D., Bettica, P., Brooks, B.R., Pioro, E.P., 2020. Real-world evidence of riluzole effectiveness in treating amyotrophic lateral sclerosis. Amyotroph Lateral Scler Frontotemporal Degener 21, 509–518. https://doi.org/10.1080/21678421.2020.1771734

Arai, T., Hasegawa, M., Akiyama, H., Ikeda, K., Nonaka, T., Mori, H., Mann, D., Tsuchiya, K., Yoshida, M., Hashizume, Y., Oda, T., 2006. TDP-43 is a component of ubiquitin-positive tau-negative inclusions in frontotemporal lobar degeneration and amyotrophic lateral sclerosis. Biochemical and Biophysical Research Communications 351, 602–611. https://doi.org/10.1016/j.bbrc.2006.10.093

Araki, W., Minegishi, S., Motoki, K., Kume, H., Hohjoh, H., Araki, Y.M., Tamaoka, A., 2014. Disease-associated mutations of TDP-43 promote turnover of the protein through the proteasomal pathway. Mol Neurobiol 50, 1049–1058. https://doi.org/10.1007/s12035-014-8644-6

Austin, J.A., Wright, G.S.A., Watanabe, S., Grossmann, J.G., Antonyuk, S.V., Yamanaka, K., Hasnain, S.S., 2014. Disease-causing mutants of TDP-43 nucleic acid binding domains are resistant to aggregation and have increased

stability and half-life. Proc Natl Acad Sci U S A 111, 4309–4314. https://doi.org/10.1073/pnas.1317317111

Ayala, Y.M., De Conti, L., Avendaño-Vázquez, S.E., Dhir, A., Romano, M., D'Ambrogio, A., Tollervey, J., Ule, J., Baralle, M., Buratti, E., Baralle, F.E., 2011. TDP-43 regulates its mRNA levels through a negative feedback loop. EMBO J 30, 277–288. https://doi.org/10.1038/emboj.2010.310

Balendra, R., Isaacs, A.M., 2018. C9orf72-mediated ALS and FTD: multiple pathways to disease. Nat Rev Neurol 14, 544–558. https://doi.org/10.1038/s41582-018-0047-2

Bansal, M., Moharir, S.C., Sailasree, S.P., Sirohi, K., Sudhakar, C., Sarathi, D.P., Lakshmi, B.J., Buono, M., Kumar, S., Swarup, G., 2018. Optineurin promotes autophagosome formation by recruiting the autophagy-related Atg12-5-16L1 complex to phagophores containing the Wipi2 protein. J Biol Chem 293, 132–147. https://doi.org/10.1074/jbc.M117.801944

Barmada, S.J., Serio, A., Arjun, A., Bilican, B., Daub, A., Ando, D.M., Tsvetkov, A., Pleiss, M., Li, X., Peisach, D., Shaw, C., Chandran, S., Finkbeiner, S., 2014. Autophagy induction enhances TDP43 turnover and survival in neuronal ALS models. Nat Chem Biol 10, 677–685. https://doi.org/10.1038/nchembio.1563

Baruch, K., Deczkowska, A., David, E., Castellano, J.M., Miller, O., Kertser, A., Berkutzki, T., Barnett-Itzhaki, Z., Bezalel, D., Wyss-Coray, T., Amit, I., Schwartz, M., 2014. Aging. Aging-induced type I interferon response at the choroid plexus negatively affects brain function. Science 346, 89–93. https://doi.org/10.1126/science.1252945

Beers, D.R., Henkel, J.S., Xiao, Q., Zhao, W., Wang, J., Yen, A.A., Siklos, L., McKercher, S.R., Appel, S.H., 2006. Wild-type microglia extend survival in PU.1 knockout mice with familial amyotrophic lateral sclerosis. Proceedings of the National Academy of Sciences 103, 16021–16026. https://doi.org/10.1073/pnas.0607423103

Beers, D.R., Henkel, J.S., Zhao, W., Wang, J., Appel, S.H., 2008. CD4+ T cells support glial neuroprotection, slow disease progression, and modify glial morphology in an animal model of inherited ALS. Proceedings of the National Academy of Sciences 105, 15558–15563. https://doi.org/10.1073/pnas.0807419105

Beers, D.R., Henkel, J.S., Zhao, W., Wang, J., Huang, A., Wen, S., Liao, B., Appel, S.H., 2011a. Endogenous regulatory T lymphocytes ameliorate amyotrophic lateral sclerosis in mice and correlate with disease progression in patients with amyotrophic lateral sclerosis. Brain 134, 1293–1314. https://doi.org/10.1093/brain/awr074

Beers, D.R., Zhao, W., Liao, B., Kano, O., Wang, J., Huang, A., Appel, S.H., Henkel, J.S., 2011b. Neuroinflammation modulates distinct regional and temporal clinical responses in ALS mice. Brain, Behavior, and Immunity 25, 1025–1035. https://doi.org/10.1016/j.bbi.2010.12.008

Béland, L.-C., Markovinovic, A., Jakovac, H., De Marchi, F., Bilic, E., Mazzini, L., Kriz, J., Munitic, I., 2020a. Immunity in amyotrophic lateral sclerosis: blurred lines between excessive inflammation and inefficient immune responses. Brain Communications 2, fcaa124. https://doi.org/10.1093/braincomms/fcaa124

Béland, L.-C., Markovinovic, A., Jakovac, H., De Marchi, F., Bilic, E., Mazzini, L., Kriz, J., Munitic, I., 2020b. Immunity in amyotrophic lateral sclerosis: blurred

lines between excessive inflammation and inefficient immune responses. Brain Communications 2, fcaa124. https://doi.org/10.1093/braincomms/fcaa124

Béland, L.-C., Markovinovic, A., Jakovac, H., De Marchi, F., Bilic, E., Mazzini, L., Kriz, J., Munitic, I., 2020c. Immunity in amyotrophic lateral sclerosis: blurred lines between excessive inflammation and inefficient immune responses. Brain Communications 2, fcaa124. https://doi.org/10.1093/braincomms/fcaa124

Beli, E., Duriancik, D.M., Clinthorne, J.F., Lee, T., Kim, S., Gardner, E.M., 2014. Natural killer cell development and maturation in aged mice. Mechanisms of Ageing and Development 135, 33–40. https://doi.org/10.1016/j.mad.2013.11.007

Belzil, V.V., Daoud, H., Desjarlais, A., Bouchard, J.-P., Dupré, N., Camu, W., Dion, P.A., Rouleau, G.A., 2011. Analysis of OPTN as a causative gene for amyotrophic lateral sclerosis. Neurobiology of Aging 32, 555.e13-555.e14. https://doi.org/10.1016/j.neurobiolaging.2010.10.001

Benito-Cuesta, I., Ordoñez-Gutierrez, L., Wandosell, F., 2021. Trehalose Reduces the Secreted Beta-Amyloid Levels in Primary Neurons Independently of Autophagy Induction. Metabolites 11. https://doi.org/10.3390/metabo11070421

Birger, A., Ben-Dor, I., Ottolenghi, M., Turetsky, T., Gil, Y., Sweetat, S., Perez, L., Belzer, V., Casden, N., Steiner, D., Izrael, M., Galun, E., Feldman, E., Behar, O., Reubinoff, B., 2019. Human iPSC-derived astrocytes from ALS patients with mutated C9ORF72 show increased oxidative stress and neurotoxicity. EBioMedicine 50, 274–289. https://doi.org/10.1016/j.ebiom.2019.11.026

Boillee, S., Yamanaka, K., Lobsiger, C.S., Copeland, N.G., Jenkins, N.A., Kassiotis, G., Kollias, G., Cleveland, D.W., 2006. Onset and Progression in Inherited ALS Determined by Motor Neurons and Microglia. Science 312, 1389–1392. https://doi.org/10.1126/science.1123511

Bose, J.K., Huang, C.-C., Shen, C.-K.J., 2011. Regulation of Autophagy by Neuropathological Protein TDP-43. J Biol Chem 286, 44441–44448. https://doi.org/10.1074/jbc.M111.237115

Brauning, A., Rae, M., Zhu, G., Fulton, E., Admasu, T.D., Stolzing, A., Sharma, A., 2022. Aging of the Immune System: Focus on Natural Killer Cells Phenotype and Functions. Cells 11, 1017. https://doi.org/10.3390/cells11061017

Brenner, D., Sieverding, K., Bruno, C., Lüningschrör, P., Buck, E., Mungwa, S., Fischer, L., Brockmann, S.J., Ulmer, J., Bliederhäuser, C., Philibert, C.E., Satoh, T., Akira, S., Boillée, S., Mayer, B., Sendtner, M., Ludolph, A.C., Danzer, K.M., Lobsiger, C.S., Freischmidt, A., Weishaupt, J.H., 2019. Heterozygous Tbk1 loss has opposing effects in early and late stages of ALS in mice. Journal of Experimental Medicine 216, 267–278. https://doi.org/10.1084/jem.20180729

Bright, F., Chan, G., van Hummel, A., Ittner, L.M., Ke, Y.D., 2021. TDP-43 and Inflammation: Implications for Amyotrophic Lateral Sclerosis and Frontotemporal Dementia. Int J Mol Sci 22, 7781. https://doi.org/10.3390/ijms22157781

Brown, R.H., Phil, D., 2017. Amyotrophic Lateral Sclerosis. n engl j med 11.

Bruijn, L.I., Houseweart, M.K., Kato, S., Anderson, K.L., Anderson, S.D., Ohama, E., Reaume, A.G., Scott, R.W., Cleveland, D.W., 1998. Aggregation and motor neuron toxicity of an ALS-linked SOD1 mutant independent from wild-type

SOD1. Science 281, 1851–1854. https://doi.org/10.1126/science.281.5384.1851

Budini, M., Buratti, E., Morselli, E., Criollo, A., 2017. Autophagy and Its Impact on Neurodegenerative Diseases: New Roles for TDP-43 and C9orf72. Frontiers in Molecular Neuroscience 10.

Buratti, E., 2018. TDP-43 post-translational modifications in health and disease. Expert Opin Ther Targets 22, 279–293. https://doi.org/10.1080/14728222.2018.1439923

Buratti, E., 2015. Functional Significance of TDP-43 Mutations in Disease, in: Advances in Genetics. Elsevier, pp. 1–53. https://doi.org/10.1016/bs.adgen.2015.07.001

Buratti, E., Baralle, F.E., 2008. Multiple roles of TDP-43 in gene expression, splicing regulation, and human disease. Front Biosci 13, 867–878. https://doi.org/10.2741/2727

Butcher, S., Chahel, H., Lord, J.M., 2000. Ageing and the neutrophil: no appetite for killing? Immunology 100, 411–416. https://doi.org/10.1046/j.1365-2567.2000.00079.x

Byrne, S., Walsh, C., Lynch, C., Bede, P., Elamin, M., Kenna, K., McLaughlin, R., Hardiman, O., 2011. Rate of familial amyotrophic lateral sclerosis: a systematic review and meta-analysis. J Neurol Neurosurg Psychiatry 82, 623–627. https://doi.org/10.1136/jnnp.2010.224501

Chen, Z.J., 2012. Ubiquitination in signaling to and activation of IKK. Immunol Rev 246, 95–106. https://doi.org/10.1111/j.1600-065X.2012.01108.x

Chew, T.S., O'Shea, N.R., Sewell, G.W., Oehlers, S.H., Mulvey, C.M., Crosier, P.S., Godovac-Zimmermann, J., Bloom, S.L., Smith, A.M., Segal, A.W., 2015. Optineurin deficiency in mice contributes to impaired cytokine secretion and neutrophil recruitment in bacteria-driven colitis. Dis Model Mech 8, 817–829. https://doi.org/10.1242/dmm.020362

Chiò, A., Mazzini, L., Mora, G., 2020. Disease-modifying therapies in amyotrophic lateral sclerosis. Neuropharmacology 167, 107986. https://doi.org/10.1016/j.neuropharm.2020.107986

Chiu, I.M., Chen, A., Zheng, Y., Kosaras, B., Tsiftsoglou, S.A., Vartanian, T.K., Brown, R.H., Carroll, M.C., 2008. T lymphocytes potentiate endogenous neuroprotective inflammation in a mouse model of ALS. Proc Natl Acad Sci U S A 105, 17913–17918. https://doi.org/10.1073/pnas.0804610105

Cho, M.-H., Cho, K., Kang, H.-J., Jeon, E.-Y., Kim, H.-S., Kwon, H.-J., Kim, H.-M., Kim, D.-H., Yoon, S.-Y., 2014. Autophagy in microglia degrades extracellular β-amyloid fibrils and regulates the NLRP3 inflammasome. Autophagy 10, 1761–1775. https://doi.org/10.4161/auto.29647

Choi, Y., Bowman, J.W., Jung, J.U., 2018. Autophagy during viral infection - a double-edged sword. Nat Rev Microbiol 16, 341–354. https://doi.org/10.1038/s41579-018-0003-6

Cirulli, E.T., Lasseigne, B.N., Petrovski, S., Sapp, P.C., Dion, P.A., Leblond, C.S., Couthouis, J., Lu, Y.-F., Wang, Q., Krueger, B.J., Ren, Z., Keebler, J., Han, Y., Levy, S.E., Boone, B.E., Wimbish, J.R., Waite, L.L., Jones, A.L., Carulli, J.P., Day-Williams, A.G., Staropoli, J.F., Xin, W.W., Chesi, A., Raphael, A.R., McKenna-Yasek, D., Cady, J., Vianney de Jong, J.M.B., Kenna, K.P., Smith,

B.N., Topp, S., Miller, J., Gkazi, A., FALS Sequencing Consortium, Al-Chalabi, A., van den Berg, L.H., Veldink, J., Silani, V., Ticozzi, N., Shaw, C.E., Baloh, R.H., Appel, S., Simpson, E., Lagier-Tourenne, C., Pulst, S.M., Gibson, S., Trojanowski, J.Q., Elman, L., McCluskey, L., Grossman, M., Shneider, N.A., Chung, W.K., Ravits, J.M., Glass, J.D., Sims, K.B., Van Deerlin, V.M., Maniatis, T., Hayes, S.D., Ordureau, A., Swarup, S., Landers, J., Baas, F., Allen, A.S., Bedlack, R.S., Harper, J.W., Gitler, A.D., Rouleau, G.A., Brown, R., Harms, M.B., Cooper, G.M., Harris, T., Myers, R.M., Goldstein, D.B., 2015. Exome sequencing in amyotrophic lateral sclerosis identifies risk genes and pathways. Science 347, 1436–1441. https://doi.org/10.1126/science.aaa3650

Conicella, A.E., Zerze, G.H., Mittal, J., Fawzi, N.L., 2016. ALS mutations disrupt phase separation mediated by -helical structure in the TDP-43 low complexity C-terminal domain. Structure 24, 1537–1549. https://doi.org/10.1016/j.str.2016.07.007

Cook, C.N., Wu, Y., Odeh, H.M., Gendron, T.F., Jansen-West, K., Del Rosso, G., Yue, M., Jiang, P., Gomes, E., Tong, J., Daughrity, L.M., Avendano, N.M., Castanedes-Casey, M., Shao, W., Oskarsson, B., Tomassy, G.S., McCampbell, A., Rigo, F., Dickson, D.W., Shorter, J., Zhang, Y.-J., Petrucelli, L., 2020. C9orf72 poly(GR) aggregation induces TDP-43 proteinopathy. Sci Transl Med 12, eabb3774. https://doi.org/10.1126/scitranslmed.abb3774

Coque, E., Salsac, C., Espinosa-Carrasco, G., Varga, B., Degauque, N., Cadoux, M., Crabé, R., Virenque, A., Soulard, C., Fierle, J.K., Brodovitch, A., Libralato, M., Végh, A.G., Venteo, S., Scamps, F., Boucraut, J., Laplaud, D., Hernandez, J., Gergely, C., Vincent, T., Raoul, C., 2019. Cytotoxic CD8+ T lymphocytes expressing ALS-causing SOD1 mutant selectively trigger death of spinal motoneurons. Proc Natl Acad Sci U S A 116, 2312–2317. https://doi.org/10.1073/pnas.1815961116

Correia, A.S., Patel, P., Dutta, K., Julien, J.-P., 2015. Inflammation Induces TDP-43 Mislocalization and Aggregation. PLoS ONE 10, e0140248. https://doi.org/10.1371/journal.pone.0140248

Dantuma, N.P., Bott, L.C., 2014. The ubiquitin-proteasome system in neurodegenerative diseases: precipitating factor, yet part of the solution. Frontiers in Molecular Neuroscience 7.

De Giorgio, F., Maduro, C., Fisher, E.M.C., Acevedo-Arozena, A., 2019. Transgenic and physiological mouse models give insights into different aspects of amyotrophic lateral sclerosis. Disease Models & Mechanisms 12, dmm037424. https://doi.org/10.1242/dmm.037424

De Maeyer, R.P.H., Chambers, E.S., 2021. The impact of ageing on monocytes and macrophages. Immunology Letters 230, 1–10. https://doi.org/10.1016/j.imlet.2020.12.003

De Marchi, F., Munitic, I., Amedei, A., Berry, J.D., Feldman, E.L., Aronica, E., Nardo, G., Van Weehaeghe, D., Niccolai, E., Prtenjaca, N., Sakowski, S.A., Bendotti, C., Mazzini, L., 2021. Interplay between immunity and amyotrophic lateral sclerosis: Clinical impact. Neuroscience & Biobehavioral Reviews 127, 958–978. https://doi.org/10.1016/j.neubiorev.2021.06.027

De Marco, G., Lomartire, A., Calvo, A., Risso, A., De Luca, E., Mostert, M., Mandrioli, J., Caponnetto, C., Borghero, G., Manera, U., Canosa, A., Moglia, C., Restagno, G., Fini, N., Tarella, C., Giordana, M.T., Rinaudo, M.T., Chiò, A.,

2017. Monocytes of patients with amyotrophic lateral sclerosis linked to gene mutations display altered TDP-43 subcellular distribution. Neuropathol Appl Neurobiol 43, 133–153. https://doi.org/10.1111/nan.12328

DeJesus-Hernandez, M., Mackenzie, I.R., Boeve, B.F., Boxer, A.L., Baker, M., Rutherford, N.J., Nicholson, A.M., Finch, N.A., Flynn, H., Adamson, J., Kouri, N., Wojtas, A., Sengdy, P., Hsiung, G.-Y.R., Karydas, A., Seeley, W.W., Josephs, K.A., Coppola, G., Geschwind, D.H., Wszolek, Z.K., Feldman, H., Knopman, D.S., Petersen, R.C., Miller, B.L., Dickson, D.W., Boylan, K.B., Graff-Radford, N.R., Rademakers, R., 2011. Expanded GGGGCC hexanucleotide repeat in noncoding region of C9ORF72 causes chromosome 9p-linked FTD and ALS. Neuron 72, 245–256. https://doi.org/10.1016/j.neuron.2011.09.011

Deng, H.-X., Chen, W., Hong, S.-T., Boycott, K.M., Gorrie, G.H., Siddique, N., Yang, Y., Fecto, F., Shi, Y., Zhai, H., Jiang, H., Hirano, M., Rampersaud, E., Jansen, G.H., Donkervoort, S., Bigio, E.H., Brooks, B.R., Ajroud, K., Sufit, R.L., Haines, J.L., Mugnaini, E., Pericak-Vance, M.A., Siddique, T., 2011. Mutations in UBQLN2 cause dominant X-linked juvenile and adult-onset ALS and ALS/dementia. Nature 477, 211–215. https://doi.org/10.1038/nature10353

Deretic, V., 2021. Autophagy in inflammation, infection, and immunometabolism. Immunity 54, 437–453. https://doi.org/10.1016/j.immuni.2021.01.018

Dermentzaki, G., Politi, K.A., Lu, L., Mishra, V., Pérez-Torres, E.J., Sosunov, A.A., McKhann, G.M., Lotti, F., Shneider, N.A., Przedborski, S., 2019. Deletion of *Ripk3* Prevents Motor Neuron Death *In Vitro* but not *In Vivo*. eNeuro 6, ENEURO.0308-18.2018. https://doi.org/10.1523/ENEURO.0308-18.2018

Dobson-Stone, C., Hallupp, M., Shahheydari, H., Ragagnin, A.M.G., Chatterton, Z., Carew-Jones, F., Shepherd, C.E., Stefen, H., Paric, E., Fath, T., Thompson, E.M., Blumbergs, P., Short, C.L., Field, C.D., Panegyres, P.K., Hecker, J., Nicholson, G., Shaw, A.D., Fullerton, J.M., Luty, A.A., Schofield, P.R., Brooks, W.S., Rajan, N., Bennett, M.F., Bahlo, M., Shankaracharya, Landers, J.E., Piguet, O., Hodges, J.R., Halliday, G.M., Topp, S.D., Smith, B.N., Shaw, C.E., McCann, E., Fifita, J.A., Williams, K.L., Atkin, J.D., Blair, I.P., Kwok, J.B., 2020. CYLD is a causative gene for frontotemporal dementia – amyotrophic lateral sclerosis. Brain 143, 783–799. https://doi.org/10.1093/brain/awaa039

Engelhardt, J.I., Appel, S.H., 1990. IgG reactivity in the spinal cord and motor cortex in amyotrophic lateral sclerosis. Arch Neurol 47, 1210–1216. https://doi.org/10.1001/archneur.1990.00530110068019

Engelhardt, J.I., Tajti, J., Appel, S.H., 1993. Lymphocytic infiltrates in the spinal cord in amyotrophic lateral sclerosis. Arch Neurol 50, 30–36. https://doi.org/10.1001/archneur.1993.00540010026013

Evans, C.S., Holzbaur, E.L., 2020. Degradation of engulfed mitochondria is rate-limiting in Optineurin-mediated mitophagy in neurons. eLife 9, e50260. https://doi.org/10.7554/eLife.50260

Fecto, F., 2011. SQSTM1 Mutations in Familial and Sporadic Amyotrophic Lateral Sclerosis. Arch Neurol 68, 1440. https://doi.org/10.1001/archneurol.2011.250

Fernandes, N., Nero, L., Lyons, S.M., Ivanov, P., Mittelmeier, T.M., Bolger, T.A., Buchan, J.R., 2020. Stress Granule Assembly Can Facilitate but Is Not Required for TDP-43 Cytoplasmic Aggregation. Biomolecules 10, 1367. https://doi.org/10.3390/biom10101367

Fessler, J., Felber, A., Duftner, C., Dejaco, C., 2013. The Impact of Aging on Regulatory T-Cells. Frontiers in Immunology 4.

Fisher, E.M.C., Greensmith, L., Malaspina, A., Fratta, P., Hanna, M.G., Schiavo, G., Isaacs, A.M., Orrell, R.W., Cunningham, T.J., Arozena, A.A., 2023. Opinion: more mouse models and more translation needed for ALS. Molecular Neurodegeneration 18, 30. https://doi.org/10.1186/s13024-023-00619-2

Fitzgerald, K.A., McWhirter, S.M., Faia, K.L., Rowe, D.C., Latz, E., Golenbock, D.T., Coyle, A.J., Liao, S.-M., Maniatis, T., 2003. IKKepsilon and TBK1 are essential components of the IRF3 signaling pathway. Nat Immunol 4, 491–496. https://doi.org/10.1038/ni921

Franceschi, C., Bonafè, M., Valensin, S., Olivieri, F., De Luca, M., Ottaviani, E., De Benedictis, G., 2000. Inflamm-aging: An Evolutionary Perspective on Immunosenescence. Annals of the New York Academy of Sciences 908, 244–254. https://doi.org/10.1111/j.1749-6632.2000.tb06651.x

Franceschi, C., Garagnani, P., Parini, P., Giuliani, C., Santoro, A., 2018. Inflammageing: a new immune–metabolic viewpoint for age-related diseases. Nat Rev Endocrinol 14, 576–590. https://doi.org/10.1038/s41574-018-0059-4

Freischmidt, A., Müller, K., Ludolph, A.C., Weishaupt, J.H., Andersen, P.M., 2017. Association of Mutations in *TBK1* With Sporadic and Familial Amyotrophic Lateral Sclerosis and Frontotemporal Dementia. JAMA Neurol 74, 110. https://doi.org/10.1001/jamaneurol.2016.3712

Fukushi, M., Ohsawa, R., Okinaka, Y., Oikawa, D., Kiyono, T., Moriwaki, M., Irie, T., Oda, K., Kamei, Y., Tokunaga, F., Sotomaru, Y., Maruyama, H., Kawakami, H., Sakaguchi, T., 2023. Optineurin deficiency impairs autophagy to cause interferon beta overproduction and increased survival of mice following viral infection. PLoS One 18, e0287545. https://doi.org/10.1371/journal.pone.0287545

Furukawa, Y., Kaneko, K., Watanabe, S., Yamanaka, K., Nukina, N., 2011. A seeding reaction recapitulates intracellular formation of Sarkosyl-insoluble transactivation response element (TAR) DNA-binding protein-43 inclusions. J Biol Chem 286, 18664–18672. https://doi.org/10.1074/jbc.M111.231209

Garofalo, S., Cocozza, G., Porzia, A., Inghilleri, M., Raspa, M., Scavizzi, F., Aronica, E., Bernardini, G., Peng, L., Ransohoff, R.M., Santoni, A., Limatola, C., 2020. Natural killer cells modulate motor neuron-immune cell cross talk in models of Amyotrophic Lateral Sclerosis. Nat Commun 11, 1773. https://doi.org/10.1038/s41467-020-15644-8

Geissmann, F., Auffray, C., Palframan, R., Wirrig, C., Ciocca, A., Campisi, L., Narni-Mancinelli, E., Lauvau, G., 2008. Blood monocytes: distinct subsets, how they relate to dendritic cells, and their possible roles in the regulation of T-cell responses. Immunol Cell Biol 86, 398–408. https://doi.org/10.1038/icb.2008.19

Gleason, C.E., Ordureau, A., Gourlay, R., Arthur, J.S.C., Cohen, P., 2011. Polyubiquitin Binding to Optineurin Is Required for Optimal Activation of TANK-binding Kinase 1 and Production of Interferon β. Journal of Biological Chemistry 286, 35663–35674. https://doi.org/10.1074/jbc.M111.267567

Gong, Y.H., Parsadanian, A.S., Andreeva, A., Snider, W.D., Elliott, J.L., 2000. Restricted expression of G86R Cu/Zn superoxide dismutase in astrocytes results in astrocytosis but does not cause motoneuron degeneration. J Neurosci 20, 660–665. https://doi.org/10.1523/JNEUROSCI.20-02-00660.2000

Gotkine, M., de Majo, M., Wong, C.H., Topp, S.D., Michaelson-Cohen, R., Epsztejn-Litman, S., Eiges, R., Y, Y.L., Kanaan, M., Shaked, H.M., Alahmady, N., Vance, C., Newhouse, S.J., Breen, G., Nishimura, A.L., Shaw, C.E., Smith, B.N., 2021. A recessive S174X mutation in Optineurin causes amyotrophic lateral sclerosis through a loss of function via allele-specific nonsense-mediated decay. Neurobiology of Aging 106, 1–6. https://doi.org/10.1016/j.neurobiolaging.2021.05.009

Götzl, J.K., Lang, C.M., Haass, C., Capell, A., 2016. Impaired protein degradation in FTLD and related disorders. Ageing Research Reviews 32, 122–139. https://doi.org/10.1016/j.arr.2016.04.008

Gounder, S.S., Abdullah, B.J.J., Radzuanb, N.E.I.B.M., Zain, F.D.B.M., Sait, N.B.M., Chua, C., Subramani, B., 2018. Effect of Aging on NK Cell Population and Their Proliferation at Ex Vivo Culture Condition. Anal Cell Pathol (Amst) 2018, 7871814. https://doi.org/10.1155/2018/7871814

Gravel, M., Béland, L.-C., Soucy, G., Abdelhamid, E., Rahimian, R., Gravel, C., Kriz, J., 2016. IL-10 Controls Early Microglial Phenotypes and Disease Onset in ALS Caused by Misfolded Superoxide Dismutase 1. J. Neurosci. 36, 1031–1048. https://doi.org/10.1523/JNEUROSCI.0854-15.2016

Gurney, M.E., Pu, H., Chiu, A.Y., Dal Canto, M.C., Polchow, C.Y., Alexander, D.D., Caliendo, J., Hentati, A., Kwon, Y.W., Deng, H.-X., Chen, W., Zhai, P., Sufit, R.L., Siddique, T., 1994. Motor Neuron Degeneration in Mice that Express a Human Cu,Zn Superoxide Dismutase Mutation. Science 264, 1772–1775. https://doi.org/10.1126/science.8209258

Hardiman, O., Al-Chalabi, A., Chio, A., Corr, E.M., Logroscino, G., Robberecht, W., Shaw, P.J., Simmons, Z., van den Berg, L.H., 2017. Amyotrophic lateral sclerosis. Nat Rev Dis Primers 3, 17071. https://doi.org/10.1038/nrdp.2017.71

Hattula, K., Peränen, J., 2000. FIP-2, a coiled-coil protein, links Huntingtin to Rab8 and modulates cellular morphogenesis. Current Biology 10, 1603–1606.

Hellwig, S., Heinrich, A., Biber, K., 2013. The brain's best friend: microglial neurotoxicity revisited. Frontiers in Cellular Neuroscience 7.

Henkel, J.S., Beers, D.R., Wen, S., Rivera, A.L., Toennis, K.M., Appel, J.E., Zhao, W., Moore, D.H., Powell, S.Z., Appel, S.H., 2013. Regulatory T-lymphocytes mediate amyotrophic lateral sclerosis progression and survival. EMBO Mol Med 5, 64–79. https://doi.org/10.1002/emmm.201201544

Heo, J.-M., Ordureau, A., Paulo, J.A., Rinehart, J., Harper, J.W., 2015. The PINK1-PARKIN Mitochondrial Ubiquitylation Pathway Drives a Program of OPTN/NDP52 Recruitment and TBK1 Activation to Promote Mitophagy. Mol Cell 60, 7–20. https://doi.org/10.1016/j.molcel.2015.08.016

Hjerpe, R., Bett, J.S., Keuss, M.J., Solovyova, A., McWilliams, T.G., Johnson, C., Sahu, I., Varghese, J., Wood, N., Wightman, M., Osborne, G., Bates, G.P., Glickman, M.H., Trost, M., Knebel, A., Marchesi, F., Kurz, T., 2016. UBQLN2 Mediates Autophagy-Independent Protein Aggregate Clearance by the Proteasome. Cell 166, 935–949. https://doi.org/10.1016/j.cell.2016.07.001

Hock, E.-M., Polymenidou, M., 2016. Prion-like propagation as a pathogenic principle in frontotemporal dementia. J Neurochem 138 Suppl 1, 163–183. https://doi.org/10.1111/jnc.13668

Holmøy, T., 2008. T cells in amyotrophic lateral sclerosis. European Journal of Neurology 15, 360–366. https://doi.org/10.1111/j.1468-1331.2008.02065.x

Hung, S.-T., Linares, G.R., Chang, W.-H., Eoh, Y., Krishnan, G., Mendonca, S., Hong, S., Shi, Y., Santana, M., Kueth, C., Macklin-Isquierdo, S., Perry, S., Duhaime, S., Maios, C., Chang, J., Perez, J., Couto, A., Lai, J., Li, Y., Alworth, S.V., Hendricks, E., Wang, Y., Zlokovic, B.V., Dickman, D.K., Parker, J.A., Zarnescu, D.C., Gao, F.-B., Ichida, J.K., 2023. PIKFYVE inhibition mitigates disease in models of diverse forms of ALS. Cell 186, 786-802.e28. https://doi.org/10.1016/j.cell.2023.01.005

Igaz, L.M., Kwong, L.K., Chen-Plotkin, A., Winton, M.J., Unger, T.L., Xu, Y., Neumann, M., Trojanowski, J.Q., Lee, V.M.-Y., 2009. Expression of TDP-43 C-terminal Fragments in Vitro Recapitulates Pathological Features of TDP-43 Proteinopathies. Journal of Biological Chemistry 284, 8516–8524. https://doi.org/10.1074/jbc.M809462200

Ito, H., Nakamura, M., Komure, O., Ayaki, T., Wate, R., Maruyama, H., Nakamura, Y., Fujita, K., Kaneko, S., Okamoto, Y., Ihara, M., Konishi, T., Ogasawara, K., Hirano, A., Kusaka, H., Kaji, R., Takahashi, R., Kawakami, H., 2011. Clinicopathologic study on an ALS family with a heterozygous E478G optineurin mutation. Acta Neuropathol 122, 223–229. https://doi.org/10.1007/s00401-011-0842-y

Ito, Y., Ofengeim, D., Najafov, A., Das, S., Saberi, S., Li, Y., Hitomi, J., Zhu, H., Chen, H., Mayo, L., Geng, J., Amin, P., DeWitt, J.P., Mookhtiar, A.K., Florez, M., Ouchida, A.T., Fan, J., Pasparakis, M., Kelliher, M.A., Ravits, J., Yuan, J., 2016a. RIPK1 mediates axonal degeneration by promoting inflammation and necroptosis in ALS. Science 353, 603–608. https://doi.org/10.1126/science.aaf6803

Ito, Y., Ofengeim, D., Najafov, A., Das, S., Saberi, S., Li, Y., Hitomi, J., Zhu, H., Chen, H., Mayo, L., others, 2016b. RIPK1 mediates axonal degeneration by promoting inflammation and necroptosis in ALS. Science 353, 603–608.

Jayanthi, P., Joshua, E., Ranganathan, K., 2010. Ageing and its implications. J Oral Maxillofac Pathol 14, 48–51. https://doi.org/10.4103/0973-029X.72500

Kakihana, T., Takahashi, M., Katsuragi, Y., Yamashita, S.-I., Sango, J., Kanki, T., Onodera, O., Fujii, M., 2021. The optineurin/TIA1 pathway inhibits aberrant stress granule formation and reduces ubiquitinated TDP-43. iScience 24, 102733. https://doi.org/10.1016/j.isci.2021.102733

Kamada, M., Izumi, Y., Ayaki, T., Nakamura, M., Kagawa, S., Kudo, E., Sako, W., Maruyama, H., Nishida, Y., Kawakami, H., Ito, H., Kaji, R., 2014. Clinicopathologic features of autosomal recessive amyotrophic lateral sclerosis associated with optineurin mutation: Autosomal recessive OPTN-ALS. Neuropathology 34, 64–70. https://doi.org/10.1111/neup.12051

Kettenmann, H., Kirchhoff, F., Verkhratsky, A., 2013. Microglia: New Roles for the Synaptic Stripper. Neuron 77, 10–18. https://doi.org/10.1016/j.neuron.2012.12.023

King, A., Maekawa, S., Bodi, I., Troakes, C., Al-Sarraj, S., 2011. Ubiquitinated, p62 immunopositive cerebellar cortical neuronal inclusions are evident across the spectrum of TDP-43 proteinopathies but are only rarely additionally immunopositive for phosphorylation-dependent TDP-43. Neuropathology 31, 239–249. https://doi.org/10.1111/j.1440-1789.2010.01171.x

Kirisako, T., Kamei, K., Murata, S., Kato, M., Fukumoto, H., Kanie, M., Sano, S., Tokunaga, F., Tanaka, K., Iwai, K., 2006. A ubiquitin ligase complex

assembles linear polyubiquitin chains. EMBO J 25, 4877–4887. https://doi.org/10.1038/sj.emboj.7601360

Kirkin, V., 2020. History of the Selective Autophagy Research: How Did It Begin and Where Does It Stand Today? J Mol Biol 432, 3–27. https://doi.org/10.1016/j.jmb.2019.05.010

Kocur, M., Schneider, R., Pulm, A.-K., Bauer, J., Kropp, S., Gliem, M., Ingwersen, J., Goebels, N., Alferink, J., Prozorovski, T., Aktas, O., Scheu, S., 2015. IFNβ secreted by microglia mediates clearance of myelin debris in CNS autoimmunity. acta neuropathol commun 3, 20. https://doi.org/10.1186/s40478-015-0192-4

Komander, D., Rape, M., 2012. The ubiquitin code. Annu Rev Biochem 81, 203–229. https://doi.org/10.1146/annurev-biochem-060310-170328

Korac, J., Schaeffer, V., Kovacevic, I., Clement, A.M., Jungblut, B., Behl, C., Terzic, J., Dikic, I., 2012. Ubiquitin-independent function of optineurin in autophagic clearance of protein aggregates. Journal of Cell Science jcs.114926. https://doi.org/10.1242/jcs.114926

Kurashige, T., Kuramochi, M., Ohsawa, R., Yamashita, Y., Shioi, G., Morino, H., Kamada, M., Ayaki, T., Ito, H., Sotomaru, Y., Maruyama, H., Kawakami, H., 2021. Optineurin defects cause TDP43-pathology with autophagic vacuolar formation. Neurobiology of Disease 148, 105215. https://doi.org/10.1016/j.nbd.2020.105215

Kwiatkowski, T.J., Bosco, D.A., Leclerc, A.L., Tamrazian, E., Vanderburg, C.R., Russ, C., Davis, A., Gilchrist, J., Kasarskis, E.J., Munsat, T., Valdmanis, P., Rouleau, G.A., Hosler, B.A., Cortelli, P., de Jong, P.J., Yoshinaga, Y., Haines, J.L., Pericak-Vance, M.A., Yan, J., Ticozzi, N., Siddique, T., McKenna-Yasek, D., Sapp, P.C., Horvitz, H.R., Landers, J.E., Brown, R.H., 2009. Mutations in the FUS/TLS gene on chromosome 16 cause familial amyotrophic lateral sclerosis. Science 323, 1205–1208. https://doi.org/10.1126/science.1166066

Lall, D., Baloh, R.H., 2017. Microglia and C9orf72 in neuroinflammation and ALS and frontotemporal dementia. J Clin Invest 127, 3250–3258. https://doi.org/10.1172/JCI90607

Laplantine, E., Fontan, E., Chiaravalli, J., Lopez, T., Lakisic, G., Véron, M., Agou, F., Israël, A., 2009. NEMO specifically recognizes K63-linked poly-ubiquitin chains through a new bipartite ubiquitin-binding domain. EMBO J 28, 2885–2895. https://doi.org/10.1038/emboj.2009.241

Lazarou, M., Sliter, D.A., Kane, L.A., Sarraf, S.A., Wang, C., Burman, J.L., Sideris, D.P., Fogel, A.I., Youle, R.J., 2015. The ubiquitin kinase PINK1 recruits autophagy receptors to induce mitophagy. Nature 524, 309–314. https://doi.org/10.1038/nature14893

Leibiger, C., Deisel, J., Aufschnaiter, A., Ambros, S., Tereshchenko, M., Verheijen, B.M., Büttner, S., Braun, R.J., 2018. TDP-43 controls lysosomal pathways thereby determining its own clearance and cytotoxicity. Hum Mol Genet 27, 1593–1607. https://doi.org/10.1093/hmg/ddy066

Leidal, A.M., Levine, B., Debnath, J., 2018. Autophagy and the cell biology of age-related disease. Nat Cell Biol 20, 1338–1348. https://doi.org/10.1038/s41556-018-0235-8

Li, F., Xie, X., Wang, Y., Liu, J., Cheng, X., Guo, Y., Gong, Y., Hu, S., Pan, L., 2016. Structural insights into the interaction and disease mechanism of

neurodegenerative disease-associated optineurin and TBK1 proteins. Nat Commun 7, 12708. https://doi.org/10.1038/ncomms12708

Li, Y., Kang, J., Horwitz, M.S., 1998. Interaction of an Adenovirus E3 14.7-Kilodalton Protein with a Novel Tumor Necrosis Factor Alpha-Inducible Cellular Protein Containing Leucine Zipper Domains. Mol Cell Biol 18, 1601–1610.

Liao, B., Zhao, W., Beers, D.R., Henkel, J.S., Appel, S.H., 2012. Transformation from a neuroprotective to a neurotoxic microglial phenotype in a mouse model of ALS. Experimental Neurology 237, 147–152. https://doi.org/10.1016/j.expneurol.2012.06.011

Ling, S.-C., Albuquerque, C.P., Han, J.S., Lagier-Tourenne, C., Tokunaga, S., Zhou, H., Cleveland, D.W., 2010. ALS-associated mutations in TDP-43 increase its stability and promote TDP-43 complexes with FUS/TLS. Proc. Natl. Acad. Sci. U.S.A. 107, 13318–13323. https://doi.org/10.1073/pnas.1008227107

Lino, M.M., Schneider, C., Caroni, P., 2002. Accumulation of SOD1 Mutants in Postnatal Motoneurons Does Not Cause Motoneuron Pathology or Motoneuron Disease. J. Neurosci. 22, 4825–4832. https://doi.org/10.1523/JNEUROSCI.22-12-04825.2002

Liu, Z., Chen, P., Gao, H., Gu, Y., Yang, J., Peng, H., Xu, X., Wang, H., Yang, M., Liu, X., Fan, L., Chen, S., Zhou, J., Sun, Y., Ruan, K., Cheng, S., Komatsu, M., White, E., Li, L., Ji, H., Finley, D., Hu, R., 2014a. Ubiquitylation of Autophagy Receptor Optineurin by HACE1 Activates Selective Autophagy for Tumor Suppression. Cancer Cell 26, 106–120. https://doi.org/10.1016/j.ccr.2014.05.015

Liu, Z., Chen, P., Gao, H., Gu, Y., Yang, J., Peng, H., Xu, X., Wang, H., Yang, M., Liu, X., Fan, L., Chen, S., Zhou, J., Sun, Y., Ruan, K., Cheng, S., Komatsu, M., White, E., Li, L., Ji, H., Finley, D., Hu, R., 2014b. Ubiquitylation of Autophagy Receptor Optineurin by HACE1 Activates Selective Autophagy for Tumor Suppression. Cancer Cell 26, 106–120. https://doi.org/10.1016/j.ccr.2014.05.015

Liu, Z., Li, H., Hong, C., Chen, M., Yue, T., Chen, C., Wang, Z., You, Q., Li, C., Weng, Q., Xie, H., Hu, R., 2018. ALS-Associated E478G Mutation in Human OPTN (Optineurin) Promotes Inflammation and Induces Neuronal Cell Death. Front. Immunol. 9, 2647. https://doi.org/10.3389/fimmu.2018.02647

Lobo-Silva, D., Carriche, G.M., Castro, A.G., Roque, S., Saraiva, M., 2017. Interferon-β regulates the production of IL-10 by toll-like receptor-activated microglia. Glia 65, 1439–1451. https://doi.org/10.1002/glia.23172

Mankouri, J., Fragkoudis, R., Richards, K.H., Wetherill, L.F., Harris, M., Kohl, A., Elliott, R.M., Macdonald, A., 2010. Optineurin Negatively Regulates the Induction of IFNβ in Response to RNA Virus Infection. PLOS Pathogens 6, e1000778. https://doi.org/10.1371/journal.ppat.1000778

Mantovani, S., Garbelli, S., Pasini, A., Alimonti, D., Perotti, C., Melazzini, M., Bendotti, C., Mora, G., 2009. Immune system alterations in sporadic amyotrophic lateral sclerosis patients suggest an ongoing neuroinflammatory process. Journal of Neuroimmunology 210, 73–79. https://doi.org/10.1016/j.jneuroim.2009.02.012

Mao, K., Klionsky, D.J., 2017. Xenophagy: A battlefield between host and microbe, and a possible avenue for cancer treatment. Autophagy 13, 223–224. https://doi.org/10.1080/15548627.2016.1267075

Markovinovic, A., Cimbro, R., Ljutic, T., Kriz, J., Rogelj, B., Munitic, I., 2017a. Optineurin in amyotrophic lateral sclerosis: Multifunctional adaptor protein at the crossroads of different neuroprotective mechanisms. Progress in Neurobiology 154, 1–20. https://doi.org/10.1016/j.pneurobio.2017.04.005

Markovinovic, A., Cimbro, R., Ljutic, T., Kriz, J., Rogelj, B., Munitic, I., 2017b. Optineurin in amyotrophic lateral sclerosis: Multifunctional adaptor protein at the crossroads of different neuroprotective mechanisms. Progress in Neurobiology 154, 1–20. https://doi.org/10.1016/j.pneurobio.2017.04.005

Markovinovic, A., Ljutic, T., Béland, L.-C., Munitic, I., 2018. Optineurin Insufficiency Disbalances Proinflammatory and Anti-inflammatory Factors by Reducing Microglial IFN-β Responses. Neuroscience 388, 139–151. https://doi.org/10.1016/j.neuroscience.2018.07.007

Martin, G.M., 1999. A Means to an End: The Biological Basis of Aging and Death. Am J Hum Genet 65, 1477–1478.

Maruyama, H., Morino, H., Ito, H., Izumi, Y., Kato, H., Watanabe, Y., Kinoshita, Y., Kamada, M., Nodera, H., Suzuki, H., Komure, O., Matsuura, S., Kobatake, K., Morimoto, N., Abe, K., Suzuki, N., Aoki, M., Kawata, A., Hirai, T., Kato, T., Ogasawara, K., Hirano, A., Takumi, T., Kusaka, H., Hagiwara, K., Kaji, R., Kawakami, H., 2010. Mutations of optineurin in amyotrophic lateral sclerosis. Nature 465, 223–226. https://doi.org/10.1038/nature08971

Masrori, P., Beckers, J., Gossye, H., Van Damme, P., 2022. The role of inflammation in neurodegeneration: novel insights into the role of the immune system in C9orf72 HRE-mediated ALS/FTD. Mol Neurodegeneration 17, 22. https://doi.org/10.1186/s13024-022-00525-z

Mattson, M.P., Arumugam, T.V., 2018. Hallmarks of Brain Aging: Adaptive and Pathological Modification by Metabolic States. Cell Metab 27, 1176–1199. https://doi.org/10.1016/j.cmet.2018.05.011

McCauley, M.E., Baloh, R.H., 2019. Inflammation in ALS/FTD pathogenesis. Acta Neuropathol 137, 715–730. https://doi.org/10.1007/s00401-018-1933-9

McCauley, M.E., O'Rourke, J.G., Yáñez, A., Markman, J.L., Ho, R., Wang, X., Chen, S., Lall, D., Jin, M., Muhammad, A.K.M.G., Bell, S., Landeros, J., Valencia, V., Harms, M., Arditi, M., Jefferies, C., Baloh, R.H., 2020. C9orf72 in myeloid cells suppresses STING-induced inflammation. Nature 585, 96–101. https://doi.org/10.1038/s41586-020-2625-x

McGeer, P.L., Itagaki, S., Boyes, B.E., McGeer, E.G., 1988. Reactive microglia are positive for HLA-DR in the substantia nigra of Parkinson's and Alzheimer's disease brains. Neurology 38, 1285–1291. https://doi.org/10.1212/wnl.38.8.1285

McGeer, P.L., McGeer, E.G., 2011. History of Innate Immunity in Neurodegenerative Disorders. Front Pharmacol 2, 77. https://doi.org/10.3389/fphar.2011.00077

Mead, R.J., Shan, N., Reiser, H.J., Marshall, F., Shaw, P.J., 2023a. Amyotrophic lateral sclerosis: a neurodegenerative disorder poised for successful therapeutic translation. Nat Rev Drug Discov 22, 185–212. https://doi.org/10.1038/s41573-022-00612-2

Mead, R.J., Shan, N., Reiser, H.J., Marshall, F., Shaw, P.J., 2023b. Amyotrophic lateral sclerosis: a neurodegenerative disorder poised for successful therapeutic translation. Nat Rev Drug Discov 22, 185–212. https://doi.org/10.1038/s41573-022-00612-2

Meena, N.P., Zhu, G., Mittelstadt, P.R., Giardino Torchia, M.L., Pourcelot, M., Arnoult, D., Ashwell, J.D., Munitic, I., 2016a. The TBK1-binding domain of optineurin promotes type I interferon responses. FEBS Letters 590, 1498–1508. https://doi.org/10.1002/1873-3468.12176

Meena, N.P., Zhu, G., Mittelstadt, P.R., Giardino Torchia, M.L., Pourcelot, M., Arnoult, D., Ashwell, J.D., Munitic, I., 2016b. The TBK1-binding domain of optineurin promotes type I interferon responses. FEBS Lett 590, 1498–1508. https://doi.org/10.1002/1873-3468.12176

Mejzini, R., Flynn, L.L., Pitout, I.L., Fletcher, S., Wilton, S.D., Akkari, P.A., 2019. ALS Genetics, Mechanisms, and Therapeutics: Where Are We Now? Front. Neurosci. 13, 1310. https://doi.org/10.3389/fnins.2019.01310

Miller, F.D., Gauthier, A.S., 2007. Timing Is Everything: Making Neurons versus Glia in the Developing Cortex. Neuron 54, 357–369. https://doi.org/10.1016/j.neuron.2007.04.019

Miller, T.M., Cudkowicz, M.E., Genge, A., Shaw, P.J., Sobue, G., Bucelli, R.C., Chiò, A., Van Damme, P., Ludolph, A.C., Glass, J.D., Andrews, J.A., Babu, S., Benatar, M., McDermott, C.J., Cochrane, T., Chary, S., Chew, S., Zhu, H., Wu, F., Nestorov, I., Graham, D., Sun, P., McNeill, M., Fanning, L., Ferguson, T.A., Fradette, S., VALOR and OLE Working Group, 2022. Trial of Antisense Oligonucleotide Tofersen for SOD1 ALS. N Engl J Med 387, 1099–1110. https://doi.org/10.1056/NEJMoa2204705

Mittelbrunn, M., Kroemer, G., 2021. Hallmarks of T cell aging. Nat Immunol 22, 687–698. https://doi.org/10.1038/s41590-021-00927-z

Moharir, S.C., Swarup, G., 2021. Optineurin deficiency induces patchy hair loss but it is not sufficient to cause amyotrophic lateral sclerosis in mice (preprint). Neuroscience. https://doi.org/10.1101/2021.12.22.473616

Mohovic, N., Peradinovic, J., Markovinovic, A., Cimbro, R., Minic, Z., Dominovic, M., Jakovac, H., Nimac, J., Rogelj, B., Munitic, I., 2023. Neuroimmune characterization of optineurin insufficiency mouse model during ageing. Sci Rep 13, 11840. https://doi.org/10.1038/s41598-023-38875-3

Moore, A.S., Holzbaur, E.L.F., 2016. Dynamic recruitment and activation of ALS-associated TBK1 with its target optineurin are required for efficient mitophagy. Proc Natl Acad Sci U S A 113, E3349-3358. https://doi.org/10.1073/pnas.1523810113

Moreland, R.J., Dresser, M.E., Rodgers, J.S., Roe, B.A., Conaway, J.W., Conaway, R.C., Hanas, J.S., 2000. Identification of a transcription factor IIIA-interacting protein. Nucleic Acids Res. 28, 1986–1993.

Moreno-García, A., Kun, A., Calero, O., Medina, M., Calero, M., 2018. An Overview of the Role of Lipofuscin in Age-Related Neurodegeneration. Frontiers in Neuroscience 12.

Morton, S., Hesson, L., Peggie, M., Cohen, P., 2008a. Enhanced binding of TBK1 by an optineurin mutant that causes a familial form of primary open angle glaucoma. FEBS Letters 582, 997–1002. https://doi.org/10.1016/j.febslet.2008.02.047

Morton, S., Hesson, L., Peggie, M., Cohen, P., 2008b. Enhanced binding of TBK1 by an optineurin mutant that causes a familial form of primary open angle glaucoma. FEBS Letters 582, 997–1002. https://doi.org/10.1016/j.febslet.2008.02.047

Mrdjen, D., Pavlovic, A., Hartmann, F.J., Schreiner, B., Utz, S.G., Leung, B.P., Lelios, I., Heppner, F.L., Kipnis, J., Merkler, D., Greter, M., Becher, B., 2018. High-Dimensional Single-Cell Mapping of Central Nervous System Immune Cells Reveals Distinct Myeloid Subsets in Health, Aging, and Disease. Immunity 48, 380-395.e6. https://doi.org/10.1016/j.immuni.2018.01.011

Munitic, I., Giardino Torchia, M.L., Meena, N.P., Zhu, G., Li, C.C., Ashwell, J.D., 2013. Optineurin Insufficiency Impairs IRF3 but Not NF- B Activation in Immune Cells. The Journal of Immunology 191, 6231–6240. https://doi.org/10.4049/jimmunol.1301696

Munitic, Ivana, Giardino Torchia, M.L., Meena, N.P., Zhu, G., Li, C.C., Ashwell, J.D., 2013. Optineurin Insufficiency Impairs IRF3 but Not NF-κB Activation in Immune Cells. J.I. 191, 6231–6240. https://doi.org/10.4049/jimmunol.1301696

Murasko, D.M., Weiner, P., Kaye, D., 1987. Decline in mitogen induced proliferation of lymphocytes with increasing age. Clin Exp Immunol 70, 440–448.

Murdock, B.J., Zhou, T., Kashlan, S.R., Little, R.J., Goutman, S.A., Feldman, E.L., 2017. Correlation of Peripheral Immunity With Rapid Amyotrophic Lateral Sclerosis Progression. JAMA Neurol 74, 1446. https://doi.org/10.1001/jamaneurol.2017.2255

Nagabhushana, A., Bansal, M., Swarup, G., 2011a. Optineurin Is Required for CYLD-Dependent Inhibition of TNFα-Induced NF-κB Activation. PLOS ONE 6, e17477. https://doi.org/10.1371/journal.pone.0017477

Nagabhushana, A., Bansal, M., Swarup, G., 2011b. Optineurin is required for CYLD-dependent inhibition of TNFα-induced NF-κB activation. PLoS One 6, e17477. https://doi.org/10.1371/journal.pone.0017477

Nakazawa, S., n.d. Linear ubiquitination is involved in the pathogenesis of optineurin-associated amyotrophic lateral sclerosis. NATURE COMMUNICATIONS 14.

Nakazawa, S., Oikawa, D., Ishii, R., Ayaki, T., Takahashi, H., Takeda, H., Ishitani, R., Kamei, K., Takeyoshi, I., Kawakami, H., Iwai, K., Hatada, I., Sawasaki, T., Ito, H., Nureki, O., Tokunaga, F., 2016. Linear ubiquitination is involved in the pathogenesis of optineurin-associated amyotrophic lateral sclerosis. Nature Communications 7, 12547. https://doi.org/10.1038/ncomms12547

Naor, S., Keren, Z., Bronshtein, T., Goren, E., Machluf, M., Melamed, D., 2009. Development of ALS-like disease in SOD-1 mice deficient of B lymphocytes. J Neurol 256, 1228–1235. https://doi.org/10.1007/s00415-009-5097-3

Neelagandan, N., Gonnella, G., Dang, S., Janiesch, P.C., Miller, K.K., Küchler, K., Marques, R.F., Indenbirken, D., Alawi, M., Grundhoff, A., Kurtz, S., Duncan, K.E., 2019. TDP-43 enhances translation of specific mRNAs linked to neurodegenerative disease. Nucleic Acids Res 47, 341–361. https://doi.org/10.1093/nar/gky972

Neumann, M., Sampathu, D.M., Kwong, L.K., Truax, A.C., Micsenyi, M.C., Chou, T.T., Bruce, J., Schuck, T., Grossman, M., Clark, C.M., McCluskey, L.F., Miller, B.L., Masliah, E., Mackenzie, I.R., Feldman, H., Feiden, W., Kretzschmar, H.A., Trojanowski, J.Q., Lee, V.M.-Y., 2006. Ubiquitinated TDP-43 in Frontotemporal Lobar Degeneration and Amyotrophic Lateral Sclerosis. Science 314, 130–133. https://doi.org/10.1126/science.1134108

Nikodemova, M., Small, A.L., Smith, S.M.C., Mitchell, G.S., Watters, J.J., 2014. Spinal but not cortical microglia acquire an atypical phenotype with high VEGF, galectin-3 and osteopontin, and blunted inflammatory responses in

ALS rats. Neurobiology of Disease 69, 43–53. https://doi.org/10.1016/j.nbd.2013.11.009

Nishioka, T., Shimizu, J., Iida, R., Yamazaki, S., Sakaguchi, S., 2006. CD4+CD25+Foxp3+ T Cells and CD4+CD25−Foxp3+ T Cells in Aged Mice1. The Journal of Immunology 176, 6586–6593. https://doi.org/10.4049/jimmunol.176.11.6586

O'Neil, S.M., Witcher, K.G., McKim, D.B., Godbout, J.P., 2018. Forced turnover of aged microglia induces an intermediate phenotype but does not rebalance CNS environmental cues driving priming to immune challenge. Acta Neuropathologica Communications 6, 129. https://doi.org/10.1186/s40478-018-0636-8

Ormeño, F., Hormazabal, J., Moreno, J., Riquelme, F., Rios, J., Criollo, A., Albornoz, A., Alfaro, I.E., Budini, M., 2020. Chaperone Mediated Autophagy Degrades TDP-43 Protein and Is Affected by TDP-43 Aggregation. Front Mol Neurosci 13, 19. https://doi.org/10.3389/fnmol.2020.00019

Osaka, M., Ito, D., Suzuki, N., 2016. Disturbance of proteasomal and autophagic protein degradation pathways by amyotrophic lateral sclerosis-linked mutations in ubiquilin 2. Biochem Biophys Res Commun 472, 324–331. https://doi.org/10.1016/j.bbrc.2016.02.107

Ou, S.H., Wu, F., Harrich, D., García-Martínez, L.F., Gaynor, R.B., 1995. Cloning and characterization of a novel cellular protein, TDP-43, that binds to human immunodeficiency virus type 1 TAR DNA sequence motifs. J Virol 69, 3584–3596. https://doi.org/10.1128/JVI.69.6.3584-3596.1995

Paganoni, S., Macklin, E.A., Hendrix, S., Berry, J.D., Elliott, M.A., Maiser, S., Karam, C., Caress, J.B., Owegi, M.A., Quick, A., Wymer, J., Goutman, S.A., Heitzman, D., Heiman-Patterson, T., Jackson, C.E., Quinn, C., Rothstein, J.D., Kasarskis, E.J., Katz, J., Jenkins, L., Ladha, S., Miller, T.M., Scelsa, S.N., Vu, T.H., Fournier, C.N., Glass, J.D., Johnson, K.M., Swenson, A., Goyal, N.A., Pattee, G.L., Andres, P.L., Babu, S., Chase, M., Dagostino, D., Dickson, S.P., Ellison, N., Hall, M., Hendrix, K., Kittle, G., McGovern, M., Ostrow, J., Pothier, L., Randall, R., Shefner, J.M., Sherman, A.V., Tustison, E., Vigneswaran, P., Walker, J., Yu, H., Chan, J., Wittes, J., Cohen, J., Klee, J., Leslie, K., Tanzi, R.E., Gilbert, W., Yeramian, P.D., Schoenfeld, D., Cudkowicz, M.E., 2020. Trial of Sodium Phenylbutyrate-Taurursodiol for Amyotrophic Lateral Sclerosis. N Engl J Med 383, 919–930. https://doi.org/10.1056/NEJMoa1916945

Paolicelli, R.C., Sierra, A., Stevens, B., Tremblay, M.-E., Aguzzi, A., Ajami, B., Amit, I., Audinat, E., Bechmann, I., Bennett, M., Bennett, F., Bessis, A., Biber, K., Bilbo, S., Blurton-Jones, M., Boddeke, E., Brites, D., Brône, B., Brown, G.C., Butovsky, O., Carson, M.J., Castellano, B., Colonna, M., Cowley, S.A., Cunningham, C., Davalos, D., De Jager, P.L., de Strooper, B., Denes, A., Eggen, B.J.L., Eyo, U., Galea, E., Garel, S., Ginhoux, F., Glass, C.K., Gokce, O., Gomez-Nicola, D., González, B., Gordon, S., Graeber, M.B., Greenhalgh, A.D., Gressens, P., Greter, M., Gutmann, D.H., Haass, C., Heneka, M.T., Heppner, F.L., Hong, S., Hume, D.A., Jung, S., Kettenmann, H., Kipnis, J., Koyama, R., Lemke, G., Lynch, M., Majewska, A., Malcangio, M., Malm, T., Mancuso, R., Masuda, T., Matteoli, M., McColl, B.W., Miron, V.E., Molofsky, A.V., Monje, M., Mracsko, E., Nadjar, A., Neher, J.J., Neniskyte, U., Neumann, H., Noda, M., Peng, B., Peri, F., Perry, V.H., Popovich, P.G., Pridans, C., Priller, J., Prinz, M., Ragozzino, D., Ransohoff, R.M., Salter, M.W., Schaefer,

A., Schafer, D.P., Schwartz, M., Simons, M., Smith, C.J., Streit, W.J., Tay, T.L., Tsai, L.-H., Verkhratsky, A., von Bernhardi, R., Wake, H., Wittamer, V., Wolf, S.A., Wu, L.-J., Wyss-Coray, T., 2022. Microglia states and nomenclature: A field at its crossroads. Neuron 110, 3458–3483. https://doi.org/10.1016/j.neuron.2022.10.020

Parzych, K.R., Klionsky, D.J., 2014. An Overview of Autophagy: Morphology, Mechanism, and Regulation. Antioxid Redox Signal 20, 460–473. https://doi.org/10.1089/ars.2013.5371

Peradinovic, J., Mohovic, N., Bulic, K., Markovinovic, A., Cimbro, R., Munitic, I., 2023. Ageing-Induced Decline in Primary Myeloid Cell Phagocytosis Is Unaffected by Optineurin Insufficiency. Biology 12, 240. https://doi.org/10.3390/biology12020240

Philips, T., Rothstein, J.D., 2015. Rodent Models of Amyotrophic Lateral Sclerosis. Curr Protoc Pharmacol 69, 5.67.1-5.67.21. https://doi.org/10.1002/0471141755.ph0567s69

Pinarbasi, E.S., Cağatay, T., Fung, H.Y.J., Li, Y.C., Chook, Y.M., Thomas, P.J., 2018. Active nuclear import and passive nuclear export are the primary determinants of TDP-43 localization. Sci Rep 8, 7083. https://doi.org/10.1038/s41598-018-25008-4

Polymenidou, M., Lagier-Tourenne, C., Hutt, K.R., Huelga, S.C., Moran, J., Liang, T.Y., Ling, S.-C., Sun, E., Wancewicz, E., Mazur, C., Kordasiewicz, H., Sedaghat, Y., Donohue, J.P., Shiue, L., Bennett, C.F., Yeo, G.W., Cleveland, D.W., 2011. Long pre-mRNA depletion and RNA missplicing contribute to neuronal vulnerability from loss of TDP-43. Nat Neurosci 14, 459–468. https://doi.org/10.1038/nn.2779

Porcher, L., Bruckmeier, S., Burbano, S.D., Finnell, J.E., Gorny, N., Klett, J., Wood, S.K., Kelly, M.P., 2021. Aging triggers an upregulation of a multitude of cytokines in the male and especially the female rodent hippocampus but more discrete changes in other brain regions. J Neuroinflammation 18, 219. https://doi.org/10.1186/s12974-021-02252-6

Porter, A.G., Jänicke, R.U., 1999. Emerging roles of caspase-3 in apoptosis. Cell Death Differ 6, 99–104. https://doi.org/10.1038/sj.cdd.4400476

Pottier, C., Bieniek, K.F., Finch, N., van de Vorst, M., Baker, M., Perkersen, R., Brown, P., Ravenscroft, T., van Blitterswijk, M., Nicholson, A.M., DeTure, M., Knopman, D.S., Josephs, K.A., Parisi, J.E., Petersen, R.C., Boylan, K.B., Boeve, B.F., Graff-Radford, N.R., Veltman, J.A., Gilissen, C., Murray, M.E., Dickson, D.W., Rademakers, R., 2015. Whole-genome sequencing reveals important role for TBK1 and OPTN mutations in frontotemporal lobar degeneration without motor neuron disease. Acta Neuropathol 130, 77–92. https://doi.org/10.1007/s00401-015-1436-x

Pottier, C., Rampersaud, E., Baker, M., Wu, G., Wuu, J., McCauley, J.L., Zuchner, S., Schule, R., Bermudez, C., Hussain, S., Cooley, A., Wallace, M., Zhang, J., Taylor, J.P., Benatar, M., Rademakers, R., 2018. Identification of compound heterozygous variants in OPTN in an ALS-FTD patient from the CReATe consortium: a case report. Amyotroph Lateral Scler Frontotemporal Degener 19, 469–471. https://doi.org/10.1080/21678421.2018.1452947

Pourcelot, M., Zemirli, N., Silva Da Costa, L., Loyant, R., Garcin, D., Vitour, D., Munitic, I., Vazquez, A., Arnoult, D., 2016a. The Golgi apparatus acts as a

platform for TBK1 activation after viral RNA sensing. BMC Biology 14. https://doi.org/10.1186/s12915-016-0292-z

Pourcelot, M., Zemirli, N., Silva Da Costa, L., Loyant, R., Garcin, D., Vitour, D., Munitic, I., Vazquez, A., Arnoult, D., 2016b. The Golgi apparatus acts as a platform for TBK1 activation after viral RNA sensing. BMC Biol 14, 69. https://doi.org/10.1186/s12915-016-0292-z

Pramatarova, A., Laganière, J., Roussel, J., Brisebois, K., Rouleau, G.A., 2001. Neuron-Specific Expression of Mutant Superoxide Dismutase 1 in Transgenic Mice Does Not Lead to Motor Impairment. J. Neurosci. 21, 3369–3374. https://doi.org/10.1523/JNEUROSCI.21-10-03369.2001

Prasad, A., Bharathi, V., Sivalingam, V., Girdhar, A., Patel, B.K., 2019. Molecular Mechanisms of TDP-43 Misfolding and Pathology in Amyotrophic Lateral Sclerosis. Front. Mol. Neurosci. 12, 25. https://doi.org/10.3389/fnmol.2019.00025

Prinz, M., Priller, J., 2014. Microglia and brain macrophages in the molecular age: from origin to neuropsychiatric disease. Nat Rev Neurosci 15, 300–312. https://doi.org/10.1038/nrn3722

Prtenjaca, N., 2020. Optineurin Dysfunction in Amyotrophic Lateral Sclerosis: Why So Puzzling? PDBIAD 121–122, 23–34. https://doi.org/10.18054/pb.v121-122i1-2.10627

Prtenjaca, N., Rob, M., Alam, M.S., Markovinovic, A., Stuani, C., Buratti, E., Munitic, I., 2022. Optineurin Deficiency and Insufficiency Lead to Higher Microglial TDP-43 Protein Levels. IJMS 23, 6829. https://doi.org/10.3390/ijms23126829

Ramesh, N., Pandey, U.B., 2017. Autophagy Dysregulation in ALS: When Protein Aggregates Get Out of Hand. Front Mol Neurosci 10, 263. https://doi.org/10.3389/fnmol.2017.00263

Ransohoff, R.M., 2016. How neuroinflammation contributes to neurodegeneration. Science 353, 777–783. https://doi.org/10.1126/science.aag2590

Re, D.B., Le Verche, V., Yu, C., Amoroso, M.W., Politi, K.A., Phani, S., Ikiz, B., Hoffmann, L., Koolen, M., Nagata, T., Papadimitriou, D., Nagy, P., Mitsumoto, H., Kariya, S., Wichterle, H., Henderson, C.E., Przedborski, S., 2014. Necroptosis drives motor neuron death in models of both sporadic and familial ALS. Neuron 81, 1001–1008. https://doi.org/10.1016/j.neuron.2014.01.011

Renton, A.E., Majounie, E., Waite, A., Simón-Sánchez, J., Rollinson, S., Gibbs, J.R., Schymick, J.C., Laaksovirta, H., van Swieten, J.C., Myllykangas, L., Kalimo, H., Paetau, A., Abramzon, Y., Remes, A.M., Kaganovich, A., Scholz, S.W., Duckworth, J., Ding, J., Harmer, D.W., Hernandez, D.G., Johnson, J.O., Mok, K., Ryten, M., Trabzuni, D., Guerreiro, R.J., Orrell, R.W., Neal, J., Murray, A., Pearson, J., Jansen, I.E., Sondervan, D., Seelaar, H., Blake, D., Young, K., Halliwell, N., Callister, J.B., Toulson, G., Richardson, A., Gerhard, A., Snowden, J., Mann, D., Neary, D., Nalls, M.A., Peuralinna, T., Jansson, L., Isoviita, V.-M., Kaivorinne, A.-L., Hölttä-Vuori, M., Ikonen, E., Sulkava, R., Benatar, M., Wuu, J., Chiò, A., Restagno, G., Borghero, G., Sabatelli, M., ITALSGEN Consortium, Heckerman, D., Rogaeva, E., Zinman, L., Rothstein, J.D., Sendtner, M., Drepper, C., Eichler, E.E., Alkan, C., Abdullaev, Z., Pack, S.D., Dutra, A., Pak, E., Hardy, J., Singleton, A., Williams, N.M., Heutink, P., Pickering-Brown, S., Morris, H.R., Tienari, P.J., Traynor, B.J., 2011. A hexanucleotide repeat expansion in C9ORF72 is the cause of chromosome

9p21-linked ALS-FTD. Neuron 72, 257–268. https://doi.org/10.1016/j.neuron.2011.09.010

Rezaie, T., 2002. Adult-Onset Primary Open-Angle Glaucoma Caused by Mutations in Optineurin. Science 295, 1077–1079. https://doi.org/10.1126/science.1066901

Rezaie, T., Waitzman, D.M., Seeman, J.L., Kaufman, P.L., Sarfarazi, M., 2005. Molecular cloning and expression profiling of optineurin in the rhesus monkey. Invest Ophthalmol Vis Sci 46, 2404–2410. https://doi.org/10.1167/iovs.04-1243

Richter, B., Sliter, D.A., Herhaus, L., Stolz, A., Wang, C., Beli, P., Zaffagnini, G., Wild, P., Martens, S., Wagner, S.A., Youle, R.J., Dikic, I., 2016a. Phosphorylation of OPTN by TBK1 enhances its binding to Ub chains and promotes selective autophagy of damaged mitochondria. Proceedings of the National Academy of Sciences 113, 4039–4044. https://doi.org/10.1073/pnas.1523926113

Richter, B., Sliter, D.A., Herhaus, L., Stolz, A., Wang, C., Beli, P., Zaffagnini, G., Wild, P., Martens, S., Wagner, S.A., Youle, R.J., Dikic, I., 2016b. Phosphorylation of OPTN by TBK1 enhances its binding to Ub chains and promotes selective autophagy of damaged mitochondria. Proc Natl Acad Sci USA 113, 4039–4044. https://doi.org/10.1073/pnas.1523926113

Rusconi, M., Gerardi, F., Santus, W., Lizio, A., Sansone, V.A., Lunetta, C., Zanoni, I., Granucci, F., 2017. Inflammatory role of dendritic cells in Amyotrophic Lateral Sclerosis revealed by an analysis of patients' peripheral blood. Sci Rep 7, 7853. https://doi.org/10.1038/s41598-017-08233-1

Rusmini, P., Cortese, K., Crippa, V., Cristofani, R., Cicardi, M.E., Ferrari, V., Vezzoli, G., Tedesco, B., Meroni, M., Messi, E., Piccolella, M., Galbiati, M., Garrè, M., Morelli, E., Vaccari, T., Poletti, A., 2018. Trehalose induces autophagy via lysosomal-mediated TFEB activation in models of motoneuron degeneration. Autophagy 15, 631–651. https://doi.org/10.1080/15548627.2018.1535292

Ryan, M., Heverin, M., McLaughlin, R.L., Hardiman, O., 2019. Lifetime Risk and Heritability of Amyotrophic Lateral Sclerosis. JAMA Neurol 76, 1367–1374. https://doi.org/10.1001/jamaneurol.2019.2044

Sahlender, D.A., Roberts, R.C., Arden, S.D., Spudich, G., Taylor, M.J., Luzio, J.P., Kendrick-Jones, J., Buss, F., 2005a. Optineurin links myosin VI to the Golgi complex and is involved in Golgi organization and exocytosis. J Cell Biol 169, 285–295. https://doi.org/10.1083/jcb.200501162

Sahlender, D.A., Roberts, R.C., Arden, S.D., Spudich, G., Taylor, M.J., Luzio, J.P., Kendrick-Jones, J., Buss, F., 2005b. Optineurin links myosin VI to the Golgi complex and is involved in Golgi organization and exocytosis. J Cell Biol 169, 285–295. https://doi.org/10.1083/jcb.200501162

Salminen, A., Huuskonen, J., Ojala, J., Kauppinen, A., Kaarniranta, K., Suuronen, T., 2008. Activation of innate immunity system during aging: NF-kB signaling is the molecular culprit of inflamm-aging. Ageing Research Reviews 7, 83–105. https://doi.org/10.1016/j.arr.2007.09.002

Saresella, M., Piancone, F., Tortorella, P., Marventano, I., Gatti, A., Caputo, D., Lunetta, C., Corbo, M., Rovaris, M., Clerici, M., 2013. T helper-17 activation dominates the immunologic milieu of both amyotrophic lateral sclerosis and progressive multiple sclerosis. Clin Immunol 148, 79–88. https://doi.org/10.1016/j.clim.2013.04.010

Sarkar, S., Davies, J.E., Huang, Z., Tunnacliffe, A., Rubinsztein, D.C., 2007. Trehalose, a Novel mTOR-independent Autophagy Enhancer, Accelerates the Clearance of Mutant Huntingtin and α-Synuclein*. Journal of Biological Chemistry 282, 5641–5652. https://doi.org/10.1074/jbc.M609532200

Schwamborn, K., Weil, R., Courtois, G., Whiteside, S.T., Israël, A., 2000. Phorbol esters and cytokines regulate the expression of the NEMO-related protein, a molecule involved in a NF-kappa B-independent pathway. J Biol Chem 275, 22780–22789. https://doi.org/10.1074/jbc.M001500200

Schwartz, M., Cahalon, L., 2022. The vicious cycle governing the brain–immune system relationship in neurodegenerative diseases. Current Opinion in Immunology 76, 102182. https://doi.org/10.1016/j.coi.2022.102182

Scotter, E.L., Vance, C., Nishimura, A.L., Lee, Y.-B., Chen, H.-J., Urwin, H., Sardone, V., Mitchell, J.C., Rogelj, B., Rubinsztein, D.C., Shaw, C.E., 2014. Differential roles of the ubiquitin proteasome system and autophagy in the clearance of soluble and aggregated TDP-43 species. Journal of Cell Science 127, 1263–1278. https://doi.org/10.1242/jcs.140087

Sephton, C.F., Good, S.K., Atkin, S., Dewey, C.M., Mayer, P., Herz, J., Yu, G., 2010. TDP-43 Is a Developmentally Regulated Protein Essential for Early Embryonic Development. Journal of Biological Chemistry 285, 6826–6834. https://doi.org/10.1074/jbc.M109.061846

Sheean, R.K., McKay, F.C., Cretney, E., Bye, C.R., Perera, N.D., Tomas, D., Weston, R.A., Scheller, K.J., Djouma, E., Menon, P., Schibeci, S.D., Marmash, N., Yerbury, J.J., Nutt, S.L., Booth, D.R., Stewart, G.J., Kiernan, M.C., Vucic, S., Turner, B.J., 2018. Association of Regulatory T-Cell Expansion With Progression of Amyotrophic Lateral Sclerosis: A Study of Humans and a Transgenic Mouse Model. JAMA Neurology 75, 681–689. https://doi.org/10.1001/jamaneurol.2018.0035

Shen, W.-C., Li, H.-Y., Chen, G.-C., Chern, Y., Tu, P., 2015. Mutations in the ubiquitin-binding domain of OPTN/optineurin interfere with autophagy-mediated degradation of misfolded proteins by a dominant-negative mechanism. Autophagy 11, 685–700. https://doi.org/10.4161/auto.36098

Shiga, A., Ishihara, T., Miyashita, A., Kuwabara, M., Kato, T., Watanabe, N., Yamahira, A., Kondo, C., Yokoseki, A., Takahashi, M., Kuwano, R., Kakita, A., Nishizawa, M., Takahashi, H., Onodera, O., 2012. Alteration of POLDIP3 splicing associated with loss of function of TDP-43 in tissues affected with ALS. PLoS One 7, e43120. https://doi.org/10.1371/journal.pone.0043120

Sidibé, H., Khalfallah, Y., Xiao, S., Gómez, N.B., Tank, E.M.H., Di Tomasso, G., Bareke, E., Aulas, A., McKeever, P.M., Melamed, Z., Destroimaisons, L., Deshaies, J.-E., Zinman, L., Parker, J.A., Legault, P., Tétreault, M., Barmada, S.J., Robertson, J., Vande Velde, C., 2020. TDP-43 stabilizes transcripts encoding stress granule protein G3BP1: potential relevance to ALS/FTD (preprint). Neuroscience. https://doi.org/10.1101/2020.09.15.298455

Slowicka, K., Vereecke, L., Mc Guire, C., Sze, M., Maelfait, J., Kolpe, A., Saelens, X., Beyaert, R., van Loo, G., 2016. Optineurin deficiency in mice is associated with increased sensitivity to *Salmonella* but does not affect proinflammatory NF-κB signaling. Eur. J. Immunol. 46, 971–980. https://doi.org/10.1002/eji.201545863

Smith, A.M., Sewell, G.W., Levine, A.P., Chew, T.S., Dunne, J., O'Shea, N.R., Smith, P.J., Harrison, P.J., Macdonald, C.M., Bloom, S.L., Segal, A.W., 2015. Disruption of macrophage pro-inflammatory cytokine release in Crohn's disease is associated with reduced optineurin expression in a subset of patients. Immunology 144, 45–55. https://doi.org/10.1111/imm.12338

Smith, R., Pioro, E., Myers, K., Sirdofsky, M., Goslin, K., Meekins, G., Yu, H., Wymer, J., Cudkowicz, M., Macklin, E.A., Schoenfeld, D., Pattee, G., 2017. Enhanced Bulbar Function in Amyotrophic Lateral Sclerosis: The Nuedexta Treatment Trial. Neurotherapeutics 14, 762–772. https://doi.org/10.1007/s13311-016-0508-5

Steinlechner, S., 2012. Chapter 2.12 - Biological Rhythms of the Mouse, in: Hedrich, H.J. (Ed.), The Laboratory Mouse (Second Edition). Academic Press, Boston, pp. 383–407. https://doi.org/10.1016/B978-0-12-382008-2.00017-9

Stolz, A., Ernst, A., Dikic, I., 2014. Cargo recognition and trafficking in selective autophagy. Nat Cell Biol 16, 495–501. https://doi.org/10.1038/ncb2979

Sundaramoorthy, V., Sultana, J.M., Atkin, J.D., 2015. Golgi fragmentation in amyotrophic lateral sclerosis, an overview of possible triggers and consequences. Front. Neurosci. 9. https://doi.org/10.3389/fnins.2015.00400

Swarup, V., Audet, J.-N., Phaneuf, D., Kriz, J., Julien, J.-P., 2012. Abnormal Regenerative Responses and Impaired Axonal Outgrowth after Nerve Crush in TDP-43 Transgenic Mouse Models of Amyotrophic Lateral Sclerosis. Journal of Neuroscience 32, 18186–18195. https://doi.org/10.1523/JNEUROSCI.2267-12.2012

Swarup, V., Phaneuf, D., Bareil, C., Robertson, J., Rouleau, G.A., Kriz, J., Julien, J.-P., 2011a. Pathological hallmarks of amyotrophic lateral sclerosis/frontotemporal lobar degeneration in transgenic mice produced with TDP-43 genomic fragments. Brain 134, 2610–2626. https://doi.org/10.1093/brain/awr159

Swarup, V., Phaneuf, D., Dupré, N., Petri, S., Strong, M., Kriz, J., Julien, J.-P., 2011b. Deregulation of TDP-43 in amyotrophic lateral sclerosis triggers nuclear factor κB–mediated pathogenic pathways. Journal of Experimental Medicine 208, 2429–2447. https://doi.org/10.1084/jem.20111313

Talbott, E.O., Malek, A.M., Lacomis, D., 2016. The epidemiology of amyotrophic lateral sclerosis. Handb Clin Neurol 138, 225–238. https://doi.org/10.1016/B978-0-12-802973-2.00013-6

Tang, Y., Le, W., 2016. Differential Roles of M1 and M2 Microglia in Neurodegenerative Diseases. Mol Neurobiol 53, 1181–1194. https://doi.org/10.1007/s12035-014-9070-5

Taylor, J.P., Brown, R.H., Cleveland, D.W., 2016. Decoding ALS: from genes to mechanism. Nature 539, 197–206. https://doi.org/10.1038/nature20413

Thonhoff, J.R., Beers, D.R., Zhao, W., Pleitez, M., Simpson, E.P., Berry, J.D., Cudkowicz, M.E., Appel, S.H., 2018. Expanded autologous regulatory T-lymphocyte infusions in ALS: A phase I, first-in-human study. Neurol Neuroimmunol Neuroinflamm 5, e465. https://doi.org/10.1212/NXI.0000000000000465

Thonhoff, J.R., Berry, J.D., Macklin, E.A., Beers, D.R., Mendoza, P.A., Zhao, W., Thome, A.D., Triolo, F., Moon, J.J., Paganoni, S., Cudkowicz, M., Appel, S.H., 2022. Combined Regulatory T-Lymphocyte and IL-2 Treatment Is Safe,

Tolerable, and Biologically Active for 1 Year in Persons With Amyotrophic Lateral Sclerosis. Neurol Neuroimmunol Neuroinflamm 9, e200019. https://doi.org/10.1212/NXI.0000000000200019

Tokunaga, F., 2013. Linear ubiquitination-mediated NF-κB regulation and its related disorders. J Biochem 154, 313–323. https://doi.org/10.1093/jb/mvt079

Toth, R.P., Atkin, J.D., 2018. Dysfunction of Optineurin in Amyotrophic Lateral Sclerosis and Glaucoma. Frontiers in Immunology 9. https://doi.org/10.3389/fimmu.2018.01017

Trabjerg, B.B., Garton, F.C., van Rheenen, W., Fang, F., Henderson, R.D., Mortensen, P.B., Agerbo, E., Wray, N.R., 2020. ALS in Danish Registries: Heritability and links to psychiatric and cardiovascular disorders. Neurol Genet 6, e398. https://doi.org/10.1212/NXG.0000000000000398

Troost, D., van den Oord, J.J., de Jong, J.M., Swaab, D.F., 1989. Lymphocytic infiltration in the spinal cord of patients with amyotrophic lateral sclerosis. Clin Neuropathol 8, 289–294.

Tu, D., Zhu, Z., Zhou, A.Y., Yun, C., Lee, K.-E., Toms, A.V., Li, Y., Dunn, G.P., Chan, E., Thai, T., Yang, S., Ficarro, S.B., Marto, J.A., Jeon, H., Hahn, W.C., Barbie, D.A., Eck, M.J., 2013. Structure and ubiquitination-dependent activation of TANK-binding kinase 1. Cell Rep 3, 747–758. https://doi.org/10.1016/j.celrep.2013.01.033

Tumbarello, D.A., Manna, P.T., Allen, M., Bycroft, M., Arden, S.D., Kendrick-Jones, J., Buss, F., 2015. The Autophagy Receptor TAX1BP1 and the Molecular Motor Myosin VI Are Required for Clearance of Salmonella Typhimurium by Autophagy. PLOS Pathogens 11, e1005174. https://doi.org/10.1371/journal.ppat.1005174

Tumbarello, D.A., Waxse, B.J., Arden, S.D., Bright, N.A., Kendrick-Jones, J., Buss, F., 2012. Autophagy receptors link myosin VI to autophagosomes to mediate Tom1-dependent autophagosome maturation and fusion with the lysosome. Nature Cell Biology 14, 1024–1035. https://doi.org/10.1038/ncb2589

Tümer, Z., Bertelsen, B., Gredal, O., Magyari, M., Nielsen, K.C., LuCamp, Grønskov, K., Brøndum-Nielsen, K., 2012. A novel heterozygous nonsense mutation of the OPTN gene segregating in a Danish family with ALS. Neurobiology of Aging 33, 208.e1-208.e5. https://doi.org/10.1016/j.neurobiolaging.2011.07.001

Urushitani, M., Kurisu, J., Tsukita, K., Takahashi, R., 2002. Proteasomal inhibition by misfolded mutant superoxide dismutase 1 induces selective motor neuron death in familial amyotrophic lateral sclerosis. J Neurochem 83, 1030–1042. https://doi.org/10.1046/j.1471-4159.2002.01211.x

Urushitani, M., Sato, T., Bamba, H., Hisa, Y., Tooyama, I., 2010. Synergistic effect between proteasome and autophagosome in the clearance of polyubiquitinated TDP-43. Journal of Neuroscience Research 88, 784–797. https://doi.org/10.1002/jnr.22243

Van Damme, P., Robberecht, W., Van Den Bosch, L., 2017. Modelling amyotrophic lateral sclerosis: progress and possibilities. Disease Models & Mechanisms 10, 537–549. https://doi.org/10.1242/dmm.029058

van der Zee, J., Gijselinck, I., Van Mossevelde, S., Perrone, F., Dillen, L., Heeman, B., Bäumer, V., Engelborghs, S., De Bleecker, J., Baets, J., Gelpi, E., Rojas-García, R., Clarimón, J., Lleó, A., Diehl-Schmid, J., Alexopoulos, P., Perneczky, R., Synofzik, M., Just, J., Schöls, L., Graff, C., Thonberg, H.,

Borroni, B., Padovani, A., Jordanova, A., Sarafov, S., Tournev, I., de Mendonça, A., Miltenberger-Miltényi, G., Simões do Couto, F., Ramirez, A., Jessen, F., Heneka, M.T., Gómez-Tortosa, E., Danek, A., Cras, P., Vandenberghe, R., De Jonghe, P., De Deyn, P.P., Sleegers, K., Cruts, M., Van Broeckhoven, C., Goeman, J., Nuytten, D., Smets, K., Robberecht, W., Damme, P.V., Bleecker, J.D., Santens, P., Dermaut, B., Versijpt, J., Michotte, A., Ivanoiu, A., Deryck, O., Bergmans, B., Delbeck, J., Bruyland, M., Willems, C., Salmon, E., Pastor, P., Ortega-Cubero, S., Benussi, L., Ghidoni, R., Binetti, G., Hernández, I., Boada, M., Ruiz, A., Sorbi, S., Nacmias, B., Bagnoli, S., Sorbi, S., Sanchez-Valle, R., Llado, A., Santana, I., Rosário Almeida, M., Frisoni, G.B., Maetzler, W., Matej, R., Fraidakis, M.J., Kovacs, G.G., Fabrizi, G.M., Testi, S., 2017. TBK1 Mutation Spectrum in an Extended European Patient Cohort with Frontotemporal Dementia and Amyotrophic Lateral Sclerosis. Hum Mutat 38, 297–309. https://doi.org/10.1002/humu.23161

Ventevogel, M.S., Sempowski, G.D., 2013. Thymic Rejuvenation and Aging. Curr Opin Immunol 25, 516–522. https://doi.org/10.1016/j.coi.2013.06.002

Vignali, D.A.A., Collison, L.W., Workman, C.J., 2008. How regulatory T cells work. Nat Rev Immunol 8, 523–532. https://doi.org/10.1038/nri2343

Wang, Jiajia, Wang, Jiaying, Hong, W., Zhang, L., Song, L., Shi, Q., Shao, Y., Hao, G., Fang, C., Qiu, Y., Yang, L., Yang, Z., Wang, Jincheng, Cao, J., Yang, B., He, Q., Weng, Q., 2021. Optineurin modulates the maturation of dendritic cells to regulate autoimmunity through JAK2-STAT3 signaling. Nat Commun 12, 6198. https://doi.org/10.1038/s41467-021-26477-4

Wang, P., n.d. Acetylation-induced TDP-43 pathology is suppressed by an HSF1-dependent chaperone program. NATURE COMMUNICATIONS 15.

Wang, X., Fan, H., Ying, Z., Li, B., Wang, H., Wang, G., 2010. Degradation of TDP-43 and its pathogenic form by autophagy and the ubiquitin-proteasome system. Neurosci Lett 469, 112–116. https://doi.org/10.1016/j.neulet.2009.11.055

Watanabe, S., Kaneko, K., Yamanaka, K., 2013. Accelerated Disease Onset with Stabilized Familial Amyotrophic Lateral Sclerosis (ALS)-linked Mutant TDP-43 Proteins. Journal of Biological Chemistry 288, 3641–3654. https://doi.org/10.1074/jbc.M112.433615

Watts, G.D.J., Wymer, J., Kovach, M.J., Mehta, S.G., Mumm, S., Darvish, D., Pestronk, A., Whyte, M.P., Kimonis, V.E., 2004. Inclusion body myopathy associated with Paget disease of bone and frontotemporal dementia is caused by mutant valosin-containing protein. Nat Genet 36, 377–381. https://doi.org/10.1038/ng1332

Webster, C.P., Smith, E.F., Bauer, C.S., Moller, A., Hautbergue, G.M., Ferraiuolo, L., Myszczynska, M.A., Higginbottom, A., Walsh, M.J., Whitworth, A.J., Kaspar, B.K., Meyer, K., Shaw, P.J., Grierson, A.J., De Vos, K.J., 2016. The C9orf72 protein interacts with Rab1a and the ULK1 complex to regulate initiation of autophagy. EMBO J 35, 1656–1676. https://doi.org/10.15252/embj.201694401

Wertz, I.E., O'Rourke, K.M., Zhou, H., Eby, M., Aravind, L., Seshagiri, S., Wu, P., Wiesmann, C., Baker, R., Boone, D.L., Ma, A., Koonin, E.V., Dixit, V.M., 2004. De-ubiquitination and ubiquitin ligase domains of A20 downregulate NF-kappaB signalling. Nature 430, 694–699. https://doi.org/10.1038/nature02794

White, M.A., Kim, E., Duffy, A., Adalbert, R., Phillips, B.U., Peters, O.M., Stephenson, J., Yang, S., Massenzio, F., Lin, Z., Andrews, S., Segonds-Pichon, A., Metterville, J., Saksida, L.M., Mead, R., Ribchester, R.R., Barhomi, Y., Serre, T., Coleman, M.P., Fallon, J.R., Bussey, T.J., Brown, R.H., Sreedharan, J., 2018. TDP-43 gains function due to perturbed autoregulation in a Tardbp knock-in mouse model of ALS-FTD. Nat Neurosci 21, 552–563. https://doi.org/10.1038/s41593-018-0113-5

Wild, P., Farhan, H., McEwan, D.G., Wagner, S., Rogov, V.V., Brady, N.R., Richter, B., Korac, J., Waidmann, O., Choudhary, C., Dotsch, V., Bumann, D., Dikic, I., 2011. Phosphorylation of the Autophagy Receptor Optineurin Restricts Salmonella Growth. Science 333, 228–233. https://doi.org/10.1126/science.1205405

Wild, Philipp, Farhan, H., McEwan, D.G., Wagner, S., Rogov, V.V., Brady, N.R., Richter, B., Korac, J., Waidmann, O., Choudhary, C., Dötsch, V., Bumann, D., Dikic, I., 2011. Phosphorylation of the autophagy receptor optineurin restricts Salmonella growth. Science 333, 228–233. https://doi.org/10.1126/science.1205405

Wise, J.P., Price, C.G., Amaro, J.A., Cannon, J.R., 2018. Autophagy Disruptions Associated With Altered Optineurin Expression in Extranigral Regions in a Rotenone Model of Parkinson's Disease. Front Neurosci 12, 289. https://doi.org/10.3389/fnins.2018.00289

Wong, Y.C., Holzbaur, E.L.F., n.d. Optineurin is an autophagy receptor for damaged mitochondria in parkin-mediated mitophagy that is disrupted by an ALS-linked mutation. CELL BIOLOGY 10.

Writing Group, Edaravone (MCI-186) ALS 19 Study Group, 2017. Safety and efficacy of edaravone in well defined patients with amyotrophic lateral sclerosis: a randomised, double-blind, placebo-controlled trial. Lancet Neurol 16, 505–512. https://doi.org/10.1016/S1474-4422(17)30115-1

Yamanaka, K., Chun, S.J., Boillee, S., Fujimori-Tonou, N., Yamashita, H., Gutmann, D.H., Takahashi, R., Misawa, H., Cleveland, D.W., 2008. Astrocytes as determinants of disease progression in inherited amyotrophic lateral sclerosis. Nat Neurosci 11, 251–253. https://doi.org/10.1038/nn2047

Yildiz, O., Schroth, J., Tree, T., Turner, M.R., Shaw, P.J., Henson, S.M., Malaspina, A., 2023. Senescent-like Blood Lymphocytes and Disease Progression in Amyotrophic Lateral Sclerosis. Neurology - Neuroimmunology Neuroinflammation 10. https://doi.org/10.1212/NXI.0000000000200042

Ying, H., Shen, X., Park, B., Yue, B.Y.J.T., 2010. Posttranslational Modifications, Localization, and Protein Interactions of Optineurin, the Product of a Glaucoma Gene. PLoS ONE 5, e9168. https://doi.org/10.1371/journal.pone.0009168

Zhang, Y.-J., Gendron, T.F., Xu, Y.-F., Ko, L.-W., Yen, S.-H., Petrucelli, L., 2010. Phosphorylation regulates proteasomal-mediated degradation and solubility of TAR DNA binding protein-43 C-terminal fragments. Molecular Neurodegeneration 5, 33. https://doi.org/10.1186/1750-1326-5-33

Zhao, W., Beers, D.R., Appel, S.H., 2013. Immune-mediated mechanisms in the pathoprogression of amyotrophic lateral sclerosis. J Neuroimmune Pharmacol 8, 888–899. https://doi.org/10.1007/s11481-013-9489-x

Zhao, W., Beers, D.R., Bell, S., Wang, J., Wen, S., Baloh, R.H., Appel, S.H., 2015. TDP-43 activates microglia through NF-κB and NLRP3 inflammasome. Experimental Neurology 273, 24–35. https://doi.org/10.1016/j.expneurol.2015.07.019

Zhao, X., Wang, H., Sun, G., Zhang, J., Edwards, N.J., Aronowski, J., 2015. Neuronal Interleukin-4 as a Modulator of Microglial Pathways and Ischemic Brain Damage. Journal of Neuroscience 35, 11281–11291. https://doi.org/10.1523/JNEUROSCI.1685-15.2015

Zhong, Z., Umemura, A., Sanchez-Lopez, E., Liang, S., Shalapour, S., Wong, J., He, F., Boassa, D., Perkins, G., Ali, S.R., McGeough, M.D., Ellisman, M.H., Seki, E., Gustafsson, A.B., Hoffman, H.M., Diaz-Meco, M.T., Moscat, J., Karin, M., 2016. NF-κB Restricts Inflammasome Activation via Elimination of Damaged Mitochondria. Cell 164, 896–910. https://doi.org/10.1016/j.cell.2015.12.057

Zhu, G., Wu, C.-J., Zhao, Y., Ashwell, J.D., 2007. Optineurin Negatively Regulates TNFα- Induced NF-κB Activation by Competing with NEMO for Ubiquitinated RIP. Current Biology 17, 1438–1443. https://doi.org/10.1016/j.cub.2007.07.041

Zhu, J., Cynader, M.S., Jia, W., 2015. TDP-43 Inhibits NF-κB Activity by Blocking p65 Nuclear Translocation. PLoS One 10, e0142296. https://doi.org/10.1371/journal.pone.0142296

Zou, Z.-Y., Zhou, Z.-R., Che, C.-H., Liu, C.-Y., He, R.-L., Huang, H.-P., 2017. Genetic epidemiology of amyotrophic lateral sclerosis: a systematic review and meta-analysis. J Neurol Neurosurg Psychiatry 88, 540–549. https://doi.org/10.1136/jnnp-2016-315018

Zuo, L., Prather, E.R., Stetskiv, M., Garrison, D.E., Meade, J.R., Peace, T.I., Zhou, T., 2019. Inflammageing and Oxidative Stress in Human Diseases: From Molecular Mechanisms to Novel Treatments. Int J Mol Sci 20, 4472. https://doi.org/10.3390/ijms20184472

8. List of Abbreviations

Abbreviation	Definition
aa	amino acids
ABIN	A20 binding inhibitor of NF-kB
ALS	amyotrophic lateral sclerosis
AMPK	5' adenosine monophosphate-activated protein kinase
Atg	autophagy-related gene
ATP	adenosine triphosphate
BBB	blood-brain barrier
BDNF	brain cell-derived neurotrophic factors
CC	coiled-coil
cDC	conventional dendritic cells
CC3	cleaved caspase 3
$CD4^+$	helper T lymphocytes
$CD8^+$	cytotoxic T lymphocytes
CHMP2B	multivesicular body protein 2B
cIAPs	and cellular inhibitor of apoptosis proteins
CMA	chaperone-mediated autophagy
CNS	central nervous system
CRP	C-reactive protein
CSF	cerebrospinal fluid
CYLD	cylindromatosis
C9orf72	chromosome 9 open reading frame 72
DAMPs	damage-associated molecular patterns
DC	dendritic cells
DNase I	Deoxyribonuclease I
fALS	familial amyotrophic lateral sclerosis
FIP-2	adenoviral E3-14.7K interacting protein 2
FIP200	focal adhesion kinase family interacting protein of 200
FOXP3	forkhead box P3
FTD	frontotemporal dementia
FUS	fused in sarcoma
GABARAP	GABA Type A Receptor-Associated Protein
GDNF	glial cell-derived neurotrophic factors

G3bp1	Ras-GAP SH3 domain-binding protein 1
HACE1	HECT Domain and Ankyrin Repeat Containing E3 Ubiquitin Protein Ligase 1
HIV-1	Human Immunodeficiency Virus 1
hnRNP	heterogeneous nuclear ribonucleoprotein
hSOD1	human mutations in SOD1
IκB	inhibitor of kappa B
IKK	Inhibitor of kappa B kinase
IRF3	interferon regulatory factor 3
IFN-β	interferon-β
IL	interleukin
K	lysin
KO	knockout
LC3	microtubule-associate protein 1A/1B-light chain 3
LIR	LC3-interacting region
LPS	lipopolysaccharide
LUBAC	linear ubiquitin chain assembly complex
M	methionine
MFI	mean fluorescence intensity
MΦ	macrophages
mTOR	mammalian target of rapamycin
NES	nuclear export signal
NEMO	NF-κB essential modulator
NF-κB	nuclear factor kappa-light-chain-enhancer of activated B cells
NK cells	natural killer cells
NLS	nuclear localization signal
NPR	NEMO-related protein
OPTN	optineurin
PBMC	peripheral blood mononuclear cell
PAMPs	pathogen-associated molecular patterns
PE	phosphatidyl ethanolamine
PET	positron emission tomography
PINK1	PTEN-induced kinase 1
PI3P	phosphatidylinositol 3-phosphate
POAG	primary open-angle glaucoma

Poldip3	Polymerase delta-interacting protein 3
RIPK1	receptor-interacting protein 1
RRM	RNA recognition motifs
ROS	reactive oxygen species
sALS	sporadic amyotrophic lateral sclerosis
Ser	serine
SIP	Stock isotonic Percoll
SQSTM1	sequestosome 1
SOD1	superoxide dismutase 1
TAK1	transforming growth factor-β-activated kinase 1
TARDBP	transactive response (TAR) DNA-binding protein
TBK1	TANK-binding kinase 1
T_{CM}	central memory T lymphocytes
T_{EM}	effector memory T lymphocytes
TFEB	transcription factor EB
TGF-β	transforming growth factor β
TLR	toll-like receptors
T_N	naïve T lymphocytes
TNF	tumor necrosis factor
TRAF	tumor necrosis factor receptor-associated factor
Tregs	regulatory T cells
TDP-43	TAR DNA binding protein of 43 kDa
UBAN	ubiquitin-binding region of ABIN and NEMO proteins
UBQLN2	ubiqulin-2
ULK1	unc-51 like autophagy activating kinase 1
UPS	ubiquitin-proteasomal system
UPR	ER stress-activated unfolded protein response
VPS34	phosphatidylinositol 3-kinase
Wipi2	WD repeat domain phosphoinositide-interacting protein 2
WT	wild-type
ZF	zinc finger

9. List of Figures

10. List of Tables

11. Biography

Nikolina Mohović

Nationality: Croatian **Date of birth:** 06/03/1994

Phone number: (+385) 992148597

Email address: nikolina.prtenjaca.np@gmail.com **Skype:** nikolina.prtenjaca

Home: Antončićeva 9, 51211 Matulji (Croatia)

WORK EXPERIENCE

University research assistant

Department of Biotechnology, University of Rijeka [03/2019 – Current]

City: Rijeka

Country: Croatia

Laboratory of Molecular Immunology (Rijeka, Croatia), a project founded by the Croatian science foundation (HRZZ) Career development of young scientists DOK-2018-09-7739; PI: Associate Prof. Ivana Munitić, PhD

Student Teaching Fellow

Department of Biotechnology, University of Rijeka [01/10/2016 – 15/11/2016]

City: Rijeka

Country: Croatia

Help before and during laboratory exercises in the Immunology course for students.

Student Teaching Fellow

Department of Biotechnology, University of Rijeka [01/01/2016 – 15/02/2016]

City: Rijeka

Country: Croatia

Help before and during laboratory exercises in the Organic chemistry course for students.

Erasmus visiting PhD student

Jožef Stefan Institute [01/09/2022 – 01/12/2022]

City: Ljubljana

Country: Slovenia

EDUCATION AND TRAINING

PhD student

Department of Biotechnology, University of Rijeka [10/2019 – Current]

City: Rijeka

Country: Croatia

Website: https://www.biotech.uniri.hr/en/

Doktorski sveučilišni studij *Medicinska kemija*
Laboratorij za molekularnu imunologiju; mentor: dr.sc. Ivana Munitić

Master of Science (M.Sc.) in Biotechnology in Medicine (mag. biotech. in med.)

Department of Biotechnology, University of Rijeka [2016 – 2018]

City: Rijeka

Country: Croatia

Website: https://www.biotech.uniri.hr/en/

Final grade: 93.4 % (Summa cum laude)

Thesis: Autophagy analyses in Neuro2A cell line with CRISPR/Cas9-mediated deletion of optineurin

Bachelor of Science (B.Sc.) in Biotechnology and Drug Research (univ. bacc. biotech. et pharm. inv.)
Department of Biotechnology, University of Rijeka [2013 – 2016]

City: Rijeka
Country: Croatia
Website: https://www.biotech.uniri.hr/en/
Final grade: 87.3% (Magna cum laude)

High school graduate
Gymnasium "Eugena Kumičića Opatija" [2008 – 2013]

City: Opatija
Country: Croatia
Website: https://gek-opatija.hr/hr/

JOB-RELATED SKILLS

Laboratory and research skills

Cell cultures, transfection, silencing; cloning; Isolation and cultivation of primary cells; western blotting; RT-PCR; ELISA; flow cytometry; immunofluorescence and immunohistochemistry; work with experimental animals (cognitive and motor coordination tests); ImageJ; GraphPad Prism; FlowJo; MS Office

ADDITIONAL INFORMATIONS

Publications

Nikolina Mohovic, Josip Peradinovic, Andrea Markovinovic, Raffaello Cimbro, Zeljka Minic, Marin Dominovic, Hrvoje Jakovac, Jerneja Nimac, Boris Rogelj, and Ivana Munitic. **Neuroimmune characterization of optineurin insufficiency mouse model during ageing.** Scientific Reports, (2023) 13:11840; https://doi.org/10.1038/s41598-023-38875-3

Josip Peradinovic, **Nikolina Mohovic**, Katarina Bulic, Andrea Markovinovic, Raffaello Cimbro and Ivana Munitic. **Ageing-Induced Decline in Primary Myeloid Cell Phagocytosis Is Unaffected by Optineurin Insufficiency**. Biology 2023, 12(2), 240; https://doi.org/10.3390/biology12020240

Nikolina Prtenjaca, Matea Rob, Muhammad S. Alam, Andrea Markovinovic, Cristiana Stuani, Emanuele Buratti and Ivana Munitic. **Optineurin Deficiency and Insufficiency Lead to Higher Microglial TDP-43 Protein Levels.** Int. J. Mol. Sci. 2022, 23, 6829; https://doi.org/10.3390/ijms23126829

De Marchi F, Munitic I, Amedei A, Berry JD, Feldman EL, Aronica E, Nardo G, Van Weehaegh D, Niccolai E, **Prtenjaca N**, Sakowski SA, Bendotti C, and Mazzini L. Interplay between immunity and amyotrophic lateral sclerosis: Clinical impact. Neuroscience & Biobehavioral Reviews, Volume 127, 958-978; 10.1016/j.neubiorev.2021.06.027

Nikolina Prtenjača, Marin Dominović, Josip Peradinović, Rozalija Šajn and Ivana Munitić ;**Optineurin Dysfunction in Amyotrophic Lateral Sclerosis: Why So Puzzling?**; Periodicum Biologorum; VOL. 121–122, No 1–2, 23–34, 2020; 10.3390/ijms23126829

Conferences

Mohović N. **Crosstalk of Optineurin and TDP-43 in ALS and FTD;** oral presentation; SiNAPSA Neuroscience Conference '23, Ljubljana, Slovenia, 28th -30th September 2023.

Mohović N. **Optineurin and TDP-43 crosstalk in ALS and FTD in microglia**; poster presentation; 1st biennial conference on TDP-43 function and dysfunction in disease, Trieste, Italy, 8th-9th September 2023.

Mohović N. **Optineurin downregulates microglial TDP-43 protein levels**; poster presentation; ALS Rijeka 2022 Symposium, Rijeka, Croatia, 30th June-3rd July 2022.

Mohović N. **Optineurin downregulates microglial TDP-43 protein levels**; poster presentation; ENCALS meeting 2022 Edinburgh, Edinburgh, UK, 1st-3rd June 2022.

Prtenjača N. **Differential Crosstalk of Optineurin and TDP-43 in Myeloid Cells in Steady State Versus Inflammation**; poster presentation; 32nd International Symposium on ALS/MND, online, 7th-10th December 2021.

Prtenjača N. **Crosstalk of Optineurin and TDP-43 in microglia**; poster presentation; Microglia 2021, online, 28th-29th October 2021.

Prtenjača N. **Regulation of TDP-43 by optineurin**; oral presentation; Mechanistic insights into the pathophysiology of ALS, online, 26th-28th May 2021.

Prtenjača N. **Crosstalk of TDP-43 and Optineurin**; poster presentation; ENCALS; online, 10th-12th December 2020.

Prtenjača N. **Regulation of TDP-43 by Optineurin**; poster presentation; Glia in Health & Disease; online, 16th-19th July 2020.

Prtenjača N. **Elucidating the role of Optineurin in neuroinflammation and autophagy**; poster presentation; HDBMB 2019.; Lovran, Croatia, 25th-28th September 2019.

Prtenjača N. **Elucidating the complex role of Optineurin in inflammation and autophagy**; oral presentation; 23. *Young Neuroscientist Meeting (YNM2019)*; Trieste, Italy, 13th June 2019.

Grants and scholarships

Travel grant for SiNAPSA Neuroscience Conference 2023 (SNC'23), Ljubljana, Slovenia (2023)

Erasmus+ grant for an internship, University of Rijeka; internship at Jožef Stefan Institute, Ljubljana, Slovenia (2022)

Erasmus+ grant for student exchange, University of Rijeka, semester abroad at University of Milano, Milano, Italy (2018)

Scholarship for gifted high school students and college students of the Matulji municipality (2013-2018)

Awards

Best poster award; 2nd prize for the best poster titled **Elucidating the role of Optineurin in neuroinflammation and autophagy**; Congress of the Croatian Society of Biochemistry and Molecular Biology Crossroads in Life Sciences; Lovran, Croatia, 25th-28th September 2019.

Trainings

28th-30th September 2021: ICGEB Course Flow cytometry: from basic principles to advanced application, online

25th-28th September 2019: Workshop on Education; Better Skills for Better Jobs: Education and Training for Successful Research Careers; Croatian Society of Biochemistry and Molecular Biology Crossroads in Life Sciences; Lovran, Croatia

July 2019: Advanced Zeiss Confocal Microscopy Course LSM 880 with Airyscan, Departmant of Biotechnology, Rijeka

June 2019: Course for work with laboratory animals, Veterinary Faculty, Zagreb

Networks and memberships

2014-2018. Student Council of Department of Biotechnology

2016-2018. Department of Biotechnology Council; one of the student representative

2014-2018. Student Association of Biotechnology of Rijeka; supervisor of the volunteer activity

LANGUAGE SKILLS

Mother tongue(s): **Croatian**

Other language(s):

English	**Italian**
LISTENING C1 **READING** C1 **WRITING** B2	**LISTENING** A2 **READING** A2 **WRITING** A2
SPOKEN PRODUCTION B2 **SPOKEN INTERACTION** B2	**SPOKEN PRODUCTION** A2 **SPOKEN INTERACTION** A2

Levels: A1 and A2: Basic user; B1 and B2: Independent user; C1 and C2: Proficient user